

## INFORMATION TO USERS

This manuscript has been reproduced from the microfilm master. UMI films the text directly from the original or copy submitted. Thus, some thesis and dissertation copies are in typewriter face, while others may be from any type of computer printer.

**The quality of this reproduction is dependent upon the quality of the copy submitted.** Broken or indistinct print, colored or poor quality illustrations and photographs, print bleedthrough, substandard margins, and improper alignment can adversely affect reproduction.

In the unlikely event that the author did not send UMI a complete manuscript and there are missing pages, these will be noted. Also, if unauthorized copyright material had to be removed, a note will indicate the deletion.

Oversize materials (e.g., maps, drawings, charts) are reproduced by sectioning the original, beginning at the upper left-hand corner and continuing from left to right in equal sections with small overlaps.

Photographs included in the original manuscript have been reproduced xerographically in this copy. Higher quality 6" x 9" black and white photographic prints are available for any photographs or illustrations appearing in this copy for an additional charge. Contact UMI directly to order.

ProQuest Information and Learning  
300 North Zeeb Road, Ann Arbor, MI 48106-1346 USA  
800-521-0600


UMI<sup>®</sup>



**UNIVERSITY OF ALBERTA**

**THE FAMILY OF COMPACTION CURVES FOR  
FINE-GRAINED SOILS AND THEIR ENGINEERING  
BEHAVIORS**

by

Hua Li 

A thesis submitted to the Faculty of Graduate Studies and Research in partial fulfillment  
of the requirements for the degree of Doctor of Philosophy

in

Geotechnical Engineering

Department of Civil and Environmental Engineering

Edmonton, Alberta

Spring 2001



**National Library  
of Canada**

**Acquisitions and  
Bibliographic Services**

395 Wellington Street  
Ottawa ON K1A 0N4  
Canada

**Bibliothèque nationale  
du Canada**

**Acquisitions et  
services bibliographiques**

395, rue Wellington  
Ottawa ON K1A 0N4  
Canada

*Your file Votre référence*

*Our file Notre référence*

The author has granted a non-exclusive licence allowing the National Library of Canada to reproduce, loan, distribute or sell copies of this thesis in microform, paper or electronic formats.

The author retains ownership of the copyright in this thesis. Neither the thesis nor substantial extracts from it may be printed or otherwise reproduced without the author's permission.

L'auteur a accordé une licence non exclusive permettant à la Bibliothèque nationale du Canada de reproduire, prêter, distribuer ou vendre des copies de cette thèse sous la forme de microfiche/film, de reproduction sur papier ou sur format électronique.

L'auteur conserve la propriété du droit d'auteur qui protège cette thèse. Ni la thèse ni des extraits substantiels de celle-ci ne doivent être imprimés ou autrement reproduits sans son autorisation.

0-612-60319-9

**Canada**

# UNIVERSITY OF ALBERTA

## Library Release Form

**Name of Author:** Hua Li

**Title of Thesis:** The Family of Compaction Curves for Fine-grained Soils and Their Engineering Behaviors

**Degree:** Doctor of Philosophy

**Year this Degree Granted:** 2001

Permission is hereby granted to the University of Alberta Library to reproduce single copies of this thesis and to lend or sell such copies for private, scholarly or scientific research purposes only.

The author reserves all other publication and other rights in association with the copyright in the thesis, and except as herein before provided, neither the thesis nor any substantial portion thereof may be printed or otherwise reproduced in any material form whatever without the author's prior written permission.

A handwritten signature in black ink, appearing to be 'Hua Li', written over a horizontal line.

Hua Li

611C, Michener Park  
Edmonton, Alberta  
Canada, T6H 5A1

December 12, 2000

# UNIVERSITY OF ALBERTA

## Faculty of Graduate Studies and Research

The undersigned certify that they have read, and recommend to the Faculty of Graduate Studies and Research for acceptance, a thesis entitled The Family of Compaction Curves for Fine-grained Soils and Their Engineering Behaviours submitted by Hua Li in partial fulfillment of the requirements for the degree of Doctor of Philosophy in Geotechnical Engineering.



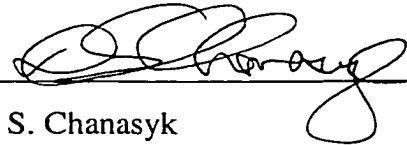
Dr. D. C. Sego



Dr. R. J. Chalaturnyk



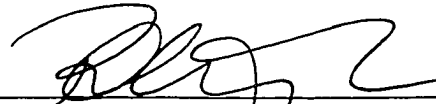
Dr. K. W. Biggar



Dr. D. S. Chanasyk



Dr. D. D. Tannant



for Dr. J. M. Konrad

Date: December 11, 2000

**To my wife Betty and daughter Alice**

for their support, love and understanding

**To my parents**

for all their encouragement and help through my education

**To my sister and brother**

for all the good time we had along the way

## ABSTRACT

The family of compaction curves has been found and used in construction quality control as the one-point method for many years. The objective of this study is to investigate soil compaction theory for fine-grained soils, especially the fundamental aspects related to the family of compaction curves, and its influence on their engineering behaviors.

Studies of the characteristics of the complete compaction curve allowed a promising equation for describing the compaction curve for fine-grained soils to be proposed. The equation has four parameters which physically define the boundary conditions, shape and size of the compaction curve. The relationships between the compaction parameters and the physical properties of a given soil are studied. The equation can easily be used to predict a family of compaction curves for the same soil for varying compactive efforts. In order to explain the origin of the family of compaction curves, the evolution of particle size distribution for residual soils due to weathering is analyzed using uniform fragmentation theory. The profiles of unconfined compression strength along the complete compaction curves are presented. It is found that the matric suction value at the compaction sensitivity threshold is equal to compactive stress applied during the test, which is important for understanding the compaction mechanism and determining the effective compaction region and the water content where the maximum compressive strength occurs.

The deformation behavior of the compacted fine-grained soils is another focus of this research. A new testing procedure using undisturbed compacted samples is developed that combines compaction, one-dimensional compression and wetting collapse testing in one apparatus. A series of soil deformation behaviors are summarized with variation in water content, compactive efforts, and wetting-flooding sequences. A continuous model to describe the one-dimensional compression curve over the complete stress range is proposed. Based on the equation and the concept of the family of compression curves, a new method is proposed to estimate the settlement of a thick compacted layer.



## **ACKNOWLEDGEMENTS**

I would like to express my sincere gratitude and appreciation to Dr. David C. Sego for his consistent guidance and advice throughout this study. The opportunity to work with him and witness his insight covering the field of geotechnical engineering was an invaluable experience.

The support and direction offered by Dr. Norbert R. Morgenstern was critical to this research at the early stage and greatly appreciated.

I would like to appreciate the encouragement and support by Dr. Rick Chalaturnyk during the research. The helpful editorial suggestion of Dr. Kevin Biggar significantly improved the manuscript of the thesis. My acknowledgement is also extended to Dr. Dwayne Tannant and Dr. David Chanasyk for their valuable comments during my candidacy and final examination.

I would like particularly to thank Dr. Jean-Marie Konrad from Laval University for accepting to be the external examiner and for his valuable comments.

I would also like to thank Dr. David Cruden and Dr. Stan Thomson for their inputs during the research.

The never-ending help from Mr. Gerry Cyre, Mr. Steve Gamble, and Ms. Christine Hereygers in laboratory testing is gratefully acknowledged.

I wish to thank Syncrude Canada Ltd. for providing the overburden soil samples used for this study. Helpful suggestions by Ms. Danielle Romanick of Campbell Scientific, Inc. and Dr. Fangsheng Shuai of University of Saskatchewan during suction measurement are greatly acknowledged.

The financial supports through National Sciences and Engineering Research Council grant (NSERC) held by Dr. Sego and University of Alberta Ph.D. Scholarship are gratefully acknowledged.

I would also like to thank my fellow graduate students in geotechnical group of department of civil and environmental engineering and in department of mathematical sciences for the challenging discussions and fresh ideas. My thanks are also extended to my former colleagues in department of geotechnical engineering at Tongji University, Shanghai, China, for the knowledge and experience they gave me.

## TABLE OF CONTENTS

<b>TABLE OF CONTENTS .....</b>	<b>I</b>
<b>LIST OF TABLES .....</b>	<b>VI</b>
<b>LIST OF FIGURES .....</b>	<b>VII</b>
<b>LIST OF SYMBOLS .....</b>	<b>XIV</b>
<b>CHAPTER 1 INTRODUCTION.....</b>	<b>1</b>
1.1 OUTLINE OF THESIS .....	3
1.2 REFERENCES .....	6
<b>CHAPTER 2 EQUATION FOR COMPACTION CURVE OF FINE-GRAINED SOILS: ITS ORIGIN, IMPLEMENTATION AND APPLICATION<sup>1</sup>.....</b>	<b>9</b>
2.1 INTRODUCTION.....	9
2.2 THE COMPLETE COMPACTION CURVE FOR FINE-GRAINED SOIL .....	12
2.2.1 Identifiable regions of the compaction curve.....	13
2.2.2 Boundaries of compaction curve .....	14
2.2.3 Shape of compaction curve.....	15
2.2.4 Size (Compactable moisture range) of compaction curve .....	15
2.3 DERIVATION OF THE COMPACTION CURVE FOR FINE-GRAINED SOIL 16	
2.3.1 The hypothesis .....	16
2.3.2 Expression for $f(w)$ .....	18
2.4 INFLUENCE OF PARAMETERS .....	19
2.5 DETERMINATION OF COMPACTION PARAMETERS .....	21
2.5.1 Direct method.....	21
2.5.2 Regression method.....	22
2.6 APPLICATION I – FITTING COMPACTION CURVES.....	23

2.7	APPLICATION II – PREDICTING A FAMILY OF COMPACTION CURVES	
	24	
2.7.1	Analyses of a family of compaction curves.....	24
2.7.2	Creating a family of compaction curves.....	26
2.7.3	Examples.....	27
2.8	CONCLUSIONS.....	28
2.9	REFERENCES.....	29
2.10	APPENDIX 2-A DERIVATION OF PROPOSED EQUATION 2-6 AND 2-7	
	33	
2.11	APPENDIX 2-B DETERMINATION OF PARAMETER “N” FROM S VERSUS <i>W</i> CURVE.....	36
2.12	APPENDIX 2-C DETERMINATION OF PARAMETER “P” FROM S VERSUS <i>W</i> CURVE.....	40
2.13	APPENDIX 2-D DERIVATION OF SUGGESTED EQUATION 2-9 ( <i>KP=CONST</i> ).....	42
<b>CHAPTER 3</b>	<b>SOIL COMPACTION PARAMETERS AND THEIR RELATIONSHIP WITH SOIL PHYSICAL PROPERTIES<sup>1</sup></b>	<b>67</b>
3.1	INTRODUCTION.....	67
3.2	COMPLETE COMPACTION CURVE FOR FINE-GRAINED SOILS.....	68
3.3	CHARACTERISTICS OF A COMPLETE COMPACTION CURVE.....	69
3.3.1	The Boundary Conditions.....	69
3.3.2	The Curve Shape.....	70
3.3.3	The Compactable Moisture Range.....	71
3.4	THE FORMULATION.....	71
3.5	DISCUSSION OF PARAMETERS IN PROPOSED EQUATION.....	73
3.5.1	Parameter $S_m$ .....	73
3.5.2	Parameter $w_m$ ( $\gamma_{dd}$ , or $k$ ).....	73
3.5.3	Parameter $n$ .....	74
3.5.4	Parameter $p$ .....	74
3.6	COMPACTION PARAMETERS IN DIFFERENT SOILS.....	75

3.7	CONCLUSIONS .....	77
3.8	REFERENCES .....	77
<b>CHAPTER 4</b>	<b>THE STRENGTH BEHAVIOR ALONG COMPLETE</b>	
	<b>COMPACTION CURVES<sup>1</sup> .....</b>	<b>86</b>
4.1	INTRODUCTION .....	86
4.2	REGIONS OF THE COMPLETE COMPACTION CURVE .....	88
4.3	MATERIALS AND TESTS .....	89
4.4	VARIATION OF UNCONFINED COMPRESSION STRENGTHS WITH COMPACTION CURVE .....	90
4.5	MEASUREMENT OF MATRIC SUCTION AND ANALYSIS .....	92
4.6	APPLICATIONS .....	94
4.7	CONCLUSIONS .....	95
4.8	REFERENCES .....	95
<b>CHAPTER 5</b>	<b>THE EVOLUTION OF PARTICLE SIZE DISTRIBUTION DUE</b>	
	<b>TO WEATHERING WITH UNIFORM FRAGMENTATION .....</b>	<b>104</b>
5.1	INTRODUCTION .....	104
5.2	WEATHERING EFFECT ON A SINGLE PARTICLE – UNIFORM FRAGMENTATION .....	105
5.3	GENERAL ANALYSIS METHOD ON EVOLUTION OF PARTICLE SIZE DISTRIBUTION .....	107
5.4	CALCULATING THE EVOLUTION OF PARTICLE SIZE DISTRIBUTION DUE TO WEATHERING WITH UNIFORM FRAGMENTATION .....	109
5.5	RELATIONSHIP BETWEEN PARALLEL PARTICLE SIZE DISTRIBUTIONS AND THE FAMILY OF COMPACTION CURVES .....	112
5.6	CONCLUSIONS .....	113
5.7	REFERENCES .....	114
<b>CHAPTER 6</b>	<b>ONE-DIMENSIONAL COMPRESSION BEHAVIOR OF LESS</b>	
	<b>COMPACTED FINE-GRAINED SOIL<sup>1</sup> .....</b>	<b>120</b>

6.1	INTRODUCTION.....	120
6.2	TESTING METHOD .....	121
6.3	COMPRESSION BEHAVIOR OF AS-DUMPED SOIL AND CLOD EFFECTS 122	
6.4	PNEUMATIC COMPACTION ON DUMPED FINE-GRAINED SOILS .....	124
6.5	ONE-DIMENSIONAL COMPRESSION OF LESS COMPACTED FINE- GRAINED SOILS .....	125
6.5.1	The influence of water content on the behavior of one-dimensional compression curves .....	126
6.5.2	The influence of compactive effort on the behavior of one-dimensional compression curve.....	128
6.6	WETTING-INDUCED COLLAPSE OF LESS COMPACTED FINE-GRAINED SOIL 131	
6.7	CONCLUSIONS .....	135
6.8	REFERENCES .....	136

**CHAPTER 7      MODELING      AND      PREDICTING      ONE-DIMENSIONAL  
COMPRESSION CURVES FOR COMPACTED SOILS..... 151**

7.1	INTRODUCTION.....	151
7.2	CHARACTERISTICS OF ONE-DIMENSIONAL COMPRESSION CURVE	152
7.3	REVIEW OF EQUATIONS FOR ONE-DIMENSIONAL COMPRESSION CURVE.....	154
7.4	PROPOSED EQUATION FOR ONE DIMENSIONAL COMPRESSION CURVE.....	158
7.5	INFLUENCES OF THE PARAMETERS .....	161
7.6	EXPERIMENTAL EVALUATION OF PROPOSED EQUATION .....	164
7.7	PREDICTION OF A FAMILY OF COMPRESSION CURVES .....	167
7.8	CONCLUSIONS AND RECOMMENDATIONS.....	168
7.9	REFERENCES .....	169

<b>CHAPTER 8</b>	<b>SETTLEMENT ESTIMATION FOR A THICK COMPACTED LAYER USING A FAMILY OF COMPRESSION CURVES.....</b>	<b>191</b>
8.1	INTRODUCTION.....	191
8.2	EQUATION FOR ONE-DIMENSIONAL COMPRESSION CURVE AND A FAMILY OF COMPRESSION CURVES.....	194
8.3	ESTIMATING SETTLEMENT OF THIN SUBLAYER USING PROPOSED COMPRESSION EQUATION.....	196
8.4	SETTLEMENT ESTIMATION FOR A THICK COMPACTED LAYER.....	199
8.5	METHODS AND EXAMPLES.....	201
8.6	DISCUSSION.....	204
8.7	CONCLUSIONS.....	206
8.8	REFERENCES.....	207
8.9	APPENDIX 8-A DERIVATION OF EQUATION 8-9.....	209
<b>CHAPTER 9</b>	<b>SUMMARY AND CONCLUSIONS, AND RECOMMENDATION FOR FUTURE WORK.....</b>	<b>217</b>
9.1	SUMMARY.....	217
9.2	CONCLUSIONS.....	220
9.3	RECOMMENDATIONS FOR FUTURE WORK.....	222
<b>APPENDIX</b>	<b>INSTRUMENT PHOTOS AND MATRIC SUCTION MEASUREMENT RESULTS.....</b>	<b>224</b>

## LIST OF TABLES

Table 2-1	Properties of tested Syncrude overburden soils.....	45
Table 2-2	Parameters regressed from Equation 2-7 in Figures 2-14 and 2-15 .....	46
Table 2-3	Predicting parameters of lacustrine clay during kneading compaction tests in Fig. 2-20 .....	47
Table 3-1	Physical properties of tested Syncrude overburden soils .....	79
Table 3-2	Results from standard compaction test and compaction parameters.....	80
Table 4-1	Properties of tested Syncrude overburden soils.....	98
Table 7-1	Regression results for normal consolidated clay, Drammen, Norway .....	174
Table 7-2	Regression results for overconsolidated clay, San Francisco Bay Mud.....	175
Table 7-3	Regression results for overconsolidated clay, Chicago silty clay .....	176
Table 7-4	Special normal consolidated clay, Mexico City clay .....	176
Table 7-5	Compacted lacustrine clay of Syncrude overburden ( $P_1$ at $w= 15\%$ ) .....	177
Table 7-6	Leda clay.....	178
Table 7-7	Louiseville clay (Tavenas 1981) .....	178
Table 7-8	Prediction of compression curve ( $P_1$ -17%) with known compactive pressure .....	179
Table 7-9	Prediction of compression curve ( $P_1$ -17%) with compactive pressure unknown (using Equation 7-15).....	179
Table 8-1	Parameters for $P_1$ at $w= 17\%$ under compaction of 98 kPa foot pressure and 25 applications .....	210



## LIST OF FIGURES

Figure 2-1 Characteristics of a typical complete compaction curve for fine-grained soils .....	48
Figure 2-2 Transformed complete degree of saturation versus moisture content curve.	48
Figure 2-3 Equations 2-6 and 2-7 and their represented compaction curves.....	49
Figure 2-4 Effect of parameter $S_m$ on $S$ versus $w$ curves ( $w_m=31\%$ , $n=9$ , and $p=12\%$ )	50
Figure 2-5 Effect of parameter $S_m$ on compaction curves ( $w_m=31\%$ , $n=9$ , and $p=12\%$ ) .....	50
Figure 2-6 Effect of parameter $w_m$ (or $\gamma_{dd}$ ) on $S$ versus $w$ curves ( $S_m=93\%$ , $n=9$ and $p=12\%$ ) .....	51
Figure 2-7 Effect of parameter $w_m$ (or $\gamma_{dd}$ ) on compaction curves ( $S_m=93\%$ , $n=9$ and $p=12\%$ ) .....	51
Figure 2-8 Effect of parameter $n$ on $S$ versus $w$ curves ( $S_m=93\%$ , $w_m=31\%$ , $p=12\%$ )	52
Figure 2-9 Effect of parameter $n$ on compaction curves ( $S_m=93\%$ , $w_m=31\%$ , $p=12\%$ )	52
Figure 2-10 Effect of parameter $p$ on $S$ versus $w$ curves ( $S_m=93\%$ , $w_m=31\%$ , and $n=9$ ) .....	53
Figure 2-11 Effect of parameter $p$ on compaction curves ( $S_m=93\%$ , $w_m=31\%$ , and $n=9$ ) .....	53
Figure 2-12 Determination of parameter $n$ .....	54
Figure 2-13 Determination of parameter $p$ .....	55
Figure 2-14 Standard compaction tests on Syncrude overburden soils and their fitting curves .....	56
Figure 2-15 Curve fitting on kneading test by Seed et al. (1960).....	57
Figure 2-16 A family of complete kneading compaction curves with different number of tamps on lacustrine clay (Li and Segó 1998).....	58
Figure 2-17 Faure FK series with energy E1 (0.6 MJ/m <sup>3</sup> ) and E2 (2.4 MJ/m <sup>3</sup> ) (redrawn from Faure and Da Mata, 1994).....	59
Figure 2-18 Effect of foot pressure in kneading compaction test for as-air-dried lacustrine clay.....	60

Figure 2-19	Effect of numbers of applications of 700 kPa foot pressure in kneading compaction test for as-air-dried lacustrine clay .....	60
Figure 2-20	A family of complete compaction curves of glacial lacustrine clay for different compactive efforts (revised from Li and Segoo 2000).....	61
Figure 2-21	Curve A in x-y coordinates and $S$ - $w$ coordinate systems (Equation 2-A1 and 2-A3 in Appendix 2-A) .....	62
Figure 2-22	Curve A' (revised curve A) (Equation 2-A5 in Appendix 2-A) .....	63
Figure 2-23	Determination of parameter “ $n$ ” from $S$ versus $w$ curve (Appendix 2-B)..	64
Figure 2-24	Determination of parameter “ $p$ ” from $S$ versus $w$ curve (Appendix 2-C)..	65
Figure 2-25	Derivation of suggested Equation 2-9 in paper (Appendix 2-D) .....	66
Figure 3-1	Sketch of complete compaction curve ( $\gamma_d - w$ ) .....	81
Figure 3-2	Characteristics of degree of saturation versus water content .....	81
Figure 3-3	Parameters $n$ , $p$ , $S_m$ , and $w_m$ on the complete compaction .....	82
Figure 3-4	Particle size distribution of Syncrude overburden soils .....	82
Figure 3-5	Standard compaction test results of Syncrude overburden soils .....	83
Figure 3-6	Relationship between soil dry density at dry condition ( $\gamma_{dd}$ ) and average particle size ( $D_{50}$ ) .....	84
Figure 3-7	Relationship between $w_m$ and average particle size ( $D_{50}$ ) .....	84
Figure 3-8	Relationship between shape factor ( $n$ ) and soil uniformity coefficient ( $C_u=D_{60}/D_{10}$ ).....	85
Figure 3-9	Relationship between index of compactable moisture range ( $p$ ) and $w_m - w_p$	85
Figure 4-1	Complete compaction curve for fine-grained soils .....	99
Figure 4-2	A schematic of general arrangement for measurement of matric suction...	100
Figure 4-3	Complete compaction curve and unconfined compression strength (UCS) for Pleistocene lacustrine clay ( $P_l$ ).....	101
Figure 4-4	Complete compaction curve and unconfined compression strength (UCS) for glacial till ( $P_g$ ) .....	101
Figure 4-5	Stress - strain curve in unconfined compression test for Pleistocene lacustrine clay ( $P_l$ ) .....	102
Figure 4-6	Stress - strain curve in unconfined compression test for glacial till ( $P_g$ ) ....	102

Figure 4-7 Relationship between matric suction and mixed water content for Pleistocene lacustrine clay ( $P_l$ ) and glacial till ( $P_g$ ).....	103
Figure 5-1 The concept model of uniform fragmentation .....	116
Figure 5-2 Evolution of particle size distributions from an original log-linear distribution curve .....	117
Figure 5-3 Evolution of particle size distributions from an original power-law distribution curve .....	117
Figure 5-4 Decreasing of grain size during drying-wetting cycles (revised from Yamaguchi et al. 1988) .....	118
Figure 5-5 The particle size distribution of alluvial deposits in Anderson Exploration Ltd., Alberta, Canada (Sego and Li 1999) .....	118
Figure 5-6 The compaction curves based on experimental data covering 1,383 Ohio soils (revised from Woods 1938) .....	119
Figure 6-1 Schematic clod aggregates during soil mixing with water.....	139
Figure 6-2 Compression curves of as-dumped soils prepared at different water content .....	140
Figure 6-3 Void ratio progress of as-dumped soil prepared at different water contents .....	140
Figure 6-4 Progress of dry density as-dumped soil during one-dimensional compression test .....	141
Figure 6-5 Increase of dry density after various applications of compaction test (98 kPa) .....	141
Figure 6-6 Compression curves of soils with 98 kPa of compaction prepared at different initial water contents .....	142
Figure 6-7 Compression curves of compacted soil prepared with water content at dry zone (dry of CST).....	142
Figure 6-8 Compression curves of compacted soil prepared with water content at transition zone (between CST and OWC).....	143
Figure 6-9 Compression curves of compacted soil prepared with water content at wet zone (wet of OWC) .....	143

Figure 6-10	Void ratio progress of 98 kPa compacted soil during one-dimensional compression test .....	144
Figure 6-11	Dry density progress of 98 kPa compacted soil during one-dimensional compression test .....	144
Figure 6-12	Comparison of void ratio for compacted and as-dumped samples at some compression pressures.....	145
Figure 6-13	Compression curves of various samples prepared with water content at 1% (where Pl- Pleistocene lacustrine clay; 1%- water content; 98 kPa- compaction pressure; N25- number of compaction applications; fld0- flooding sample at beginning) .....	146
Figure 6-14	Compression curves of various samples prepared with water content at 10% (sample identification as Fig. 6-13) .....	146
Figure 6-15	Compression curves of various samples prepared with water content at 15% (sample identification as Fig. 6-13) .....	147
Figure 6-16	Compression curves of various samples prepared with water content at 17% (sample identification as Fig. 6-13) .....	147
Figure 6-17	Compression curves of samples prepared with water content at 21% (sample identification as Fig. 6-13) .....	148
Figure 6-18	Compression curves of samples prepared with water content at 46% (sample identification as Fig. 6-13) .....	148
Figure 6-19	Compression curves of air-dried samples with different loading-wetting sequences.....	149
Figure 6-20	The compression curves for samples with various initial water contents and flooded at beginning (sample identification as Fig. 6-13) .....	149
Figure 6-21	Collapse potential versus as-prepared water content under different compression pressure .....	150
Figure 7-1	Characteristics of a typical compression curve.....	180
Figure 7-2	The fitting curves by Hardin (1989) and Liu and Znidarcic (1991) on field samples of overconsolidated Drammen Clay (data from Butterfield 1979) ..	180
Figure 7-3	The curves from two original functions and the combined proposed Equation 7-8 .....	181

Figure 7-4	The curve of solid ratio versus logarithm compression stress .....	181
Figure 7-5	The effects of parameter $e$ (initial void ratio) on the compression curve (Eq. 7-9).....	182
Figure 7-6	The effects of parameter $p$ (pre-compression stress) on the compression curve (Eq. 7-9) .....	182
Figure 7-7	The effects of parameter $M$ on the compression curve ( $N = 0.8$ ) (Eq. 7-9)	183
Figure 7-8	The effects of parameter $N$ on the compression curve ( $M = 0.8$ ) (Eq. 7-9)	183
Figure 7-9	The effects of $N/M$ on the compression curve when $MN$ is a constant (Eq. 7-9 and Eq. 7-13).....	184
Figure 7-10	The compression curve with consideration of elastic recompression effects (Eq. 7-14 and Eq. 7-9).....	184
Figure 7-11	Fitting normal consolidated Drammen clay by equations from simplified Hardin (1989), Liu & Znidarcic (1991), and proposed Equation 7-9 (Berre and Iversen 1972).....	185
Figure 7-12	Fitting over consolidated San Francisco Bay Mud by equations from proposed Equation 7-9 with or without $M = 1$ , simplified Hardin (1989), and Liu-Znidarcic (Holtz and Kovacs 1981) .....	185
Figure 7-13	Fitting over consolidated Chicago silty clay (Taylor 1948) by proposed Equation 7-9.....	186
Figure 7-14	Fitting structured Mexico City clay by proposed Equation 7-9 (Mesri et al. 1975) .....	186
Figure 7-15	Regression of one-dimensional compression curve for $P_1$ at $w = 15\%$ after compaction .....	187
Figure 7-16	The regression of consolidation curve of Canadian marine clay - Leda clay (Quigley and Thompson 1966) .....	188
Figure 7-17	The curve of solid ratio ( $1/e$ ) versus stress of Canadian marine clay -Leda clay (Quigley and Thompson 1966).....	188
Figure 7-18	The consolidation curve of two Eastern Canadian marine clays (Tavenas et al. 1981).....	189
Figure 7-19	The curve of solid ratio ( $1/e$ ) versus stress of two Eastern Canadian marine clay (Tavenas et al. 1981) .....	189

Figure 7-20 The prediction of compression curves for $P_1$ -17% with known previous compactive pressure .....	190
Figure 7-21 The prediction of compression curves for $P_1$ -17% without knowing the previous compactive pressure .....	190
Figure 8-1 The cross-section of a thick-layer and multi-sublayer system .....	211
Figure 8-2 The one-dimension compression curve and fitting for compacted Pleistocene Lacustrine clay prepared at 17% water content using a foot pressure of 98 kPa .....	211
Figure 8-3 The calculated settlement and vertical strain ( $\varepsilon = \Delta s/H_0$ ) for thin compacted layer of Pleistocene Lacustrine Clay using Equation 8-10 .....	212
Figure 8-4 Void ratio profile $e_0(z)$ and dry density profile $\gamma_d(z)$ over the thick layer..	213
Figure 8-5 Stress distribution over the thick layer.....	214
Figure 8-6 Influence of the total number of divided sublayers on the results of calculated settlement .....	215
Figure 8-7 The settlement estimation for thick compacted layer (10 m) under different surcharge loading using Equation 8-12.....	215
Figure 8-8 The vertical strain at each sublayer and its accumulated settlement under surcharge of 700 kPa.....	216
Figure 0-1 Kneading compaction machine (photo) .....	225
Figure 0-2 Thermo-conductivity sensor and mold for suction measurement (photo) ..	226
Figure 0-3 Apparatus that combines pneumatic compaction test and one-dimensional compression test (photo) .....	227
Figure 0-4 The suction measurement of glacial till ( $P_g$ ): sample suc-P2g-3%-c1 .....	228
Figure 0-5 The suction measurement of glacial till ( $P_g$ ): sample suc-P2g-7%-c2 .....	228
Figure 0-6 The suction measurement of glacial till ( $P_g$ ): sample suc-P2g-9%-c3 .....	229
Figure 0-7 The suction measurement of glacial till ( $P_g$ ): sample suc-P2g-12%-c4 .....	229
Figure 0-8 The suction measurement of lacustrine clay ( $P_l$ ): sample suc-P2l-11%-a1	230
Figure 0-9 The suction measurement of lacustrine clay ( $P_l$ ): sample suc-P2l-14%-a2	230
Figure 0-10 The suction measurement of lacustrine clay ( $P_l$ ): sample suc-P2l-18%-a3 .....	231

Figure 0-11 The suction measurement of lacustrine clay ( $P_1$ ): sample suc-P21-24%-a4

..... 231

## LIST OF SYMBOLS

### Compaction theory and strength (Chapter 2 to 5)

$G_s$	specific gravity of soil particles
$k$	slope of approach line in $S$ versus $w$ curve
$n$	shape factor of compaction curve
$p$	compactable moisture range of compaction curve (%)
$S$	degree of saturation (%)
$S_m$	maximum degree of saturation (%)
$w$	water content (%)
$w_m$	water content at wet side of compaction curve when dry density is equal to $\gamma_{dd}$
$\gamma_d$	dry density ( $\text{Mg/m}^3$ )
$\gamma_{dd}$	constant dry density at dry side of a complete compaction curve ( $\text{Mg/m}^3$ )
$\gamma_w$	density of water ( $\text{Mg/m}^3$ )
$\psi$	matric suction (kPa)

### Deformation behavior (Chapter 6 to 8)

$A$	a constant from ultimate compression curve
$C_k$	recompression index (1/kPa)
$e$	void ratio
$e_f$	final void ratio
$e_i$	initial void ratio
$e_k$	void ratio when applied stress is unity
$e_0$	void ratio when applied stress is zero
$H_i$	initial thickness of a thin layer (or sublayer) (m)
$H_o$	initial thickness of a layer (m)
$S_c$	total settlement of a layer (m)
$M$	parameter in proposed compression equation



$N$	parameter in proposed compression equation
$p$	compression history parameter in proposed compression equation (kPa)
$\Delta e$	void ratio change
$\Delta s$	settlement of a sublayer (m)
$\sigma$	normal stress (kPa)
$\sigma'$	effective normal stress (kPa)
$\sigma_f$	final stress after construction (kPa)

## CHAPTER 1 INTRODUCTION

Of the number of methods used to improve soil at a site, compaction is usually the least expensive and the most widely used. It is a procedure employed frequently to densify soils to enhance its strength and reduce its compressibility and hydraulic conductivity. It is virtually the universal method used for placement of engineered fills. Since Proctor introduced the compaction concept in 1933, compacted soils have been used extensively in dams, embankments, and for the substructure of road pavements. Compacted clays are also often used in landfills and other waste containment facilities as barriers to water and contaminant movement.

As early as 1938, Woods et al. presented a typical family of compaction curves by classifying and averaging data on 1383 Ohio soils. The average curves are all rather similar in shape (Woods et al. 1938). Analyzing these compaction test results from a particular geographic area or geological formation, it was observed that the compaction curves have characteristic shapes that can be represented by a family of typical curves (Joslin 1959). The family of curves exists because the variation of soil particle size in the same region follows similar geologic evolution. The curve moves up and to the left on the dry density versus water content plot when the soil particle size is coarser. This type of family of curves is referred as Type A in this thesis.

For the same soil, when compacting by using different compactive energy or effort, many laboratory and field tests show similar shape to the compaction curves (Lambe 1958; Turnbull and Foster 1958; Seed et al. 1960; Lee and Haley 1968). The curve moves up and to the left when the applied compactive effort increases. This creates another family of compaction curves, which is identified as Type B. In embankment construction, different compaction equipment is generally used that vary in weight and number of passes used to apply different field compaction effort. It is also true, when different thickness of placement lifts are compacted, the compactive effort differs within the lift itself (Turnbull and Foster 1958; Parson 1992). Therefore, knowing the family of

compaction curves is useful for the designer to assist in selecting the layer thickness or compaction efforts that should be used in the field on a given project.

The need to use the Type B family of compaction curves has increased recently. Overburden excavation by the mining industry such as oil sands mining in Northern Alberta results in a large volume of material for disposal. The use of increasing larger trucks to haul, dump, and compact these waste materials results in the use of thick placement layers in the waste dumps (Morgenstern et al. 1988; Cameron et al. 1995). The applied compaction effort varies within these thick lifts. This results in the need for a family of compaction curves within each placement layer. Knowledge of the family of compaction curves makes it possible to predict a compaction curve from a single laboratory compaction test and to determine the dry density profile over the thick layer, which is useful in later settlement estimation.

The family of compaction curves has been used in practice as the one-point method for many years and is recommended by AASHTO (1990). However, there is no method used to predict a family of compaction curves for a given soil. In fact, prior to the prediction, other works need to be done in terms of the characteristics of the complete compaction curve for fine-grained soils, and the determination of the curve shape, location and boundaries. The origin of the family of curves is also of interest.

The deformation behavior for a given compacted soil varies with its compactive efforts. This increases the complexity for the settlement estimation particularly within a thick layer. Since the same soil is compacted, it is possible to have a series of compression curves with a similar characteristic. This new concept is based on the test results that, no matter what initial void ratio, structure or previous stress history, the void ratio at high pressure for a given soil is unique. The variation of the curves suggests the same features as observed for samples with different degree of disturbance (Rutledge 1944; Bozozuk 1971; Lacerda et al. 1977; Holtz and Kovacs 1981; Kabbaj et al. 1985; Wang and Wei 1996). The knowledge on the family of compression curves could be used to simplify the procedures for the settlement estimation of engineered fills.

The objective of this study is to investigate soil compaction theory for fine-grained soils, especially the fundamental aspects related to the family of compaction curves, and its influence on engineering behaviors. Materials obtained from overburden soils at Syncrude Canada Ltd., Fort McMurray, Alberta are used in the study. The test program was designed and carried out to study the compaction, compression, and matric suction behavior of the soils. The objective of the thesis was achieved by introducing and applying two versatile equations that describe and predict a family of compaction curves and compression curves for a given soil.

## **1.1 OUTLINE OF THESIS**

This thesis is presented in paper format. Each chapter is a modified version of a paper or two, published or submitted for publication. The chapters in general are divided into two parts. The first part, from Chapters 2 to 5, is related to the compaction theory of compacted soils. It discusses the characteristics of the complete compaction curve for fine-grained soils, its formulation and prediction, determination of compaction parameters, the strength profile along complete compaction curve, and the origin of the family of compaction curves. The second part, from Chapters 6 to 8, studies one-dimensional compression behavior of compacted soils, its formulation and prediction, and presents a method for estimating settlement for a thick compacted layer.

The contents are as follows. The second chapter discusses the characteristics of complete compaction curves for fine-grained soils. Based on the testing results during the research and the observation from Faure and Da Mata (1994), a comprehensive description of a rational equation to describe the complete compaction curve of a fine-grained soil from the dry to wet condition is proposed. It is the first pure non-curve-fitting equation to represent the compaction curve since Proctor introduced the compaction method in 1933. The equation is versatile in its ability to quantify the shape, size and boundary conditions of compaction curves. Each of its four parameters is physically related to the soil composition or compaction method, and imparts specific influences on the predicted

compaction curve. All parameters can be obtained directly from a single compaction curve carried out on a soil. The relationship shows good agreement with measured compaction test results. By using the shape factor, the equation can successfully predict a family of compaction curves when the applied compactive effort is varied.

Based on the theoretical advances in the second chapter, an effort to study the soil compaction parameters and their relationship with soil physical properties is followed in the third chapter. Standard compaction test results from four different soils are used to estimate the relationship between the parameters and physical properties of the soil. It is found that the shape factor, which is very useful because it remains unchanged when soil is compacted using different compaction energy, is related to the soil uniformity coefficient. The dry density of soil for the very dry condition increases with average particle size in a certain compaction tests. The index of compactable range is a function of the soil plasticity and average particle size.

The fourth chapter studies how the unconfined compressive strength and deformation modulus vary along the complete compaction curves. The variation of the unconfined compression strength with water content and location along this complete compaction curve is presented. It is concluded that the maximum compressive strength and stiffness modulus occurs between the compaction sensitivity threshold (CST) and the optimum water content (OWC). This behavior is useful for design and construction control of highway subgrades and embankments. In addition, matric suction measurements during the laboratory testing indicate that the suction measured at the CST equals the applied compactive pressure. This will assist in establishing the CST and therefore the water content with the maximum compressive strength.

A further effort is made in the fifth chapter to explain the origin of the family of compaction curves, which is frequently found in regions with residual soils. The evolution of the particle size distribution due to weathering is analyzed using the concept of the uniform fragmentation. A general analytical method is described to calculate the evolution of the particle size distribution. The particle size distribution curves after

weathering remain parallel to each other with a gradual decrease in average particle size of the weathered soil. The results are compared with test results in the literature and explain the existence of the family of compaction curves of residual soils, which is the fundamental of the one-point compaction method that is commonly used in the region of residual soils.

The testing program of one-dimensional compression of less compacted fine-grained soil is presented in the sixth chapter. A special testing procedure that combined the compaction and compression tests in one apparatus was designed. The one-dimensional compression curves with different water content, compaction pressure, and flooding procedures are presented. The initial water content of the soil is important during soil deposition and influenced the long-term performance of the deposited soil. Compaction can substantially decrease the placement void ratio and thus improve the subsequent compression behavior of the compacted soil. When the sample is prepared dry of the optimum water content (OWC), the compaction pressure has a similar effect on the compression curve as the preconsolidation pressure on the consolidation behavior of a given soil. When the sample is prepared wet of OWC, compaction is less effective in its influence on the compressibility. There is little influence from compaction effects when the applied compression pressure is greater than the compactive effort.

The collapse of a compacted soil is independent of loading-wetting sequence. The collapse potential decreases when either the initial water content increases or the compression pressure increases. It is also shown that the wetting collapse is less affected by compaction if the sample is prepared wet of OWC or if the wetting takes place at a higher applied vertical stress than the applied compaction foot pressure. Therefore, choosing an appropriate compaction pressure that covers the subsequent loading level is very important for controlling the future wetting collapse of waste soil dumps.

A four-parameter equation is proposed to aid in prediction of a family of compression curves in the seventh chapter. The equation is continuous over the complete stress range and is able to describe the sharp curvature associated with the yield point. It is evaluated

for its ability to fit real behavior using various soil compression or consolidation curves. The equation is based on the fact that, for different initial void ratio, structure and stress history, the void ratio at high stress for a given soil is unique. Therefore it can be used to describe and predict a family of compression curves for use in settlement estimation of thick compacted non-uniform layer. The parameters in the equation are well defined and are related to the initial void ratio, previous compactive pressure and physical properties of the soil. The settlement of a thin layer can be then calculated directly using the equation.

The settlement estimation for a thick compacted layer is more complicated and can result in large errors if one uses the simplified straight line with slope of the compression index to estimate the settlement. An analysis method is described in the eighth chapter based on the proposed compression equation and the concept of a family of compression curves. The thick layer is first divided into multi-sublayers and the settlement is calculated separated. The final settlement of the thick compacted layer is integrated from the settlement of multi-sublayers. The method only requires a single one-dimensional compression curve and the dry density profile of the thick layer.

Conclusions and recommendation for further studies are presented in the ninth chapter. The last section of the thesis includes processed test data in the course of this study.

## **1.2 REFERENCES**

- AASHTO (American Association of State Highway and Transportation Officials). 1990. T 272-86, Family of curves – one point method. Standard specifications for transportation materials and methods of sampling and testing, 15<sup>th</sup> Ed. Part 2. AASHTO, Washington, pp. 820-823.
- Bozozuk, M. 1971. Effect of sampling, size, and storage on test results for marine clay. Sampling of Soil and Rock, ASTM STP 483, American Society for Testing and Materials: 121-131.

- Cameron, R., Ashton, C., Fong, V., and Strueby, B. 1995. Syncrude's highway berm: Part 1 of 5 – Project overview and design philosophy. *In Proceedings of 48<sup>th</sup> Canadian Geotechnical Conference*, Vol. 2, 789-797.
- Faure, A.G. and Da Mata, J.D.V. 1994. Penetration resistance value along compaction curves. *ASCE Journal of Geotechnical Engineering*, **120**(1): 46-59.
- Holtz, R.D. and Kovacs, W.D. 1981. **An Introduction to Geotechnical Engineering**, Prentice-Hall, New Jersey, p291-293, p327.
- Kabbaj, M., Oka, F., Leroueil, S., and Tavenas, F. 1985. Consolidation of natural clays and laboratory testing. *Symposium on Consolidation Behavior of Soils*, Fort Lauderdale, *ASTM STP 892*: 378-403.
- Lambe, T.W. 1958. The engineering behavior of compacted clay. *ASCE Journal of Soil Mechanics and Foundation Division*, **84**(SM2): 1655-1 to -35.
- Lacerda W.A., Costa Filho, L.M., Coutinho, R.Q., Duarte, A.E.R. 1977. Consolidation characteristics of Rio de Janeiro soft clay. *In Proceeding of International Symposium on Soft Clay*, Bangkok, Thailand: 231-235.
- Joslin, J.G. 1959. Ohio's Typical Moisture-density curves. *Symposium on application of soil testing in highway design and construction*, *ASTM Special Technical Publications 239*, pp. 111-118.
- Lee, K.L. and Haley, S.C. 1968. Strength of compacted clay at high pressure. *ASCE Journal of Soil Mechanics and Foundation Division*, **94**(SM1): 1303-1332.
- Morgenstern, N.R., Fair, A.E., and McRoberts, E.C. 1988. Geotechnical engineering beyond soil mechanics – a case study. *Canadian Geotechnical Journal*, **25**: 637-661.
- Parsons, A.W. 1992. *Compaction of Soils and Granular Materials: A review of Research Performed at the Transport Research Laboratory*, London: H.M.S.O.
- Proctor, R.R. 1933. The design and construction of rolled earth dams. *Engineering News Record III*, August 31, Sept. 7, 21, and 28.
- Rutledge, G.P. 1944. Relation of undisturbed sampling to laboratory testing. *Transactions of American Society of Civil Engineers*, **109**: 1155-1183.
- Seed, H.B., Mitchell, J.K. and Chan, C.K. 1960. The strength of compacted cohesive soils. *Research Conference on Shear Strength of Cohesive Soils*, ASCE, pp. 877-964.



- Turnbull, W.J. and Foster, C.R. 1957. Compaction of graded crushed stones base course. *In Proceedings of 4th International Conference on Soil Mechanics and Foundation Engineering*, **2**: 181-185.
- Wang, N. and Wei, R. 1996. Evaluation of sample quality of soft clay. *In Proceeding of 2nd International Conference on Soft Soil Engineering*, Nanjing, 120-125.
- Woods, K.B. et al. 1938. Compaction of earth embankments. *In Proceeding of Highway Research Board*, Washington, **18(2)**: 155.

# **CHAPTER 2 EQUATION FOR COMPACTION CURVE OF FINE-GRAINED SOILS: ITS ORIGIN, IMPLEMENTATION AND APPLICATION<sup>1</sup>**

## **2.1 INTRODUCTION**

Of the number of methods used to improve soils at a site, compaction is usually the least expensive and the most widely used. It is a procedure employed frequently to densify in-situ soils, thus enhancing their strength and reducing compressibility and hydraulic conductivity. It is virtually the universal method used during the placement of engineered fills. Compacted soils are used extensively in dams, embankments, and the substructure of roads. Compacted clays are also often used in landfills and other waste containment facilities as barriers to water and contaminant movement.

Much research on compaction has been carried out since the first paper by Proctor in 1933. Most laboratory and field tests focused on the physical properties of the soil near or at the maximum dry density, such as hydraulic conductivity, compressibility, and strength. Tremendous contributions to our understanding of compacted soils have been made by various individuals (e.g. Woods 1938; Leonards 1955; Hilf 1956 and 1959; Turnbull 1957 and 1958; Lambe 1958a and 1958b; Seed 1959 and 1960), and organizations (e.g. Waterways Experiment Station 1949; Bureau of Reclamation 1963; U.S. Navy 1962 and 1982).

---

<sup>1</sup> This chapter has been submitted for publication. Li, H. and Segoo, D.C. 2000. Canadian Geotechnical Journal. Some information presented in this chapter is also contained in Li, H. and Segoo, D. C. 2000. Constructing and Controlling Compaction of Earth Fills, ASTM STP 1384, Shanklin, D.W., Rademacher, K.R., and Talbot, J.R. (Eds.), American Society for Testing and Materials, West Conshohocken, PA. pp. 113-125.

When a fine-grained soil is densified under a constant compactive effort but with varying moisture contents, a typical dry density versus water content relationship develops. The shape of the compaction curve is related strongly to the particle size distribution of the soil and compaction method utilized. Compaction curves of fine-grained soils are essential to establish practical and reliable criteria for effective control of field compaction on most projects.

As early as 1938, Woods et al. presented a typical family of compaction curves by classifying and averaging data from 1383 tests on Ohio soils. The average curves are all rather similar in shape (Woods et al. 1938). From an analysis of these compaction test results from a particular geographic area or geologic formation, it was observed that the compaction curves have characteristic shapes that can be represented by a family of typical curves (Joslin 1959). The family of curves exists because the variation of soil particle size in the same region follows a similar geologic evolution. The curve moves up and to the left when the soil particle size becomes coarser. This type of family of curves is referred as **Type A** in this paper.

Knowledge of the family of compaction curves makes it possible to predict a compaction curve from a single laboratory compaction test and thus determine the maximum dry density and optimum water content. This concept, the one-point method, has been used in practice for many years and is a recommended method by AASHTO (1990). It will also be included in ASTM Manual: Testing Compaction of Earth Fills Using ASTM Standards (Shanklin 1999). The family of curves from Ohio was created to identify 26 typical standard Proctor curves and the corresponding maximum dry density and optimum moisture content are then obtained directly from a table (Joslin 1959).

For the same soil, when compacted by using different compactive energies or efforts, many laboratory and field tests show the compaction curves to have a similar shape (Lambe 1958; Turnbull and Foster 1958; Seed et al. 1960; Lee and Haley 1968). The curves move up and to the left when the applied compactive effort increases. This creates

another family of compaction curves, which is identified as **Type B**. In embankment construction in general, the equipment varies in weight and number of passes used to apply different field compaction energy. It is also true, when different thickness of lifts are compacted, in which the compactive effort differs within the lift itself (Turnbull and Foster 1958; Parson 1992). Therefore, knowledge of the Type B family of compaction curves is useful in assisting the designer to select the layer thickness or compaction energy that should be used in the field on a given project.

The need to understand and predict the Type B family of compaction curves has increased recently. Overburden excavation by the mining industry, such as oil sands mining in Northern Alberta, results in a large volume of material for disposal. The use of increasingly larger trucks to haul, dump and compact these waste materials results in the use of thick placement layers in the waste dumps. The applied compaction energy varies within each thick lift and this results in the need for a family of compaction curves within each placement layer. The family of compaction curves therefore becomes an important input in understanding the compaction achieved within the layer and then analyzing the future deformation behavior of the thick-layered waste dumps (Chapter 7 and 8).

Although the apparent bell-shaped curve is widely recognized, knowledge for describing the compaction curve is not well developed. Little research was found that focused on understanding what controls the location and the shape of the compaction curve.

Polynomial equations have been used to represent the compaction curves in the past. Usually a second, third or fourth-order polynomial equation was used in studies reported by Hilf (1990), Bradet (1997), and Howell (1997). Pandian et al. (1997) presented two separate equations to represent separate portions of the compaction curves that intersect to form a cusp at the optimum compaction point. Although using polynomial equations is expeditious, their application is restricted because they are only curve fitting equations. There are no parameters that physically represent the soil in the predicted compaction curve and that control its shape, size and location. It is common for the values of the fitting parameters to change by up to three-orders of magnitude or even from positive to

negative values (Howell et al. 1997). Therefore it is difficult to establish an appropriate value for use in practice. Another disadvantage is that the equations work well only over a limited moisture content range for a specific test or soil. The predicted dry density may also become negative or the relationship predicts that the compaction curve exceeds the zero air void curve (ZAVC) which is not physically possible.

From this introduction, one concludes that there is a need for a relationship that describes the compaction curve. The control of field compaction, the application of the one-point compaction method, the deformation estimation within a thick compacted layer, and the need to represent a compaction curve adequately makes it necessary and useful to have a powerful relationship to characterize the shape, size and position of a compaction curve for fine-grained soils. To define a curve mathematically, knowledge over a wider moisture range than is typically tested is necessary. The emergence and presentation of the complete compaction curve for fine-grained soils has addressed this need (Faure 1981; Faure and Da Mata 1994; Li and Sego 1998).

The objective of this chapter is to study and mathematically formulate the compaction curve. The application of the equation, especially related to the prediction of a family of compaction curves, is also studied.

## **2.2 THE COMPLETE COMPACTION CURVE FOR FINE-GRAINED SOIL**

The complete compaction curve for a soil differs from the traditionally presented compaction curve with respect to the range of moisture content tested. It starts from the completely dry condition and ends well wet of the optimum water content. The use of the dry and wet conditions allows rational boundary conditions of the complete compaction curve to be defined.

A number of compaction tests over a wide range of water content for fine-grained soils have been presented by Faure (1981) and Faure and Da Mata (1994). Their results show a nearly constant dry density on the dry side before the water content reaches an

important point called the **compaction sensitivity threshold (CST)** (Fig. 2-1). Faure and Da Mata (1994) presented compaction curves with this feature for thirty-four materials prepared by mixing clay with either fine or coarse sand and for thirty-six natural soils from locations in France and four from Brazil. Other evidence includes heavy clay (Johnson and Sallberg 1960), tills and lacustrine material in New Brunswick (Saini and Chow 1984), clay liner of landfills (Daniel 1990; Benson 1997), lacustrine clay from northern Alberta (Li and Seg0 1998). It was shown that the water content at CST is a linear function of clay content and was linked to the clay mineralogy and the compactive effort (Faure and Da Mata 1994). How the CST relates to the soil behavior is still not fully understood at present.

With the addition of water to the soil, the density increases due to the lubrication of water that improves the workability (Holtz and Kovacs 1981), and also due to the decrease of matric suction (Delage and Graham 1996; Li 1996). This behavior prevails until a point where further addition of water does not contribute to more lubrication or suction decrease, but, on the contrary, would cause displacement of the heavier soil by the lighter water, thus resulting in a decrease in the dry density achieved. This point is the optimum compaction point (point A in Fig. 2-1), which represents the maximum dry density (MDD) and the optimum water content (OWC). Soil compacted at or near OWC is of most interest in engineering embankment design. A sample slightly wet of OWC generally achieves the lowest hydraulic conductivity, while the sample slightly dry of OWC represents a higher strength than that compacted at OWC (Seed and Chan 1959; Mitchell 1976).

### **2.2.1 Identifiable regions of the compaction curve**

With the existence of the points CST and A, the complete compaction curve can be separated into three identifiable regions (Fig. 2-1): namely, the dry region, the transition region (effective compaction region), and the wet region (wet of optimum region).

The dry region indicates the dominance of the air phase surrounding the soil particles. The air is continuous and the small portions of water are discontinuous. The sparse isolated water is not effective in lubricating the soil particles thus it has little or no influence on the soil compaction behavior. The water becomes effective in lubricating the soil particles in the transition region when it is believed the water becomes partially continuous. The addition of water in this region helps to increase the packing of the soil particles. Therefore, the transition region is also called the effective compaction region. Beyond the OWC, the water phase dominates and only small air bubbles are trapped within the water. The trapped air phase is discontinuous and has little effect on the soil macro behavior. The wet region is limited by  $w_m$  where the dry density decreases to the same value as the constant dry density found on the dry side of the compaction curve. Practically, compacting a soil beyond  $w_m$  is difficult and has little engineering use.

### **2.2.2 Boundaries of compaction curve**

Figure 2-1 also illustrates the boundary conditions of a typical complete compaction curve. When the soil is in the very dry condition, the dry density of fine-grained soil is nearly constant ( $\gamma_{dd}$ ). The fact that the dry density remains constant ( $\gamma_{dd}$ ) is an important characteristic for fine-grained soils. Unfortunately, this important boundary condition has been neglected over the years. It is also the lower limit of density on the dry side of the complete compaction curve.

The soil compacted on the wet side is generally not completely saturated because a portion of the air trapped during compaction cannot escape. For a fine-grained soil, it is often found that the maximum degree of saturation ( $S_m$ ) remains constant (Seed et al. 1960; Lee and Haley 1968). In practice, one can find  $S_m$  from the wet side of a given compaction curve which runs nearly parallel to the zero air void curve (ZAVC) (Woods 1938; Hausmann 1990). Thus  $S_m$  is an important referenced value on the wet side of the compaction curve. The maximum degree of saturation ( $S_m$ ) is not related to the compactive effort, as the application of additional energy is absorbed by the water and

thus does not increase the saturation on the wet side during compaction (Seed et al. 1960). The degree of saturation around the OWC has been recognized as an important factor in the control of wetting collapse of soils (hydro-compression-induced settlement) following the review of over 900 laboratory tests in California by McMahon and Kropp (2000).

### **2.2.3 Shape of compaction curve**

The typical shape for fine-grained soils is one of the most apparent characteristics of a compaction curve. The shape is related to the soil's physical properties and the compaction method used (Woods 1938; Hausmann 1990). Generally speaking, a flat curve denotes a poorly graded soil and a curve with a pronounced peak denotes a well-graded soil. The difficulty is how to quantify the special bell-shape of the compaction curve. If the shape of a curve can be quantified, a family of compaction curves could be described and predicted for future use by engineers.

The consistent shape is the key to creating a family of compaction curves. It can be used to predict the compaction curve for a given soil since it remains unchanged while using the same compaction method but employing different compactive energies. Unfortunately, this important characteristic cannot be utilized at present since no equation is available to quantify the generalized shape of the family of compaction curves. It is indeed puzzling that the compaction curve has not had an applicable mathematical expression developed to describe its shape, size and location since Proctor first presented the concept of soil compaction in 1933, some 67 years ago.

### **2.2.4 Size (Compactable moisture range) of compaction curve**

A traditional compaction curve shows a typical bell-shape, however, the bell-shaped curve has limits. In fact, the increasing dry density part of the curve only covers a limited moisture range, as illustrated in Figure 2-1 in the transition region. Beyond the optimum



water content, the decreasing dry density part of the curve is the wet region of the compaction curve. The width of the two zones is indicated as the compactable moisture range of the compaction curve.

## 2.3 DERIVATION OF THE COMPACTION CURVE FOR FINE-GRAINED SOIL

### 2.3.1 The hypothesis

The complete compaction curve has two important boundary conditions that are critical for mathematically defining a curve, namely  $\gamma_{dd}$  and  $S_m$  in Fig. 2-1. The complex shape of the compaction curve makes defining the mathematical relationship challenging. Therefore, a transformation to simplify the shape of the curve by using the degree of saturation instead of dry density is introduced. Equation 2-1 is used to relate the dry density to the degree of saturation.

$$[2-1] \quad S = \frac{w}{\frac{\gamma_w}{\gamma_d} - \frac{1}{G_s}}$$

where  $S$  is the degree of saturation of the soil,  $w$  is the water content,  $\gamma_w$  is the density of water,  $\gamma_d$  is the dry density of the soil and  $G_s$  is the specific gravity of the soil particles.

For convenience, the dry density versus water content curve will be called the  $\gamma_d$  versus  $w$  curve or the compaction curve. The degree of saturation and water content curve will be called  $S$  versus  $w$  curve.

In a fine-grained soil, when the soil is very dry, the density changes little with increasing water content (Fig. 2-1), therefore, the degree of saturation increases linearly with increasing water content in the  $S$  versus  $w$  curve (Fig. 2-2). The approach line exists as

shown in Fig. 2-2. As the water content approaches CST, the degree of saturation departs from the linear relationship and increases rapidly with small increases in water content. From CST to the optimum compaction point at A, the degree of saturation increases rapidly then slows beyond point A until it approaches a constant saturation called the maximum saturation ( $S_m$ ). In practice, one can find  $S_m$  from the wet branch of the conventional compaction curve that runs parallel to the zero air void curve (ZAVC) (Hausmann 1990). For all fine-grained soils, the value of  $S_m$  varies over a limited range.

The slope of the approach line ( $k$ ) is controlled by the constant dry density ( $\gamma_{dd}$ ) of an air-dried sample according to Equation 2-2:

$$[2-2] \quad k = \frac{1}{\frac{\gamma_w}{\gamma_{dd}} - \frac{1}{G_s}}$$

It is usually difficult to compact a sample at a water content well above the optimum water content as the compaction stress is greater than soil shear strength. It is therefore assumed that the maximum degree of saturation ( $S_m$ ) is reached at point M ( $w = w_m$ ) where the compaction curve intersects the constant dry density ( $\gamma_{dd}$ ) (Fig. 1). This assumption does not result in large errors since the degree of saturation is nearly constant on the wet side of the OWC.

$w_m$  can be calculated as:

$$[2-3] \quad w_m = \frac{S_m}{k} = S_m \cdot \left( \frac{\gamma_w}{\gamma_{dd}} - \frac{1}{G_s} \right)$$

where  $S_m$  is the maximum degree of saturation,  $w_m$  is the water content when  $S_m$  is achieved (Fig. 2-2).

The governing equation that defines the shape of the  $S$  versus  $w$  curve and thus the compaction curve is based on the relationship between the degree of saturation ( $S$ ) and the water content ( $w$ ), i.e.:

$$[2-4] \quad S = f(w)$$

Therefore the relationship for the dry density versus water content curve ( $\gamma_d$  versus  $w$ ) can be written as

$$[2-5] \quad \gamma_d = \frac{G_s \gamma_w}{1 + \frac{w G_s}{f(w)}}$$

### 2.3.2 Expression for $f(w)$

A detailed derivation of the mathematical expression for  $f(w)$  is presented in Appendix 2-A. The equation for the  $S$  versus  $w$  curve is written as:

$$[2-6] \quad f(w) = S = S_m - \frac{S_m}{w_m} \cdot \frac{(w_m - w)^{n+1}}{[(w_m - w)^n + p^n]} \quad w < w_m$$

Four parameters are included,  $S_m$  and  $w_m$  have been physically defined previously and are easily obtained at point M as shown in Figure 2-1 or 2-2. Parameters  $n$  and  $p$  are the curve-fitting parameters and each has a specific influence on the compaction curve. The detailed influence of all four parameters on the compaction curve will be discussed in following sections.

Equation 2-6 represents curve A in Figure 2-3. Although the equation represents the traditional compaction curve very well, the degree of saturation for the completely dry condition is non-zero as predicted by Equation 2-6. This causes large dry densities

according to Equation 2-5 at very low moisture contents (Figure 2-3). This can be resolved by using the following revised relationship:

$$[2-7] \quad f(w) = S = S_m - S_m \times \left( \frac{w_m - w}{w_m} \right)^{n+1} \times \left( \frac{w_m^n + p^n}{(w_m - w)^n + p^n} \right) \quad w < w_m$$

Substitute Equation 2-7 into Equation 2-5 describes curve B presented in Fig. 2-3 which does not have the same problem as curve A at low moisture contents.

## 2.4 INFLUENCE OF PARAMETERS

Four parameters ( $S_m$ ,  $w_m$ ,  $n$ , and  $p$ ) are required to use Equation 2-7 effectively. By using Equations 2-7 and 2-5, the  $S$  versus  $w$  curve and compaction curve can be calculated. The influence of each parameter on the compaction curve and the  $S$  versus  $w$  curve is discussed by changing one parameter while keeping the others constant.

$S_m$  is the maximum degree of saturation of a soil compacted wet of the optimum moisture content. It is the parameter that controls the wet side boundary of the compaction curve. Fig. 2-4 and 2-5 show the influence of  $S_m$  on both the  $S$  versus  $w$  curve and the compaction curve. Figure 2-5 indicates that the whole compaction curve shifts vertically when  $S_m$  increases. As discussed previously,  $S_m$  usually remains constant for different compactive efforts for a given fine-grained soil.

Parameter  $w_m$  is obtained by extending a horizontal line of the constant dry density ( $\gamma_{dd}$ ) to cross the compaction curve on the wet side (Fig. 2-1). The parameter  $w_m$  can also be calculated from  $\gamma_{dd}$  using Equation 2-3. A decrease of  $w_m$  indicates a steeper slope ( $k$ ) to the  $S$  versus  $w$  approach line (Fig. 2-6). A decrease of  $w_m$  is a result of an increase in  $\gamma_{dd}$ , that is a higher density on the dry side of the optimum moisture content but little change on the wet side (Fig. 2-7). It should be noted that the dry density increases as a higher compactive effort is used. The parameter  $w_m$  reflects the dry boundary condition of a

compactive curve. Since the water content has little influence on the value of  $\gamma_{dd}$ , the compactive energy is the external factor that controls  $\gamma_{dd}$  other than the basic soil properties. Therefore,  $\gamma_{dd}$  physically represents the energy absorbed by a dry compacted soil and can be used as an index for the compactive energy applied during a given compaction test.

Figure 2-8 and 2-9 shows the influence of parameter  $n$  on the shape of the compaction curve. When  $n$  increases, the belled portion of the compaction curve becomes narrower and achieves a higher optimum dry density (Fig. 2-9). Thus  $n$  controls the bell-shape of the compaction curve. Compaction curves with a characteristic bell-shape thus can be quantified by using a constant value of  $n$ . The parameter  $n$  will be called the shape factor because of its important influence on the bell shape of the compaction curves.

As previously observed the shape of a compaction curve depends on both the soil fabric and compaction method used. For soils from a particular geological region, a family of compaction curves with similar shape was found by Woods (1938). When using the same compaction method with additional energy to compact a soil, the compaction curves have a similar characteristic shape but are shifted up and to the left (Seed 1960; Hausmann 1990). Therefore, parameter  $n$  can be assumed constant for a particular soil when the compaction energy varies, or for soils from the same geological region when using the same compaction method. For the soils used in this study,  $n$  varies from 4 to 12.

Figure 2-10 and 2-11 shows that parameter  $p$  affects the width of the bell-shaped compaction curve. The compactable moisture range ( $w_m - w_{cst}$ ) was presented in the previous section. The range increases when  $p$  increases. The parameter  $p$  allows the equation to define the size of this range without changing its shape factor ( $n$ ) and/or boundary conditions (defined by  $S_m$  and  $w_m$  (or  $\gamma_{dd}$ )). Therefore  $p$  is the index of the compactable moisture range. The width of the compactable moisture range is a little greater than parameter  $p$ .

The parameter  $p$  is proportional to the difference between  $w_m$  and the water content at CST ( $w_{CST}$ ). Both  $w_m$  and  $w_{CST}$  are related to the compaction energy (or  $\gamma_{dd}$ ) and soil properties. The value of  $w_{CST}$  has been shown to be proportional to the clay content of the soil (Faure 1981; Faure and Da Mata 1994).

## 2.5 DETERMINATION OF COMPACTION PARAMETERS

Among the four parameters, two ( $S_m$ ,  $w_m$ ) are obtained directly from the complete compaction curve. Simple procedures to determine  $n$  and  $p$  directly from a complete compaction curve are also developed. These procedures will aid in selecting the input parameters for use with Equation 2-7.

### 2.5.1 Direct method

Parameter  $S_m$  is equal to the maximum saturation achieved on the wet side of the compaction curve that parallels the ZAVC. Parameter  $w_m$  can be obtained by extending the horizontal line of  $\gamma_{dd}$  to meet the compaction curve on the wet side (Fig. 2-1). It can also be calculated directly from  $\gamma_{dd}$  and  $S_m$  by using Equation 2-3.

Li and Segoo (2000) have developed simple procedures to obtain the parameters  $n$  and  $p$  directly from the  $S$  versus  $w$  curve. The detailed description and proof of these procedures are included in Appendices 2-B and 2-C. Figure 2-12 illustrates the method to establish the value of  $n$  by using the optimum compaction point (point A). By locating point B on the horizontal axis,  $n$  is the value obtained by dividing  $BM'$  by  $OA'$ . The procedure to determine parameter  $p$  is shown in Figure 2-13. It requires selecting point C ( $0, S_m/2$ ) on the vertical axis. This point is connected to M to obtain D on the  $S$  versus  $w$  curve. The difference in water content between  $M'$  and  $D'$  is equal to  $p$ .

There is a great advantage in avoiding the use of non-linear regression of the compaction data to ensure that the equation can easily be used in everyday engineering practice. The

direct method is simple and easy to use, but its application relies on knowing the constant dry density  $\gamma_{dd}$ . Its accuracy will be affected if there is no previous test result at water content dry of the CST. For most traditional compaction curves,  $\gamma_{dd}$  can be assumed based on the lowest dry density on the dry side of the compaction curve if information on air-dried soil is unavailable.

### **2.5.2 Regression method**

The regression method is a pure curve-fitting procedure that provides a best fit to test results. The best curve-fitting parameters can be obtained where the sum of the squares of deviations (SS) is least. It can be used to describe both the traditional and complete compaction curves. The concept of the regression method is widely used in engineering practice. For a non-linear equation, a computer program may need to be prepared using the same concept. Most statistical software packages have the option of defining any equations and they are easy to use. For example, when using the software SPSS for Windows, which is popular and used in first or second year statistics courses in universities, one can choose the option of non-linear regression from statistics then input the suggested equation and the parameters with name and starting value. The program allows the user to select an estimation method from sequential quadratic programming or Levenberg-Marquardt. The computer generally obtains the results in less than one minute if appropriate starting values are chosen.

Draper (1966) indicated that one of the major difficulties in using non-linear regression is choosing the starting values for a particular parameter. The suggested Equation 2-7 has special advantages when one chooses an appropriate starting value since all of the values can be first determined or estimated based on the direct method. Both  $S_m$  and  $w_m$  are easily determined. Parameter  $p$  relates to the width of the upper domed part of compaction curve and the compactable moisture range is about 1.2 to 1.5 times  $p$ . It can also be obtained by the procedure shown in Figure 2-13. Parameter  $n$  is a shape factor, which is related to the ratio of dome height to its width. It varies over the range of 4 to

12 for natural soils based on experience. Therefore a choice of 7 or 8 as a start value for the regression analysis would generally lead to rapid convergence.

The regression analyses allow fine-tuning of the parameters used in Equation 2-7 to predict different families of compaction curves.

## 2.6 APPLICATION I – FITTING COMPACTION CURVES

Four different natural soils, glacial till ( $P_g$ ), Pleistocene lacustrine clay ( $P_l$ ), Cretaceous clay shale ( $K_{ca}$ ), and lean oil sands ( $K_{cw}$ ) were used to carry out laboratory compaction tests. The soils were all acquired from overburden soils on the lease of Syncrude Canada Ltd., Fort McMurray, in northeastern Alberta. Their basic physical properties are shown in Table 2-1. The large variation in these properties provides an opportunity for evaluating how well Equation 2-7 can be used to fit the compaction curves.

All soils were oven dried and standard (Proctor) compaction tests following ASTM D698-91 were conducted. Table 2-2 summarizes the four parameters ( $S_m$ ,  $w_m$ ,  $n$ ,  $p$ ) as estimated from these compaction tests. Figure 2-14 shows the fitted curves compared to the laboratory test data. It can be observed that the curves fit the test results quite well. The original test data for  $K_{ca}$  is scattered but the fitted curve is a reasonable fit to the laboratory data.

Data from a family of compaction curves presented by Seed et al. (1960) was also utilized to test the usefulness of Equation 2-7. The soil was an inorganic silty clay of low plasticity from Vicksburg, Mississippi, with a liquid limit of 38% and a plastic limit of 24%. The soil was compacted using the kneading method with three different foot pressures being applied. As shown in Figure 2-15, the maximum degree of saturation along the wet leg of the curves was the same in the three tests. The shapes of all three curves are similar, therefore, the  $n$  parameter of all curves was assumed the same so the value obtained for curve A1 was used as the initial value to predict the other two curves.



Curve A2 and A3 were fitted by only changing  $w_m$  and  $p$  as indicated in Table 2-2. All the fitted curves show good agreement with the laboratory test data in Fig. 2-15.

## **2.7 APPLICATION II – PREDICTING A FAMILY OF COMPACTION CURVES**

### **2.7.1 Analyses of a family of compaction curves**

As discussed in the opening section, there exist two different families of compaction curves. Type A curves describes compaction of various soils from a borrow area when the same compaction method is employed for each geologically similar soil. Type B curves are created by compacting the same soil by applying different levels of compaction energy. The family of compaction curves is regarded as a family because each curve has a similar shape, therefore the same shape factor  $n$  can be used to predict the curves. In terms of the complete compaction curves, currently only the Type B family of curves are typically available, therefore the following discussion focuses on the behavior of this family of curves.

Kneading compaction tests over a wide moisture range were carried out using the Pleistocene Lacustrine clay (P<sub>i</sub>) (Li and Segó 1998). The soil was obtained from overburden soils at Syncrude Canada Ltd. The compaction test was conducted using a CS 1000 Electronic-Hydraulic Kneading Compactor which is described in ASTM Standard Practice for Preparation of Bituminous Mixture Test Specimens by Means of California Kneading Compactor (D 1561-92). Figure 2-16 displays a family of curves obtained using 12, 25 and 50 applications of a foot pressure of 700 kPa to the soil. A nearly constant degree of saturation at CST ( $S_{CST} = 44\%$ ) was observed from the data.

The results from Faure and Da Mata (1994) on their FK<sub>i</sub> series (fine sand and kaolinite mixtures) showed that the degree of saturation at the point of CST remained nearly constant at two different compaction energies E1 and E2 (Fig. 2-17). For example, the

degrees of saturation at CST for the sample K0 (100% kaolinite) is around 72% at the different levels of energy. For FK73 (73% kaolinite and 27% fine sand) and FK31 (31% kaolinite and 69% fine sand), the degree of saturation value at CST is 60% and 36% respectively.

The physical explanation of this observation is as follows. CST is a point where compaction begins to influence the dry density of a soil and where the water added becomes effective in contributing to changes in soil density. As the degree of saturation represents the percent water in the total volume of voids,  $S_{CST}$  represents the critical value when the volume of water is sufficient to lubricate the soil particles and allow them to move to denser packing. This value appears not to be affected by the magnitude of the externally applied compaction energy. Therefore,  $S_{CST}$  is considered a constant for the Type B family of compaction curves for a particular soil type. This assumption is a convenient starting point for predicting the compaction curve at different levels of compactive effort. This concept also is consistent with the general observation that the compaction curves move up and to the left when the applied compactive effort increases while maintaining its characteristic shape.

As the smooth transition around CST is usually observed, it is necessary to have a standard technique to determine a reasonable location for CST. A suggested method is illustrated in Figure 2-2. Drawing a tangent line through the inflection point on the  $S$  versus  $w$  curve, the line meets the approach line at a point where the degree of saturation equals the saturation at the CST ( $S_{CST}$ ). This approach provides a standard method for locating the CST point for a given compaction curve.  $S_{CST}$  can be calculated from Equation 2-8 as follows (see Appendix D for details of its derivation):

$$[2-8] \quad S_{CST} = S_m - \frac{S_m}{w_m} \cdot P \cdot \left( \frac{n+1}{n-1} \right)^{\frac{n+1}{n}}$$

As discussed, both  $S_{CST}$  and the soil shape factor  $n$  are constants for a given soil when subjected to a given compaction method. For fine-grained soils, a constant maximum

degree of saturation ( $S_m$ ) was observed in Type B curves (e.g. Seed 1960). Therefore the relationship of Equation 2-8 becomes surprising simple.

$$[2-9] \quad \frac{S_m}{w_m} \cdot p = k \cdot p = \text{const}$$

### 2.7.2 Creating a family of compaction curves

Given Equation 2-9, one only requires a single compaction test to create a whole family of compaction curves for the same soil subjected to different compactive efforts. Alternatively, a relationship between the applied compaction energy and dry density is required. By using different foot pressures and different number of applications of the foot in a kneading compaction test, a relationship between compactive effort and dry density was found for an air-dried soil. Figure 2-18 presents the dry density versus foot pressure, while Fig. 2-19 shows the dry density increases with number of applications under a constant foot pressure of 700 kPa.

For comparison, a logarithmic linear relation between compaction effort and maximum dry density was observed (Hausemann 1990; Parsons 1992). The reasons for using  $\gamma_{dd}$  instead of the maximum dry density ( $\gamma_{max}$ ) are: for fine-grained soil, the dry density before CST is insensitive to its water content; the sample is easy to prepare; the optimum dry density can only be obtained by carrying out many individual tests to define the compaction curve.

The procedure to create a family of compaction curves for a particular soil is:

- Obtain all four parameters from a complete compaction curve by the direct method or regression method as previously described.
- For a fine-grained soil, assume the shape factor ( $n$ ) and maximum degree of saturation ( $S_m$ ) remains constant for all levels of applied compactive effort.

- Carry out a compaction test on an air-dried sample to measure  $\gamma_{dd}$  at a given compactive energy, or use the relationship between compactive energy and  $\gamma_{dd}$  which may be available for your soil. Use Equation 2-3 to calculate  $w_m$ .
- From Equation 2-9 establish the index of compactable moisture range ( $p$ ) at the new level of compaction energy.
- Using Equation 2-5 and 2-7 calculate the compaction curves for the different levels of applied compaction energy using the established parameters.

### 2.7.3 Examples

Figure 2-20 shows a family of compaction curves for Pleistocene Lacustrine clay (P<sub>l</sub>) using the kneading compaction method. It is an expansion of the laboratory tests results presented in Figure 2-16. At first, the samples were prepared using three layers of soil under a foot pressure of 700 kPa with 50 applications per layer. The parameters of the curve were obtained by the regression method using Equation 2-7, where  $S_m$  is 88.8%,  $w_m$  is 27.2%,  $n$  is 11.38 and  $p$  is equal to 11.3%. The complete compaction curve is shown as B1 in Fig. 2-20. By using the values of  $\gamma_{dd}$  for 25 and 12 applications, which are 1.44 and 1.41 Mg/m<sup>3</sup> respectively, other parameters were obtained and are summarized in Table 2-3. Two complete compaction curves (B2 and B3) were calculated and are compared to the measured data. Results of additional laboratory compaction tests carried out at different water contents shows good agreement between the data and the predicted family of curves.

The parameters were then used to create other curves at different levels of compactive effort using the relationships from Fig. 2-18 and 2-19. The family of curves for kneading compaction tests covers foot pressure from 40 to 70,000 kPa under 25 applications and applications from 3 to 100 times using a constant pressure of 700 kPa. Due to the limitation of the kneading compaction machine applying low pressure, a separate pneumatic pressure system was used to apply footing pressures of 98 kPa. The pressure was controlled and manually applied for 1 to 2 seconds each stroke. The pneumatic

compaction test is a little different from the kneading compaction test because it has 100% coverage of the sample surface during each application and causes no kneading effect. The compaction results at 98 kPa show a similarly shaped compaction curve (Fig. 2-20). But without the kneading effect, the 98 kPa compactive effort in the pneumatic compaction test can only achieve the same level of dry density as the 80 kPa applied pressure using the kneading compaction method.

## 2.8 CONCLUSIONS

A promising mathematical approach for describing the compaction curve for fine-grained soils, based on the relationship between the degree of saturation and water content, is proposed. The equation uses four parameters that are dimensionless and can be used to describe an individual or a family of compaction curves. The four parameters clearly define the boundary conditions, shape and compactable moisture range of the compaction curve. Parameters  $S_m$  and  $w_m$  ( $\gamma_{dd}$ ) can be obtained from plots, and parameters  $n$  and  $p$  can be obtained graphically or using regression analysis. The equation can easily be used to predict a family of compaction curves by experimentally obtaining  $\gamma_{dd}$  for compactive effort. The examples show the equation adequately represents the traditional as well as the complete compaction curves for fine-grained soils. The curves predicted by the proposed equation showed excellent agreement with laboratory test results.

The relationship between the compaction parameters and various basic soil properties has been investigated (Li and Segoo 1999). It is recommended that a parameter database using various soils needs to be created in the future and the predicted compaction curve and family of compaction curves using this database would benefit practical engineering design of earthen embankment.

---

<sup>1</sup> SPSS for Windows is a proprietary product of SPSS Inc. Headquarters, 233 S. Wacker Drive, 11th floor, Chicago, Illinois 60606.

## 2.9 REFERENCES

- American Association of State Highway and Transportation Officials. 1990. T 272-86, Family of curves – one point method. Standard specifications for transportation materials and methods of sampling and testing, 15<sup>th</sup> Ed. Part 2. AASHTO, Washington, pp. 820-823.
- Benson, C.H., Gunter, J.A., Boutwell, G.P., Trautwein, S.J. and Berzanskis, P.H. 1997. Comparison of four methods to assess hydraulic conductivity. *ASCE Journal of Geotechnical and Geoenvironmental Engineering*, **123**(10): 929-937.
- Bradet, J-P. 1997. **Experimental Soil Mechanics**, Prentice Hall, pp. 161-162.
- Bureau of Reclamation. 1963. **Earth Manual**, U.S. Bureau of Reclamation, Denver, Colorado, First Edition, U.S. Government Printing Office, Washington, D.C.
- Daniel, D.E. and Benson, C.H. 1990. Water content-density criteria for compacted soil liners. *ASCE Journal of Geotechnical Engineering*, **116**(12): 1811-1830.
- Delage, P. and Graham, J. 1996. Mechanical behaviour of unsaturated soils: Understanding the behaviour of unsaturated soils requires reliable conceptual models. *Unsaturated Soils*, Alonso, E.E. and Delage, P. (Eds), Balkema, Rotterdam, pp. 1223-1256.
- Draper, N.R. and Smith, H. 1966. **Applied Regression Analysis**, John Wiley & Sons, pp. 263-301.
- Faure, A.G. 1981. A new conception of the plastic and liquid limits of clays. *Soil and Tillage Research*, **1**: 97-105.
- Faure, A.G. and Da Mata, J.D.V. 1994. Penetration resistance value along compaction curves. *ASCE Journal of Geotechnical Engineering*, **20**: 46-59.
- Hausmann, M.R. 1990. **Engineering Principles of Ground Modification**, McGraw-Hill Inc., New York, pp. 14-56.
- Hilf, J.W. 1956. An investigation of pore-water pressure in compacted cohesive soils, Technical Memorandum 654, U.S. Department of the Interior, Bureau of Reclamation, Denver, Colorado.

- Hilf, J.W. 1959. A rapid method of construction control for embankments of cohesive soil, Engineering Monograph No. 26, Bureau of Reclamation, pp.7 and 23.
- Hilf, J.W. 1990. Compacted fill. **Foundation Engineering Handbook**, Fang, H.-Y (Ed), pp. 249-316.
- Holtz, R.D. and Kovacs, W.D. 1981. **An Introduction to Geotechnical Engineering**, Prentice Hall, Englewood Cliffs, New Jersey.
- Howell, J.L., Shackelford, C.D., Amer, N.H., and Stern, R.T. 1997. Compaction of sand-processed clay soil mixtures. *Geotechnical Testing Journal*, **20**: 443-458.
- Johnson, A.W. and Sallberg, J.R. 1960. Factors that influence field compaction of soils. Highway Research Board Bulletin 272, Highway Research Board, National Research Council, Washington, D.C.
- Joslin, J.G. 1959. Ohio's Typical Moisture-density curves. Symposium on application of soil testing in highway design and construction, ASTM Special Technical Publications 239, pp. 111-118.
- Krebs, R.D. and Walker, R.D. 1971. **Highway Materials**, McGraw-Hill, pp. 215-217.
- Lambe, T.W. 1958a. The structure of compacted clay. *ASCE Journal of Soil Mechanics and Foundation Division*, **84**(SM2): 1654-1 to -34.
- Lambe, T.W. 1958b. The engineering behavior of compacted clay. *ASCE Journal of Soil Mechanics and Foundation Division*, **84**(SM2): 1655-1 to -35.
- Lee, K.L. and Haley, S.C. 1968. Strength of compacted clay at high pressure. *ASCE Journal of Soil Mechanics and Foundation Division*, **94**(SM1): 1303-1332.
- Leonards, G.A. 1955. Strength characteristics of compacted clays, *Transactions of American Society of Civil Engineers*, Vol. 120: 1420-1479.
- Li, H. and Sego, D.C. 1998. Prediction complete compaction curves of fine-grained soil. *In Proceedings of the 51st Canadian Geotechnical Conference*, Edmonton, Alberta, Canada, October 4-7, 1998. Vol. 2: 679-686.
- Li, H. and Sego, D.C. 1999. Soil Compaction Parameters and its Relationship with Soil Physical Properties. *In Proceedings of the 52nd Canadian Geotechnical Conference*, Regina, Saskatchewan, Canada, October 24-27, 1999. pp. 517-524.
- Li, H. and Sego, D. C. 2000. Equation for complete compaction curve of fine-grained soils and its applications. *Constructing and Controlling Compaction of Earth Fills*,

- ASTM STP 1384, Shanklin, D.W., Rademacher, K.R., and Talbot, J.R. (Eds.), American Society for Testing and Materials, West Conshohocken, PA. pp. 113-125.
- Li, Z.M. 1996. Compressibility and collapsibility of compacted unsaturated loessial soils. *Unsaturated Soils*, Alonso, E.E. and Delage, P. (Eds), Balkema, Rotterdam, pp. 139-144.
- McMahon, D.J. and Kropp, A.L. 2000. Proposed compaction specifications to minimize hydrocompression-induced settlements in fills supporting residential structures. *Constructing and Controlling Compaction of Earth Fills*, ASTM STP 1384, D. W. Shanklin, K. R. Rademacher, and J. R. Talbot (Eds.), American Society for Testing and Materials, West Conshohocken, PA. pp. 209-228.
- McRae, J.L. 1959. Index of compaction characteristics. *ASTM Special Technical Publications* **23**, pp. 119-123.
- Mitchell, J.K. 1976. **Fundamentals of Soil Behavior**, John Wiley & Sons, Inc., New York, N.Y., 422p.
- Pandian, N.S., Nagaraj, T.S. and Manoj, M. 1997. Re-examination of compaction characteristics of fine-grained soils. *Geotechnique*, **47**(2): 363-366.
- Parsons, A.W. 1992. *Compaction of Soils and Granular Materials: A review of Research Performed at the Transport Research Laboratory*, London: H.M.S.O.
- Proctor, R.R. 1933. The design and construction of rolled earth dams. *Engineering News Record* III, August 31, Sept. 7, 21, and 28.
- Saini, G.R. and Chow, T.L. 1984. Compactibility indices of some agricultural soils of New Brunswick, Canada. *Soil Science*, **137**: 33-38.
- Seed, H.B. and Chan, C.K. 1959. Structure and strength characteristics of compacted clays. *ASCE Journal of Soil Mechanics and Foundation Division*, **85**(SM5), pp. 87-128.
- Seed, H.B., Mitchell, J.K. and Chan, C.K. 1960. The strength of compacted cohesive soils. *Research Conference on Shear Strength of Cohesive Soils*, Boulder, Colorado, pp. 877-964.
- Shanklin, D.W. 1999. The family of curves and one point compaction test method for determining moisture-density values (draft). *ASTM Manual: Testing Compaction of*



- Earth Fills Using ASTM Standards. Talbot, J.R., Shanklin, D.W., Farrar, J.A., and Rademacher, K.R. (Eds), ASTM, West Conshohocken, PA.
- Turnbull, W.J. and Foster, C.R. 1957. Compaction of graded crushed stones base course. *In Proceedings of 4<sup>th</sup> International Conference on Soil Mechanics and Foundation Engineering*, **2**: 181-185.
- Turnbull, W.J. and Foster, C.R. 1958. Stabilization of materials by compaction. *Transactions of the American Society of Civil Engineers*, **123**: 1-15.
- U.S. Navy. 1962. Soil Mechanics, Foundations, and Earth Structures, NAVFAC Design Manual DM-7, Washington, D.C.
- U.S. Navy. 1982. Foundations, and Earth Structures, NAVFAC Design Manual DM-7-2, Washington, D.C.
- Waterways Experiment Station. 1949. Soil compaction investigation: Compaction studies on silty clay, Report No. 2, Technical Memorandum No. 3-271, U.S. Corps of Engineers, Vicksburg, Mississippi.
- Woods, K.B. et al. 1938. Compaction of earth embankments. *In Proceeding of Highway Research Board*, Washington, **18**(2): 155.

## 2.10 APPENDIX 2-A DERIVATION OF PROPOSED EQUATION 2-6 AND 2-7

The derivation starts from a relatively simple mathematical curve in an x-y coordinate system. Curve A in Figure 2-21 can be expressed as:

$$[2-A1] \quad y = \frac{kx^{n+1}}{x^n + p^n}$$

Here  $k$ ,  $p$  and  $n$  are positive real parameters which are to be determined. The approach line of curve A exists with the following form:

$$[2-A2] \quad y = kx$$

The lower part of curve A is considered to model the curve of degree of saturation versus water content.

It is necessary to shift the curve to a new origin "O" by replacing  $x$  and  $y$  by  $w_m - w$  and  $S_m - S$  respectively, which is applicable to the S versus w coordinate system. The new equation of curve A will be

$$[2-A3] \quad S = f(w) = S_m - \frac{k(w_m - w)^{n+1}}{(w_m - w)^n + p^n} \quad w < w_m$$

Equation 2-A3 is the same as Equation 2-6 in the paper by replacing  $k$  with  $\frac{S_m}{w_m}$ .

Equation 2-A3 is only applicable for  $w$  less than  $w_m$ .

Curve A will not pass through the origin "O" but will instead go through point "S<sub>0</sub>". Point S<sub>0</sub> is close to point "O" because  $w_m$  is much larger than  $p$  in a given compaction

test. The upper part of curve A can be replaced with a constant maximum degree of saturation ( $S_m$ ) by introducing a factor  $\delta$ .

$$[2-A4] \quad \delta = \frac{1}{2} \left[ 1 + \frac{\text{abs}(w_m - w)}{(w_m - w)} \right]$$

Thus, Equation 2-A3 can be rewritten as Equation 2-A5 with the restriction of  $w < w_m$  no longer being required.

$$[2-A5] \quad S = f(w) = S_m - \frac{k \cdot [\text{abs}(w_m - w)]^{n+1}}{[\text{abs}(w_m - w)]^n + p^n} \times \delta$$

Equation 2-A5 represents curve A' in Figure 2-22.

Because the curve defined in Equation 2-A3 or 2-A5 does not pass through the origin "O", it may cause errors to the compaction curve for very dry conditions. To solve this problem, the following steps are used.

Step 1:

From Equation 2-A3, when  $w=0$ ,

$$S_0 = S_m - \frac{k w_m^{n+1}}{w_m^n + p^n}$$

Step 2:

Equation 2-A4 minus  $S_0$  to move curve A to pass through point "O".

$$S' = S_m - \frac{k(w_m - w)^{n+1}}{(w_m - w)^n + p^n} - S_m + \frac{k w_m^{n+1}}{w_m^n + p^n}$$

$$= \frac{k w_m^{n+1}}{w_m^n + p^n} - \frac{k(w_m - w)^{n+1}}{(w_m - w)^n + p^n}$$

When  $w=0$ ,  $S'=0$ . It means the curve  $S'$  passes through the origin "O". But when  $w=w_m$ ,

$$S' = \frac{k w_m^{n+1}}{w_m^n + p^n} \neq S_m$$

Step 3:

To let curve pass through point M,  $S'$  is multiplied by a factor as following

$$[2-A6] \quad S = S' \times \frac{S_m}{\frac{k w_m^{n+1}}{w_m^n + p^n}} = S_m - S_m \times \left(\frac{w_m - w}{w_m}\right)^{n+1} \times \frac{w_m^n + p^n}{(w_m - w)^n + p^n} \quad w < w_m$$

Equation 2-A6 is Equation 2-7 in the paper.

## 2.11 APPENDIX 2-B DETERMINATION OF PARAMETER “*n*” FROM *S* VERSUS *w* CURVE

### Method

Procedure: As shown in Figure 2-23, from origin O, draw a tangent line on a *S-w* curve to find point A (point with maximum dry density), or use the optimum water content ( $w_{opt}$ ) obtained from the compaction curve to determine A. Extend a line through MA to cross the X-axis at point B. The difference in water content between points M and B equals to  $nw_{opt}$ . Thus,

$$n = \frac{nw_{opt}}{w_{opt}} = \frac{BM'}{OA'}$$

### Proof

For a soil in three phases,

$$[2-B1] \quad \gamma_d = \frac{\gamma_w}{\frac{1}{G_s} + \frac{w}{S}}$$

To get the maximum dry density in Equation 2-B1, the value of  $\frac{w}{S}$  is required to be the minimum, or  $\frac{S}{w}$  to be the maximum. Since the water content at the optimum compaction point is called the optimum water content,  $w$  and  $S$  can be represented by  $w_{opt}$  and  $S_{opt}$ . To obtain the maximum value of  $S/w$  we can differentiate Equation 2-B1 equal to zero, which gives:

$$\frac{d\left(\frac{S}{w}\right)}{dw} = \frac{\frac{dS}{dw} \cdot w - S}{w^2} = 0$$

Therefore, at the location of optimum water content ( $w = w_{opt}$ )

$$[2-B2] \quad \frac{dS}{dw} = \frac{S}{w}$$

According to the proposed Equation 2-6,

$$[2-B3] \quad S = S_m - \frac{S_m}{w_m} \cdot \frac{(w_m - w)^{n+1}}{(w_m - w)^n + p^n}$$

Differentiating Equation 2-B3,

$$[2-B4] \quad \frac{dS}{dw} = \frac{S_m}{w_m} \cdot \frac{(w_m - w)^n}{\left[(w_m - w)^n + p^n\right]^2} \cdot \left[(w_m - w)^n + (n+1)p^n\right]$$

Replace Equations 2-B3 setting  $w = w_{opt}$  and  $S = S_{opt}$  and 2-B4 into Equation 2-B2, one can obtain:

$$\frac{S_m}{w} - \frac{S_m}{w \cdot w_m} \cdot \frac{(w_m - w)^{n+1}}{(w_m - w)^n + p^n} = \frac{S_m}{w_m} \cdot \frac{(w_m - w)^n}{\left[(w_m - w)^n + p^n\right]^2} \cdot \left[(w_m - w)^n + (n+1)p^n\right]$$

Then eliminate  $S_m$  from each side,

$$\frac{1}{w} - \frac{1}{w \cdot w_m} \cdot \frac{(w_m - w)^{n+1}}{(w_m - w)^n + p^n} = \frac{1}{w_m} \cdot \frac{(w_m - w)^n}{\left[(w_m - w)^n + p^n\right]^2} \cdot \left[(w_m - w)^n + (n+1)p^n\right]$$

To simplify the relationship, both sides are multiplied by a factor  $w_m \cdot [(w_m - w)^n + p^n]^2$ , therefore

$$\begin{aligned} & \frac{w_m}{w} \cdot [(w_m - w)^n + p^n]^2 - \frac{1}{w} \cdot (w_m - w)^{n+1} \cdot [(w_m - w)^n + p^n] \\ &= (w_m - w)^n \cdot [(w_m - w)^n + (n+1)p^n] \end{aligned}$$

Then simplify using following steps,

$$\begin{aligned} & \frac{w_m}{w} \cdot [(w_m - w)^n + p^n]^2 - \frac{1}{w} \cdot (w_m - w)^{n+1} \cdot [(w_m - w)^n + p^n] - (w_m - w)^n \cdot [(w_m - w)^n + p^n] \\ &= (w_m - w)^n \cdot np^n \end{aligned}$$

$$\frac{w_m}{w} \cdot [(w_m - w)^n + p^n]^2 - (w_m - w)^n \cdot [(w_m - w)^n + p^n] \cdot \frac{w_m}{w} = (w_m - w)^n \cdot np^n$$

$$\frac{w_m}{w} \cdot [(w_m - w)^n + p^n] \cdot p^n = (w_m - w)^n \cdot np^n$$

By eliminating  $p^n$  from both sides of the equation, the following relationship is derived for the optimum compaction point ( $w = w_{opt}$ ,  $S = S_{opt}$ ):

$$[2-B5] \quad \frac{(w_m - w)^n}{(w_m - w)^n + p^n} = \frac{w_m}{nw}$$

By using Equation 2-B3, one can also obtain:

$$[2-B6] \quad (S_m - S) \cdot \frac{w_m}{S_m} \cdot \frac{1}{w_m - w} = \frac{(w_m - w)^n}{(w_m - w)^n + p^n}$$

Therefore, combine 2-B6 and 2-B5, one can obtain:

$$[2-B7] \quad \frac{S_m - S}{w_m - w} = \frac{S_m}{nw}$$

In Figure 2-23, noting the similar triangle, one can observe that  $BM'$  should replace  $nw$  in Equation 2-B7. Therefore,

$$[2-B8] \quad n = \frac{nw_{opt}}{w_{opt}} = \frac{BM'}{OM'}$$



## 2.12 APPENDIX 2-C DETERMINATION OF PARAMETER “ $p$ ” FROM $S$ VERSUS $w$ CURVE

### Method

In Figure 2-24, point C is a point on S-axis with coordinates of  $(0, S_m/2)$ , i.e. half of  $S_m$ . Draw a line CM to cross the  $S$  versus  $w$  curve at point D. Distance along x-axis between D and M is equal to  $p$ .

### Proof

The equation of the  $S$  versus  $w$  curve in x-y system (origin at M) is

$$[2-C1] \quad y = \frac{kx^{n+1}}{x^n + p^n}$$

The equation of line CM is

$$[2-C2] \quad y = \frac{1}{2}kx$$

Combine Equation 2-C1 and 2-C2 to get the value of point D, i.e.

$$\frac{kx^{n+1}}{x^n + p^n} = \frac{1}{2}kx$$

Solving the above equation results in:

$$[2-C3] \quad x = p$$

Equation 2-C3 implies that the value of parameter “ $p$ ” is equal to the x-coordinate of point D in Figure 2-24 if a simplified Equation 2-C1 or Equation 2-6 in paper is adopted. Because the difference between Equations 2-6 and 2-7 is on very dry side, the method suggested here, which mainly uses the wet side, should not be affected.

**2.13 APPENDIX 2-D DERIVATION OF SUGGESTED EQUATION 2-9**  
**( $kp=const$ )**

To simplify the derivation, the general equation in x-y coordinate system is used and with reference to Figure 2-25.

$$[2-D1] \quad y = \frac{kx^{n+1}}{x^n + p^n}$$

From inflection point F in  $S-w$  curve, we draw a tangent line to meet the approach line at point E. Then extend a horizontal line to cross the  $S-w$  curve at point CST, which represents the compaction sensitivity threshold (CST). The value in y-coordinate at CST and point E are the same.

As shown in Figure 2-25, the degree of saturation at point E is called  $S_E$ .

$$[2-D2] \quad S_E = S_m - y_E$$

For fine-grained soil,  $S_m$  is assumed unchanged when using different compactive effort. As discussed in the paper, it is suggested the degree of saturation at the CST ( $S_E$ ) is the same under different compactive effort. Thus, from Equation 2-D2, the value of  $y_E$  is a constant.

$$[2-D3] \quad y_E = const$$

Differentiate Equation 2-D1, one obtains:

$$[2-D4] \quad y' = \frac{kx^n \cdot [x^n + (n+1)p^n]}{(x^n + p^n)^2}$$

At the inflection point F, it is required:

$$[2-D5] \quad y'' = 0$$

By differentiate Equation 2-D4 one more time and notice  $y''$  equals zero, one obtains:

$$(n+1) \cdot p^n = (n-1) \cdot x^n$$

Therefore, the x-coordinate of point F is obtained:

$$[2-D6] \quad x_F = p \cdot \left( \frac{n+1}{n-1} \right)^{\frac{1}{n}}$$

The y-coordinate of point F is then calculated using Equation 2-D1:

$$[2-D7] \quad y_F = kp \cdot \frac{n-1}{2n} \cdot \left( \frac{n+1}{n-1} \right)^{\frac{n+1}{n}}$$

Substitute Equation 2-D6 into Equation 2-D4, the slope of the tangent line is at point F then calculated to be:

$$[2-D8] \quad y'_F = \frac{k(n+1)^2}{4n}$$

With the coordinates at F and slope of the inflection line known, the equation for the tangent line is then written as follows:

$$[2-D9] \quad y - y_F = y'_F \cdot (x - x_F)$$

By substituting Equations 2-D6, 2-D7, and 2-D8 into Equation 2-D9, one obtains:

$$[2-D10] \quad y - kp \cdot \frac{n-1}{2n} \cdot \left(\frac{n+1}{n-1}\right)^{\frac{n+1}{n}} = \frac{k(n+1)^2}{4n} \cdot \left[ x - p \cdot \left(\frac{n+1}{n-1}\right)^{\frac{1}{n}} \right]$$

The tangent line at point F will intersect the approach line ( $y = kx$  in x-y coordinate system) at point E, which gives the following relationship:

$$kx_E - kp \cdot \frac{n-1}{2n} \cdot \left(\frac{n+1}{n-1}\right)^{\frac{n+1}{n}} = \frac{k(n+1)^2}{4n} \cdot \left[ x_E - p \cdot \left(\frac{n+1}{n-1}\right)^{\frac{1}{n}} \right]$$

Simplify above equation, the x-coordinate of point E is obtained as follow:

$$[2-D11] \quad x_E = p \cdot \left(\frac{n+1}{n-1}\right)^{\frac{n+1}{n}}$$

Because point E is on approach line, the y-coordinate of point E ( $y_E$ ) can be obtained from Equation 2-D12:

$$[2-D12] \quad y_E = kx_E = kp \cdot \left(\frac{n+1}{n-1}\right)^{\frac{n+1}{n}}$$

As we concluded in the paper, for the same soil with same compaction method, the shape factor “ $n$ ” is considered the same. From Equation 2-D3 and 2-D12, following equation is proven:

$$[2-D6] \quad kp = \text{const}$$

**Table 2-1 Properties of tested Syncrude overburden soils**

Soil types	Specific gravity	Plastic limit (%)	Liquid limit (%)	Plastic Index (%)	Particle size distribution
P <sub>i</sub>	2.69	20.1	37	16.9	sand 22%, silt 44%, clay 34%
P <sub>g</sub>	2.54	12.7	22.2	9.5	gravel 16%, sand 37%, silt 30%, clay 17%
K <sub>ca</sub>	2.76	79.5	108.2	28.7	silt 36%, clay 63%
K <sub>cw</sub>	2.66	21.2	36.8	15.6	gravel 15%, sand 36%, silt 26%, clay 22%

**Table 2-2 Parameters regressed from Equation 2-7 in Figures 2-14 and 2-15**

Case No.	Soil type	$S_m(\%)$	$w_m(\%)$	$n$	$p$ (%)	$R^2$ *
Standard compaction test on Syncrude overburden soils	P <sub>1</sub>	86.7	31.5	7.81	13.74	0.994
	P <sub>g</sub>	83.0	18.0	6.49	5.74	0.980
	K <sub>ca</sub>	86.7	34.8	4.80	3.84	0.530
	K <sub>cw</sub>	90.7	21.9	7.46	5.10	0.992
Kneading compaction test on silty clay (Seed et al. 1960)	A1	89.9	21.4	6.48	4.03	0.959
	A2	same <sup>†</sup>	23.0	same <sup>†</sup>	7.90	0.963
	A3	same <sup>†</sup>	23.3	same <sup>†</sup>	10.12	0.930

\*  $R^2$  is correlation coefficient;

† Maximum degree of saturation ( $S_m$ ) and <sup>†</sup> shape factor ( $n$ ) are assumed the same

**Table 2-3 Predicting parameters of lacustrine clay during kneading compaction tests in Fig. 2-20**

Test	$S_m$ (%)	$n$			$w_m$ (%)	$p$ (%)	$R^{2*}$
B1 (N= 50) †	88.8	11.38			27.2	11.30	0.999
Predicted parameters			$\gamma_{dd} ‡$ (Mg/m <sup>3</sup> )	$k$ from Eq. 2-2	$w_m$ (%) from Eq. 2-3	$p$ (%) from Eq. 2-9	
B2 (N= 25)	same	same	1.441	3.10	28.6	11.89	0.984
B3 (N= 12)	same	same	1.411	2.97	29.9	12.43	0.986

\*  $R^2$  is correlation coefficient;

† Parameters of test B1 are used as base for prediction of B2 and B3;

‡  $\gamma_{dd}$  is dry density of soil compacted at air dried condition.



**Figure 2-1 Characteristics of a typical complete compaction curve for fine-grained soils**

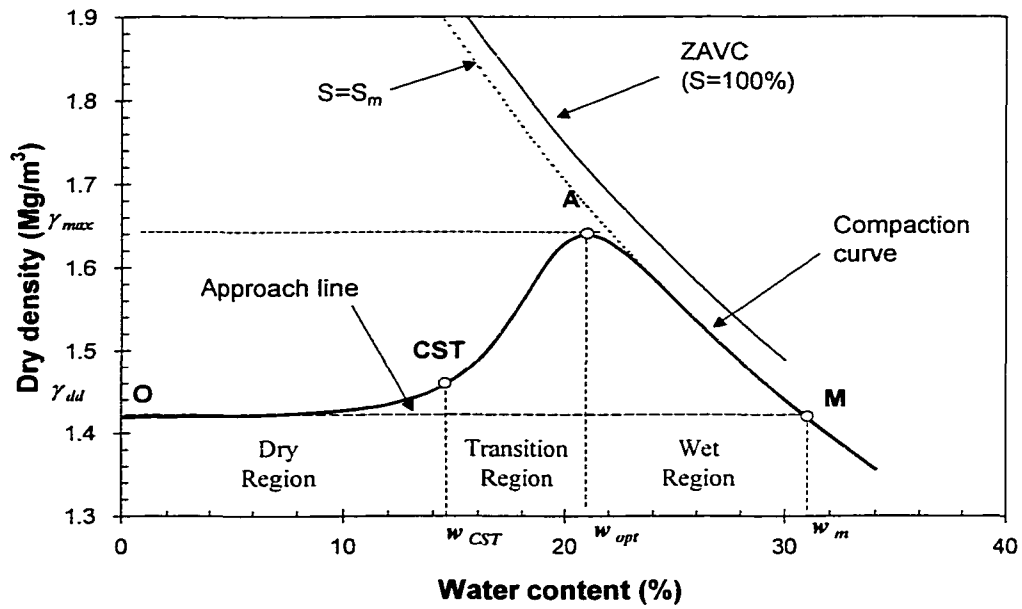


**Figure 2-2 Transformed complete degree of saturation versus moisture content curve**

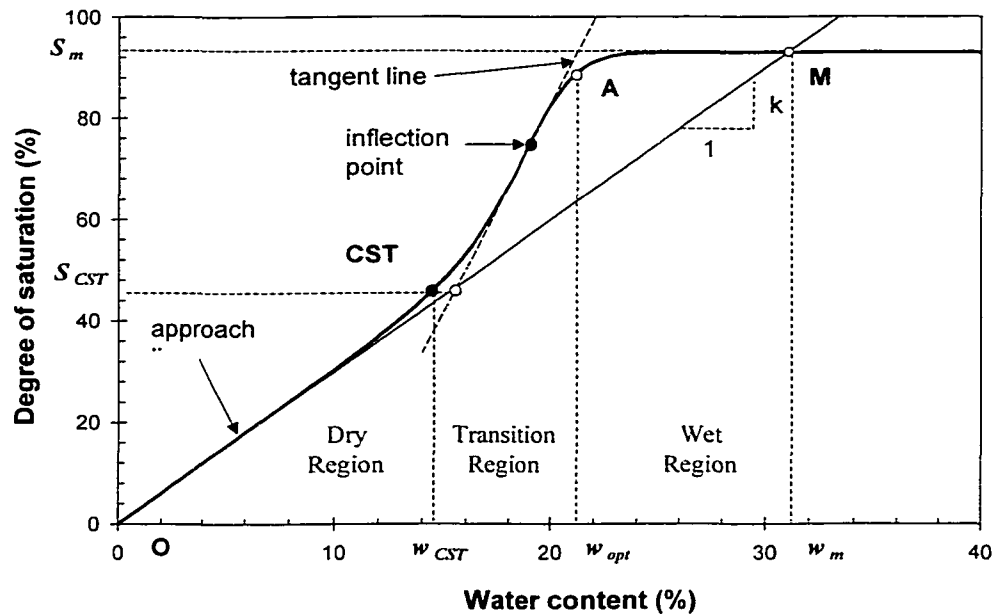


**Figure 2-3 Equations 2-6 and 2-7 and their represented compaction curves**

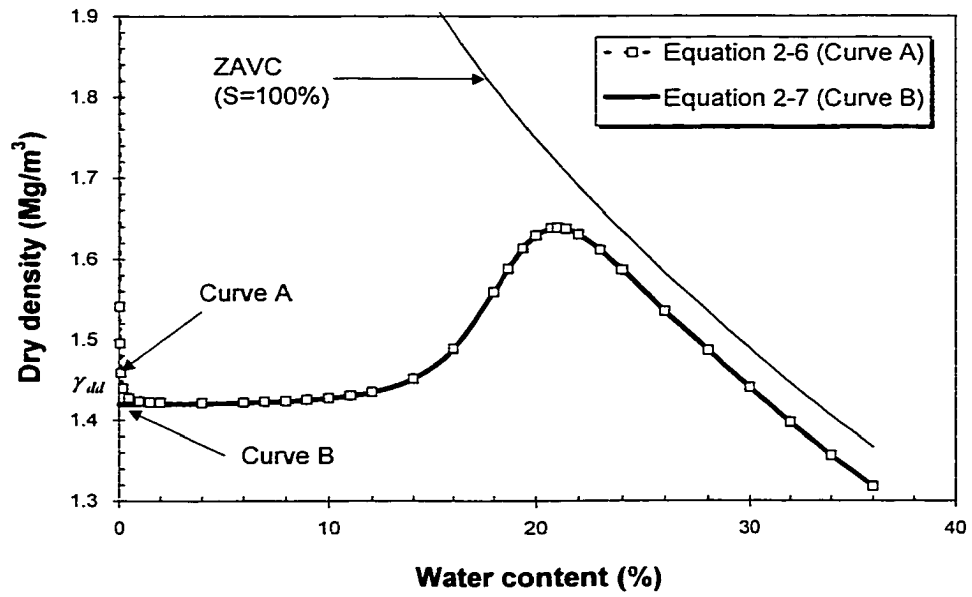


**Figure 2-4 Effect of parameter  $S_m$  on  $S$  versus  $w$  curves ( $w_m = 31\%$ ,  $n = 9$ , and  $p = 12\%$ )**

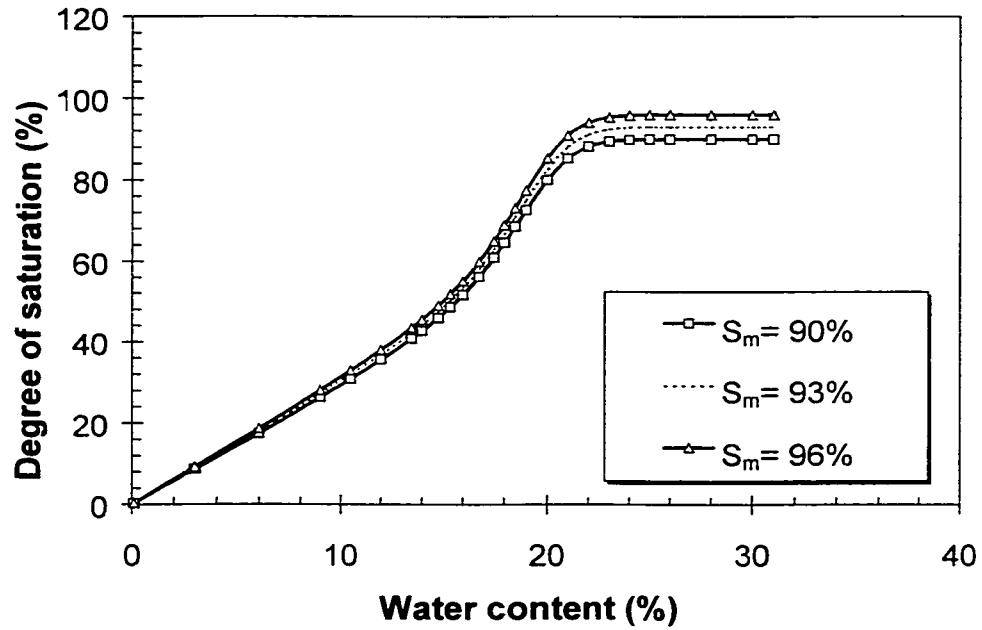


**Figure 2-5 Effect of parameter  $S_m$  on compaction curves ( $w_m = 31\%$ ,  $n = 9$ , and  $p = 12\%$ )**

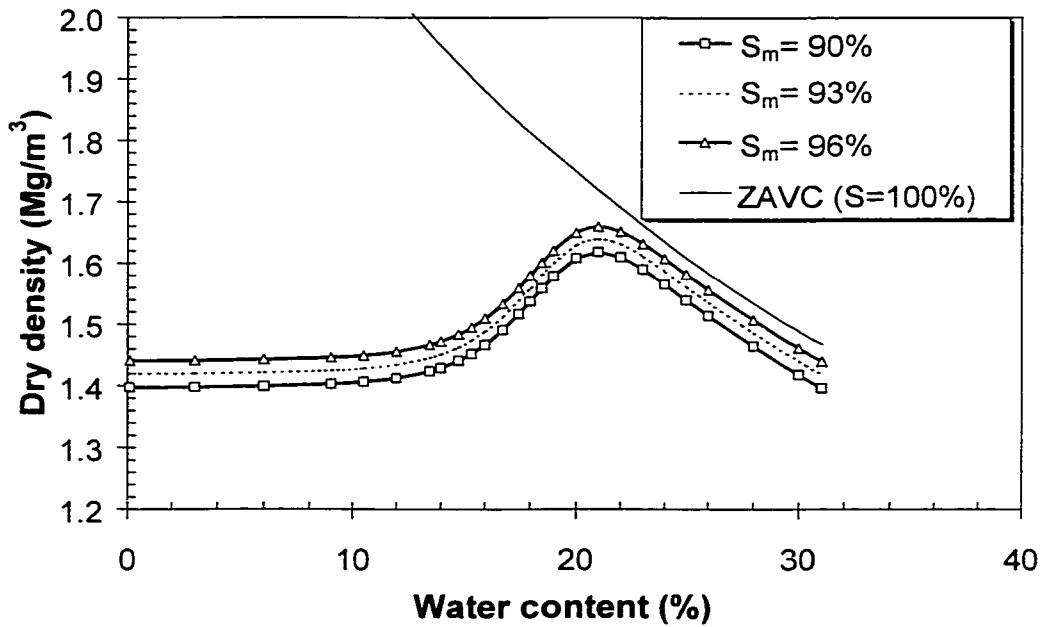


**Figure 2-6 Effect of parameter  $w_m$  (or  $\gamma_{dd}$ ) on  $S$  versus  $w$  curves ( $S_m = 93\%$ ,  $n = 9$  and  $p = 12\%$ )**

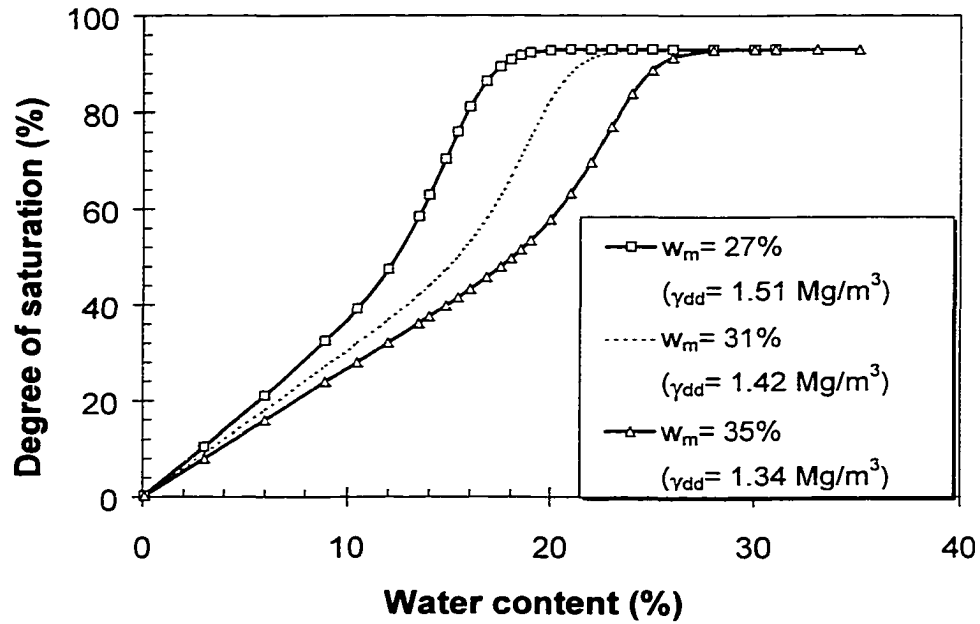


**Figure 2-7 Effect of parameter  $w_m$  (or  $\gamma_{dd}$ ) on compaction curves ( $S_m = 93\%$ ,  $n = 9$  and  $p = 12\%$ )**

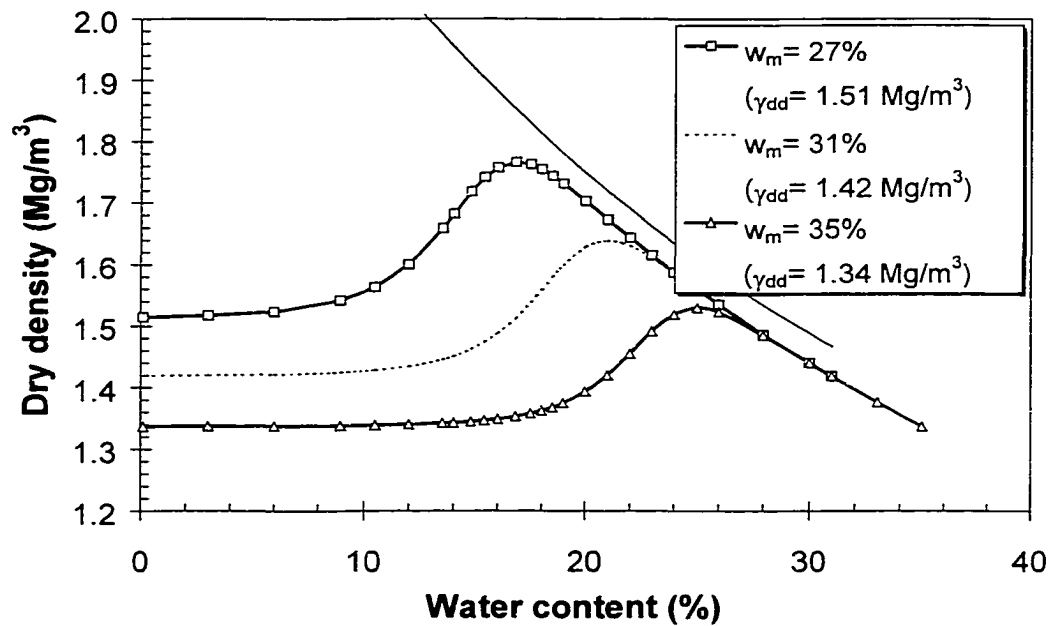


**Figure 2-8** Effect of parameter  $n$  on  $S$  versus  $w$  curves ( $S_m = 93\%$ ,  $w_m = 31\%$ ,  $p = 12\%$ )

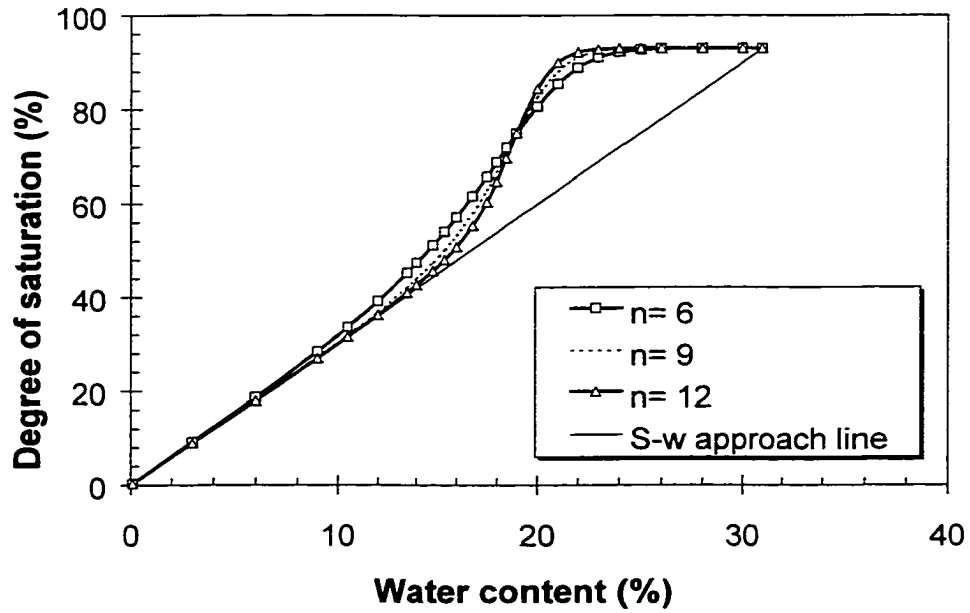


**Figure 2-9** Effect of parameter  $n$  on compaction curves ( $S_m = 93\%$ ,  $w_m = 31\%$ ,  $p = 12\%$ )

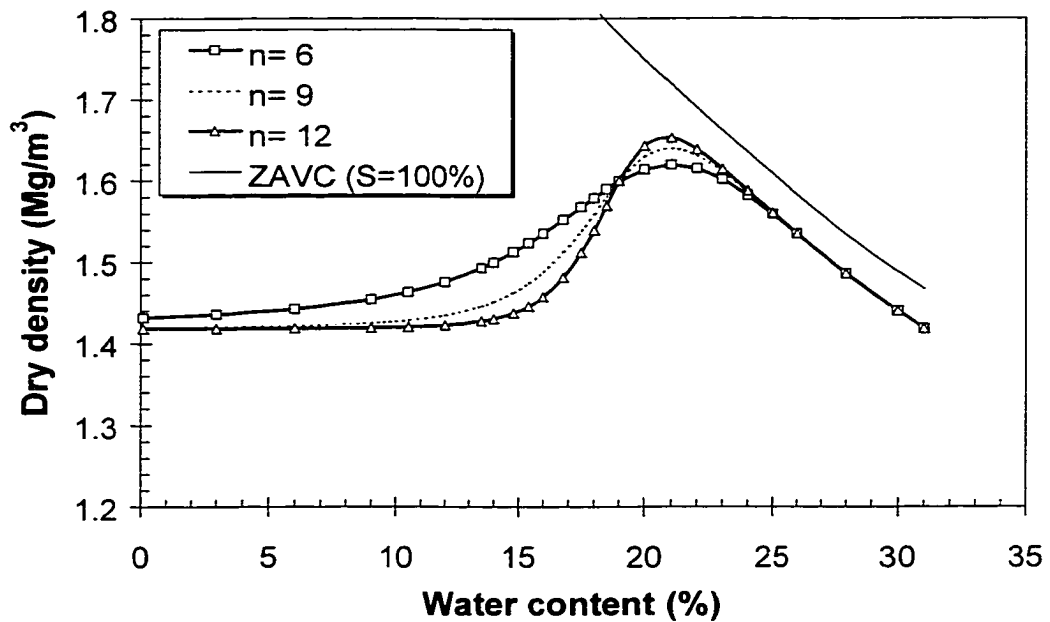


**Figure 2-10** Effect of parameter  $p$  on  $S$  versus  $w$  curves ( $S_m=93\%$ ,  $w_m=31\%$ , and  $n=9$ )

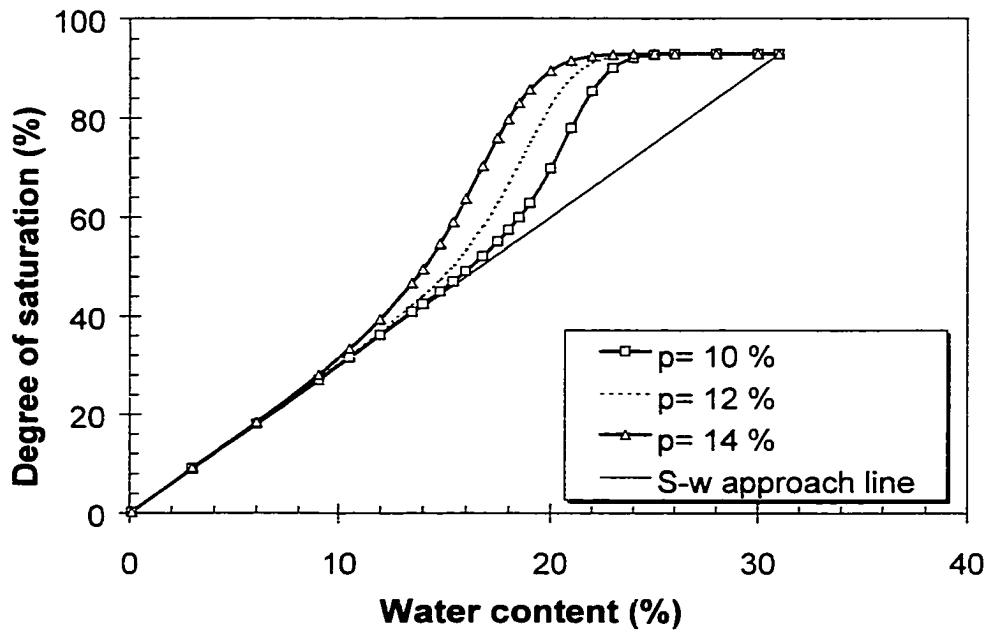


**Figure 2-11** Effect of parameter  $p$  on compaction curves ( $S_m=93\%$ ,  $w_m=31\%$ , and  $n=9$ )

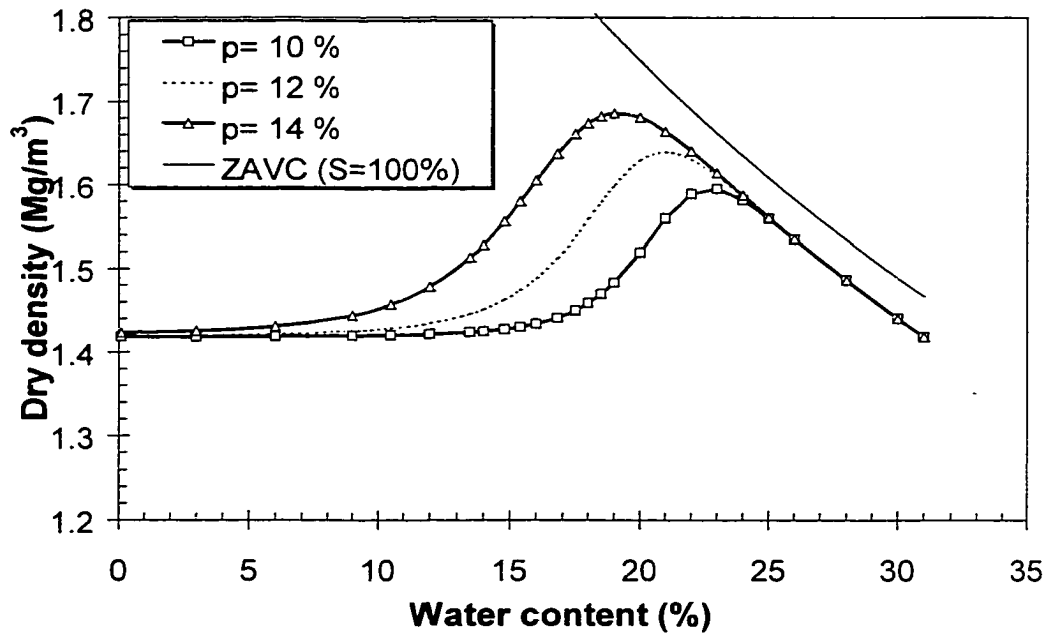


**Figure 2-12 Determination of parameter  $n$**

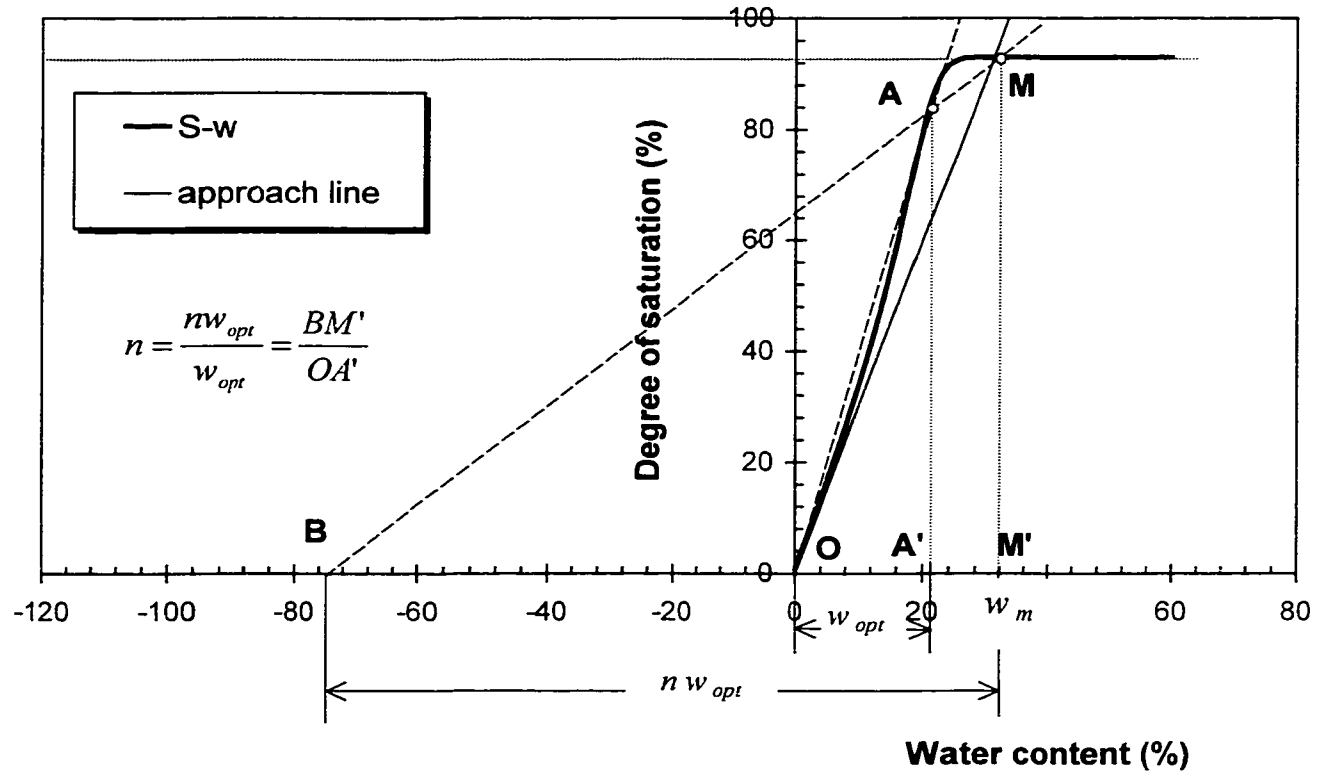
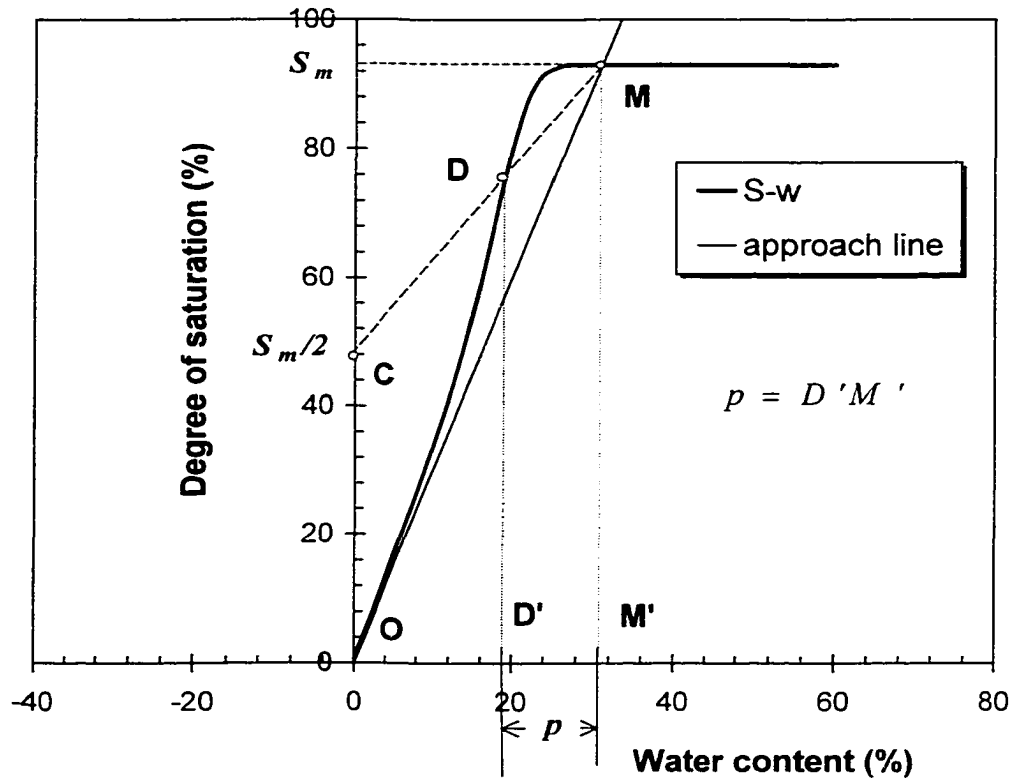


Figure 2-13 Determination of parameter  $p$





**Figure 2-14 Standard compaction tests on Syncrude overburden soils and their fitting curves**

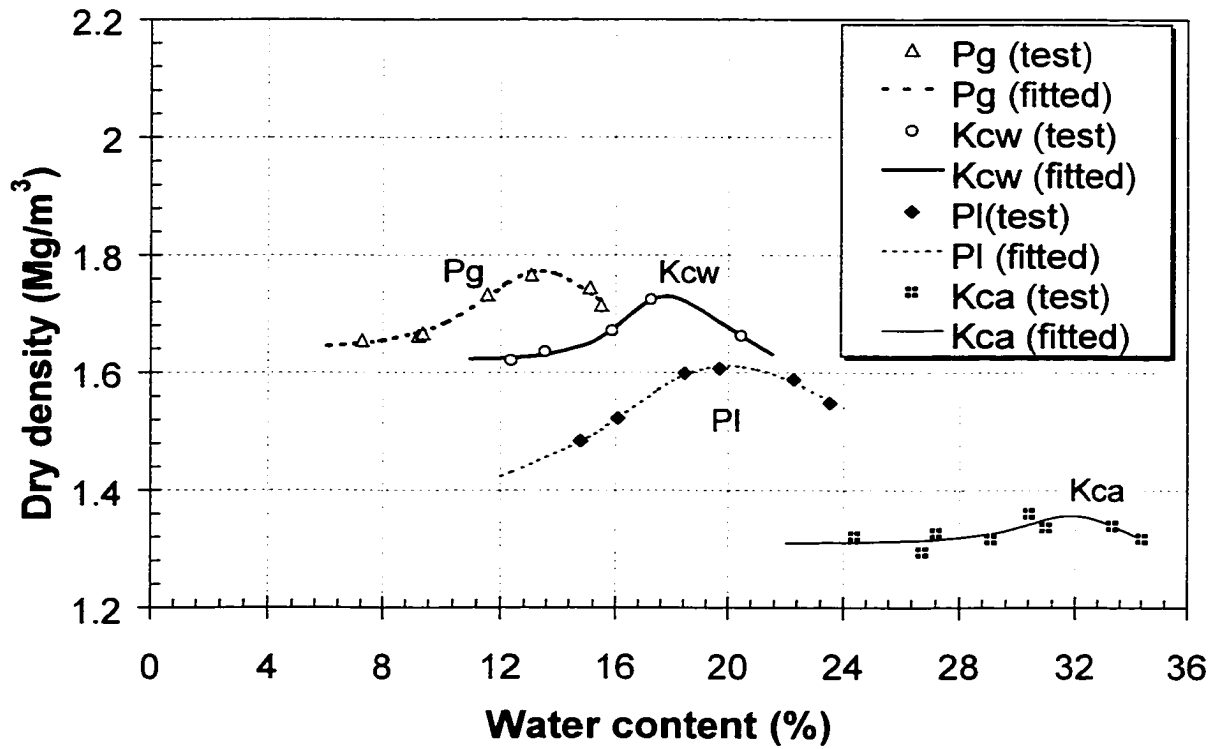
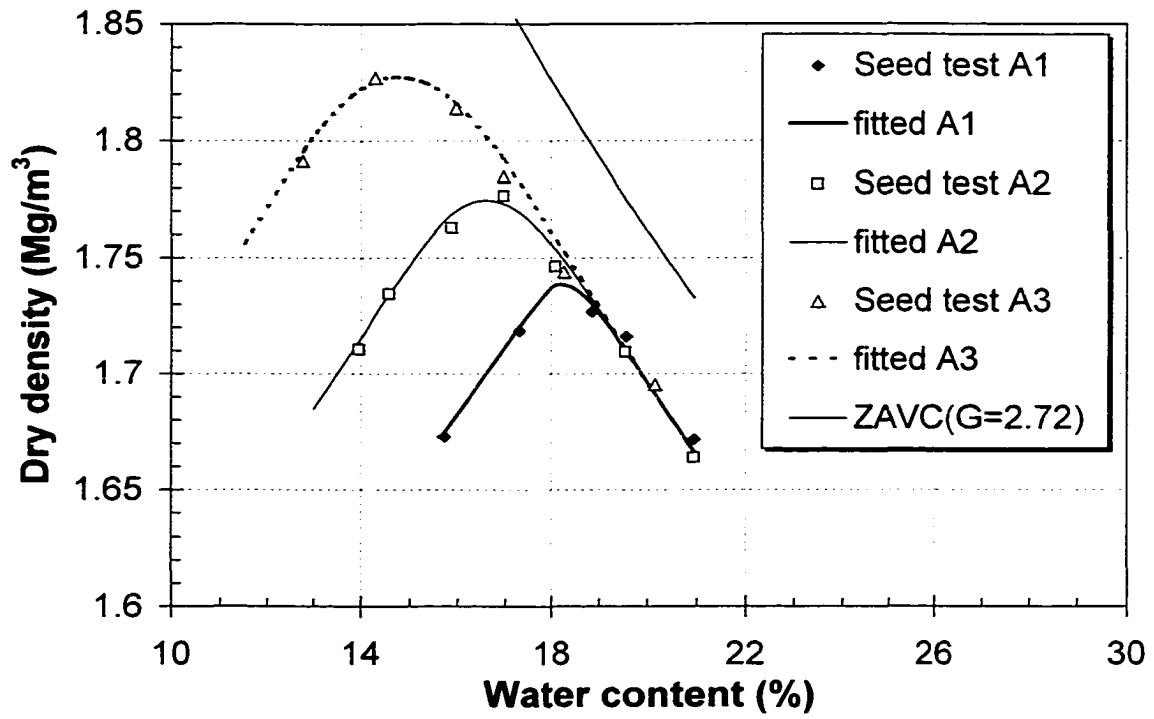
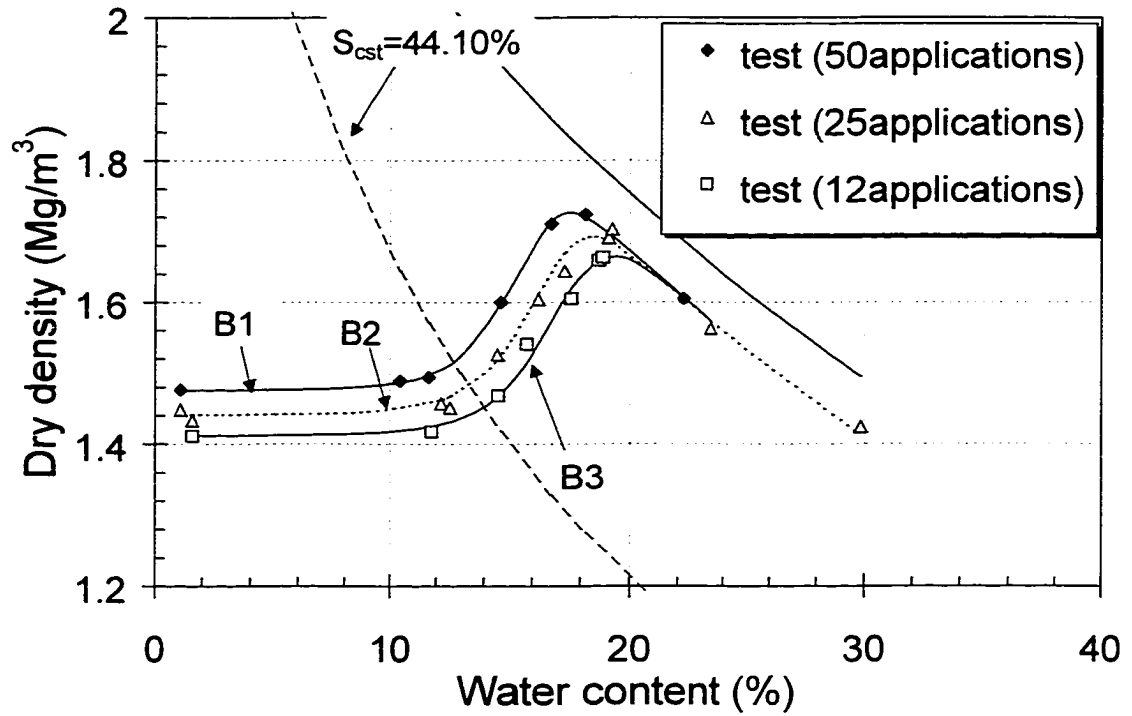


Figure 2-15 Curve fitting on kneading test by Seed et al. (1960)



**Figure 2-16 A family of complete kneading compaction curves with different number of tamps on lacustrine clay (Li and Seg0 1998)**



**Figure 2-17 Faure FK series with energy E1 (0.6 MJ/m<sup>3</sup>) and E2 (2.4 MJ/m<sup>3</sup>) (redrawn from Faure and Da Mata, 1994)**

\* K0 = kaolinite, FK31 = mixtures of fine sand and kaolinite with 31% kaolinite content, FK73 = mixtures of fine sand and kaolinite with 73% kaolinite content

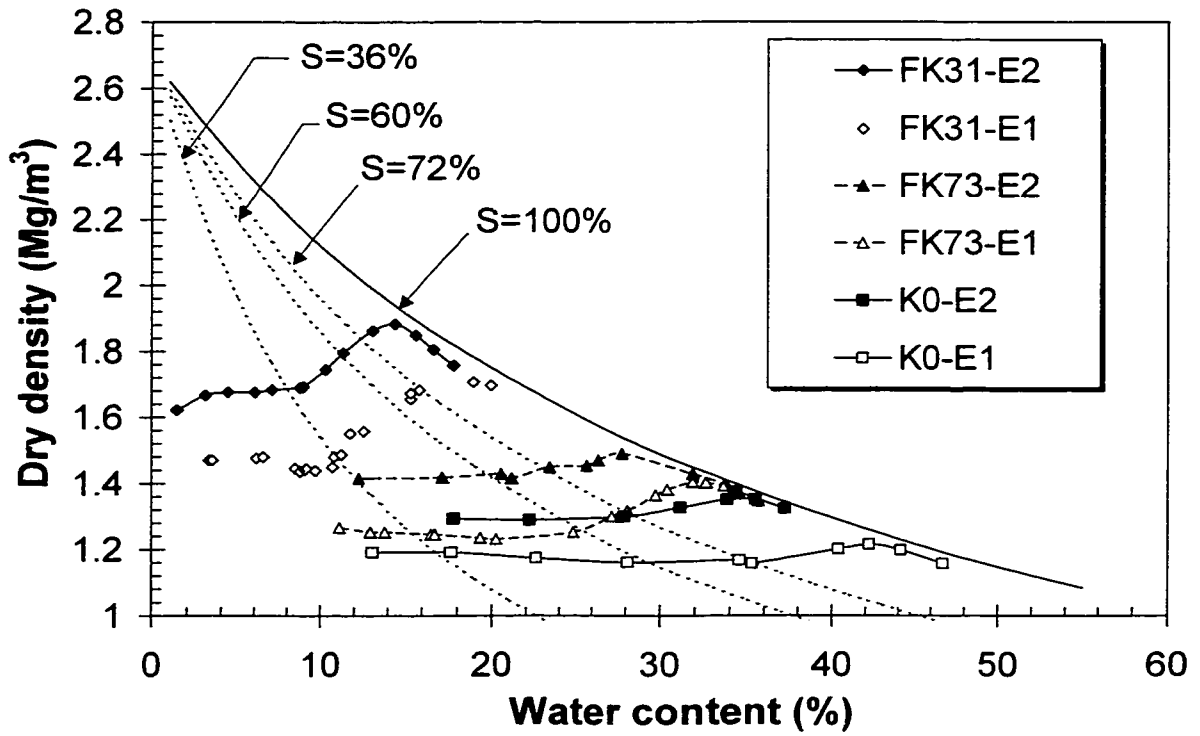


**Figure 2-18 Effect of foot pressure in kneading compaction test for as-air-dried lacustrine clay**

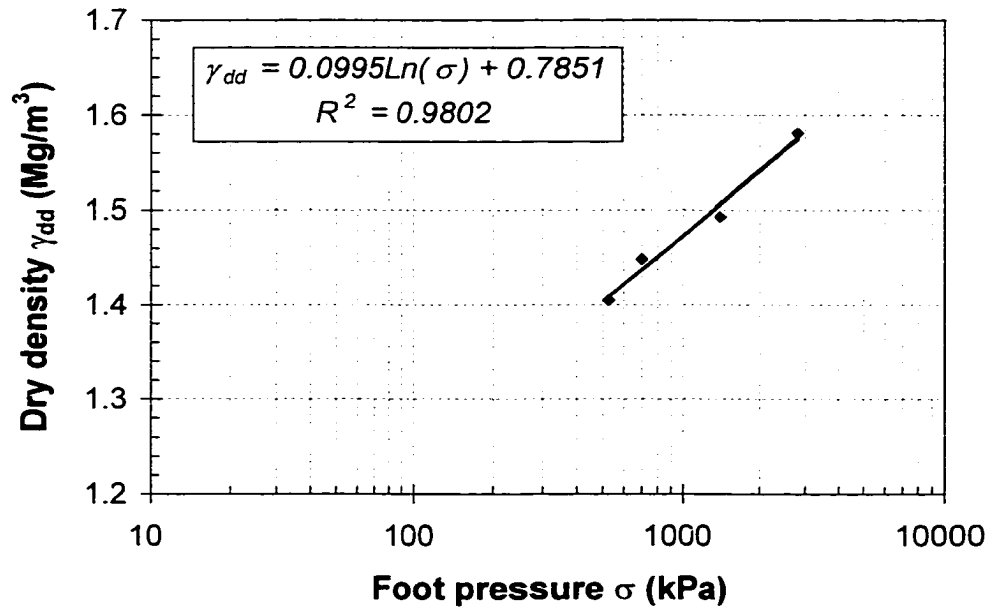


**Figure 2-19 Effect of numbers of applications of 700 kPa foot pressure in kneading compaction test for as-air-dried lacustrine clay**

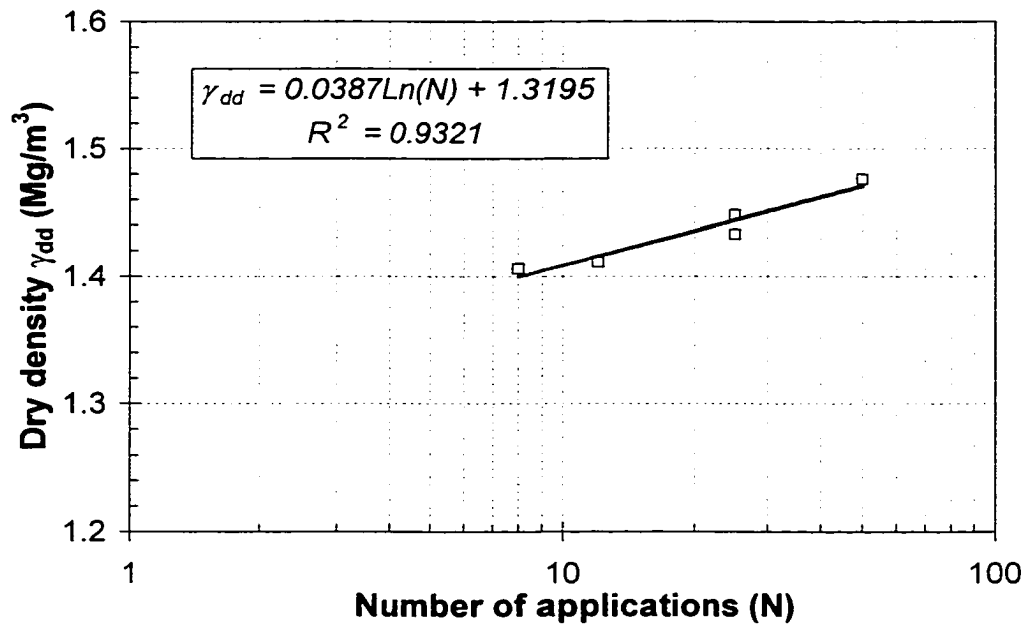


**Figure 2-20 A family of complete compaction curves of glacial lacustrine clay for different compactive efforts (revised from Li and Seg0 2000).**

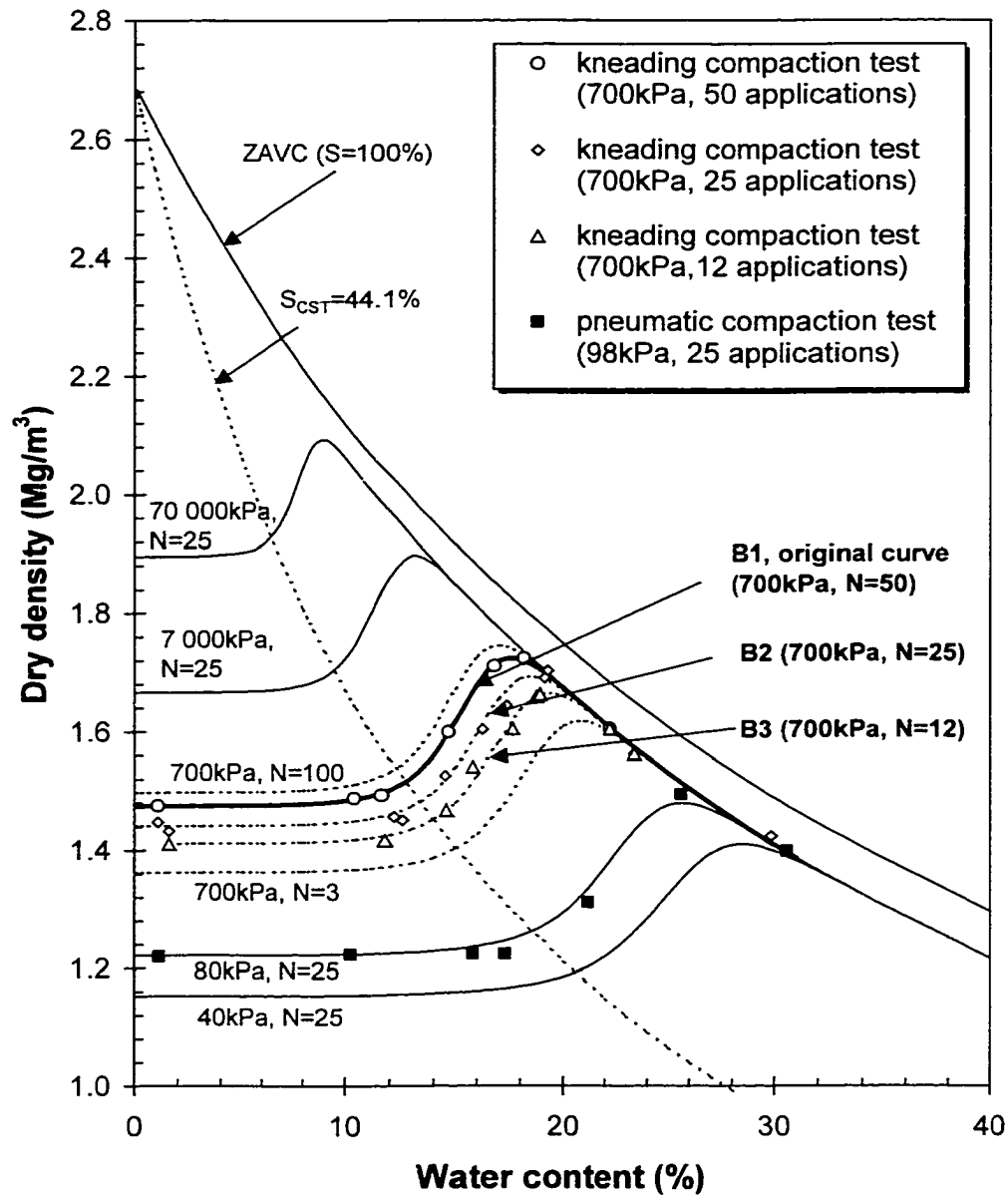


**Figure 2-21** Curve A in x-y coordinates and S-w coordinate systems (Equation 2-A1 and 2-A3 in Appendix 2-A)

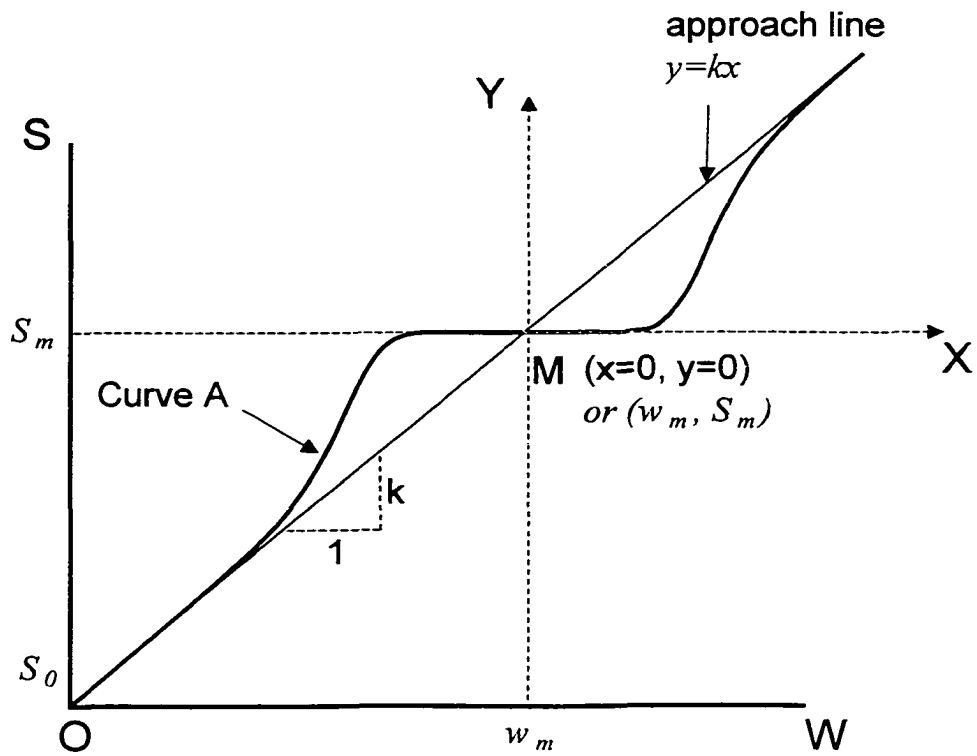


**Figure 2-22 Curve A' (revised curve A) (Equation 2-A5 in Appendix 2-A)**

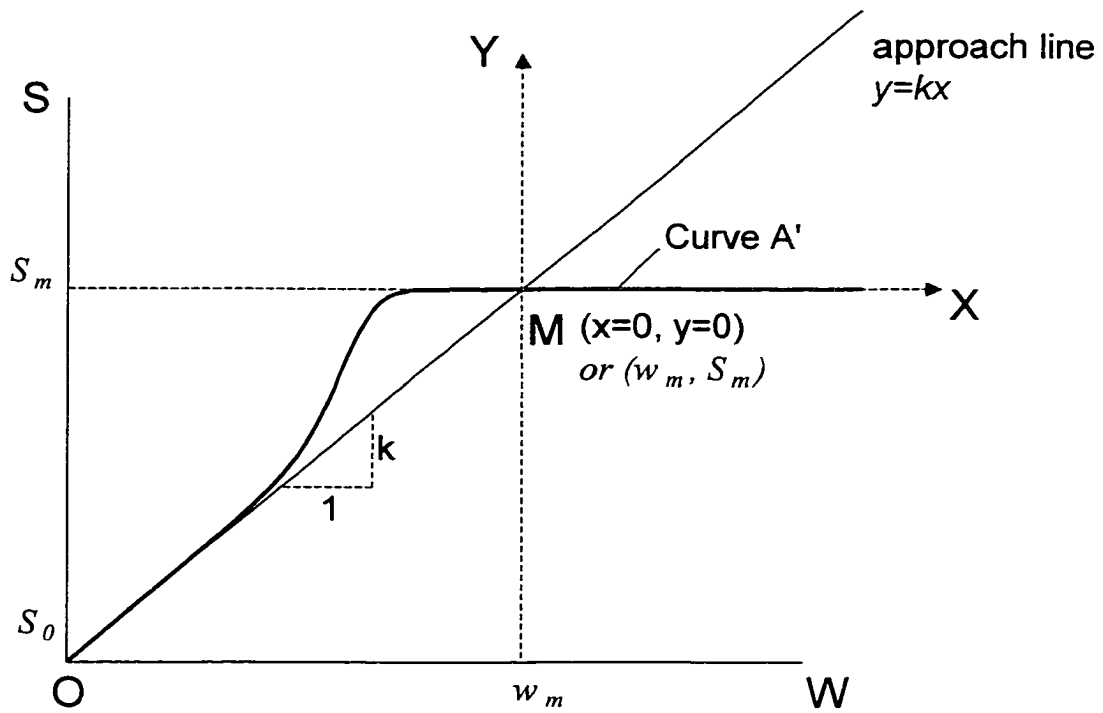




**Figure 2-23 Determination of parameter “ $n$ ” from  $S$  versus  $w$  curve (Appendix 2-B)**

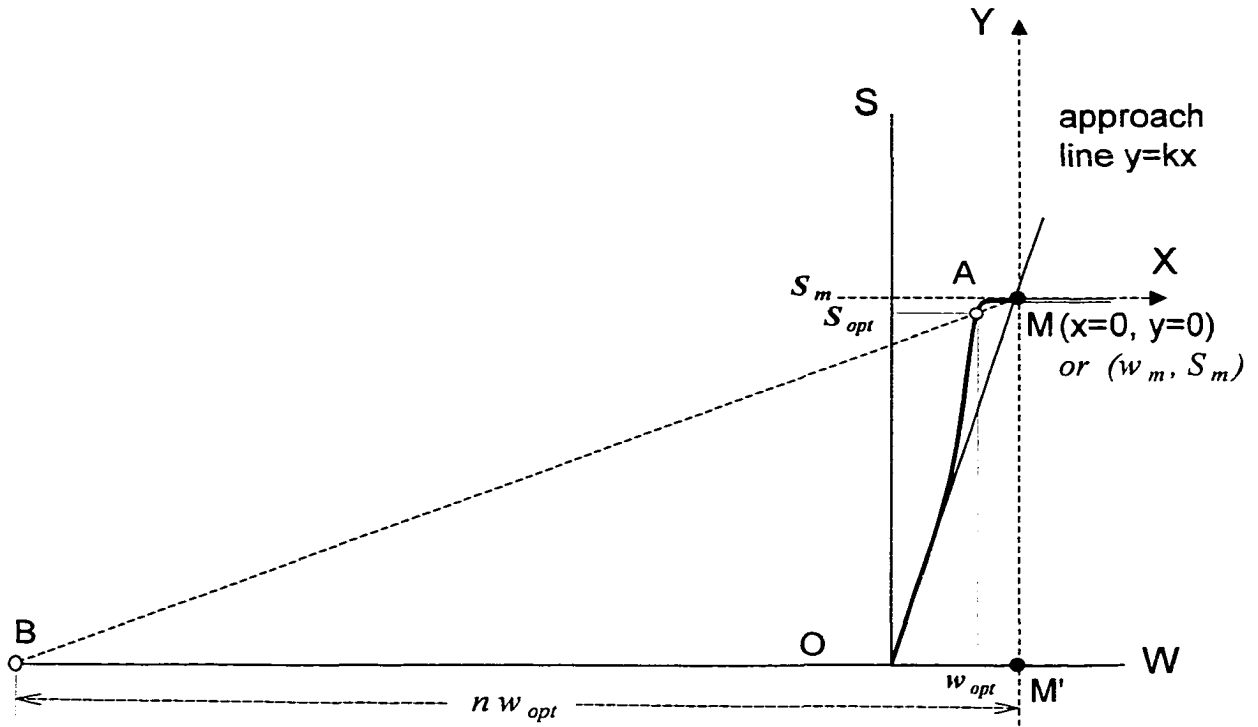
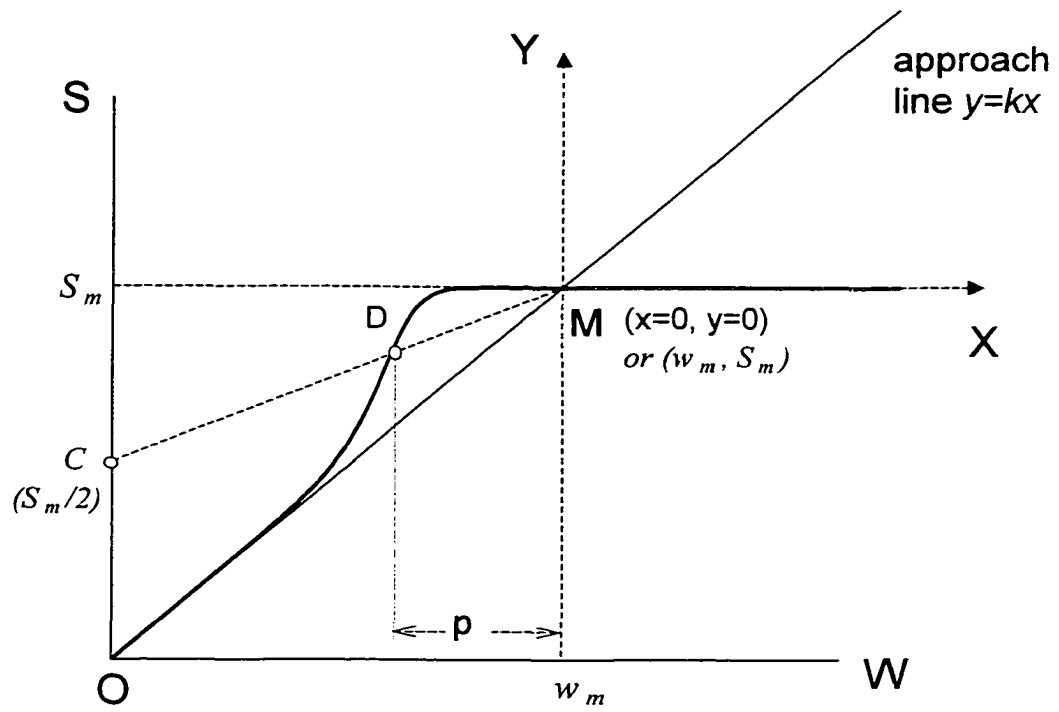
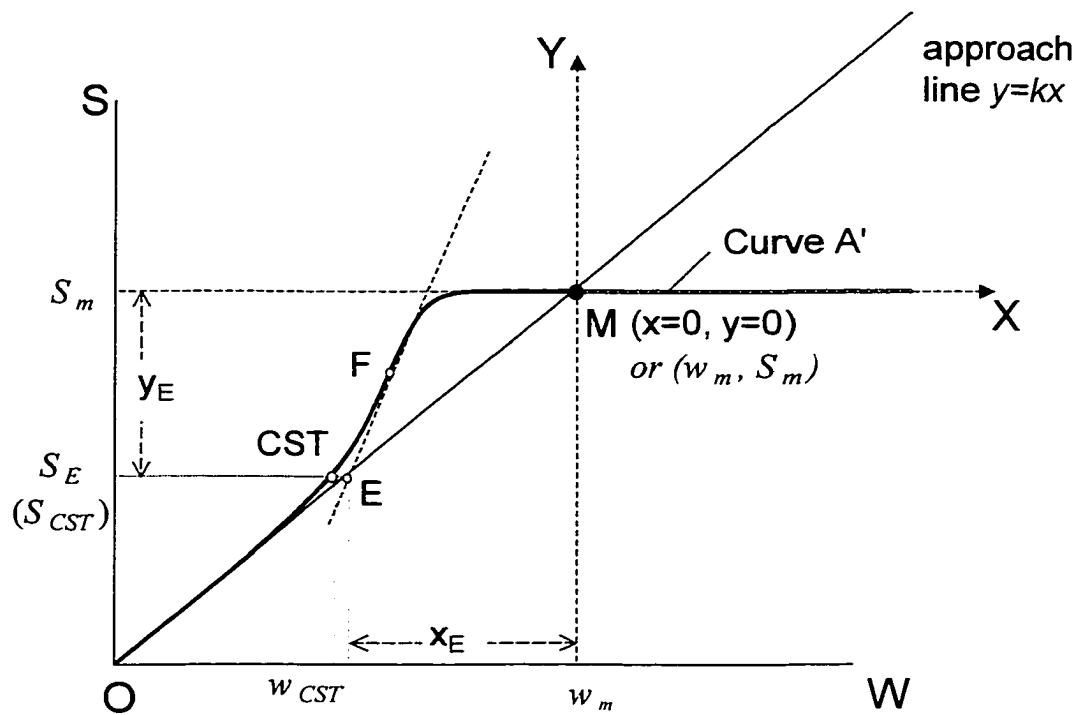


Figure 2-24 Determination of parameter "p" from S versus w curve (Appendix 2-C)



**Figure 2-25 Derivation of suggested Equation 2-9 in paper (Appendix 2-D)**



# CHAPTER 3 SOIL COMPACTION PARAMETERS AND THEIR RELATIONSHIP WITH SOIL PHYSICAL PROPERTIES<sup>1</sup>

## 3.1 INTRODUCTION

In 1933 Proctor showed that: 1) there exists a relationship between the soil moisture content and the dry density to which a soil may be compacted; 2) that for a specific amount of compaction energy applied to a soil there is one water content termed the “optimum water content” at which a particular soil attains its maximum dry density. Since then, the compaction method has become one of the most widely used soil improvement techniques around the world. Most laboratory and field test programs are concerned with the physical properties of the soil near or at the optimum water content. However, the relationship between the dry density and the soil water content for the whole range has seldom been studied in detail.

For fine-grained soil, the complete compaction curve has a number of important characteristics. The position, shape and size of the curve have been quantified in Chapter 2 using four parameters to describe the complete compaction curve from the dry to very wet condition for a given soil. The equation of the complete compaction curve is the first formulation except for attempts which used pure fitting with polynomial equations (Li and Sego 1998, 2000). It can be used to predict a family of compaction curves for a given soil subjected to different inputs of compaction energies. All parameters can be obtained directly from the compaction curve or a transformed curve of degree of the

---

<sup>1</sup> A version of this paper was published in Proceedings of 52<sup>nd</sup> Canadian Geotechnical Conference, Regina, Saskatchewan.

saturation versus water content for a given soil. The method has been discussed in Chapter 2 in detail. The parameters used in the formulation are physically clearly defined and their relationships with soil physical properties are of interested. The objective of this chapter is to explain the relationship between the parameters and the physical properties of the soils.

### 3.2 COMPLETE COMPACTION CURVE FOR FINE-GRAINED SOILS

The complete compaction curve for a soil differs from the traditionally presented compaction curve with respect to the moisture range considered. It starts from the completely dry condition and ends well wet of the optimum water content.

Faure (1981) might be the first to study the complete compaction curve for fine-grained soil. Faure (1981), Saini and Chow (1984) and Faure and Da Mata (1994) studied the evolution of these curves with increasing clay content, clay mineralogy, and compactive effort. The complete curve for a fine-grained soil shows a nearly constant dry density on the dry side before the water content reaches a point called the **compaction sensitivity threshold** (CST) (Fig. 3-1). Faure (1994) presented compaction curves with this feature for thirty-four materials prepared by mixing clay with either fine or coarse sand, and thirty-six natural soils from France and four from Brazil, with exception of some samples with substantial montmorillonite content. The same behavior was also illustrated from results from standard compaction tests and kneading compaction tests carried out at the University of Alberta using glacial lacustrine clay, glacial till, lean oil sands and clay shale (Li and Segó 1998).

Figure 3-1 shows a typical complete compaction curve. When the soil is very dry, the dry density of the fine-grained soil is almost constant ( $\gamma_{dd}$ ). If using degree of saturation instead of dry density, this character can be observed in Fig. 3-2 where the degree of saturation increases linearly with water content. The linear portion is called the approach line. As the water content approaches CST, the degree of saturation departs from the

linear relationship and begins to increase rapidly. The degree of saturation increases rapidly between CST and point A, then the rate of increase slows until it reaches a constant value called the maximum saturation ( $S_m$ ) after which it remains constant for increasing water content (Fig. 3-2). Figure 3-2 also displays a recommend technique to determine the position of CST proposed in Chapter 2.

### 3.3 CHARACTERISTICS OF A COMPLETE COMPACTION CURVE

#### 3.3.1 The Boundary Conditions

The fact that the dry density at the very dry condition remains constant ( $\gamma_{dd}$ ) is an important characteristic of fine-grained soils. For some reason, this has been neglected for many years. It is the limit of the complete compaction curve on the dry side. In Fig. 3-2, the slope of the approach line ( $k$ ) is related to  $\gamma_{dd}$  as follows:

$$[3-1] \quad k = \frac{1}{\frac{\gamma_w}{\gamma_{dd}} - \frac{1}{G_s}}$$

where  $\gamma_w$  is the density of water and  $G_s$  is specific gravity of soil particles.

It is assumed that the maximum degree of saturation ( $S_m$ ) is reached at point M where the compaction curve intersects the approach line of the  $S$  versus  $w$  curve (Fig. 3-2). This assumption does not result in large errors because the degree of saturation only changes by a small amount on the wet side of the optimum water content. The water content at M ( $w_m$ ) can be easily determined as:

$$[3-2] \quad w_m = \frac{S_m}{k}$$

For a given fine-grained soil, it is also shown that the maximum degree of saturation ( $S_m$ ) usually remains constant and does not change as the compactive effort changes (Seed et al. 1960; Lee and Haley 1968; Leroueil et al. 1992). In practice, one can find  $S_m$  from the wet side of the compaction curve which runs roughly parallel to the zero air void curve (ZAVC) (Hausmann, 1990). Thus  $S_m$  is another important referenced value and it controls the limit of the compaction curve on the wet side for a soil.

### **3.3.2 The Curve Shape**

When a fine-grained soil is densified under a constant compactive effort but at varying moisture contents, a typical dry density versus water content relationship becomes apparent. The shape of a compaction curve refers to the similar shape of the dome area of the compaction curve, i.e. traditional dry density versus moisture content curve of interest. The shape of the compaction curve is mostly controlled by the particle size distribution of the soil and compaction method used to compact the soil. For example, compaction curves have different shapes when using the standard compaction method compared to the kneading compaction method. Different soils will generally also result in different shaped curves.

When compacting the same soil using the same compaction method, many laboratory tests and field tests show the same shape of the compaction curves despite using different compactive energy or effort (Turnbull and Foster 1958; Lambe 1958; Seed et al. 1960; Lee and Haley 1968). In embankment construction, different compaction equipment are generally used and they have different weights and use a different number of passes to accomplish different field compaction effort. It also occurs when different thicknesses of lifts are compacted because the compactive effort differs with depth within the lift (Turnbull and Foster 1958; Parson 1992). Therefore knowing the family of compaction curves is useful for the designer as it assists with evaluation of different layer thickness or different compaction effort that is possible in the field. The quantification of the curve shape becomes a key to define the family of curves.

### 3.3.3 The Compactable Moisture Range

In addition to the shape of the curve, the size of the compaction curve also needs to be quantified. The dry density of a soil increases over only a certain water content range. The width of the range is referred as the compactable moisture range of compaction curve.

During soil compaction, water at a certain volume becomes effective at lubricating the soil particles and decreasing the matric suction allowing compaction stress overcome the matric suction inside the soil. This allows the density of the soil to increase. Compactibility depends on the properties of the water adjacent to the soil particles. The less tightly adsorbed or highly oriented the water, the more the freedom of movement of water and solids. Therefore, increasing the clay content limits the soil particles to pack together at lower water content (i.e.,  $w_{CST}$  is larger), and the dry density start to increase at a higher water content (Faure 1981, 1994).

### 3.4 THE FORMULATION

The analytical approach presented in Chapter 2 employs the degree of saturation ( $S$ ) versus water content ( $w$ ), i.e.

$$[3-3] \quad S = f(w)$$

The equation for the compaction curve therefore can be written as:

$$[3-4] \quad \gamma_d = \frac{G\gamma_w}{1 + \frac{wG}{f(w)}}$$

where  $\gamma_d$  is the dry density of soil.



This can be converted as illustrated in Fig. 3-2 to give a more convenient curve for use, since the degree of saturation and water content are both dimensionless. Thus the shape of the curve and the parameters used to describe it are unique for a soil.

The derivation of the mathematical expression of  $f(w)$  has been explained in Chapter 2 and can be written as

$$[3-5] \quad f(w) = S = S_m - \frac{S_m}{w_m} \cdot \frac{(w_m - w)^{n+1}}{(w_m - w)^n + p^n} \quad w < w_m$$

where  $S_m$  is the maximum degree of saturation,  $w_m$  is the water content when  $S_m$  is reached,  $n$  and  $p$  are two parameters which control the shape and width of the compaction curve.

One should observe that the degree of saturation for the dry condition is not zero as predicted by Equation 3-5. This causes a large dry density according to Equation 3-4 when the water content approaches zero. During tests with very high compaction energy, the error may not be neglected since the compaction curve moves to the left and close to the dry condition. This concern can be solved by employing the revised relationship presented in Chapter 2.

$$[3-6] \quad f(w) = S = S_m - S_m \times \left( \frac{w_m - w}{w_m} \right)^{n+1} \times \left( \frac{w_m^n + p^n}{(w_m - w)^n + p^n} \right) \quad w < w_m$$

The parameters  $S_m$  and  $w_m$  (or  $\gamma_{dd}$ ,  $k$ ) are illustrated in Fig. 3-1 and 3-2 and can be easily obtained. Simple procedures have been recently developed to determine  $n$  and  $p$  directly from a transformed  $S$ - $w$  curve (Li and Segoo 2000a). Therefore, all four parameters can be obtained from a compaction curve and a transformed  $S$ - $w$  curve. It is a great advantage to avoid having to use non-linear regression of the compaction data and to ensure the equation can be easily used in engineering practice.

## 3.5 DISCUSSION OF PARAMETERS IN PROPOSED EQUATION

### 3.5.1 Parameter $S_m$

$S_m$  is the maximum degree of saturation used to define the wet boundary of compaction curve. The analytical curves shown in Fig. 3-3 indicate the compaction curve shifts vertically when  $S_m$  changes. A more detailed figure has been shown in Figure 2-5. As discussed previously,  $S_m$  is usually constant for different compactive efforts for a given fine-grained soil. For different fine-grained soils, it also varies over a small range of values.

### 3.5.2 Parameter $w_m$ ( $\gamma_{dd}$ , or $k$ )

Parameter  $w_m$  can be obtained by extending a horizontal line from the point of a dried soil sample ( $\gamma_{dd}$ ) to cross the compaction curve on the wet side (Fig. 3-1). The parameter  $k$ ,  $w_m$  or  $\gamma_{dd}$  are interrelated as shown in Equation 3-1 and 3-2.  $\gamma_{dd}$  is a parameter used to determine the dry boundary of compaction curve. A decrease of  $w_m$  can be also considered as an increase of  $\gamma_{dd}$ , which means the compaction curve shows higher density on the dry side of the optimum water content but changes little on the wet side (Fig. 3-3). Figure 2-7 in Chapter 2 provides a detailed illustration. This is the general observation when a higher compaction effort is used to compact a soil, or a coarser material is compacted.

As the water content has little influence on the value of  $\gamma_{dd}$ , the compaction energy and the soil type are the only other factors that can have an important influence. For a given soil,  $\gamma_{dd}$  is the index of compaction energy used during a test (Li and Segoo 1998). For different kinds of fine-grained soils using the same compaction method,  $\gamma_{dd}$  (or  $w_m$ ) is related to the soil properties, especially soil particle size as discussed below. It is evident

that the traditional compaction curve of sandy soil has higher dry density than clayey soil (Johnson and Sallberg 1960; Krebs and Walker 1971).

### 3.5.3 Parameter $n$

Fig. 3-3 shows the influence of parameter  $n$  on the dome shape of the compaction curve. The detail of the variation has been presented in Figure 2-9 of Chapter 2. When  $n$  increases, the compaction curve becomes narrower and achieves a higher maximum dry density. The curve tends to flatten when  $n$  decreases. As discussed before, when using the same compaction method with more input energy to compact a given soil, the compaction curves have a similar characteristic shape that is shifted up and to the left. Therefore parameter  $n$  can be assumed constant for a particular soil when compacted using the same method. Compaction curves with a characteristic shape thus can be quantified by using a constant value of  $n$ . This provides the engineer with the ability to predict a family of compaction curves for a given soil for different compactive energy inputs. Therefore, parameter  $n$  will be called the shape factor because of its important influence on the shape of the compaction curves. For natural soils it generally varies over a range 4 to 12.

As mentioned before, the shape of a compaction curve also depends on both its soil fabrics and compaction method used, such as kneading compaction method or dynamic compaction method. Only the influence of soil fabrics during Proctor (standard) compaction tests is considered in this chapter.

### 3.5.4 Parameter $p$

Parameter  $p$  controls the width of the upper curved part of the compaction curve, which can be called the index of the compactable moisture range (Fig. 3-3). Parameter  $p$  allows the equation to define the size of this range without changing its shape factor ( $n$ ) and boundary conditions (defined by  $S_m$  and  $\gamma_{dd}$ ). A detail of the influences has been shown

in Figure 2-11 of Chapter 2. The width of the compactable moisture range is about 1.2~1.5 times  $p$ . Because  $p$  is a measure of the dome width ( $w_m - w_{CST}$ ) for a compaction curve, it is directly related to  $w_{CST}$  of a soil and this depends on the clay content of the soil according to Faure (1991). For convenience, the plastic limit instead of clay content is used in later discussions.

### 3.6 COMPACTION PARAMETERS IN DIFFERENT SOILS

Four different natural soils, Pleistocene glacial till ( $P_g$ ), Pleistocene lacustrine clay ( $P_l$ ), Cretaceous clay shale ( $K_{ca}$ ), and lean oil sands ( $K_{cw}$ ), were used in this study and compaction tests were carried out. The soils were all acquired from the overburden soils on the lease of Syncrude Canada Ltd., Fort McMurray, Alberta. Their basic properties are summarized in Table 3-1 and their particle size distributions are shown in Fig. 3-4.  $P_l$ ,  $K_{ca}$ , and  $K_{cw}$ , consist predominantly of fines and are fine-grained soils. Although glacial till  $P_g$  has only 25% fines (silt and clay), and 20% fine sands, it is traditionally considered as a fine-grained soil. More important is that it displays a typical flat branch on the dry side of the compaction curve (Fig. 3-5). The large variation in soil properties provides an opportunity to evaluate the relationship between the compaction parameters and the basic soil properties.

All soils were oven-dried prior to carrying out standard (Proctor) compaction tests following ASTM D698-91. The results are shown in Fig. 3-5. It can be observed that the curves separate from each other as their particle size distribution would suggest. Table 3-2 summarizes the compaction results when the four parameters ( $S_m$ ,  $w_m$ ,  $n$ ,  $p$ ) are estimated from Equation 3-6. The curves to fit the laboratory compaction data shown in Fig. 3-5 have a good agreement. The original test data for  $K_{ca}$  is scattered but the curve is a reasonable fit to the data.

Fig. 3-6 displays the strong relationship ( $R^2 = 0.916$ ) between the dry density of soil at its dry condition ( $\gamma_{dd}$ ) and the log of average particle size of each soil ( $D_{50}$ ). This indicates

that the position of compaction curve on the dry side is particle size sensitive as observed by Faure and Da Mata (1994). When the same standard compaction test was carried out, a soil with larger average particle size has higher dry density than a soil with finer particle size. Results in literature agree with this conclusion (Johnson and Sallberg 1960; Krebs and Walker 1971). As parameter  $w_m$  is directly related to  $\gamma_{dd}$  and  $S_m$  from Equation 3-1 and 3-2,  $w_m$  is also dependent on the average particle size of soil (Fig. 3-7).

Uniformly graded materials typically respond poorly to compaction (Krebs and Walker 1971). As particle size distribution (PSD) becomes increasingly well graded, the dry density of the material will increase. A well-graded soil can have greater dry density than a uniform soil because its small particles can fill the void formed by the larger particles. In the proposed equation to describe the compaction curve (Equation 3-6), parameter  $n$  should be related to soil gradation which is represented by uniformity coefficient  $C_u$ . Here  $C_u$  is equal to  $D_{60}/D_{10}$  of soil particle size distribution. Based on the database from the four available soils, Figure 3-8 shows the relationship between parameter  $n$  and  $C_u$ . Although there are some scattered points in the figure, the lean oil sands ( $K_{cw}$ ) with the highest value of  $C_u$  gives the highest value of  $n$  (7.46), and the most uniform soil  $K_{ca}$  lead to a smaller value of  $n$  (4.8). This trend agrees with the physical explanation. However, increasing the size of database would be the key in future discussion.

The value of soil plastic limit ( $w_p$ ) has been compared to the standard Proctor optimum water content ( $w_{opt}$ ) by many researchers (Daniel 1984; Hilf 1990; Daniel and Benson 1990; Leroueil et al. 1992; Chapuis 2000). As discussed before, Faure (1981) found the soil water content at CST ( $w_{CST}$ ) depends on clay content of a given soil, which is also related to the plastic limit. From the direct method to determine  $p$  in Fig. 2-13 of Chapter 2, it is found that the value of  $p$  ( $D'M'$ ) is in fact between  $w_m - w_{CST}$  and  $w_m - w_{opt}$ . Therefore, the index of compactable moisture range ( $p$ ) is considered a function of  $w_m - w_p$ . The relationship of  $w_m - w_p$  with parameter  $p$  is linear as shown in Fig. 3-9. Soil  $P_1$  with the largest difference between  $w_m$  and  $w_p$  (10.0) has largest value of  $p$  (8.39%).

### 3.7 CONCLUSIONS

An equation for use with fine-grained soils based on the relationship between degree of saturation and water content is proposed. Four parameters in the equation are clearly defined and their connections with the physical properties of a particular soil are discussed. Standard Proctor compaction test results from four different soils are used to estimate the parameter's value for the different soils. It is found that the shape factor, which is very useful because it is constant when a soil is compacted using different energy, is related to the soil uniformity coefficient. The dry density of soil at the dry condition increases with average particle size for a compaction test. The index of compactable range is related to the soil plastic limit and average particle size. The maximum degree of saturation only shows a small range for different soils.

### 3.8 REFERENCES

- Chapuis, R.P. 2000. Full-scale hydraulic performance of soil-bentonite and clay liners. R.M. Hardy Keynote Address, 53<sup>rd</sup> Canadian Geotechnical Conference, Montreal, Quebec, Canada, Oct. 14-18.
- Daniel, D.E. 1984. Predicting hydraulic conductivity of clay liners. *ASCE Journal of Geotechnical Engineering*, **110**(2): 285-300.
- Daniel, D.E., and Benson, C.H. 1990. Water content-density criteria for compacted clays. *ASCE Journal of Geotechnical Engineering*, **116**(12): 1811-1830.
- Faure, A.G. 1981. A new conception of the plastic and liquid limits of clays. *Soil and Tillage Research*, **1**: 97-105.
- Faure, A.G. and Da Mata, J.D.V. 1994. Penetration resistance value along compaction curves. *ASCE Journal of Geotechnical Engineering*, **120**(1): 46-59.
- Hausmann, M.R. 1990. **Engineering Principles of Ground Modification**, McGraw-Hill Inc., New York, pp. 14-56.
- Hilf, J.W. 1990. Compacted fill. *Foundation Engineering Handbook*, Fang, H.-Y (Ed), pp.249-316.

- Johnson, A.W. and Sallberg, J.R. 1960. Factors that influence field compaction of soils. Highway Research Board Bulletin 272, Highway Research Board, National Research Council, Washington, D.C.
- Krebs, R.D. and Walker, R.D. 1971. **Highway Materials**, McGraw-Hill Inc., New York, pp. 175-223.
- Lambe, T.W. 1958. The engineering behaviour of compacted clay. ASCE Journal of Soil Mechanics and Foundation Division, **84**(2): 1655-1 to -35.
- Lee, K.L. and Haley, S.C. 1968. Strength of compacted clay at high pressure. ASCE Journal of Soil Mechanics and Foundation Division, **94**(1): 1303-1332.
- Leroueil, S., Le Bihan, J.P., and Bouchard, R. 1992. Remarks on the design of clay liners used in lagoons as hydraulic barriers. Canadian Geotechnical Journal, **29**: 512-515.
- Li, H. and Segoo, D.C. 1998. Prediction complete compaction curves of fine-grained soil. *In* Proceedings of 51st Canadian Geotechnical Conference, Edmonton, Alberta, Canada, October 4-7, 1998. **2**: 679-686.
- Li, H. and Segoo, D. C. 2000. Equation for complete compaction curve of fine-grained soils and its applications. Constructing and Controlling Compaction of Earth Fills, ASTM Special Technical Publication 1384, Shanklin, D.W., Rademacher, K.R., and Talbot, J.R. (Eds.), American Society for Testing and Materials, West Conshohocken, PA. pp. 113-125.
- Parson, A.W. 1992. Compaction of Soils and Granular Materials: A review of Research Performed at the Transport Research Laboratory, HMSO, London, pp. 1-11.
- Proctor, R.R. 1933. The design and construction of rolled earth dams. Engineering News Record, Aug. 31, Sept. 7, Sept. 21, and Sept. 28, pp. 245-248, 286-289, 348-351, and 372-376, respectively.
- Saini, G.R. and Chow, T.L. 1984. Compactibility indexes of some agricultural soils of New Brunswick, Canada. Soil Science, **137**(1): 33-38.
- Seed, H.B., Mitchell, J.K. and Chan, C.K. 1960. The strength of compacted cohesive soils. Research Conference on Shear Strength of Cohesive Soils, Boulder, Colorado, pp. 877-964.
- Turnbull, W.J. and Foster, C.R. 1958. Stabilization of materials by compaction. Transactions of the American Society of Civil Engineers, **123**(1): 1-15.

**Table 3-1 Physical properties of tested Syncrude overburden soils**

Soil	Specific gravity (G)	Liquid limit ( $w_L$ ) (%)	Plastic limit ( $w_p$ ) (%)	Plastic index (PI) (%)	$D_{50}$ (mm)*	$C_u=D_{60}/D_{10}$ †
K <sub>ca</sub>	2.76	108.2	28.7	79.5	0.00095	12.3
P <sub>1</sub>	2.69	37.0	16.9	20.1	0.0055	20.7
K <sub>cw</sub>	2.66	36.8	15.6	21.2	0.075	818.2
P <sub>g</sub>	2.65	22.2	9.5	12.7	0.61	105.3

\*  $D_{50}$  is the average particle size with 50% finer by weight; Similar as  $D_{60}$  and  $D_{10}$ .

†  $C_u$  is uniformity coefficient of soil and is calculated from  $C_u=D_{60}/D_{10}$ .



**Table 3-2 Results from standard compaction test and compaction parameters**

Soil	OWC* (%)	$\gamma_{d \max}$ (Mg/m <sup>3</sup> )	$S_m$ (%)	$w_m$ (%)	$n$	$p$ (%)	$R^2$	$\gamma_{dd}$ (Mg/m <sup>3</sup> )	$w_m-w_p$ (%)
K <sub>ca</sub>	31.7	1.35	86.8	34.8	4.8	3.85	0.53	1.31	6.1
P <sub>1</sub>	20.2	1.62	86	26.9	7.15	8.39	0.98	1.46	10.0
K <sub>cw</sub>	17.8	1.73	90.7	21.9	7.46	5.1	0.99	1.62	6.3
P <sub>g</sub>	13.5	1.78	77.2	18.2	5.98	5.74	0.99	1.63	8.7

\* OWC is optimum water content;  $\gamma_{d \max}$  is maximum dry density.

\*  $S_m$ ,  $w_m$  (or  $\gamma_{dd}$ ),  $n$ ,  $p$  are compaction parameters;  $R^2$  is correlation coefficient.

Figure 3-1 Sketch of complete compaction curve ( $\gamma_d - w$ )

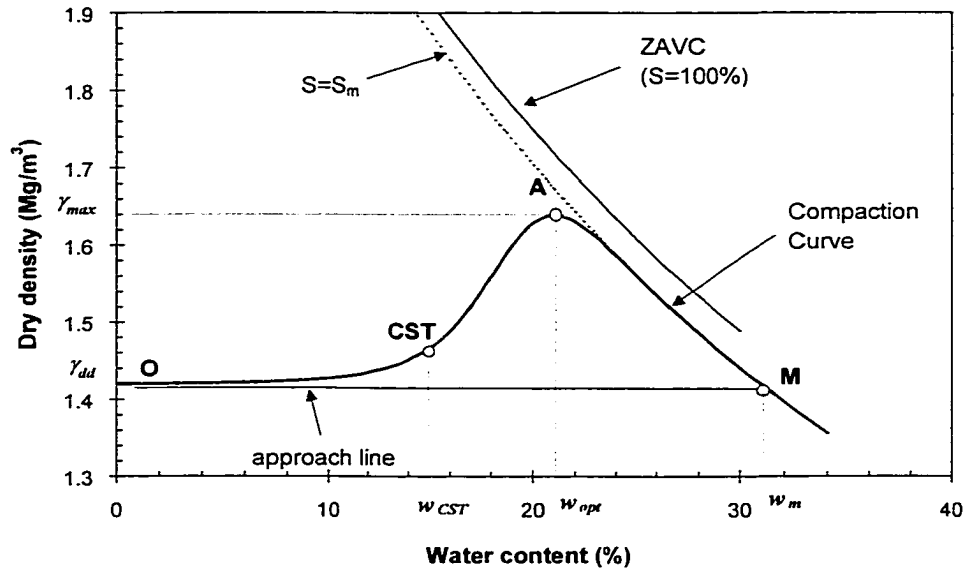
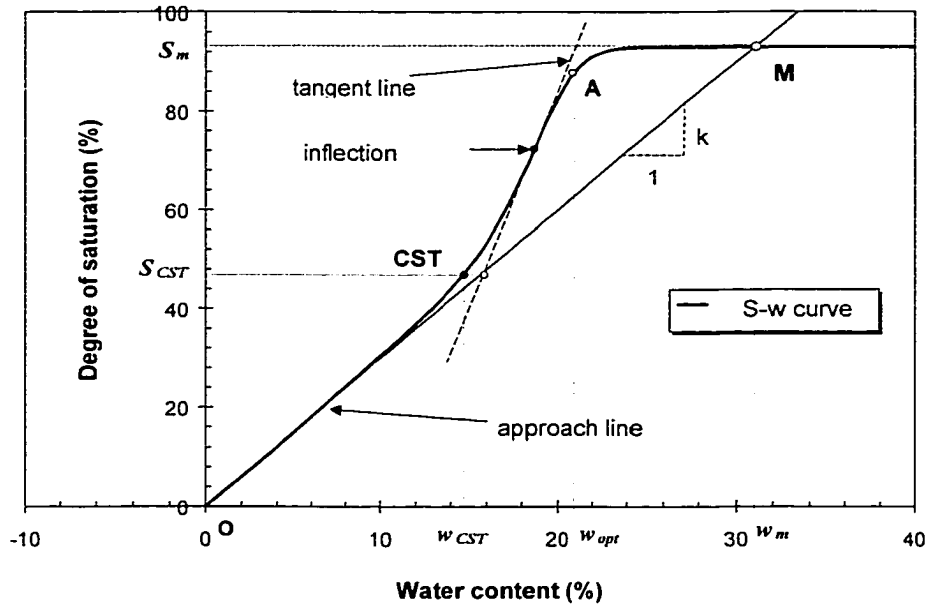
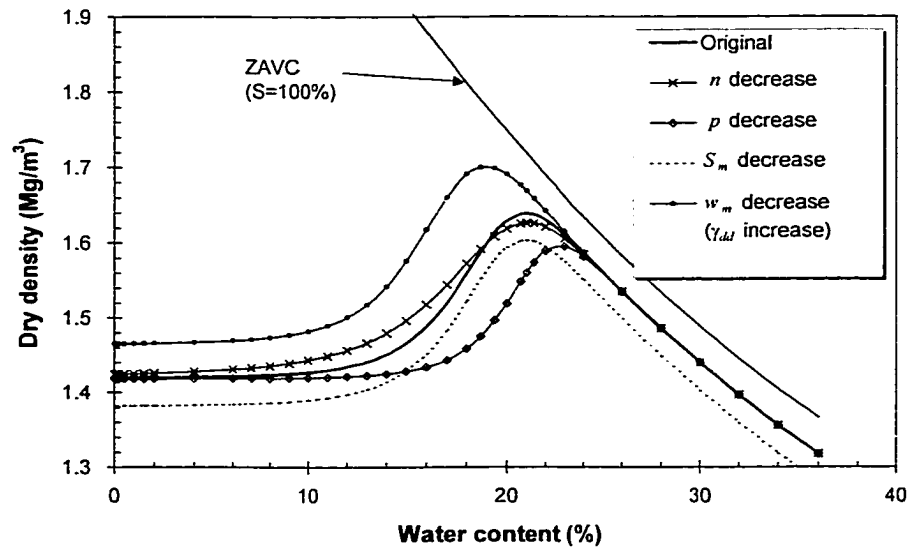


Figure 3-2 Characteristics of degree of saturation versus water content



**Figure 3-3 Parameters  $n$ ,  $p$ ,  $S_m$ , and  $w_m$  on the complete compaction**



**Figure 3-4 Particle size distribution of Syncrude overburden soils**

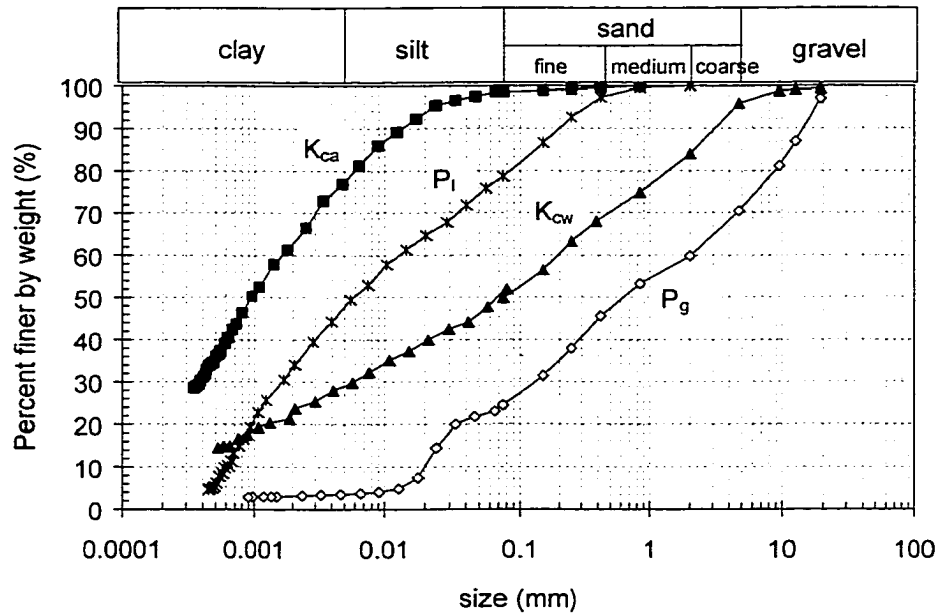


**Figure 3-5 Standard compaction test results of Syncrude overburden soils**

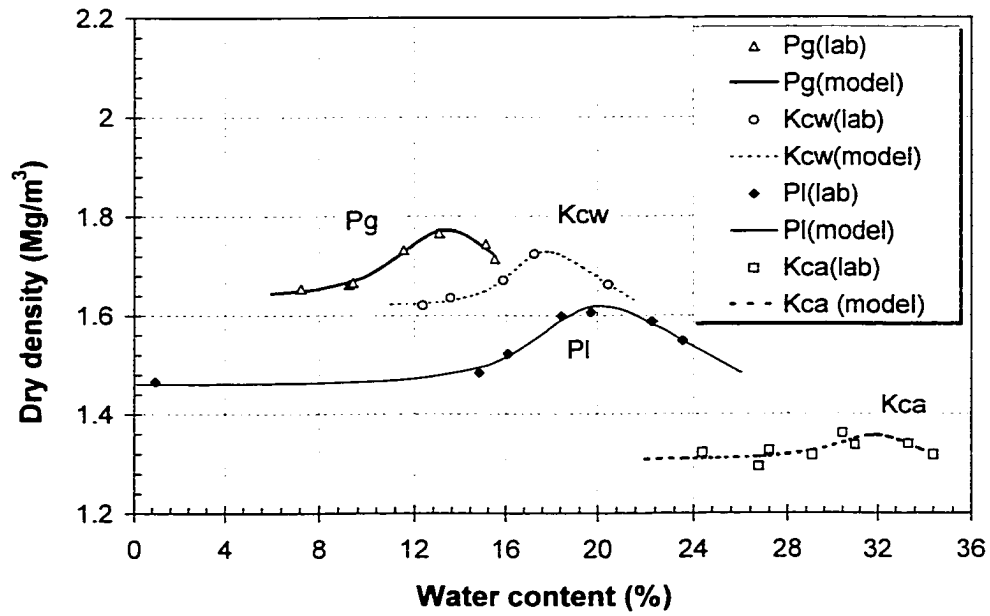


**Figure 3-6 Relationship between soil dry density at dry condition ( $\gamma_{dd}$ ) and average particle size ( $D_{50}$ )**

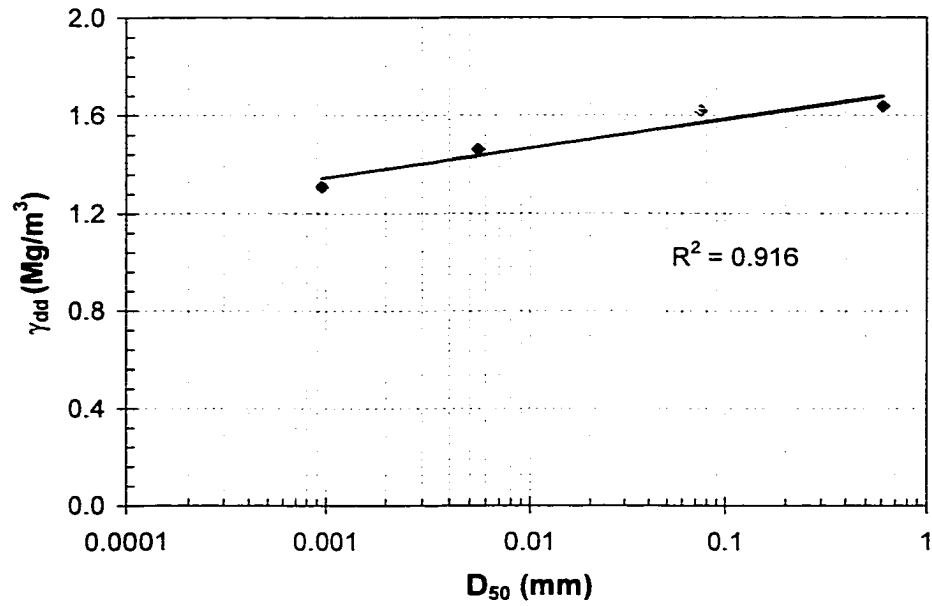


**Figure 3-7 Relationship between  $w_m$  and average particle size ( $D_{50}$ )**

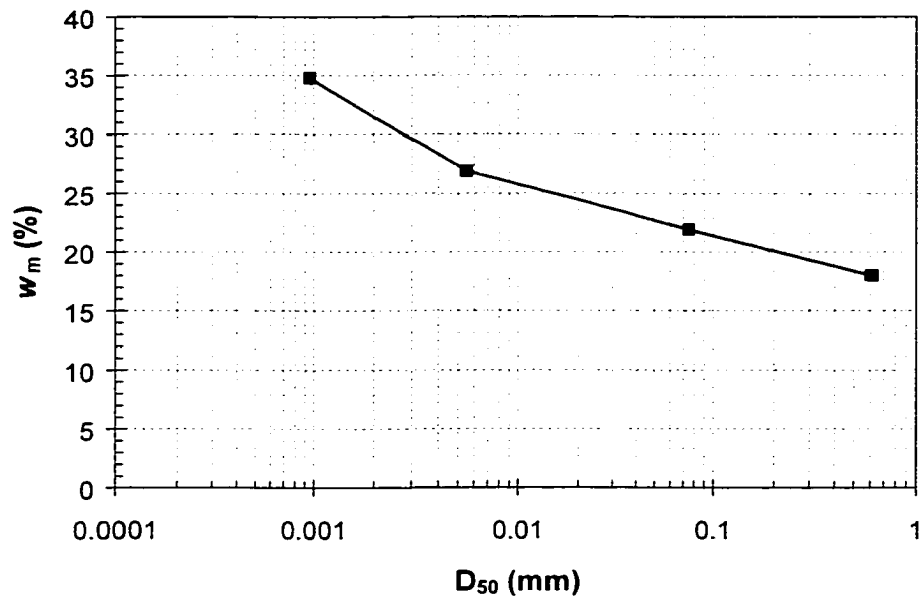


**Figure 3-8 Relationship between shape factor ( $n$ ) and soil uniformity coefficient ( $C_u=D_{60}/D_{10}$ )**

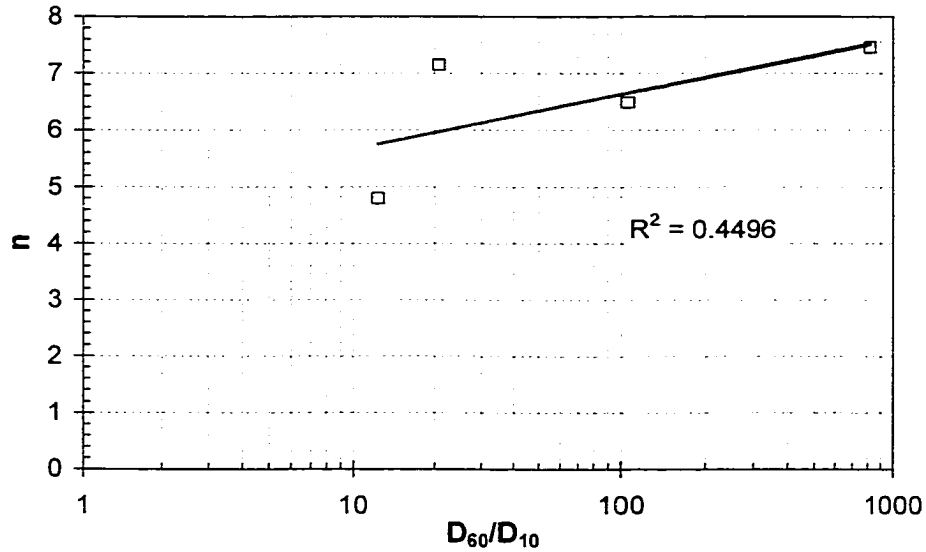
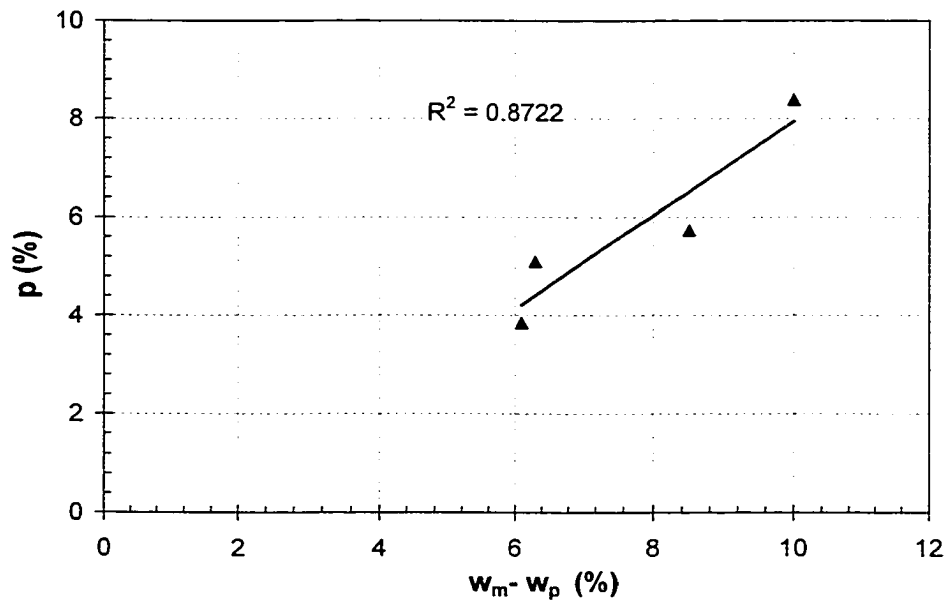


**Figure 3-9 Relationship between index of compactable moisture range ( $p$ ) and  $w_m - w_p$**



# CHAPTER 4 THE STRENGTH BEHAVIOR ALONG COMPLETE COMPACTION CURVES<sup>1</sup>

## 4.1 INTRODUCTION

For many civil engineering projects, soils have to be compacted to a denser state to improve their engineering behavior and properties. When a fine-grained soil is densified under a constant compactive effort but with varying water contents, a typical dry density versus water content relationship develops. Compaction curves of fine-grained soils are essential to establish practical and reliable criteria for effective field compaction control on most projects.

Much research on compaction has been carried out since the first paper by Proctor in 1933. Most laboratory and field tests programs focused on the physical properties of the soil near or at the maximum dry density, such as hydraulic conductivity, compressibility, and strength. Soil compacted at or near **optimum water content** (OWC) is of most interest for embankment design. Samples slightly wet of OWC generally achieve the lowest hydraulic conductivity, while samples slightly dry of OWC generate higher strength than when compacted at OWC (Mitchell 1976; Seed and Chan 1959; Leroueil et al. 1992).

A number of compaction tests over a wider range of water contents for fine-grained soils have been presented by Faure (1981) and Faure and Da Mata (1994). Their results show a nearly constant dry density on the dry side before the water content reaches an important point called the **compaction sensitivity threshold** (CST) (Fig. 4-1). Other evidence includes tests on heavy clay (Johnson and Sallberg 1960), tills and lacustrine

---

<sup>1</sup> A version of this paper was published in Proceedings of 53<sup>rd</sup> Canadian Geotechnical Conference, Montreal, Quebec.

material in New Brunswick (Saini and Chow 1984), clay liner of landfills (Benson et al. 1997; Daniel and Benson 1990), lacustrine clay from northern Alberta (Li and Sego 1998, 2000). Faure and Da Mata (1994) showed that the CST is a linear function of clay content and is linked to the clay mineralogy. How the CST relates to the compactive effort imparted to the soil is not fully understood at present.

The CST is an important location on the compaction curve like the optimum compaction point. Its location is critical to understanding the compaction mechanism over the whole moisture range. This study on the strength variation along the complete compaction curve enhances the understanding of the compaction mechanism and its impact on the design of earth structures.

Faure and Da Mata (1994) studied the strength along the complete compaction curve via triaxial and unconfined compression tests using samples of pure kaolinite or prepared as mixtures of fine sand and kaolinite. Their results showed that the unconfined compression strength reached the maximum at the CST. In triaxial tests, the samples had the maximum cohesion near the CST. The friction angle decreased linearly and slightly as the water content increased from zero to the CST, but beyond the CST, the friction angle decreased rapidly.

The objective of this chapter is to study the strength behaviors along the complete compaction curve. Two different soils, lacustrine clay and glacial till from Northern Alberta, were used in this study. The soils were compacted using the kneading compaction method over the complete water content range. Unconfined compression tests were conducted to determine the strength of the compacted sample. For an unsaturated compacted soil, the air-water surfaces create matric suction between particles. To understand its contribution to soil strength, matric suctions were measured using thermal conductivity sensors on samples prepared at different water contents.



## 4.2 REGIONS OF THE COMPLETE COMPACTION CURVE

With the existence of the compaction sensitivity threshold (CST) and the optimum water content (OWC), the complete compaction curve can be separated into three identifiable regions: namely, the dry region, the transition region (effective compaction region), and the wet region (wet of optimum region) (Fig. 4-1).

The dry region indicates the dominance of the air phase surrounding the soil particles. The air is continuous and the small portions of water are discontinuous. The sparse isolated water is not effective at lubricating the soil particles and the contribution from soil matric suction is very little due to the discontinuous water phase, thus the water has little or no influence on the soil compaction behavior. With increased water content, the water become effective at lubricating the soil particles in the transition region where it is believed the water becomes partially continuous. The suction within the soil helps to held soil clods together. The addition of water in this region helps at increasing the packing of soil particles. Therefore the transition region is also called the effective compaction region. Beyond the OWC, the water phase dominates and only small air bubbles are trapped. The water phase is fully continuous. The trapped air phase is discontinuous and has little effect on the soil behavior. The compacted sample in the wet region thus behaves as a saturated soil.

Figure 4-1 also illustrates the boundary conditions of a typical complete compaction curve. When the soil is in the very dry condition, the dry density of fine-grained soil is nearly constant ( $\gamma_{dd}$ ). The fact that the dry density remains constant ( $\gamma_{dd}$ ) is an important characteristic of fine-grained soils. It is also the boundary condition on the dry side of the complete compaction curve.

The soil compacted in the wet region is generally not completely saturated because a portion of the air trapped during compaction cannot escape. For a fine-grained soil, it is often found that the maximum degree of saturation ( $S_m$ ) remains constant (Seed et al. 1960; Lee and Haley 1968). In practice, one can find  $S_m$  from the wet side of a given

compaction curve which runs nearly parallel to the zero air void curve (ZAVC) (Woods 1938; Hausmann 1990).

### **4.3 MATERIALS AND TESTS**

Two natural soils, glacial till ( $P_g$ ) and Pleistocene lacustrine clay ( $P_l$ ), were used to carry out the compaction tests. The soils were acquired from overburden soils on the lease of Syncrude Canada Ltd., Fort McMurray, Alberta. Their basic physical properties are shown in Table 4-1. The soil was initially air-dried and then had a prescribed amount of water added prior to each sample being stored for at least 24 hours in the moisture room. Kneading compaction tests were carried out using a CS 1000 Electronic-Hydraulic Kneading Compactor. The soils were compacted in a 100-mm diameter mold using three layers. Each layer was subjected to 25 applications under a peak foot pressure of 700 kPa.

To minimize sample disturbance by sub-sampling from the compacted specimen, the whole sample was extruded from the mold and its strength was immediately determined using the conventional unconfined compression test procedure. Since the height to diameter ratio of the sample is about 1.15, plastic wrap along with grease was used to fabricate lubricated ends. Observation during the tests showed that the method was efficient in reducing end effects. The sample was deformed to failure using a deformation rate of 0.5mm/min while both the load and deformation were recorded throughout the test.

Matric suctions were measured using a thermal conductivity sensor. This method uses a measurement of the thermal conductivity of a specially designed ceramic block, which is correlated to the matric suction of the ceramic that achieves equilibrium with the surrounding soil (Fredlund et al. 1998). The sensor along with a constant current sink and amplifier was developed by the Unsaturated Soils Group of the University of Saskatchewan. The sensor was connected to a Campbell Scientific, Inc. CR10 data logger and multiplexer.

A schematic of the suction measurement is illustrated in Figure 4-2. The mold is 100 mm in diameter. The thermal conductivity sensor sits close to the bottom plate with a cable connected to the multiplexer through the bottom of the mold. The sensor was air dried before the test for at least two days. It was embedded by placing soil at prepared water content into the mold. To prevent moisture loss, the soil was covered with plastic wrap before the load cap was installed and sealed using tape. Water content measurements before and after the test showed that only small moisture loss occurred (about 0.2%) during the test.

The computer program automatically took the measurement every two hours by interacting with the data logger. Each time voltage and temperature from the sensor in the soil was recorded. The matric suction was then calculated using the calibration curve from the voltage and revised by the temperature. The aforementioned computer program and the calculation methods were all provided by the supplier of the sensor.

Initially the test was designed to measure the matric suction of soils prepared using pneumatic compaction method. However, the ceramic block could not withstand the applied compaction pressure of 700 kPa during preliminary tests. Therefore the measurement was only carried out for soils under a token pressures in the pneumatic compression apparatus. The influence of soil density on the matric suction will be discussed in later part of this chapter.

#### **4.4 VARIATION OF UNCONFINED COMPRESSION STRENGTHS WITH COMPACTION CURVE**

Compaction curves for the Pleistocene lacustrine clay  $P_1$  and the glacial till  $P_g$  are presented in Figures 4-3 and 4-4. From the complete compaction curve of lacustrine clay, the constant density on the dry side was  $1.44 \text{ Mg/m}^3$  (Fig. 4-3). The maximum dry density of  $1.68 \text{ Mg/m}^3$  was achieved at OWC of 19.1%. The water content at the CST was approximate 15.3%. The maximum dry density of compacted glacial till was 1.85

Mg/m<sup>3</sup> at OWC of 13.0% (Fig. 4-4). Its compaction curve showed a slight increase of dry density on the dry side. The dry density increased rapidly after the water content reached 8.4%, which is considered to be CST.

The variation of unconfined compression strength (UCS) with water content is also shown in the Figures 4-3 and 4-4. Compressive stress versus strain curves for each unconfined compression test is shown in Figures 4-5 and 4-6. The initial axial strain for glacial till P<sub>g</sub> at 8.5% and 15.5% were adjusted because the samples were reloaded after electronic problems were discovered during the first few minutes of the test. The correction was based on the previous loading time. The unconfined compression strength was determined using the maximum compression stress. For two samples of P<sub>l</sub> tested on the wet side of OWC, the strengths were chosen at an axial strain 10% due to observation of bulging failure (Fig. 4-5).

The driest samples on the dry side of the compaction curve (3.3% for P<sub>l</sub> and 0.9% for P<sub>g</sub>) could not be tested because the samples fell apart as they were extruded from the compaction mold, so their strengths were recorded as zero (Fig. 4-3 and 4-4). When the water contents were very high, the strength was again low. The greatest strengths were achieved near the middle of the effective compaction region. The maximum strength for the lacustrine clay P<sub>l</sub> was 322 kPa at the water content of 17.2%, and the maximum strength for the glacial till P<sub>g</sub> was 238 kPa at 10.5% water content. Both these tests occurred near the water content midway between CST and OWC for the individual soil.

It is interesting to observe that the plots of strength versus water content for both soils have a similar curvature to their compaction curves around the CST point. It indicates the direct influence on soil strength from the soil dry density. The coincidence implies that important change takes place at the CST and its relationship with the soil properties and compaction effort are of fundamental interest (Li and Segoo 2000b).

These results differs from Faure and Da Mata's results in 1994 where the maximum strength occurred at a water content close to CST for both soils tested: one was prepared

by mixing 69% fine sand and 31% kaolinite (FK31) and the other was pure kaolinite (K0). The difference may be due to difference in compaction method or compression test. In their compaction tests, samples were compacted by drop-hammer in a smaller mold (70-mm diameter and 78-mm high). In compression test, both test samples have a height to diameter ratio less than 2, but no report on using grease and plastic wrap to decrease the end friction was presented by Faure and Da Mata (1994).

The Young's moduli from Figures 4-5 and 4-6 also show the importance of the mid-point between CST and OWC. The modulus of the lacustrine clay  $P_1$  remains virtually unchanged before 17.2% water content, as does the glacial till  $P_g$  before 10.6% water content. The slope of the stress-strain curves decreased for samples tested at higher water contents. Significant differences in stress-strain behavior can be observed in the samples compacted at OWC, which showed more plastic deformation. The arrangements of the soil particles (soil structure) begin to change from the mid-point. After OWC, the soil clods are largely destroyed and the compacted sample will produce the greater degree of particle orientation (Lambe 1958). The modulus after OWC is substantially lower.

#### **4.5 MEASUREMENT OF MATRIC SUCTION AND ANALYSIS**

Since compacted soils are unsaturated soils, matric suction can have an important contribution to their compressive strength. Therefore measuring the suction can be useful in understanding the strength behavior of compacted soils and the mechanisms at work during compaction.

Figure 4-7 shows the measurements of matric suction versus water content for soil  $P_1$  and  $P_g$ . The soils were mixed to the specified water content and loose-filled into the compaction mold. Both results were fitted using a semi-log linear relationship giving the equations presented in the figures. The results agree with the findings of Marinho and Chandler (1993), Juca (1993), Tsai and Petry (1995), and Ridley and Perez-Romero (1998) who found a linear relationship between water content and the logarithm of matric suction within compacted samples.

Previous studies reported in the literature show that at low water contents (generally dry of OWC), the density has no influence on the measured suction (Li 1996; Ridley and Perez-Romero 1998). Consequently, the measurement of matric suction in the loose condition in this study should be comparable with those after compaction. This is probably because changes in density are concentrated in air-filled parts of soil, while the smaller water-filled pores remain unaffected. However, as the water content increase to OWC, the matric suction would be affected by the dry density as shown by Delage and Graham (1996). Higher plastic clays are more sensitive to changes in suction because they contain more deformable aggregates.

In Figure 4-7, the suction of 700 kPa for Pleistocene lacustrine clay ( $P_l$ ) and glacial till ( $P_g$ ) were achieved at water contents of 15.3% and 8.4%. These values coincide with the water contents at the CST in Figures 4-3 and 4-4. The compaction foot pressure used in the tests was also 700 kPa. This suggests that the CST is the water content when the soil matric suction equals the externally applied pressure. This finding indicates that **effective compaction (after CST) can only be achieved when external applied stress overcomes the internal soil matric suction.**

This observation is very interesting and the following explanation is presented. Considering that the soil was originally air-dried, the matric suction was very high at the beginning and greater than the compaction pressure (700 kPa in this case). The matric suction helps to hold the particles together as clods. When the compaction stress of 700 kPa was applied at water content less than CST, the external applied pressure was less than the value of the matric suction, and therefore the clods were not broken. The clods could only be rearranged but with little volume compression, which means a constant or small increase in dry density. As more water was added to the soil, the matric suction of the mixed soil decreased until it reached 700 kPa or less, where the applied compactive effort can now break the clods. The breaking of the clods would eliminate some macro internal pores and thus increase the dry density of the compacted soils. Therefore, the curvature of the compaction curve around the CST becomes apparent.

The previous finding suggests both the soil type and the applied compactive effort will influence the water content at CST. When compactive effort increases, the soil would be effectively compacted at a greater value of matric suction, which means a smaller water content at CST. This agrees with the observation that the compaction curve moves up and to the left under higher compactive effort (Seed and Chan 1959; Lee and Haley 1968). When comparing a finer material (e.g. clay) with a coarser material (e.g. silt), the water content at a certain level of suction (e.g. 700 kPa) for clay is higher than that for silt (Fredlund 1996). This indicates that, for the same compactive effort, the water content at CST for the clay is greater than that for the silt. It agrees well with the results in this test program that the suction of 700 kPa occurs for the lacustrine clay ( $P_l$ ) at water content of 15.3% while for the glacial till ( $P_g$ ) it is 8.4%. The results from Faure and Da Mata (1994) also support this finding. In Figure 2-17 of Chapter 2, the sample with more clay content (e.g. K0 or 100% kaolinite) has greater water content at CST than samples with less clay contents (e.g. FK73 or 73% kaolinite, and FK 31 or 31% kaolinite).

#### 4.6 APPLICATIONS

The maximum unconfined compressive strength and the modulus is important for road construction, where the strength and Young's modulus (stiffness) control the design. The mid- point between CST and OWC indicates there is a limit for the strength increase on the dry side of OWC. Young's modulus begins to decrease beyond the mid-point between CST and OWC.

With the greatest strength occurring for a sample compacted at the mid-point between CST and OWC compared with the sample compacted at OWC, the potential for wetting collapse of soils prepared at the mid-point is also greater. This could be overcome by chemical additives, which are designed to repel water. The embankment designer must balance the need for increased strength and stiffness against the potential for wetting collapse.

The location of the CST turned out to be another critical point on the compaction curves. Matric suction measurement can help to locate CST, which is important for determination of the effective compaction region and the water content with the maximum compressive strength.

#### **4.7 CONCLUSIONS**

Complete profiles of unconfined compression strength along the complete compaction curves were studied. The strength shows a significant increase at the point of the compaction sensitivity threshold (CST) where the dry density of the compacted soil also increases substantially. The strength reached a maximum midway between CST and OWC, and then the strength and Young's modulus decreased.

The location of CST turned out to be another critical point on the compaction curves. The CST appears to occur where the compactive effort (stress) exceeds the matric suction of the soil. This explains why the CST changes with compactive effort and soil type. Matric suction measurement can help to locate CST, which is important for determination of the effective compaction region and the water content with the maximum compressive strength.

#### **4.8 REFERENCES**

- Benson, C.H., Gunter, J.A., Boutwell, G.P., Trautwein, S.J. and Berzanskis, P.H. 1997. Comparison of four methods to assess hydraulic conductivity. *ASCE Journal of Geotechnical and Geoenvironmental Engineering*, 123(10): 929-937.
- Daniel, D.E. and Benson, C.H. 1990. Water content-density criteria for compacted soil liners. *ASCE Journal of Geotechnical Engineering*, 116(12): 1811-1830.
- Delage, P. and Graham, J. 1996. Mechanical behaviour of unsaturated soils: Understanding the behaviour of unsaturated soils requires reliable conceptual models.



- Unsaturated Soils, Alonso, E.E. and Delage, P. (Eds), Balkema, Rotterdam, pp. 1223-1256.
- Faure, A.G. 1981. A new conception of the plastic and liquid limits of clays. *Soil and Tillage Research*, 1: 97-105.
- Faure, A.G. and Da Mata, J.D.V. 1994. Penetration resistance value along compaction curves. *ASCE Journal of Geotechnical Engineering*, 20: 46-59.
- Fredlund, D.G. 1996. The scope of unsaturated soil mechanics: An overview. Keynote Address, *Unsaturated Soils*, Alonso, E.E. and Delage, P. (Eds), Balkema, Rotterdam, pp. 1155-1178.
- Fredlund, D.G., Shuai, F., Yazdani, J. and Feng, M. 1998. Recent developments on a sensor for the insitu measurement of matric suction. *In Proceedings of 51 Canadian Geotechnical Conference*, Edmonton, Vol. 1: 81-86.
- Hausmann, M.R. 1990. *Engineering Principles of Ground Modification*, McGraw-Hill Inc., New York, pp. 14-56.
- Johnson, A.W. and Sallberg, J.R. 1960. Factors that influence field compaction of soils. *Highway Research Board Bulletin 272*, Highway Research Board, National Research Council, Washington, D.C.
- Juca, J.F.T. 1993. Flow properties of unsaturated soils under controlled suction. *Unsaturated Soils*, ASCE Geotechnical Special Publication No. 39, S.L. Houston and W.K. Wray (Eds.).
- Lambe, T.W. 1958a. The structure of compacted clay. *ASCE Journal of Soil Mechanics and Foundation Division*, 84(SM2): 1654-1 to -34.
- Lee, K.L. and Haley, S.C. 1968. Strength of compacted clay at high pressure. *ASCE Journal of Soil Mechanics and Foundation Division*, 94(SM1): 1303-1332.
- Leroueil, S., Le Bihan, J.P., and Bouchard, R. 1992. Remarks on the design of clay liners used in lagoons as hydraulic barriers. *Canadian Geotechnical Journal*, 29: 512-515.
- Li, H. and Sego, D.C. 1998. Prediction complete compaction curves of fine-grained soil. *In proceedings of 51st Canadian Geotechnical Conference*, Edmonton, Alberta, Canada, October 4-7, 1998. Vol. 2: 679-686.
- Li, H. and Sego, D. C. 2000a. Equation for complete compaction curve of fine-grained soils and its applications. *Constructing and Controlling Compaction of Earth Fills*,

- ASTM STP 1384, Shanklin, D.W., Rademacher, K.R., and Talbot, J.R. (Eds.), American Society for Testing and Materials, West Conshohocken, PA. pp. 113-125.
- Li, H. and Sego, D. C. 2000b. Equation for compaction curve of fine-grained soils: its origin, implementation and application. Submitted to Canadian Geotechnical Journal.
- Li, Z.M. 1996. Compressibility and collapsibility of compacted unsaturated loessial soils. *Unsaturated Soils*, Alonso, E.E. and Delage, P. (Eds), Balkema, Rotterdam, pp. 139-144.
- Marinho, F.A.M. and Chandler, R.J. 1993. Aspects of the behavior of clays on drying. *Unsaturated Soils*, ASCE Geotechnical Special Publication No. 39, S.L. Houston and W.K. Wray (Eds).
- Mitchell, J.K. 1976. **Fundamentals of Soil Behavior**, John Wiley & Sons, Inc., New York, N.Y., 422p.
- Proctor, R.R. 1933. The design and construction of rolled earth dams. *Engineering News Record* III, August 31, Sept. 7, 21, and 28.
- Ridley, A.M. and Perez-Romero, J. 1998. Suction-water content relationships for a range of compacted soils. *In Proceedings of the Second International Conference on Unsaturated Soils*, Beijing, China, Vol. 1, pp. 114-118.
- Saini, G.R. and Chow, T.L. 1984. Compactability indexes of some agricultural soils of New Brunswick, Canada. *Soil Science*, 137: 33-38.
- Seed, H.B. and Chan, C.K. 1959. Structure and strength characteristics of compacted clays. *ASCE Journal of Soil Mechanics and Foundation Division*, 85(SM5), pp. 87-128.
- Seed, H.B., Mitchell, J.K. and Chan, C.K. 1960. The strength of compacted cohesive soils. *Research Conference on Shear Strength of Cohesive Soils*, ASCE, pp. 877-964.
- Tsai, C.H. and Petry, T.M. 1995. Suction study on compacted clay using three measurement methods. *Transportation Research Record* No. 1481. Transportation Research Board, National Research Council, Washington, D.C., pp. 28-34.
- Woods, K.B. et al. 1938. Compaction of earth embankments. *In Proceeding of Highway Research Board*, Washington, 18(2): 155.

**Table 4-1 Properties of tested Syncrude overburden soils**

Soil types	Specific gravity ( $G_s$ )	Plastic limit (%)	Liquid limit (%)	Plastic Index (%)	Particle size fraction
$P_1^*$	2.61 <sup>†</sup>	23.5	39.7	16.2	sand 13%, silt 37%, clay 49%
$P_g$	2.54 <sup>†</sup>	12.7	22.2	9.5	gravel 16%, sand 37%, silt 30%, clay 17%

\* The properties of the material ( $P_1$ ) used here differs from the material tested in Chapters 2 and 3, which was obtained three years earlier.

† Low specific gravity is caused by dry grass roots in  $P_1$  and trace of bitumen found in  $P_g$ .

**Figure 4-1 Complete compaction curve for fine-grained soils**

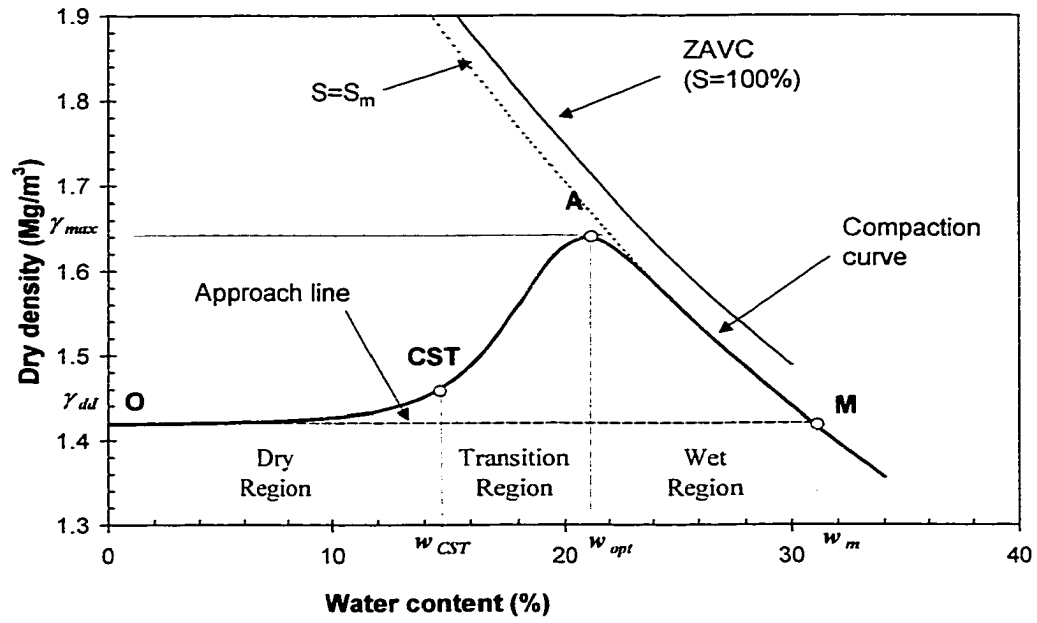


**Figure 4-2 A schematic of general arrangement for measurement of matric suction**

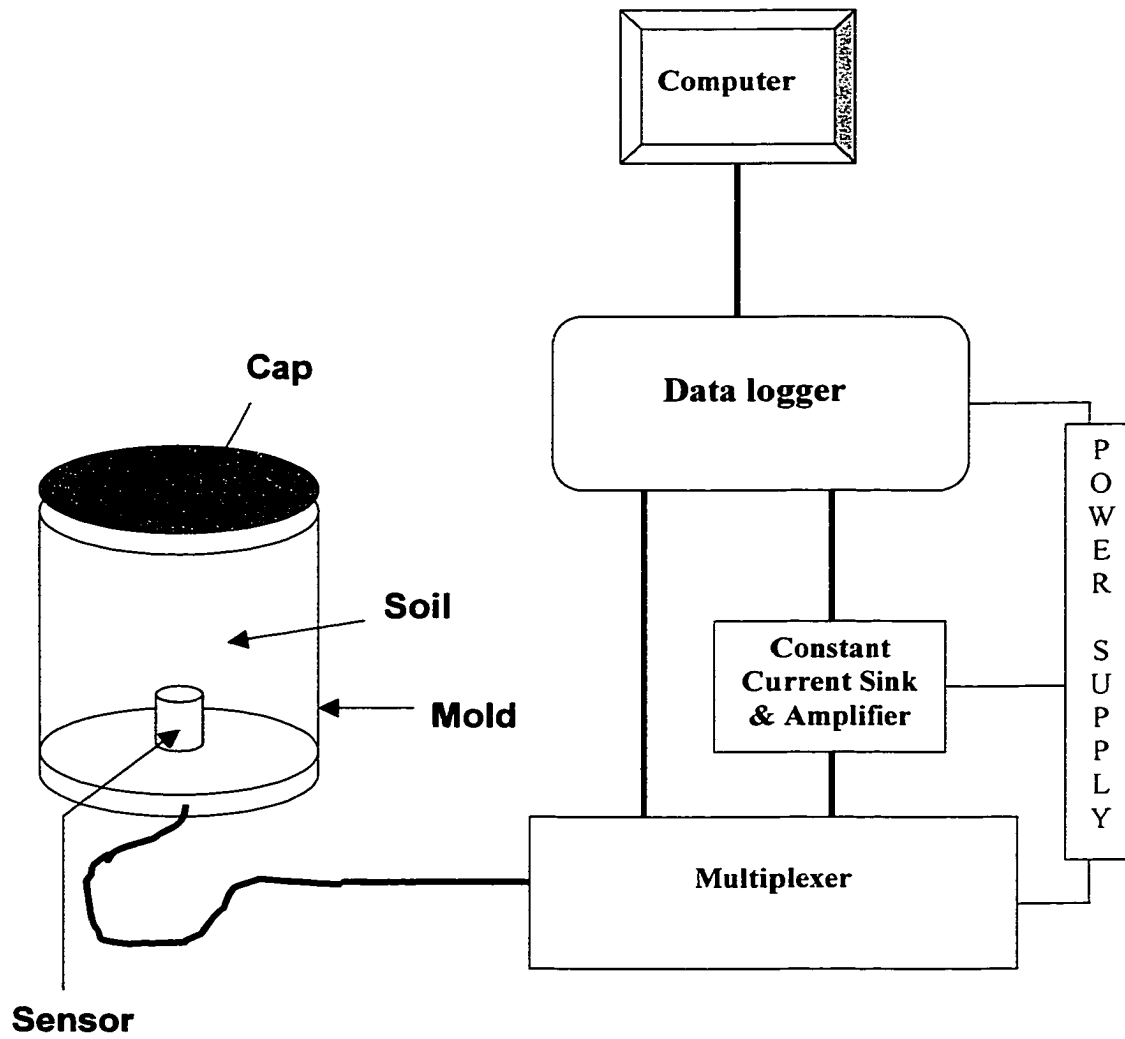


**Figure 4-3 Complete compaction curve and unconfined compression strength (UCS) for Pleistocene lacustrine clay (P<sub>l</sub>)**

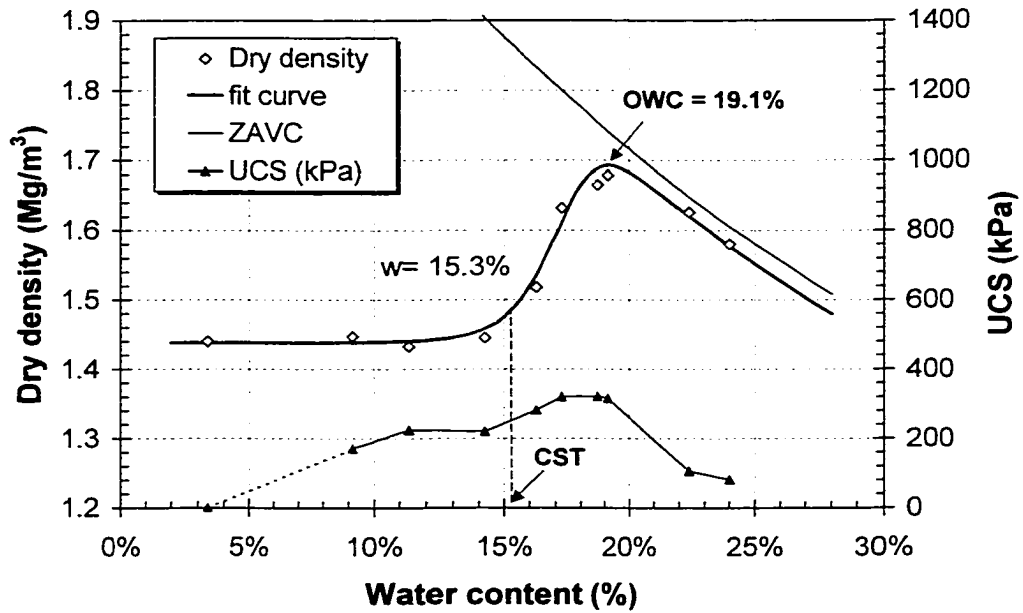


**Figure 4-4 Complete compaction curve and unconfined compression strength (UCS) for glacial till (P<sub>g</sub>)**

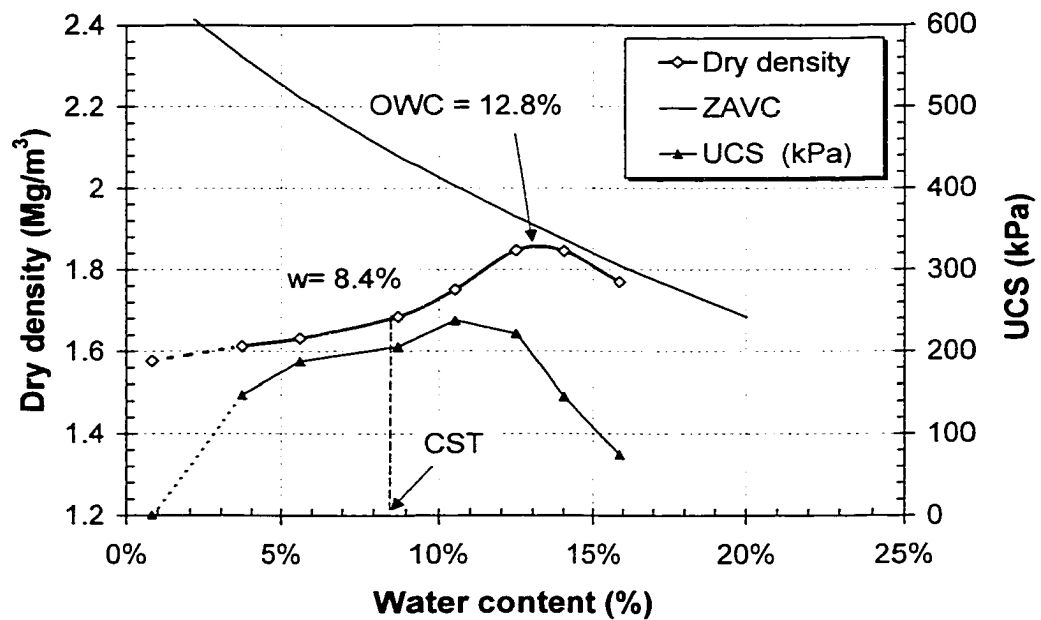


**Figure 4-5 Stress - strain curve in unconfined compression test for Pleistocene lacustrine clay ( $P_l$ )**

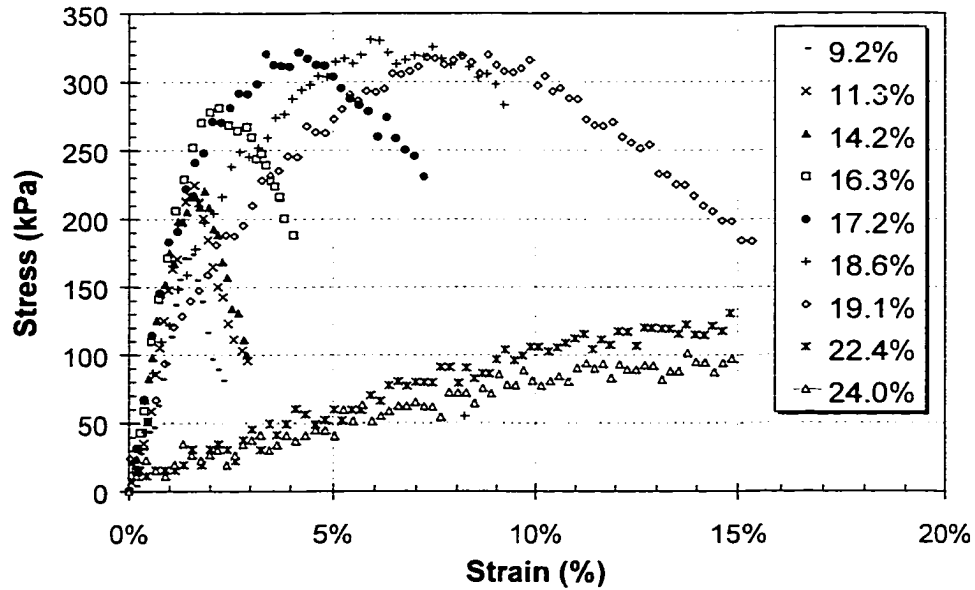


**Figure 4-6 Stress - strain curve in unconfined compression test for glacial till ( $P_g$ )**

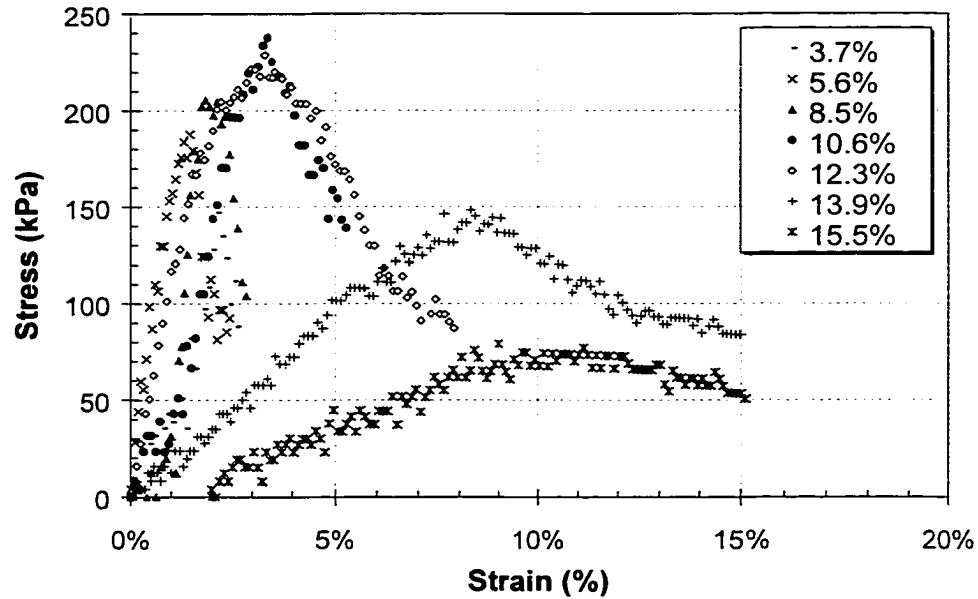
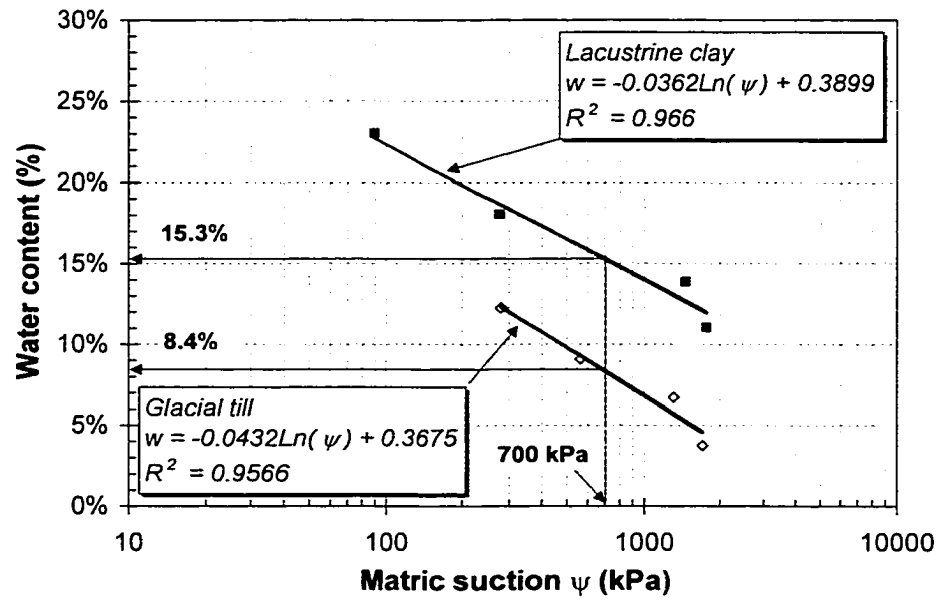


**Figure 4-7 Relationship between matric suction and mixed water content for Pleistocene lacustrine clay (P<sub>l</sub>) and glacial till (P<sub>g</sub>)**





# **CHAPTER 5 THE EVOLUTION OF PARTICLE SIZE DISTRIBUTION DUE TO WEATHERING WITH UNIFORM FRAGMENTATION**

## **5.1 INTRODUCTION**

The particle size distribution (PSD) is one of the most important and frequently used physical properties of soil. It has major influence on many other soil properties such as plastic limit, liquid limit, and other engineering behaviors such as the compaction curve, compression and consolidation behavior, strength, and stress and strain relationship.

The particle size distribution can provide an indication of a soil's history (McCarthy 1988). It is a product of a series of complicated natural processes and human activities such as weathering, loading, erosion, movement of water, wind or glacial, and blasting. It is obvious that no simple model can be found to describe the whole processes. Further, even each of the processes would not be a simple procedure, e.g. weathering (Ollier 1984).

However, the evolution of particle size distribution is of interest theoretically and from a practical engineering perspective. Previous researchers have unveiled that some rules can be used to describe these natural processes mathematically. For example, particle crushing or blasting of rocks follows a scale-invariant process that is widely referred as fractal (Mandelbrot 1982; McDowell and Bolton 1996; Gimenez et al. 1997; Turcotte 1997). For residual soils, their particle sizes constantly decrease with time as the particles continue to break down due to weathering in situ.

Based on the discussion in Chapter 2, there are two types of family of compaction curves, Type A and Type B. Type B family of compaction curves is created when different compactive efforts are applied to the same soil. The same shape of compaction curves is

believed to be due to the increased energy being applied to the same soil used during the test. Type A family of compaction curves is usually found in borrowed sites of residual soils and alluvial deposit. These curves are obtained when using the same compaction method and effort to compact the samples obtained from a borrowed site with different particle size distributions. Since the PSD of the samples are different, the explanation about why a Type A family of compaction curves exists is a challenge and has not been well studied.

The objective of this chapter is to theoretically simulate the evolution of PSD due to weathering for residual soils and to explain the origin of Type A family of compaction curves. The concept of uniform fragmentation is first introduced to model the weathering process. A general analysis method is then described to calculate the evolution of the PSD. The analyzed results evolved using uniform fragmentation are used to explain the existence of a family of compaction curves for residual soils.

## **5.2 WEATHERING EFFECT ON A SINGLE PARTICLE – UNIFORM FRAGMENTATION**

Weathering is the breakdown and alteration of materials near the earth's surface to products that are more in equilibrium with newly imposed physio-chemical condition (Ollier 1984). Many rocks were originally formed at high temperature, high pressure and in the absence of air and water, and a large part of weathering is, in fact, a response to low temperatures, low pressures, and the presence of air and water. The actual weathering phenomena of rocks are very complicated since many kinds of alteration are possible. It includes the influences from variation of water, air, temperature, and the rock property itself. Rocks from the same origin and area may suffer different stages of weathering depending on their location relative to the earth's surface.

Little effort has been made to describe the weathering process mathematically. Fukumoto (1990) studied one of the typical residual soils from decomposed granite.

With the assumption of constant retained percentage of soil grains under each cycle of weathering, a discrete equation for the weathering process was proposed. The equation was used to describe the PSD curve of various soils, but was not used to model the evolution of the curve during the weathering process. The discrete form of the equation is difficult to apply and was then modified and replaced with a continuous equation (Fukumoto 1994). However, the new equation is a pure empirical fitting equation that offers no physical explanation for the assumptions used.

The geometric degrading process of a large block of rock due to weathering can be assumed to follow uniform fragmentation. This is considered to be close to the weathering effects because it assumes that the probability of breakage of a given particle in a given time is proportional to its particle size.

The simplest possible model of a random fragmentation is the unit segment that splits into smaller segments of random numbers. If the density of these random numbers is constant (i.e. Poisson distribution), their probability is linear with the segment  $r$  in the unit segment (Fig. 5-1). This kind of random fragmentation is called uniform fragmentation (Tenchov and Yanev 1986). Uniform fragmentation means the probability of breakage of a given particle is proportional to the size of the particle. After the  $n$ th cycles of fragmentation, the integral probability of the fragment size  $r$  in the unit segment (represented using percent finer  $P(r)$ ) is obtained by induction from Tenchov and Yanev (1986) as follows:

$$[5-1] \quad P(r) = 1 - (1 - r)^n$$

If considering a spherical particle with original diameter  $D$ , the relative particle size after the  $n$ th cycle of fragmentation is  $x/D$  in Fig. 5-1, where  $x$  is the current particle size. The probability of particles less than a particle size  $x$  (or percentage finer than diameter  $x$ ) will be

$$[5-2] \quad P(x) = 1 - \left(1 - \frac{x}{D}\right)^n$$

With an increase in the number of fragmentations, Equation 5-2 moves asymptotically into the exponential distribution (i.e.  $n \rightarrow \infty$ ), which would be the same partial set of the Weibull distribution.

$$[5-3] \quad P(x) = 1 - e^{-\frac{x}{D}}$$

The Weibull distribution is a lognormal distribution that is widely used in particle size distribution of fine natural materials, such as clay. The concept of uniform fragmentation that indicates the existence of lognormal distribution for the finest soils agrees with this fact. Epstein (1946) showed, using the Central Limit Theorem, that any initial particle distribution, no matter how skewed, eventually tends to a lognormal distribution.

### **5.3 GENERAL ANALYSIS METHOD ON EVOLUTION OF PARTICLE SIZE DISTRIBUTION**

Based on the evolution equation discussed above, a method to calculate new particle size distributions after weathering can be developed. Assuming the original particle size distribution is described with a function  $f(x)$ , the weight frequency at particle size  $x$  is therefore  $f'(x)$  or  $\frac{df(x)}{dx}$ . The amount by weight at size  $x$  that undergoes the evolution in a small segment  $dx$  is then  $f'(x) dx$ .

$P(x)$  in Equation 5-2 is a function representing the evolving percentage at the grain size  $x$  after a certain evolution from the original size  $D$ . For a particle at size  $z$  which is larger than  $x$ , after evolution, it may be weathered into many smaller size of particles including some pieces of segments less than size  $x$ . The finer percentage at size  $x$  contributed by

size  $z$  is now designated by the symbol  $P(x, z)$ , where  $x < z$ . The total percentage should be 100% at  $z$  if without any loss of weight during the evolution, i.e.  $P(z, z) = 1$ .

After evolution, the new percentage of the particle size at  $x$  should consist of two sources. For a given grain size originally smaller than size  $x$ , the evolving particle sizes are still smaller than  $x$  (which only changes to even smaller size). Therefore the total contribution from the smaller size part to new percentage is kept as  $f(x)$ .

For a given particle size originally larger than  $x$ , say  $z$ , some of the particles would be decreased to a size at  $x$  or less due to weathering, crushing, or other reasons. According to the evolution function  $P(x, z)$ , the percent contribution from size  $z$  would be  $f'(z) \cdot P(x, z)$ . Therefore the contribution from the larger size part ( $z > x$ ) is integration from the  $z$  to its upper limit, i.e.

$$\int_x^a f'(z) \cdot P(x, z) \cdot dz$$

The evolving new particle size distribution (PSD) can be obtained from contributions of the above two sources as follows:

$$[5-4] \quad f_{new}(x) = f(x) + \int_x^a f'(z) \cdot P(x, z) \cdot dz$$

Equation 5-4 is the general equation to calculate any kind of evolution of PSD. The method requires its original function of PSD (i.e.  $f(x)$ ) and evolving function  $P(x, z)$  from geological or human activities such as weathering or crushing.  $f(x)$  can be easily obtained by fitting the existing PSD using various existing equations (Fukumoto 1994). However  $P(x, z)$  has to be assumed based on the characteristics of the natural or human activities. For example, sudden blasting would usually separate a block of rock into a fractal PSD (i.e. power law), and ideal weathering could be modeled using concept of the uniform fragmentation described in the previous section.

#### 5.4 CALCULATING THE EVOLUTION OF PARTICLE SIZE DISTRIBUTION DUE TO WEATHERING WITH UNIFORM FRAGMENTATION

With the development of Equation 5-4, one can calculate any new evolving PSD, i.e.  $f_{new}(x)$  based on an evolving function  $P(x, z)$ . For weathering with uniform fragmentation, particle size distributions with different initial particle sizes can be calculated based on the Equation 5-2 and 5-4.

Figure 5-2 shows the evolution of the PSD originally with a log-linear form, which is commonly used in laboratory tests. The distribution can be mathematically represented as

$$[5-5] \quad f(x) = \frac{\log_{10}\left(\frac{x}{a}\right)}{\log_{10}\left(\frac{b}{a}\right)} = \frac{\ln\left(\frac{x}{a}\right)}{\ln\left(\frac{b}{a}\right)}$$

where  $a$  and  $b$  are the lower and upper limits of particle sizes respectively. In this case, it is seen that  $b = 1$  and  $a = 10$  in Fig. 5-2.

The calculation is separated into two parts. When considering the size smaller than  $a$ , the contribution of particle size is from the particles from all ranges from  $b$  to  $a$ . When considering the percentage at a particle size greater than  $a$ , the concept in Equation 5-4 is used during the derivation. Therefore, the equation used in this case is:

$$[5-6] \quad \left\{ \begin{array}{l} f_{new}(x) = \frac{\ln\left(\frac{x}{a}\right)}{\ln\left(\frac{b}{a}\right)} + \int_x^b \frac{1}{\ln\left(\frac{b}{a}\right)} \cdot \frac{1}{z} \cdot \left[1 - \left(1 - \frac{x}{z}\right)^n\right] dz \quad \text{when } a < x < b \\ \\ f_{new}(x) = \int_a^b \frac{1}{\ln\left(\frac{b}{a}\right)} \cdot \frac{1}{z} \cdot \left[1 - \left(1 - \frac{x}{z}\right)^n\right] dz \quad \text{when } x < a \end{array} \right.$$

The evolving curves from cycle 1 to cycle 16 of uniform fragmentation are shown in Fig. 5-2. The curves move parallel to smaller size except during the first cycle.

Another example using an original distribution of a power-law is shown in Fig. 5-3, which is commonly found in gravel materials. The power-law (or fractal) relationship is easily formulated as following Equation 5-7.

$$[5-7] \quad f(x) = \left(\frac{x}{D}\right)^m$$

where  $D$  is the original maximum particle size and  $m$  is the power index. According Equation 5-4, the new equation for evolved PSD is derived.

$$[5-8] \quad f_{new}(x) = \left(\frac{x}{D}\right)^m + \int_x^D \frac{m}{D} \cdot \left(\frac{z}{D}\right)^{m-1} \cdot \left[1 - \left(1 - \frac{x}{z}\right)^n\right] dz \quad x < D$$

Again assuming the cycle  $n$  from 1 to 16, the evolving PSDs again shows a series of parallel curves in Fig. 5-3. In this case, the original maximum particle size  $D$  equals 10 mm and the parameter of power index  $m$  is 0.5.

It is important to note that there are no analytical solutions for both Equation 5-6 and 5-8 at the moment. However, all results shown in Fig. 5-2 and 5-3 are easily obtained using spreadsheets or commercial mathematical software such as Maple<sup>1</sup>.

These predicted parallel PSD curves agree with the results shown by Fukumoto (1990) on decomposed granite soils. The PSDs shown by Nishida (1963), as shown in Fukumoto 1990) and Gardner (1994) displayed the same feature, when soils at different depths receive different amount of weathering.

Yamaguchi et al. (1988) studied the weathering evolution of PSD for mudstone using drying and wetting cycles. The results are shown in Figure 5-4. The particle sizes in the test continuously decreased for each cycle. More interesting and important is that the measured curves at each cycle are generally parallel to each other.

Many construction projects use alluvial deposits. It is not difficult to find a series of parallel PSD curves for gravel, sand and silt in practical cases (Fukumoto 1993). Figure 5-5 shows the distribution curves of construction materials used in a road construction project (Sego and Li 1999). The bank clay and sand were obtained from the same borrowed site of alluvial deposits. Their PSD curves are parallel in their maximum slope and do not cross each other. To compare with these two natural soil curves, the PSD curves of two artificial products (wood fly ash and crushed gravel) are not parallel to natural PSD curves and cross over the curve of the sand.

It is obvious that the alluvial deposits have different geological history when compared to residual soils. Water flow carries the soil particles depending on its velocity. The weight of the particles (third order of particle size) is proportional to the square of the flow velocity. Once the flow slows down, the larger sizes settle first, and then smaller particles follow. However how the parallel PSD curves of the alluvial deposits develop is not fully understood.



Nevertheless, the same parallel features of both residual and alluvial soils suggest that the uniform fragmentation is an appropriate function for describing the evolving of their particle sizes. And the parallel feature of PSD is the major reason for the existence of a family of compaction curves in both residual and alluvial soils, which will be discussed in next section.

It is understood that the geological process is not as simple as a single expression. Both uniform fragmentation model and fractal model are ideal models. Each model represents an extreme condition in terms of time scale. The uniform fragmentation represents quite a long geological time during weathering, while fractal describes the particle change in a very short period, such as blasting. Most evolution of PSD in natural or human activities would be sort of a combination of these two models. Therefore, the two ideal models provide a useful approach in studying the soil's history through the evolution of the PSD of the soil.

## **5.5 RELATIONSHIP BETWEEN PARALLEL PARTICLE SIZE DISTRIBUTIONS AND THE FAMILY OF COMPACTION CURVES**

A larger number of compaction curves from the same geological origin obtained using the same compaction method may produce a family of similar curves (Woods 1938). The necessary relationship exists most often when residual soils have been formed in place from the weathering of the parent rock materials. Alluvial materials in flood plains exhibit these same relationships if they are derived from materials that have a common geological origin (Shanklin 1999). The curves in the family of PSD do not cross each other and usually are evenly spaced. These behavior create the bases of one-point compaction test method in earth work control in the field, which is widely used in practice and adopted by AASHTO and ASTM as their recommend methods (Joslin 1959; AASHTO 1990; Shanklin 1999).

A large amount of data collected by Woods (1938) on 1,383 Ohio soils is illustrated in Fig. 5-6. The soils were collected in similar geological region and represents Type A

family of compaction curves as defined in Chapter 2. The average curves are evenly spaced and are all rather similar in shape.

According to the study on the compaction curve reported in Chapter 2, the shape of compaction curve can be defined using the shape factor  $n$  in Equation 2-6 and 2-7. Based on the discussion in Chapter 3, it is found that the shape factor  $n$  can be related to the soil uniformity coefficient  $C_u$  (equal to  $D_{60}/D_{10}$ ) of the soil particle size distribution. Since  $C_u$  is the same for all parallel PSD curves, the related shape factor,  $n$ , of its represented compaction curve is also the same. Therefore, the family of compaction curves with the similar shape will be developed.

This study explains why the compaction curves of residual soils are evenly separated and would not cross each other within a particular borrow site. The fact that the PSD curves for a given soil moves parallel to the finer side under uniform fragmentation can theoretically explain the origin of the Type A family of compaction curves, which provides a foundation for applying the one-point method in construction quality control.

## 5.6 CONCLUSIONS

The particle size distribution is a key factor in understanding the physical properties of a soil. The evolving particle size for residual soils due to weathering was analyzed using uniform fragmentation theory. Using a general analysis method described to calculate the evolution of the particle size distribution, the calculated curves of particle size distribution curves after weathering were found to be parallel to each other. This was supported by empirical evidence found in the literature and can theoretically explain the origin of Type A family of compaction curves, which is the foundation for the one-point method used in practice.

In addition to the uniform fragmentation for a long geological period, crushing by loading or blasting in a short time can be described by the concept of fractal. Combining these

two concepts together, it would be possible and useful to discuss the evolution of particle size distribution of any soil types mathematically in the future.

---

<sup>1</sup> Maple is a proprietary product of Waterloo Maple Inc., 57 Erb Street W. Waterloo, Ontario, Canada N2L 6C2.

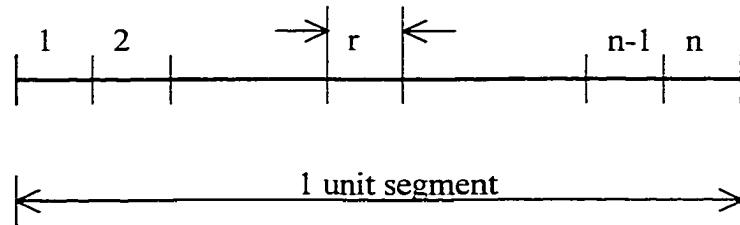
## 5.7 REFERENCES

- AASHTO- American Association of State Highway and Transportation Officials. 1990. T 272-86, Family of curves – one point method. Standard specifications for transportation materials and methods of sampling and testing, 15<sup>th</sup> Ed. Part 2. AASHTO, Washington, pp. 820-823.
- Epstein, B. 1946. The mathematical description of certain breakage mechanisms leading to the logarithmico-normal distribution. *Journal of Franklin Institute*. **244**: 471-477.
- Fukumoto, T. 1990. A grading equation for decomposed granite soil. *Soils and Foundations*. **30**(1): 27-34.
- Fukumoto, T. 1993. A study of the grain size distribution of various soils. *In Proceedings of Japanese Society of Civil Engineers*, **475** (III-24): 11-18. (in Japanese)
- Fukumoto, T. 1994. A continuous type grading equation for soil. *In Proceedings of Japanese Society of Civil Engineers*, **493**(III-27): 147-153. (in Japanese)
- Gardner, R.A.M. 1994. Silt production from weathering of metamorphic rocks in the Southern Himalaya. *Rock Weathering and Landform Evolution*, D.A. Robinson and R.B.G. Williams (eds). John Wiley & Sons Ltd.
- Gimenez, D., Perfect, E., Rawl, W.J. and Pachepsky, Ya. 1997. Fractal models for predicting soil hydraulic properties: a review. *Engineering Geology*, **48**: 161-183.
- Joslin, J.G. 1959. Ohio's Typical Moisture-density curves. *Symposium on application of soil testing in highway design and construction*, ASTM Special Technical Publications 239, pp. 111-118.

- Li, H. and Seg0, D.C. 1999. Soil Compaction Parameters and its Relationship with Soil Physical Properties. *In* Proceedings of the 52nd Canadian Geotechnical Conference, Regina, Saskatchewan, Canada, October 24-27, 1999. pp. 517-524.
- Mandelbrot, B.B. 1982. **The Fractal Geometry of Nature**. Freeman, New York.
- McCarthy, D.F. 1988. Essentials of Soil Mechanics and Foundations: Basic Geotechnics. Prentice Hall, New Jersey. Pp. 66-68.
- McDowell, G.R., Bolton, M.D., and Robertson, D. 1996. The fractal crushing of granular materials. *Journal of the Mechanics and Physics of Solids*, **44**(12): 2079-2102.
- Nishida, K. 1963. Engineering properties of decomposed granite soil. *In* Proceeding of Annual Meeting of Kansai Branch, JSCE, pp. 81-82. (In Japanese)
- Ollier, C. 1984. **Weathering** (2<sup>nd</sup> edition), Longman.
- Sego, D.C. and Li, H. 1999. Laboratory Test for Mixed Soil and Wood Fly Ash for Road Construction for Anderson Exploration, Report prepared by the Department of Civil and Environmental Engineering, University of Alberta, Edmonton, Alberta, Canada. 15p.
- Shanklin, D.W. 1999. The family of curves and one point compaction test method for determining moisture-density values. ASTM Manual: Testing Compaction of Earth Fills Using ASTM Standards (draft).
- Tenchov, B.G. and Yanev, T.K. 1986. Weibull distribution of particle sizes obtained by uniform random fragmentation. *Journal of Colloid and Interface Science*, **111**(1): 1-7.
- Turcotte, D.L. 1997. **Fractals and Chaos in Geology and Geophysics** (2<sup>nd</sup> edition), Cambridge University Press.
- Woods, K.B. 1938. Compaction of earth embankments. *In* Proceeding of Highway Research Borad, Washington, **18**(2): 155.
- Yamaguchi, H., Kuroshima, I., and Fukuda, M. 1988. Pore size distribution of Pleistocene mudstone. *Soils and Foundations*, **36**(12): 55-60.

**Figure 5-1 The concept model of uniform fragmentation**

After  $n$ th cycle of fragmentation



After  $n$ th cycle of fragmentation

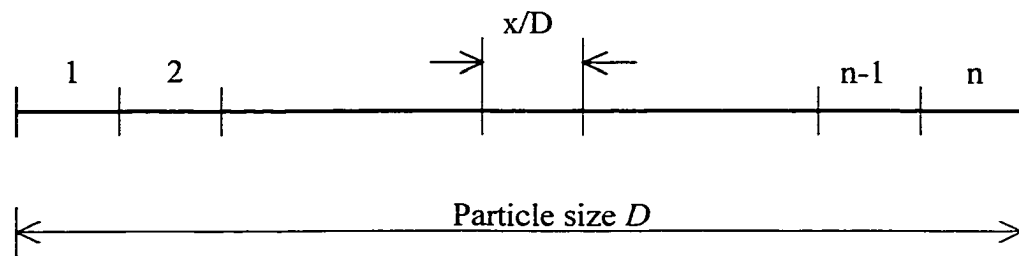


**Figure 5-2 Evolution of particle size distributions from an original log-linear distribution curve**

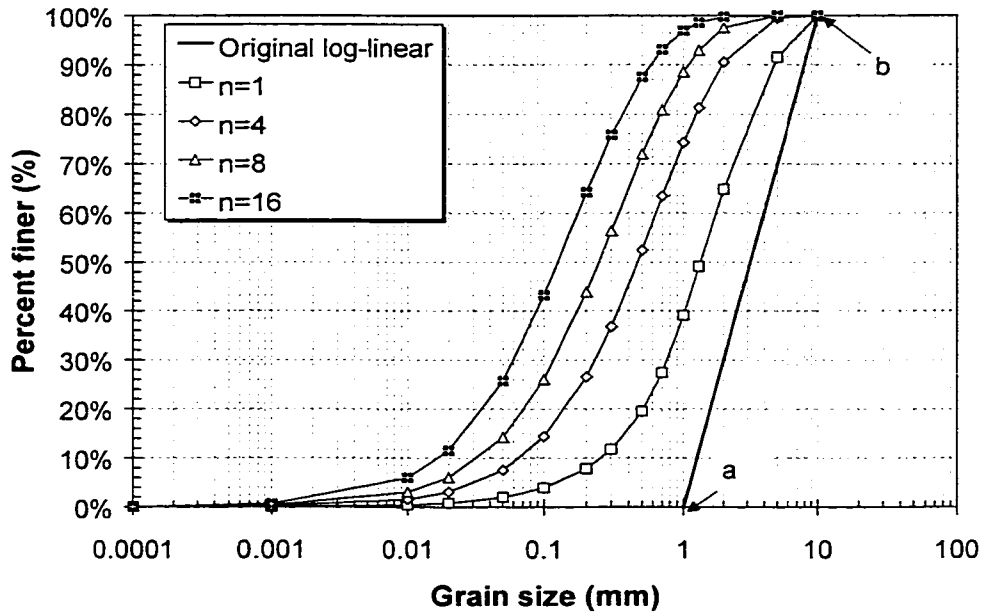


**Figure 5-3 Evolution of particle size distributions from an original power-law distribution curve**

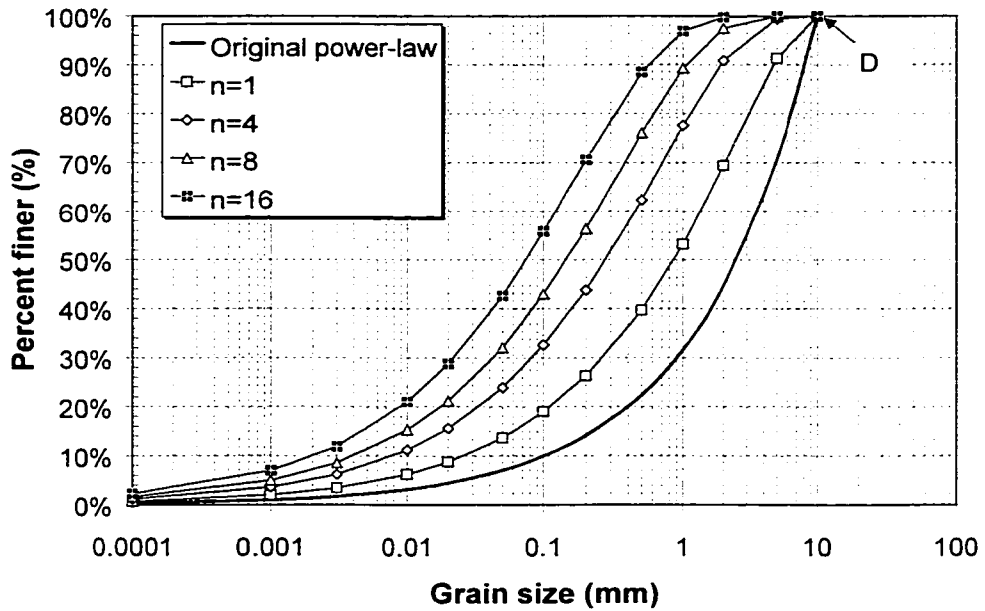


**Figure 5-4 Decreasing of grain size during drying-wetting cycles (revised from Yamaguchi et al. 1988)**

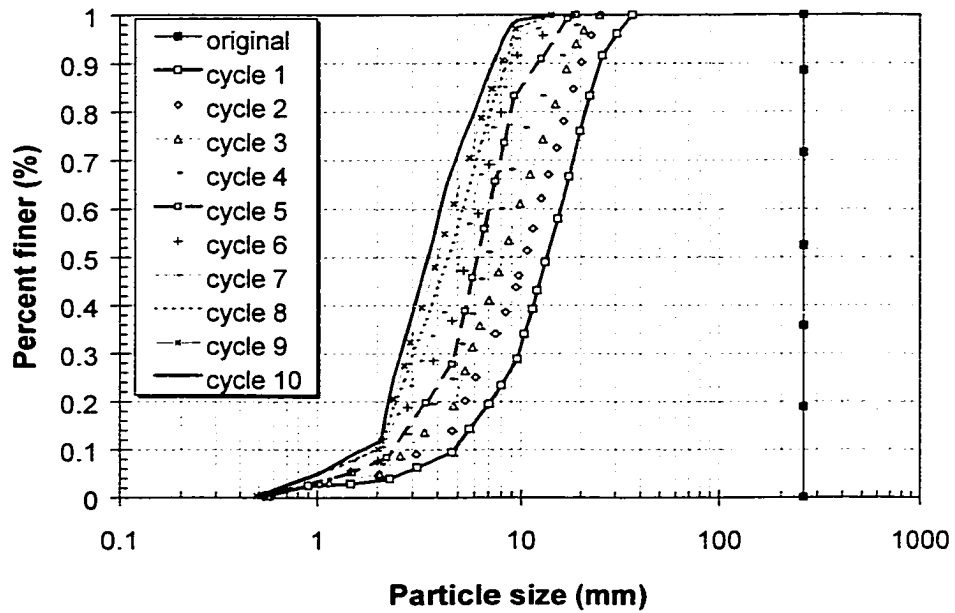


**Figure 5-5 The particle size distribution of alluvial deposits in Anderson Exploration Ltd., Alberta, Canada (Sego and Li 1999)**

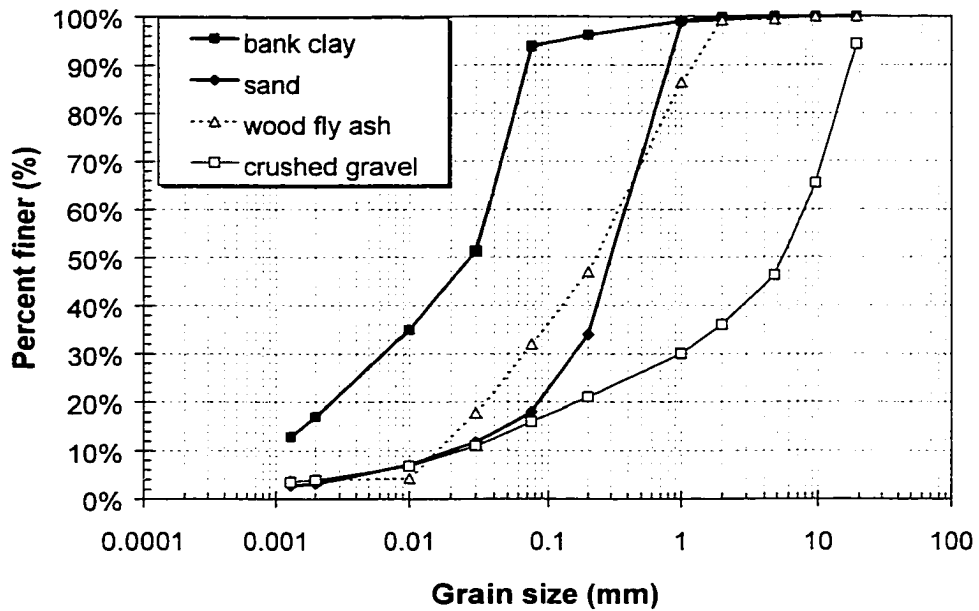
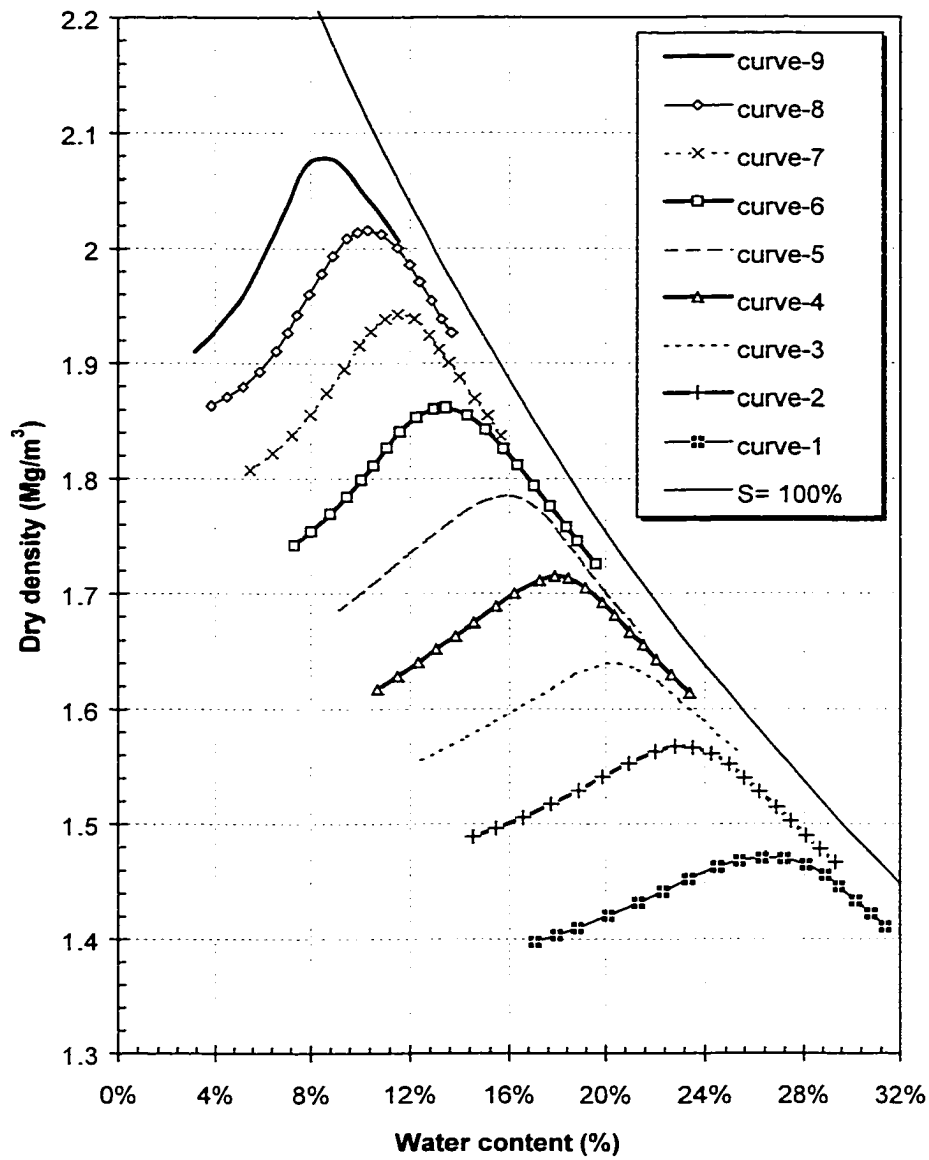


**Figure 5-6 The compaction curves based on experimental data covering 1,383 Ohio soils (revised from Woods 1938)**





# CHAPTER 6 ONE-DIMENSIONAL COMPRESSION BEHAVIOR OF LESS COMPACTED FINE-GRAINED SOIL<sup>1</sup>

## 6.1 INTRODUCTION

Overburden excavation for oil sands mining results in a large volume of soil for disposal. This soil generally undergoes little compaction and has highly variable geotechnical characteristics resulting from its genesis, excavation and placement procedure. The overburden has a significant potential to undergo volume change after deposition when subjected to construction loading or future submergence by water. When buildings and highways are subsequently founded on such fills, large ground movements can occur. It is important to understand the deformation behavior of this kind of spoil and to be able to estimate the possible settlement prior to applying ground treatment to prepare the site for future construction.

The deformation behavior of compacted soil is important in embankment design and has been studied by a number of researchers (Leonards 1955; Lambe 1958; Lee and Haley 1968; Nwaboukei and Lovell 1986; Hausmann 1990). But these previous laboratory studies only focused on the behavior near optimum water content, which is generally used in the field for highway embankment construction. However, dumped waste soils may vary over a large natural water content range. They can be either very dry or very wet when placed. The change of their deformation behavior over the moisture condition

---

<sup>1</sup> This paper is revised and expanded from the following papers:

- a. Deformation of dumped fine-grained soil. Proceeding of 52<sup>nd</sup> Canadian Geotechnical Conference, Regina, Saskatchewan, Canada, October 25-27, 1999, pp. 453-460.
- b. Deformation behaviors of oil sands mine waste soils: Compaction effects. Environmental Issues and Management of Waste in Energy and Mineral Production, Singhal and Mehrotra (Eds.), 2000, Balkema, Rotterdam, pp. 761-766.

is of interest to the designer of the waste dumps.

The objective of this research is to study the one-dimensional compression behavior of soils placed with little or no compactive effort. Samples were carried out with a series of tests of compaction, compression, and flooding. The water content was varied from the air-dried condition (about 1%) to 1.25 times the liquid limit ( $w_L$ ), which should cover the complete practical range of potential water contents. The soil mixed at different water contents was used to carry out compaction and compression tests in the same oedometer cylinder. Because the fill was initially unsaturated when placed, the soil was anticipated to subsequently undergo more volume change (wetting collapse) when submerged by water.

## **6.2 TESTING METHOD**

Pleistocene lacustrine clay ( $P_1$ ) was used in this study. The soil was acquired from the overburden soils on the lease of Syncrude Canada Ltd. at Fort McMurray, Alberta. Its specific gravity is 2.69. The plastic limit is 16.9%, and the liquid limit is 37%. The soil as tested consists of 34% clay, 44% silt and 21% sand. The particle size distribution can be found in Figure 3-4 in Chapter 3.

Air-dried soil was mixed to a certain water content and stored in the moisture room for at least 48 hours prior to use in this experimental study. The water contents were selected from 1% (air-dried condition) to 46%, which is about 1.25 times the liquid limit ( $w_L$ ). According to Burland (1990), the properties of remolded soil samples at water content between  $w_L$  and  $1.5w_L$  are independent of the natural and in-situ state of the soil and are therefore representative of its intrinsic nature. The wide range of water content would display a whole picture of the variation of one dimensional compression behavior and thus would help to understand the development of a family of compression curves for the Pleistocene clay.

The loose soils mixed at different water contents were first pored through a funnel into a rigid cylinder with a diameter of 63.4 mm. The compaction tests were then carried out by applying a pneumatic pressure directly to the sample in the cylinder via a loading cap the same diameter as the cylinder. The pressure was manually increased and then decreased a number of times with each cycle lasting about 2 seconds. The pressure application rate was designed to model the slow speed of haul truck traveling at 4 to 6 km/hr across the surface of a dump. The compaction method resulted in 100% coverage via the loading cap, therefore produced no kneading effects during compaction.

Both the compaction and subsequent one-dimensional compression tests were carried out in the same cylinder, which was designed to eliminate the disturbance during sample extraction and trimming. The compression tests provided a no lateral yield condition, which is similar to an oedometer. Compression tests were conducted by applying vertical pressure to each sample. The applied stresses ranged from 2.4 kPa to 1,569 kPa with each new increment doubling the previous applied pressure. The next load was only applied once the soil underwent deformation of less than 0.005mm in two hours. The applying time of each load varied from several hours to several days depending on the mixed water content and the magnitude of pressure. Free drainage was allowed during the compression test. The maximum applied pressure represents about 80 meters of natural deposited soil, which is expected to cover the practical range of overburden pressure found within typical waste dumps.

During the loading process, some samples were flooded via the top and bottom porous platens under different vertical stresses. The amount of wetting collapse and its relationship to the initial water content and applied pressure was evaluated.

### **6.3 COMPRESSION BEHAVIOR OF AS-DUMPED SOIL AND CLOD EFFECTS**

Soil samples were mixed at water contents of 1%, 10%, 15%, 21% and 46%. These were allowed to condition for 48 hours in a moisture room prior to being placed into the

oedometer. The compression tests were carried out without any compaction being applied, hence the soil was initially in a very loose state. A small initial vertical stress of 2.4 kPa due to the weight of the cap was applied prior to application of the vertical stresses via the air pressure system.

The initial void ratio of each sample varied for the different prepared water content. When samples were mixed at the water content, the fine clay plates aggregate to form various size clods as sketched in (Fig. 6-1). The clods were grouped in a loose open arrangement (Barden et al. 1973). The initial void ratio of 2.42 was the largest for the molding water content of 21% in Figure 6-2. The large void ratio was mostly contributed by the macrostructure of the large clods, which was formed during mixing and remained due to internal matric suction ( $u_a - u_w$ ). The matric suction was a direct contribution from water tension at the soil-water surface and  $u_a$  is the atmospheric pore-air pressure (typically 101.3 kPa). As shown in Figure 6-1, the initial void ratio of air-dried soil ( $w = 1\%$ ,  $e_0 = 1.31$ ) and the very wet soil ( $w = 46\%$ ,  $e_0 = 1.36$ ) both were lower than the other samples. The air-dried soil contained too little water to form soil clods, while the very wet soil at 46% had all clods eliminated due to the nature of the saturated sample.

The clod size formed during the soil preparation has a dominant influence on the initial void ratio (Figure 6-2). As the loading progressed, it was seen that the void ratio of all soils decreased but the sample with greater initial void ratio dropped faster. The curves converge around 100 kPa, where the contribution of atmospheric pressure was balanced.

The compression behavior became more consistent above the applied stress of 98 kPa. The samples with greater water contents resulted in smaller void ratios (Fig. 6-3) or high dry densities (Fig. 6-4). This difference can also be easily recognized in the compression curves of the air-dried soil ( $w = 1\%$ ) and wet soil of 46%. The air-dried soil has the voids filled with air and the wet soil has mostly water filled voids. The water helped to decrease the friction between particle as well as reducing due to the matric suction, which allows the individual particles to pack together.

According to Delage and Graham (1996), constant suctions are observed at low water contents, showing that the density has little influence on the suction at these lower water contents. This is probably because the compression is concentrated in the air-filled parts of the soil, while smaller water-filled pores remain unchanged. The large matric suction within the air-dried soil allows for larger potential collapse deformation once the sample is flooded and the matric suction drops to zero.

With the increase of water content from 1% to 10%, 15% and 21%, beyond 98 kPa compression pressure, the compression curves move closer to the curve at 46% water content. The samples join the same curve as the 46% water content sample at different applied stresses. The wetter the soil, the lower the pressure required to join the 46% water content sample. For example the curve at 15% reaches the same void ratio as the curve at 46% with a pressure of 1569 kPa while the curve at 21% only required about 392 kPa. For samples at water content of 10% and 1%, the maximum applied pressure (1569 kPa) was not sufficient to eliminate the air-filled voids within these samples.

Extra water within the sample may be squeezed out during the compression test. The saturation line ( $S=100\%$ ) in Figure 6-3 represents where the sample would become saturated under the vertical stress. It is seen that the 46% sample was almost saturated at the beginning of the test. When the pressure increased to 392 kPa, the sample with water content of 21% became saturated (Fig. 6-3). With high-applied pressure at 1569 kPa, the sample with water content of 15% became saturated (Fig. 6-3). These two samples in Fig. 2 illustrate that the compression curves converge when the sample are saturated.

#### **6.4 PNEUMATIC COMPACTION ON DUMPED FINE-GRAINED SOILS**

According to the previous discussion, the loose placed soil had to be compacted at 98 kPa or more foot pressure to eliminate the effect of clods. Therefore, a compaction pressure of 98 kPa was chosen to compact samples in each cylinder. This pressure represents about 5 to 6 meter depth within a dump and is still much smaller than the possible

compaction pressure applied by the inflation pressure of heavy truck tires at a mine (about 700 kPa).

Figure 6-5 shows the compaction results obtained by applying a pneumatic compaction pressure of 98 kPa and up to a total of 25 applications. The plots show a continuous evolution of the compaction curves with increasing number of applications of the foot. Because each foot application has complete coverage, the compaction under the first application was able to substantially eliminate the voids formed by the clods, therefore a large increase in the dry density at  $N=1$  was observed. The dry densities subsequently showed little increase with each application at water content less than 17% and greater than 25%. Only small increases between 17% and 25% molding water content were observed. The complete compaction curve was nearly achieved after four applications.

Figure 6-5 shows that the compacted samples have a constant dry density for all water content less than 17%. Faure and De Mata (1994) and Chapter 2 discussed this characteristic of the complete compaction curves for fine-grained soils. The compaction sensitivity threshold (CST) is at approximate 17% for the soil tested and the maximum dry density occurred at optimum water content (OWC) near 26%.

## **6.5 ONE-DIMENSIONAL COMPRESSION OF LESS COMPACTED FINE-GRAINED SOILS**

Compression tests were carried out immediately after the compaction test in the same cylinder to avoid any disturbances associated with removing and mounting the samples. This design is believed the first of its type and no other publications that combined compaction and 1-D compression tests in the same cell were found. The one-dimensional compression tests were carried out to study various factors that influence the deformation behavior of the compacted soil, such as the prepared water content and the compactive effort. Since the compacted soil was unsaturated, a flooding test was also carried out to study the loading-wetting sequence and the wetting collapse potential. The results are summarized and discussed in following sections.

### 6.5.1 The influence of water content on the behavior of one-dimensional compression curves

Samples were prepared with initial water content of 1%, 10%, 15%, 17%, 21%, 26%, 30%, and 46%, and each was compacted using 98 kPa foot pressure with 25 applications. The compaction curve obtained for these samples is illustrated in Fig. 6-5. The one-dimensional compression tests were carried out with loading from 2.4 to 1569 kPa and shown in Fig. 6-6. Flooding was performed at the end of the compression test.

The complete compaction curve can be subdivided into three zones using the CST and OWC according to Chapter 2, i.e. the dry zone ( $w < 17\%$ ), the transition zone ( $17\% < w < 26\%$ ), and the wet zone ( $w > 26\%$ ). The compression curves are therefore regrouped and their behavior is examined for each of these three zones.

Figure 6-7 represents the compression curves for soils compacted in the dry zone. The as-compacted dry density or the initial void ratio for the samples is almost the same. There is little volume change until 98 kPa and then the deformation suddenly increased. It is believed that the compacted soils in the dry zone behave similar to overconsolidated soils since little or no deformation occurred until at least 98 kPa is applied. The influence of the preparation water content dominates the deformation behavior above the compaction pressure (i.e. normal compression range). The sample with less moisture deforms less or has a smaller compressibility index. At the end of the test, it is seen there is still plenty of potential for the sample prepared at 1% water content to collapse with the addition of water while the sample prepared at 17% had achieved saturated condition with no potential for further collapse. This observation indicates the importance of the water lubrication of particles even though it may not be effective during the compaction stage it contributes throughout subsequent compression.

The one-dimensional compression curves for samples prepared in the transition zone (effective compaction zone) are shown in Fig. 6-8. A substantial difference in initial void

ratio was observed with the increase of water content. The minimum void ratio was achieved at 26% water content that represents the maximum dry density from the compaction curves. Although the compression test for the sample at 21% water content had a sharp curvature around 50 kPa, which could be decreased due to the unusual friction between load-transfer rod and load cap, the other two samples showed the maximum curvature at 98 kPa applied stress. In general, the specimens exhibit a more compressible behavior for vertical stresses greater than the as-compacted pressure of 98 kPa.

Figure 6-9 shows variation of the compression curves in the wet zone, where water is in oversupply during compaction. Extra water occupied the space in the voids and created pore pressure during the compaction. An increase of water content decreases the dry density, or increases the initial void ratio. It is also noted in Fig. 6-9 that the sharp curvature of the compression curves is lower than the applied compaction pressure of 98 kPa. For samples at 30% and 46% water content the values are around 50 and 12 kPa respectively, which indicate their effective pre-stress values. This is evidence of positive pore pressures being developed during the compaction test that lowers the net effective stresses felt by the soil particles. Therefore, the effective compaction pressures on these samples are smaller than the actual applied compaction pressure. It should also be observed that the deformation behavior beyond this net effective stress converge which is evidence of saturated soil behavior.

The compression curves in Figure 6-6 can also be displayed using void ratio versus water content (Fig. 6-10) or dry density versus water content (Fig. 6-11). An optimum water content (OWC) around 26% was found after compaction where its initial void ratio was the minimum (or the dry density is the maximum). Both figures illustrate the change in the void ratio or dry density at each stress stage. It also shows that some samples reach saturation at different pressure resulting in additional water content change.

In the wet zone, the void ratio decreased with the application of compression pressure (Fig. 6-9). The static load is more effective in reducing void volume on the wet side



because it has sufficient time to consolidate the sample, while the compactive effort could not achieve it within the 2 seconds during each application. It is also because the wet samples allow the soil particles to move closer together with lubrication from the water. It is clear in Figure 6-12 that the compaction effect almost disappears if the applied compression stress is equal to or greater than the applied compaction pressure (98 kPa) since there is little difference in void ratio between the compacted and the as-dumped samples.

### **6.5.2 The influence of compactive effort on the behavior of one-dimensional compression curve**

The compression curves at a given water content are illustrated in Fig. 6-13 to -17. Each figure includes several curves with different applied compactive efforts.

Figure 6-13 shows the results from air-dried samples (about 1% water content) subjected to compaction stresses of 98, 196, 392, 784 kPa, which subsequently underwent a compression test. The three greatest pressures were applied 25 times while the 98 kPa was applied 50 times. It is observed that maximum curvatures of the compression curves were coincidentally close to their respective compaction pressures that indicate an induced pre-compression pressure due to compaction. All the compression curves joined the virgin compression curve after being loaded beyond the compaction pressure, except the sample P<sub>1</sub>-1%-fld0 which was flooded at the beginning and thus underwent a change in initial moisture content.

The influence of the number of applications of compaction stress on the deformation behavior is illustrated in Fig. 6-14. The sample was prepared at the uniform water content of 10.2% and compacted using 98 kPa foot pressure under 3, 6, and 50 applications. It was not surprising that the initial void ratio changed little after three stress cycles, which was supported by Parson (1992) and Hausemann (1990). It is also observed that the compression curves for all these three compacted samples were similar to each other, and the sharp curvatures in each curve occurred around the compaction

pressure of 98 kPa. It was therefore concluded that the number of cycles of applied stress has a minor influence on the post-compaction deformation behavior compared with the magnitude of the compaction pressure. The sample flooded at the beginning of the test (P1-10%-fld0) will be discussed in next section.

Figure 6-15 shows the results from sample prepared at water content 15.8%, which was simply represented in the figure as 15%. The compacted sample had its maximum curvature near 98 kPa, which equals the compaction stress. Once the applied stress increases to 98 kPa, the difference in void ratio between samples with or without compaction became insignificant. All the curves merged with the flooded sample at the 1596 kPa, which indicates all samples were saturated at this point.

Different initial compaction pressures were used to compact samples at 17.3% water content samples. Compression tests were then carried out and the data are presented in Figure 6-16. The applied compaction pressure of 98 kPa is located at the maximum curvature of the compression curve and controls the deformation behavior for sample compacted using a foot pressure of 98 kPa. However, it was found that the applied pressure at the maximum curvature for the samples prepared using compaction efforts of 196 and 784 kPa foot pressure were less than these applied pressures. The reasons could be that some positive pore pressure was generated during a higher compaction pressure for these 17% water content samples. For embankment design in which the as-compacted compressibility is important, the as-compacted pre-stress should be determined in the laboratory to effectively control the post construction deformation behavior.

The results for the 21% initial water content samples are shown in Figure 6-17. The initial void ratio was substantially reduced from compaction compared to the as-dumped samples and the clod effects were also eliminated. It is unusual that the maximum curvature was located at around 50 kPa while the compaction stress was 98 kPa. Since the location for both compression curves for sample 17% and 26% water content has the same stress of 98 kPa (Fig. 6-8), the measure value at 50 kPa for the 21% water content

sample could be a testing error. It is also observed that the compaction substantially decreased the potential for wetting collapse, as shown the compression curve was closer to the curve for the sample that had been flooded at the beginning of the compression test.

The compactive effort has little influence on the compression curve when the initial water content is greater than the optimum water content (OWC), as was shown in Fig. 6-9. Figure 6-18 displays three curves with different loading-wetting procedures. The compaction did not have any influence on the post compaction compression test data. The maximum curvature occurred around 10 kPa so the influence of applying 98 kPa stress during compaction had little or no influence. Flooding also had little effect on the 46% water content sample as shown in Fig. 6-18.

In general, the following three conclusions can be summarized regarding the influence of compactive effort on the behavior of one-dimensional compression curve:

- When the sample is prepared dry of the optimum water content (OWC), the compaction pressure has a similar effect on the compression curve as the pre-consolidation pressure in natural soils has on the consolidation curve. Initial void ratio decreases depending on the preparation water contents and the compactive efforts.
- When the sample is prepared wet of the OWC, compaction is much less efficient. The stress at the maximum curvature of the compression curve is smaller than the actual compaction pressure. This is because during compaction pore pressures develop and the water cannot be squeezed from the pore space during the 2 seconds application period. The sample at 1.25  $w_L$  (46%) showed little influence due to the compaction.
- Once the applied compression stress is above the applied compaction pressure, the compaction effect become less significant. If the applied compression pressure

continues to increase or flooding of the sample occurs, all compression curves would merge.

## **6.6 WETTING-INDUCED COLLAPSE OF LESS COMPACTED FINE-GRAINED SOIL**

As less compacted waste dumps, high earth dams, deep compacted highway embankments, and other thick compacted fills become more common, it is imperative that engineers consider and control the potential for wetting-induced collapse in these fills. Problems associated with collapse settlements in compacted fills include damage to structures and foundations placed on the fills; cracking and slope failure within the fills; damage to pavements and subgrades placed on highway embankments; piping, seepage losses, and failure in earth dams; as well as distress or failure of underground utilities (Brandon et al. 1990; Charles 1992; Lawton et al. 1992; and Noorany 1997). In contrast to naturally deposited soils, whose potential for collapse is determined by natural processes, an engineer can control the potential for collapse in a compacted fill during its placement.

Vulnerability to collapse depends on overburden soil type, placement method, moisture content, stress level and stress history. Under moderate stresses a poorly compacted mudstone and sandstone backfill underwent collapse compressions of up to 2% when the fill was submerged by a rising water table (Charles et al. 1984). A poorly compacted stiff clay fill suffered up to 6% collapse compression on inundation from surface trenches during studies reported by Charles (1992). Lawton et al. (1989) studied the relative density as a guide for clayey sand or silt, and concluded that a relative density of between 85% and 90% was needed to prevent structural damage of buildings from potential collapse settlement during inundation. There is no doubt the dumped soil with little or no compaction would have potential for substantial settlement on inundation.

There is in general good agreement between predicted wetting collapses based on laboratory testing and observed field performance (Kropp and McMahon 2000). In this

study, one-dimensional compression tests were conducted to clarify the influences of compaction water content, vertical stress level, and load-wet sequence on post-compaction wetting-induced volume changes in the soil.

Figure 6-19 shows the deformation behavior of air-dried soil with different loading-wetting sequences after compression under applied stresses of 2.4, 49, 196, and 1586 kPa. The final void ratios of as-dumped soil after these loading-wetting cycle were generally the same. The wetting collapses of the compacted samples prepared using 25 application of 98 kPa foot pressure were smaller than the as-dumped sample within the compaction pressure (i.e. 98 kPa), but had similar amounts to the as-dumped soils when flooding took place at 196 and 1569 kPa. This indicates that the magnitude of wetting collapse is not affected by the compaction if the overburden pressure exceeds the applied compaction pressure.

Flooding of samples with different initial water contents (1%, 10%, 15%, and 21%) under low initial stresses showed little difference from the compression curves of the sample prepared at 46% water content ( $1.25w_L$ ) (Fig. 6-20). Burland (1990) pointed out that the sample for this condition provides the intrinsic soil behavior and results are independent of any stress history.

Both results from Figure 6-18 and 6-19 indicate that the deformation behavior of the lacustrine clay used in this study is independent of the loading-wetting sequences because the same final void ratio can be achieved using either approach. Therefore, the double oedometer procedure proposed by Jennings and Knight (1957) was judged to be sufficiently accurate for use in evaluating the wetting-induced collapse. The double oedometer tests require two identical samples to be prepared. The first is incrementally loaded without saturation to provide the upper curve. In this research, samples compacted at 98 kPa were subjected to compression tests without flooding. The second sample is flooded under the initial vertical stress to provide the lower saturated loading curve. The difference in void ratio between the two reflects the collapse potential at any single vertical stress (Assallay et al. 1998). The major advantage of the double-

oedometer is the large amount of data that can be obtained from a single set of tests (Lawton et al. 1992).

The amount of collapse is represented by the collapse potential recommended by Lutenegeger and Saber (1988) and given by:

$$[6-1] \quad I = \frac{\Delta e}{1 + e_0}$$

where  $I$  is the collapse potential;  $\Delta e$  is the change in void ratio resulting from saturation; and  $e_0$  is the void ratio just before saturation.

For example, for the compacted sample prepared at 15% water content, the void ratio due to wetting at 196 kPa was reduced from 0.897 to 0.633, a decrease of about 0.266. Its collapse potential is therefore equals to 13.9% according to Equation 1 (Fig. 6-15). There was no wetting collapse at 1569 kPa as no sudden void ratio change was observed.

A comprehensive description of the collapse potential for the samples compacted at 98 kPa with 25 applications is presented in Figure 6-21. The calculations were based on double oedometer tests presented in Figure 6-13 to -18. Some single oedometer tests were carried out but were not used to prepare this figure. The curve for the sample prepared at 17% water content and subsequently flooded under a low vertical stress was not available therefore the collapse potential was determined using the flooded curve from the 15.8% water content sample (Fig. 6-16).

It is shown in Figure 6-21 that the collapse potential decreases as the water content increases under the same vertical stress. This is obviously because the water helps to move soil particle closer and water occupies more of the pore volume. The collapse potential becomes smaller when the sample is subjected to higher applied pressures. This is also supported from the literature (Lawton et al. 1992; Assallay et al. 1998). The collapse potential is eliminated once the soil becomes saturated at a certain vertical stress.

As discussed earlier and supported in Figure 6-21, a sample can be saturated at a lower vertical stress if the soil has higher initial water content. An ultimate void ratio for a given soil under overburden load can be estimated from the compression curve of sample with initial water content of  $w_L$  to  $1.5w_L$  (Burland 1990).

Because compaction decreases the initial void ratio for samples prepared dry of OWC side (Fig. 6-13 to -17), it decreases the wetting collapse for dry samples within the compaction pressure (e.g. 98 kPa). However, the wetting collapse is not affected by the initial compaction stress if the sample is prepared wet of OWC (Fig. 6-18) or the wetting takes place at pressures above the applied compaction pressure.

Traditional specifications to control wetting collapse are to specify a zone of acceptable dry density. However, laboratory testing showed that the largest portion of wetting collapse occurs below about 85% saturation (Lawton et al. 1989; Kropp and McMahan 2000). A new specification was proposed to reduce the wetting collapse within the fills by specifying dry density and water content combinations based on achieving a minimum degree of saturation (McMahan and Kropp 2000).

The McMahan and Kropp criterion is better and easy to use in the field to control wetting-induced collapse. However, it still does not relate the required dry density to the future loading pressure, which could induce large compression deformation in the samples prepared wet of OWC. As previous discussed, the effective compaction pressures on these samples (yielding point) were smaller than the actually applied compaction pressure. If the future loading pressure is beyond the effective compaction pressure (which could be low), the soil compacted at the wet side should be considered to behave as a less compacted soil, therefore large compression deformation should be expected. Therefore, the control of both compression and wetting collapse has not only requirements on the dry density and the water content (or degree of saturation), but the future anticipated loading pressure which will be applied as well.

## 6.7 CONCLUSIONS

By combining compaction, compression and wetting collapse testing in one apparatus, the compression behaviors of a less compacted fine-grained soil were studied. The samples were prepared with water content from the air-dried condition to  $1.25 w_L$ . Clod size has a dominant influence on the initial void ratio of the prepared samples but can be eliminated by using a compaction pressure around 100 kPa. The wettest sample (46%) reached the lowest void ratio for each different applied stress due to the lubrication effect of the water.

When the sample is prepared dry of the optimum water content (OWC), the compaction pressure has a similar effect on the compression curve to the preconsolidation pressure on the consolidation curve of saturated soils. Initial void ratio decreases depending on the water contents and the compactive efforts used to prepare the sample.

When the sample is prepared wet of the OWC, compaction is not effective. The stress at the maximum curvature of the compression curve is smaller than the actual compaction pressure. This is due to the compaction causing pore pressure increases, and that pressures cannot dissipate during the short loading time. The sample at  $1.25 w_L$  (46%) showed little influence of the compaction effort on its deformation behavior.

Once the applied compression stress exceeds the previous compaction pressure, the compaction effect becomes insignificant. Different compression curves could join together when samples become saturated under high compression pressure.

The wetting-induced collapse potential of the samples compacted at 98 kPa was studied. The collapse was independent of loading-wetting sequence and decreased when either the initial water content increases or the compression pressure increases. The void ratio after collapse can be estimated from the compression curve of samples with initial water



content of  $w_L$  to  $1.5w_L$  or from the samples prepared at a given water content and flooded prior to conducting the compression test.

The samples compacted wet of OWC have yield pressure from their compression curves less than the applied compaction pressure. If the future applied pressure is beyond the effective compaction pressure, the compacted soil should behave as a less compacted soil and thus large compression deformation should be expected. Therefore, choosing an appropriate compaction pressure and water content and anticipating future loading pressure are all important in controlling the future compression and wetting collapse of dumped waste soils.

## 6.8 REFERENCES

- Assallay, A.M., Jefferson, I., Rogers, C.D.F. and Smalley, I.J. 1998. Fragipan formation in loess soils: development of the Bryant hydroconsolidation hypothesis. *Geoderma*, **83**: 1-16.
- Barden, L., McGown, A. and Collins, K. 1973. The collapse mechanism in partly saturated soil. *Engineering Geology*, **7**: 49-60.
- Brandon, T., Duncan, J.M., and Gardner, W. 1990. Hydrocompression settlement of deep fills. *ASCE Journal of Geotechnical Engineering*, **116**(10): 1536-1548.
- Burland, J.B. 1990. On the compressibility and shear strength of natural clays. *Geotechnique*, **40**(3): 329-378.
- Charles, J.A., Hughes, D.B. and Burford, D. 1984. The effect of a rise of water table on the settlement of backfill at Horsley restored opencast coal mining site, 1973-1983. *In Proceedings of 3<sup>rd</sup> International Conference on Ground Movements and Structures*, Cardiff, pp. 423-442.
- Charles, J.A. 1992. The causes, magnitudes and control of ground movements in fills. *Ground Movements and Structures*. Geddes, J.D. (Ed), Pentech Press, Vol. 4, pp. 3-28.

- Delage, P. and Graham J. 1996. Mechanical behavior of unsaturated soils: Understanding the behavior of unsaturated soils requires reliable conceptual models. *Unsaturated Soils*, Alonso and Delage (Eds), 1223-1256.
- Faure, A.G. and Da Mata, J.D.V. 1994. Penetration resistance value along compaction curves. *ASCE Journal of Geotechnical Engineering*, **120**(1): 46-59.
- Hausmann, M.R. 1990. **Engineering Principles of Ground Modification**, McGraw-Hill Inc., New York, pp. 72.
- Jennings, J.E. and Knight, K. 1957. The prediction of total heave from the double oedometer test, *Transactions, Symposium on expansive clays*, South African Institute of Civil Engineering, 13-19.
- Kropp, A. and McMahan, D.J. 2000. Comparison of laboratory data and field performance for fills subject to hydrocompression. *Constructing and Controlling Compaction of Earth Fills*, ASTM STP 1384, Shanklin, D.W., Rademacher, K.R., and Talbot, J.R. (Eds.), American Society for Testing and Materials, West Conshohocken, PA. 197-208.
- Lawton, E.C., Fragaszy, R.J. and Hardcastle, J.H. 1989. Collapse of compacted clayey sand. *ASCE Journal of Geotechnical Engineering*, **115**(9): 1252-1267.
- Lawton, E.C., Fragaszy, R.J. and Hardcastle, J.H. 1992. Review of wetting-induced collapse in compacted soil. *ASCE Journal of Geotechnical Engineering*, **118**(9): 1376-1394.
- Lambe, T.W. 1958. The engineering behavior of compacted clay. *ACSE Journal of Soil Mechanics and Foundation Division*, **84**(SM2): 1655-1 to -35.
- Lee, K.L. and Haley, S.C. 1968. Strength of compacted clay at high pressure. *ASCE Journal of Soil Mechanics and Foundation Division*, **94**(SM1): 1303-1332.
- Leonards, G.A. 1955. Strength characteristics of compacted clays, *Transactions of American Society of Civil Engineers*, Vol. 120: 1420-1479.
- Li, H. and Sego, D.C. 1999. Soil Compaction Parameters and its Relationship with Soil Physical Properties. *In Proceedings of 52nd Canadian Geotechnical Conference*, Regina, Saskatchewan, Canada, October 24-27, 1999. 517-524.

- Li, H. and Sego, D.C. 2000. Equation for compaction curve of fine-grained soils, its origin, implementation, and application. *Canadian Geotechnical Journal* (under review).
- Lutenegger, A.J. and Saber, R.T. 1988. Determination of collapse potential of soils. *Geotechnical Testing Journal, ASTM*, **11**(3): 173-178.
- McMahon, D.J. and Kropp, A. 2000. Proposed compaction specifications to minimized hydrocompression-induced settlement in fills supporting residential structures. *Constructing and Controlling Compaction of Earth Fills, ASTM STP 1384*, Shanklin, D.W., Rademacher, K.R., and Talbot, J.R. (Eds.), American Society for Testing and Materials, West Conshohocken, PA. 209-228.
- Noorany, I. 1997. Structural Fills: Design, Construction, and Performance Review. *Unsaturated Soil Engineering Practices, ASCE Geotechnical Special Publication No. 68*, pp. 233-254.
- Noorany, I. and Stanley, J.V. 1995. Invited Lecture: Settlement of compacted fills caused by wetting. *Vertical and Horizontal Deformations of Foundations and Embankments, ASCE Geotechnical Special Publication No. 40, Vol. 2*, pp. 1516-1530.
- Nwaboukei, S.O. and Lovell, C.W. 1986. Compressibility and settlement of compacted fills, *Consolidation of Soils: Testing and Evaluation, ASTM STP 892*, R.N. Yong and F.C. Townsend, Eds, American Society for Testing and Materials, Philadelphia, pp. 184-202.
- Parsons, A.W. 1992. *Compaction of Soils and Granular Materials: A review of Research Performed at the Transport Research Laboratory, London: H.M.S.O.*

**Figure 6-1 Schematic clod aggregates during soil mixing with water**

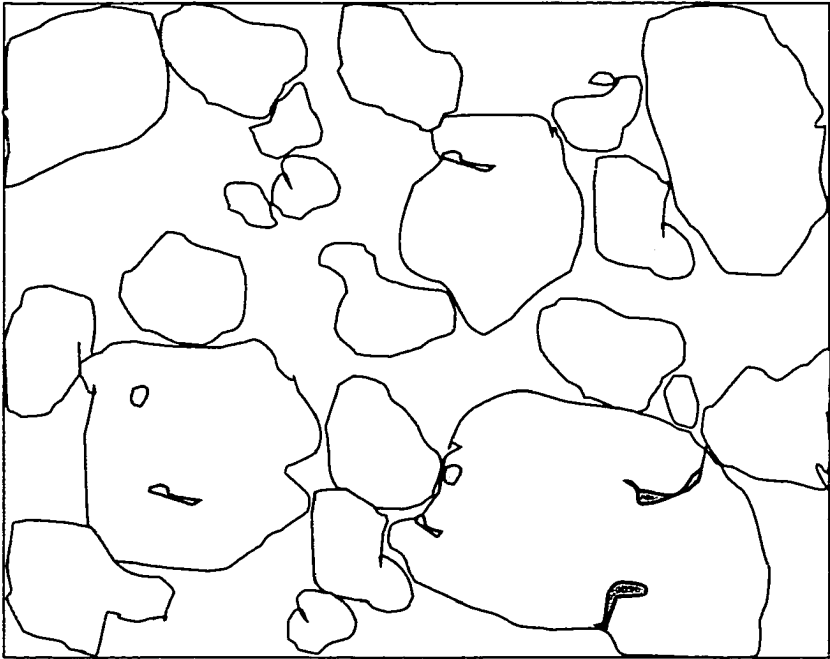


**Figure 6-2 Compression curves of as-dumped soils prepared at different water content**

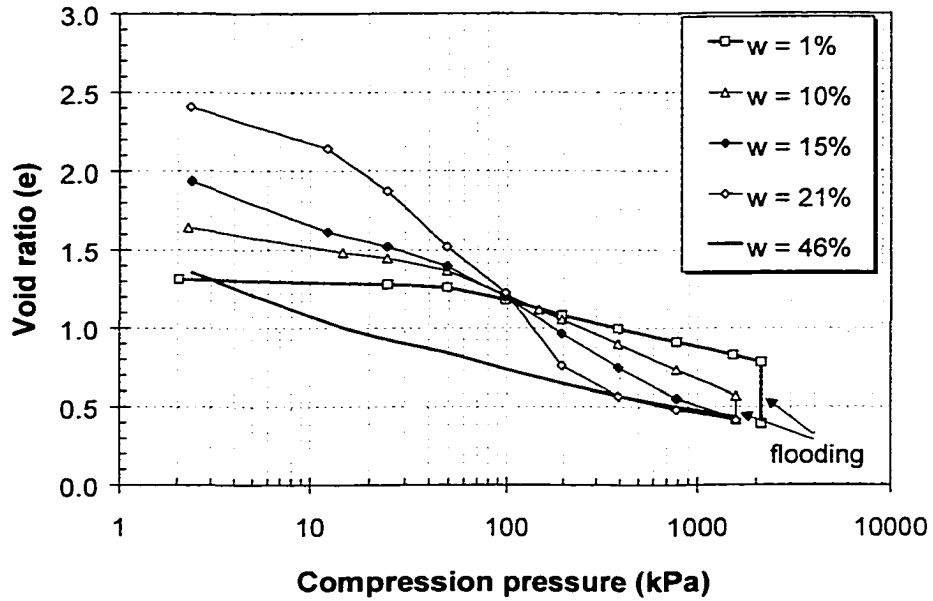


**Figure 6-3 Void ratio progress of as-dumped soil prepared at different water contents**

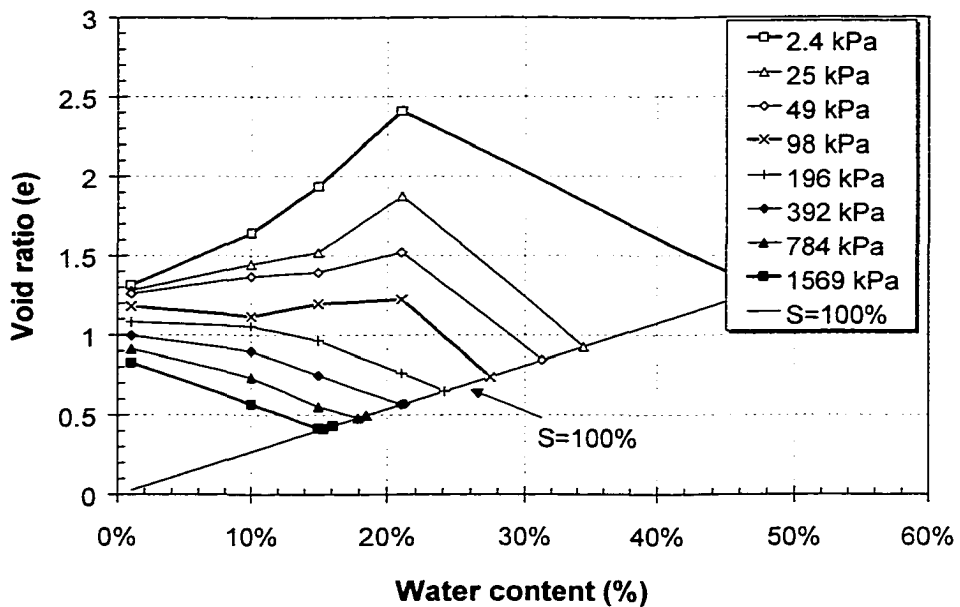


**Figure 6-4 Progress of dry density as-dumped soil during one-dimensional compression test**

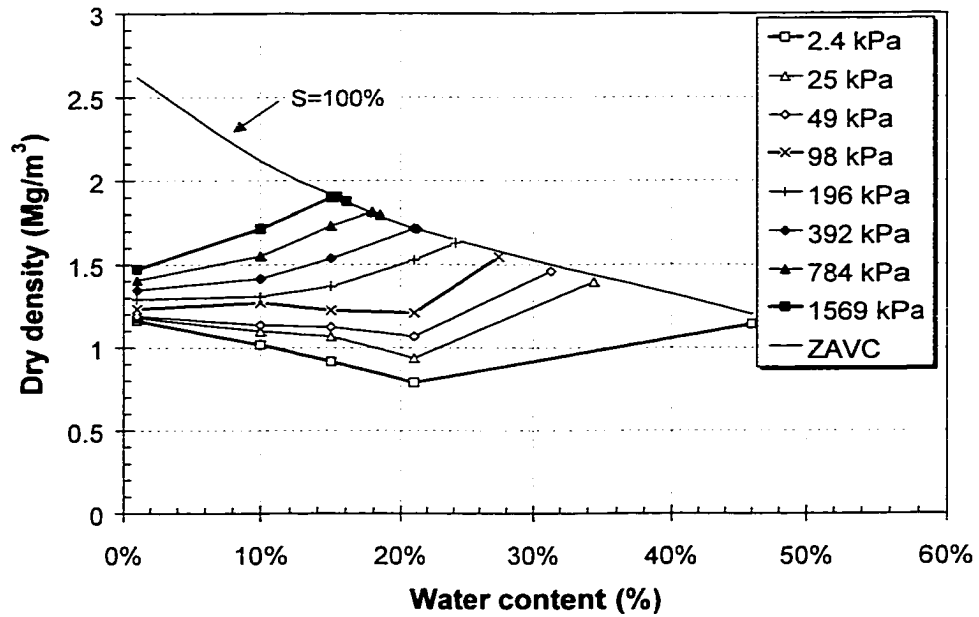


**Figure 6-5 Increase of dry density after various applications of compaction test (98 kPa)**

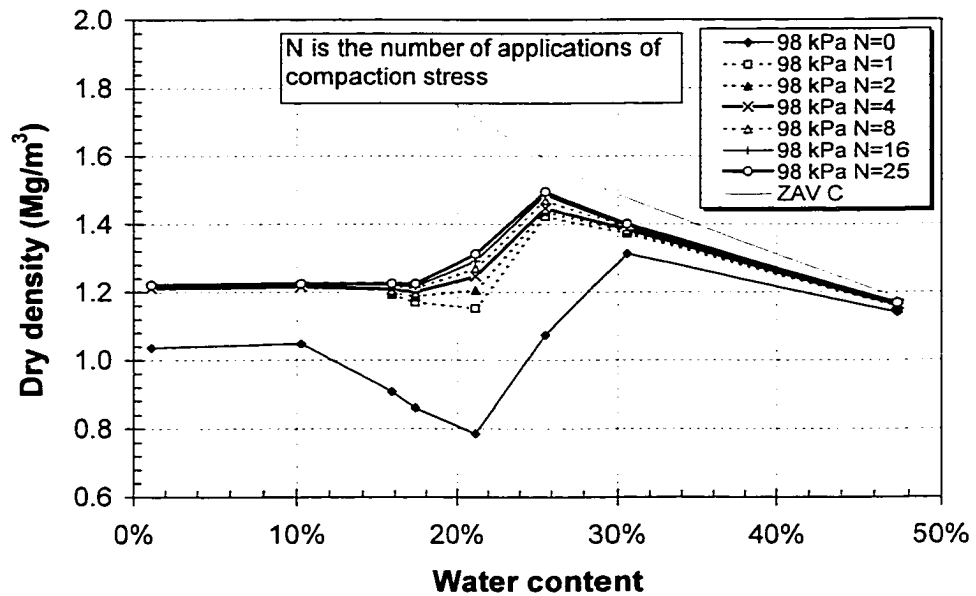


**Figure 6-6 Compression curves of soils with 98 kPa of compaction prepared at different initial water contents**

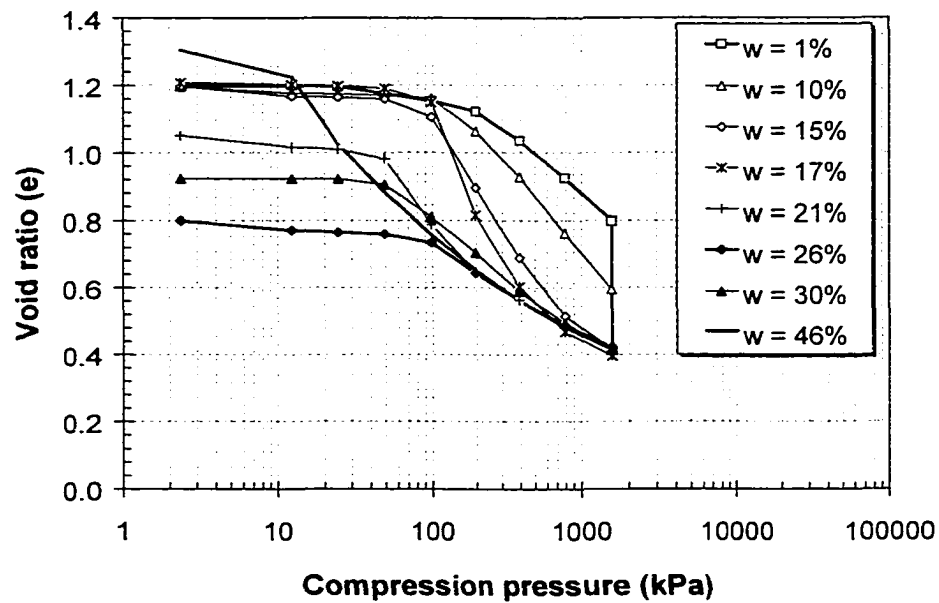


**Figure 6-7 Compression curves of compacted soil prepared with water content at dry zone (dry of CST)**

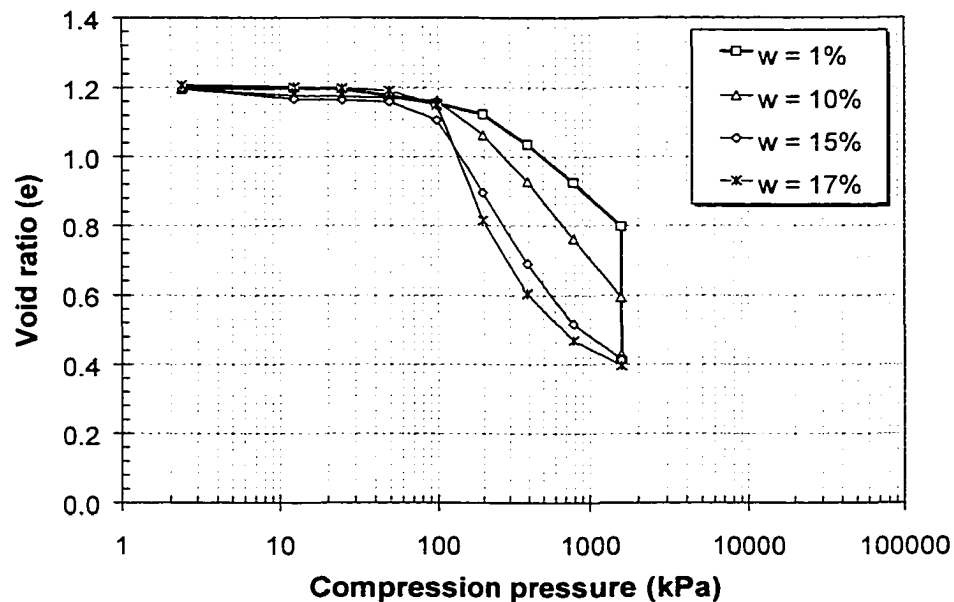


**Figure 6-8 Compression curves of compacted soil prepared with water content at transition zone (between CST and OWC)**

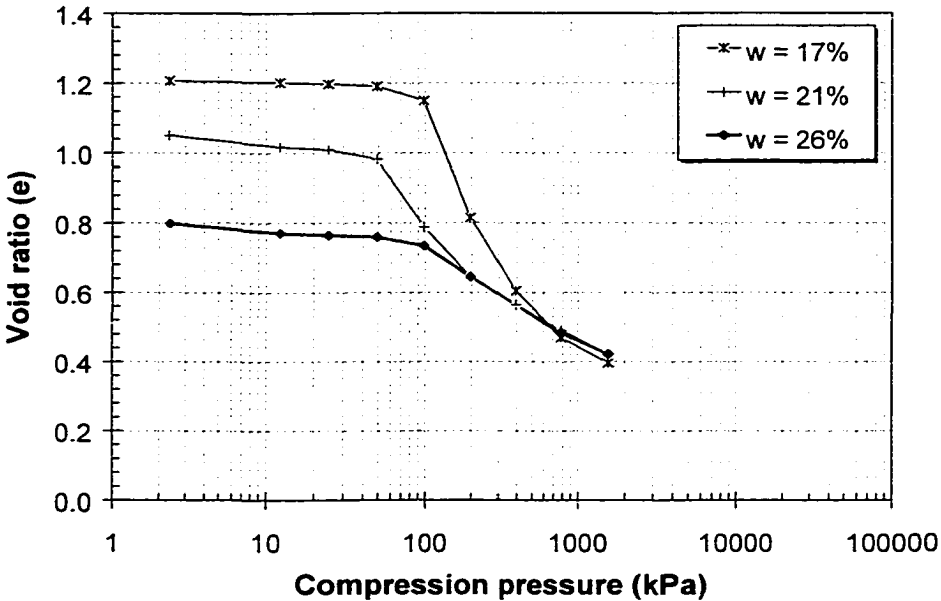


**Figure 6-9 Compression curves of compacted soil prepared with water content at wet zone (wet of OWC)**

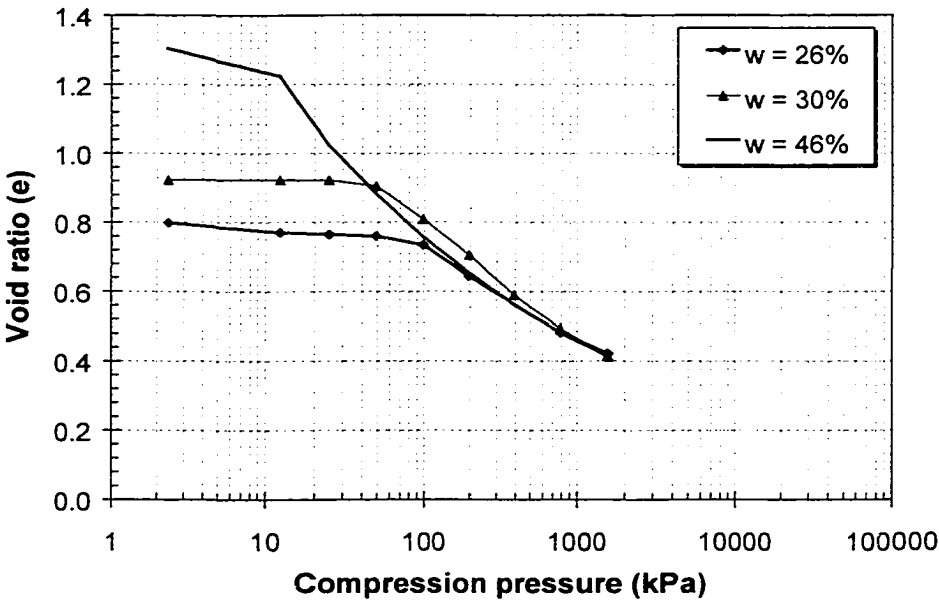




**Figure 6-10 Void ratio progress of 98 kPa compacted soil during one-dimensional compression test**

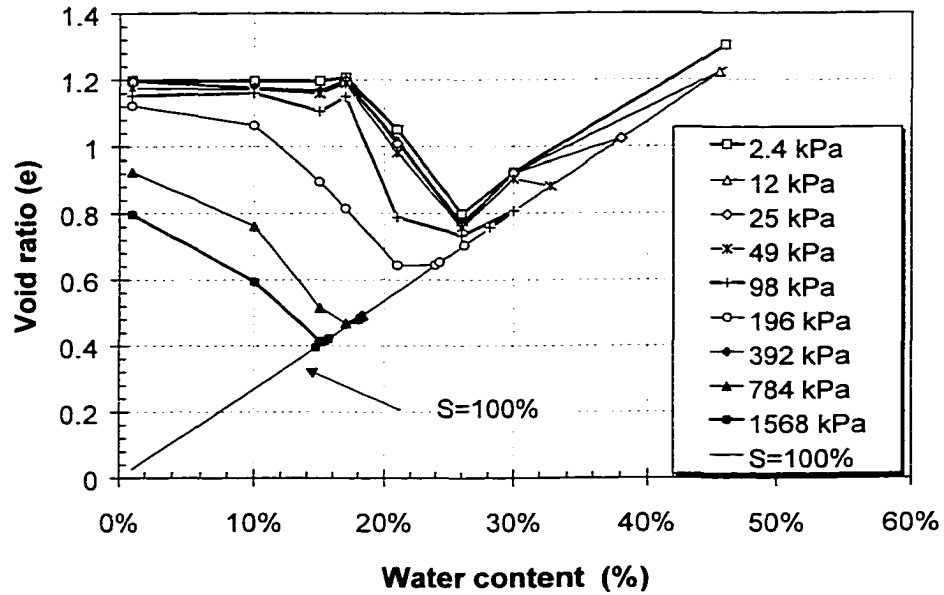


**Figure 6-11 Dry density progress of 98 kPa compacted soil during one-dimensional compression test**

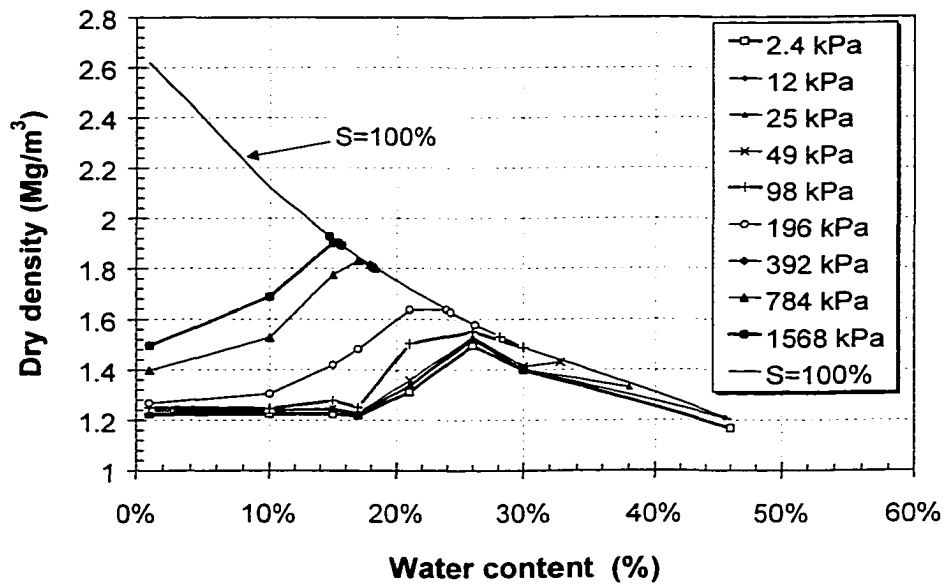


**Figure 6-12 Comparison of void ratio for compacted and as-dumped samples at some compression pressures**

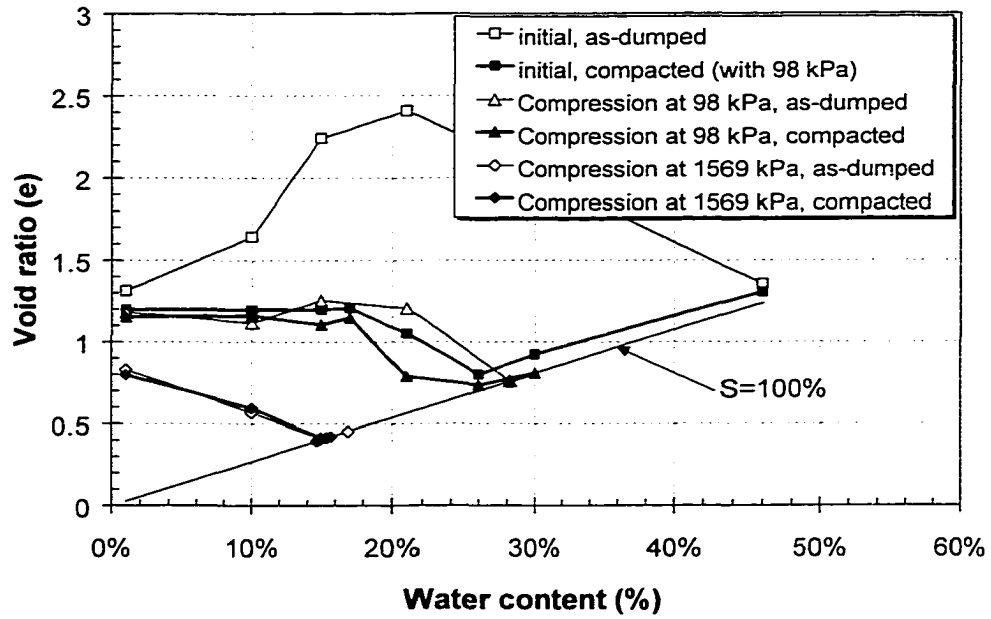


**Figure 6-13 Compression curves of various samples prepared with water content at 1% (where PI- Pleistocene lacustrine clay; 1%- water content; 98 kPa- compaction pressure; N25- number of compaction applications; fld0- flooding sample at beginning)**

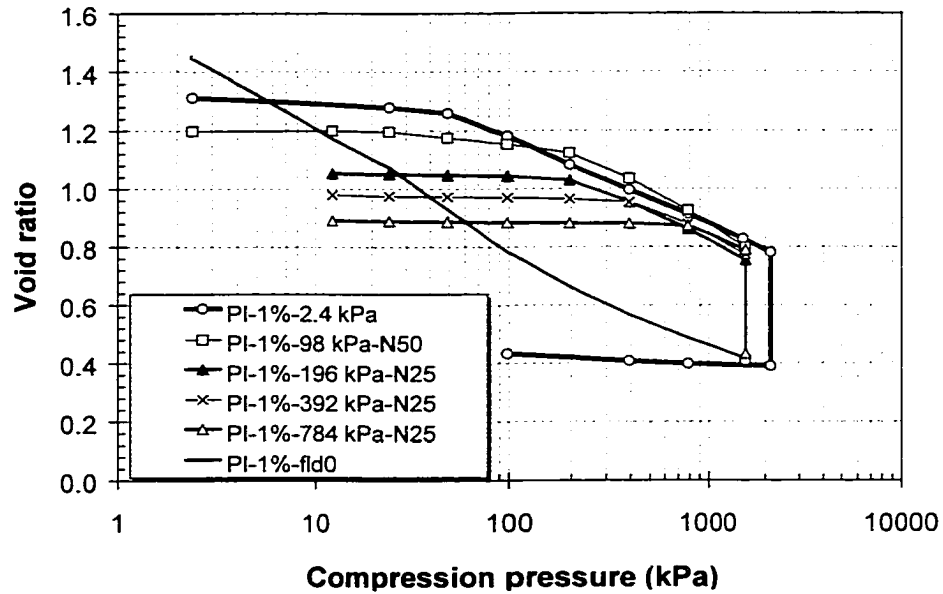


**Figure 6-14 Compression curves of various samples prepared with water content at 10% (sample identification as Fig. 6-13)**

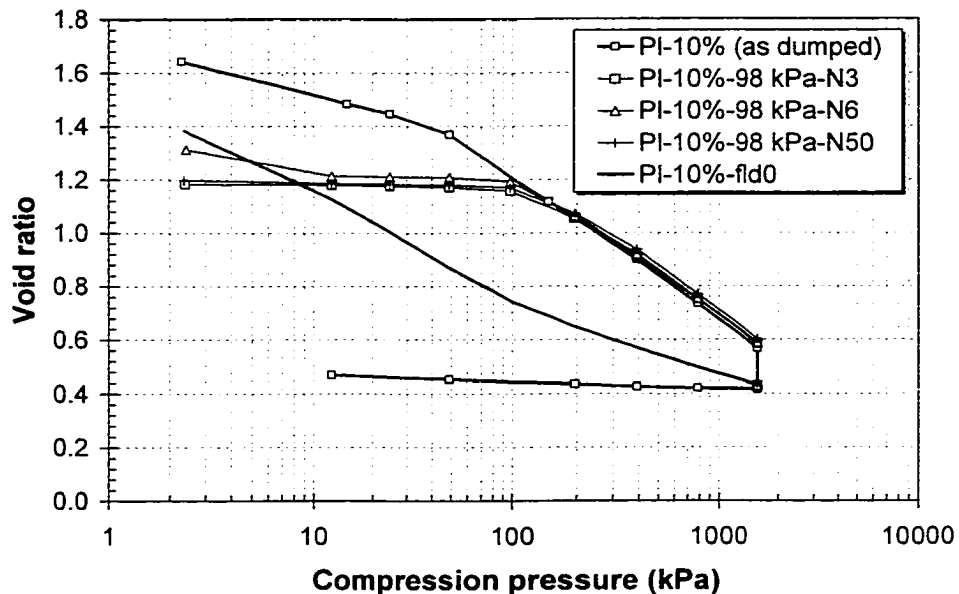


**Figure 6-15 Compression curves of various samples prepared with water content at 15% (sample identification as Fig. 6-13)**

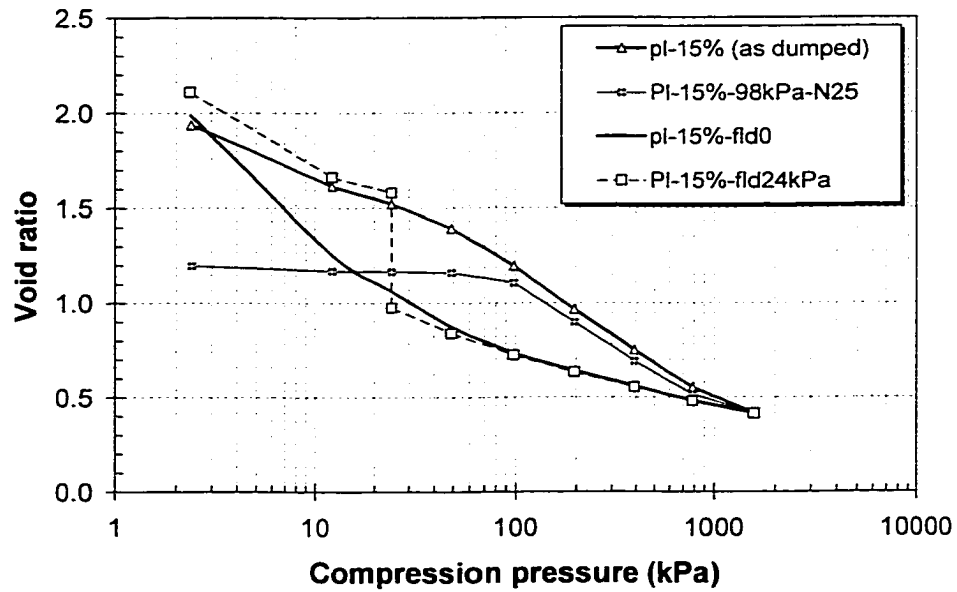


**Figure 6-16 Compression curves of various samples prepared with water content at 17% (sample identification as Fig. 6-13)**

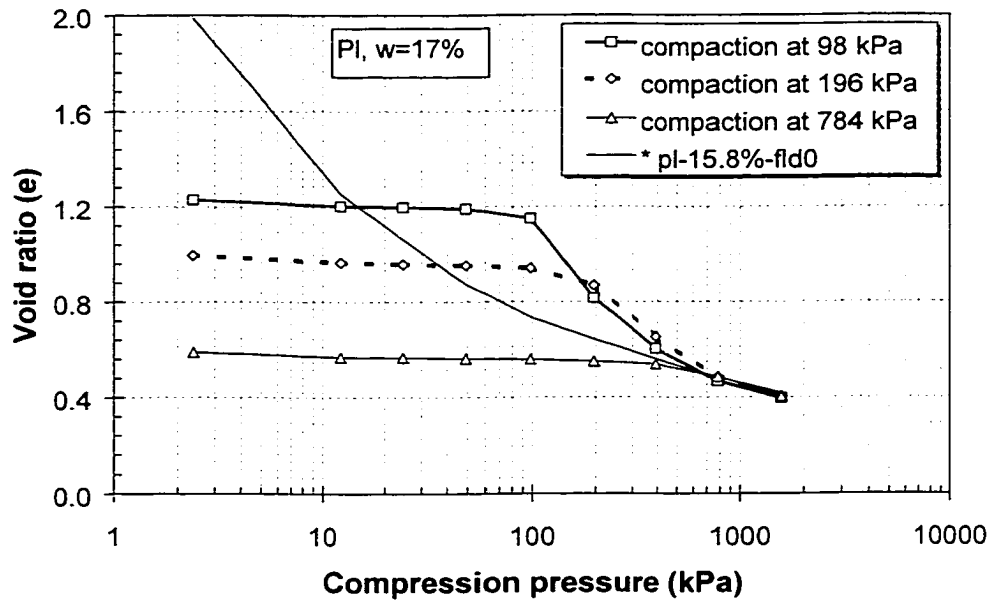


**Figure 6-17 Compression curves of samples prepared with water content at 21% (sample identification as Fig. 6-13)**

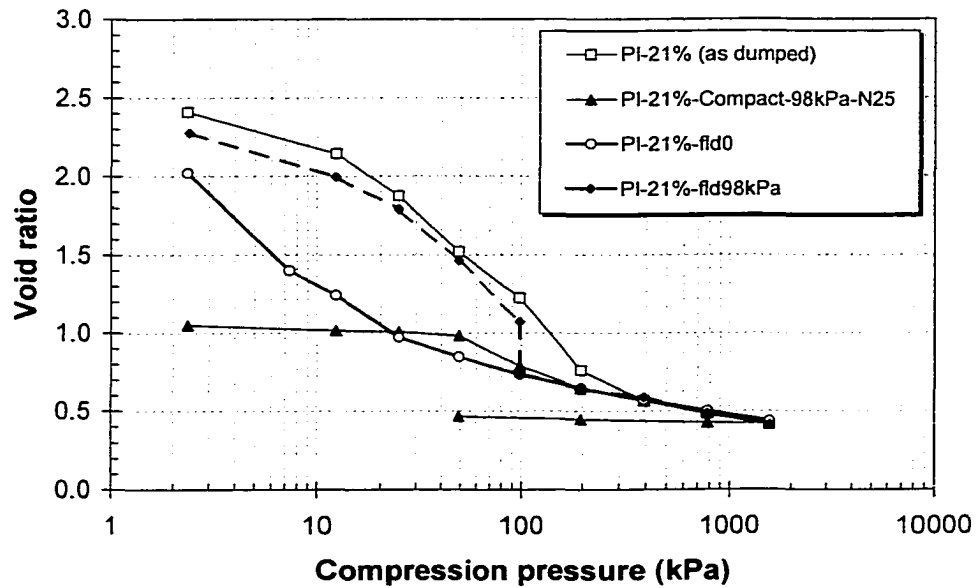


**Figure 6-18 Compression curves of samples prepared with water content at 46% (sample identification as Fig. 6-13)**

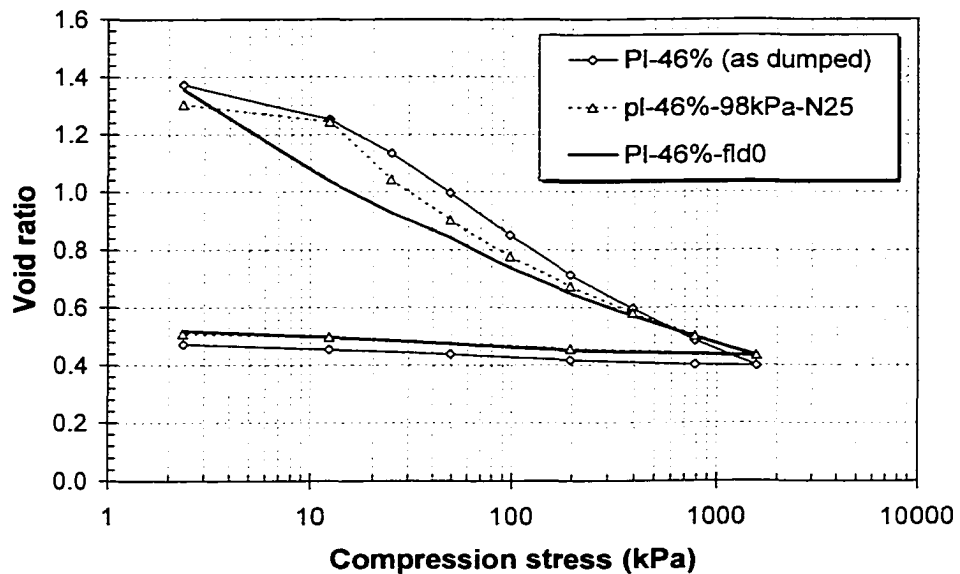


**Figure 6-19 Compression curves of air-dried samples with different loading-wetting sequences**

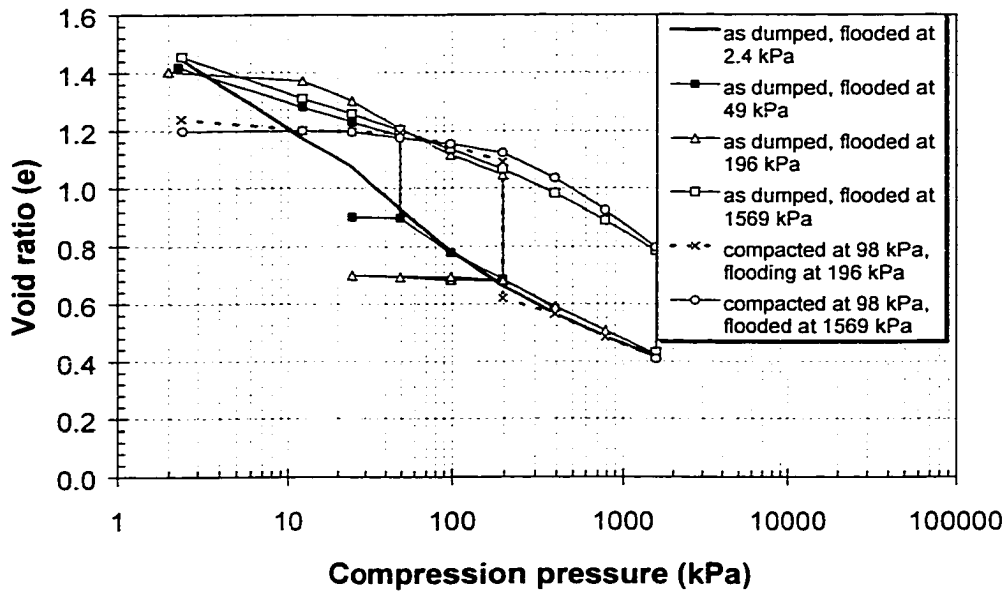


**Figure 6-20 The compression curves for samples with various initial water contents and flooded at beginning (sample identification as Fig. 6-13)**

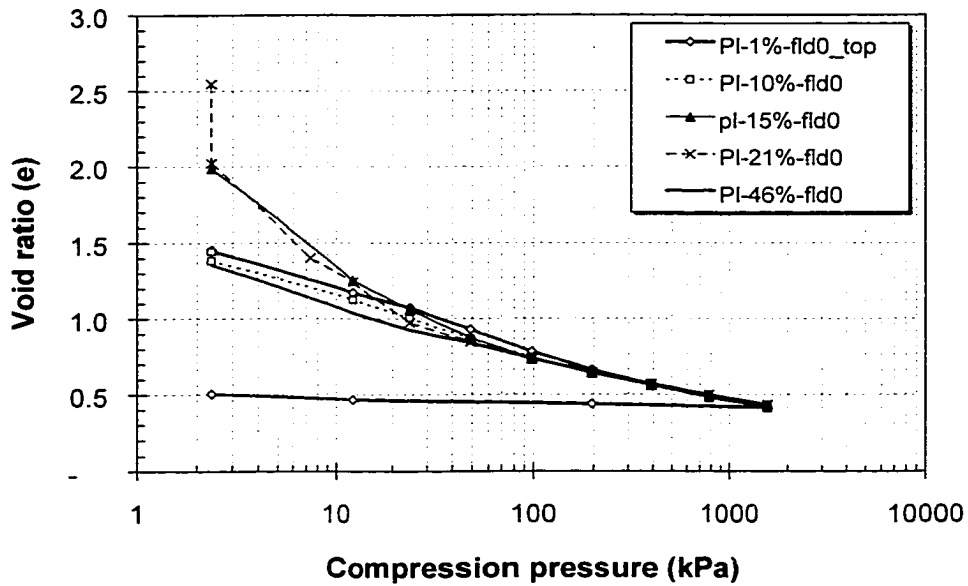
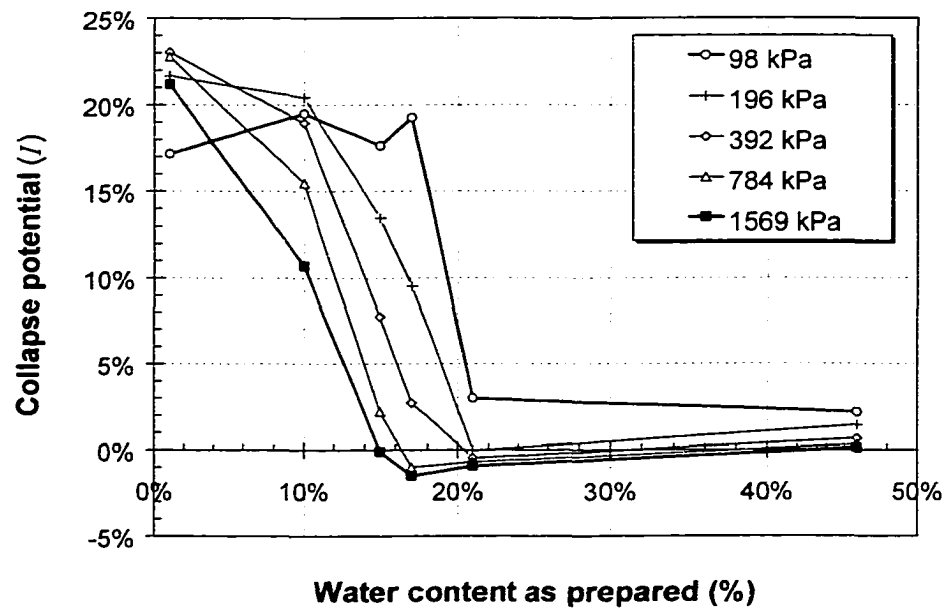


**Figure 6-21 Collapse potential versus as-prepared water content under different compression pressure**



# CHAPTER 7 MODELING AND PREDICTING ONE-DIMENSIONAL COMPRESSION CURVES FOR COMPACTED SOILS

## 7.1 INTRODUCTION

Overburden excavation by the mining industry such as oil sands mining in Northern Alberta results in a large volume of material for disposal. The use of increasing larger trucks to haul, dump and compact these waste materials results in the use of thick placement layers in the waste dumps. The applied compaction effort varies within these thick lift. This results in a variation of placement dry density within each placement layer. Therefore, the estimation of the settlement of a thick compacted layer is more complicated than a normal thin compacted layer which generally has a uniform placement dry density.

Comprehensive one-dimensional compression tests on compacted soil were carried out using the Pleistocene Lacustrine clay ( $P_1$ ) (Chapter 6 and Li and Sego 1999). The compression curves varied with the applied compactive efforts and initial water contents. It is evident that for the same soil, the one-dimensional compression behavior over the low stress range is highly dependent on the initial void ratio, but merge under high compression stress, which means the initial void ratio, pre-compression stress, and even soil structure have little influence at the high stress level (Chapter 6 and Li and Sego 1999). This observation has been supported by many researchers studying soil disturbances associated with sampling (Rutledge 1944; Terzaghi 1944; Schmertmann 1955; Mesri et al. 1975; Burland 1990; Yamamuro et al. 1996). It can be used as a basis to predict a family of compression curves and then to estimate the potential settlement for a deposit with thick layers.



The family of compaction curves has been described and can be predicted using a recently proposed method (Chapter 2 and Li and Segoo 2000a and b). The method considers the density within a thick compacted layer as a member of a family and thus all the compaction curves and individual densities can be acquired from a single compaction curve knowing the applied compactive effort. It is the first step to simplify the estimation of settlement for the thick-layered compacted soils.

One-dimensional compression tests are commonly used in settlement estimation in geotechnical practice. It is also important to research aimed at the development of three-dimensional constitutive equations for soils. Dozens of formulations have been proposed to describe the compression curve during the past fifty years. However, few are continuous over the whole stress range, and they individually have difficulty in describing the sharp curvature near the yield point (previous maximum stress) of the compression curve.

The objective in this chapter is to develop an equation that can continuously and properly describes the complete compression curve for soils with the stress history, such as compaction. The parameters in the equation must be clearly defined to quantify the variation of the initial condition, structure, and compaction pressure applied to the soil. The equation should be able to predict a family of compression curves based on the fore-mentioned behavior.

## **7.2 CHARACTERISTICS OF ONE-DIMENSIONAL COMPRESSION CURVE**

The stress-strain relationship for one-dimensional (1-D) test has been studied throughout the history of soil mechanics since Terzaghi first described the oedometer test in 1924 (Skempton 1960). The importance of this test to geotechnical engineering practice is attested by the fact that nearly all settlement estimates for structures founded on soils are based wholly or partially on 1-D no lateral yield strain behavior (Skempton and Bjerrum 1957; Lambe 1964). One-dimensional strain is also important to research aimed toward the development of three-dimensional constitutive equations for soils (Hardin 1989). The

term “compression curve” instead of “consolidation curve” is used throughout the chapter to indicate that the soil need not be saturated for the analysis being described.

Figure 7-1 shows schematically the one-dimensional compression curve of an undisturbed natural or compacted soil in the  $e$ -log  $\sigma$  space. The curve for a remolded sample is also shown. For a natural sample, the compression is negligible or it undergoes elastic compression up to a certain stress level, beyond which the soil is more compressible as indicated by the steep slope. This yielding stress (pre-compression stress),  $\sigma_p$ , is due to pre-compression or soil cementation. On further loading, the void ratio decreases with stress and theoretically approaches zero void ratio at an extremely high stress level. This results in a characteristic inverse S-shaped curve for the undisturbed sample as shown in Figure 7-1 (Nagaraj et al. 1990).

The curve has two boundaries. The initial void ratio or the initial elastic recompression controls the deformation in the stress range before the yield point. At the extremely high-stress level, the void ratio approaches zero, i.e., all voids would be eliminated.

The compression behavior in the low stress range is highly dependent on the initial void ratio. After overcoming the influence of the stress history at  $\sigma_p$ , the soil is normally (virgin) consolidated or compressed therefore the void ratio at the high-stress level is unique and only depends on the soil mineralogy, particle size, and moisture condition. This is an important characteristic of the soil compression curve and is useful in estimating the soil disturbance, cementing effects, or pre-compression stress.

In general, the complete compression curve can be divided into two zones as shown in Fig. 7-1. In Zone 1, the soil offers a nearly rigid loading response before the yield point. The steep slope in Zone 2 is due to a gradual break down of bonds or as the soil overcomes the pre-compression effect, which indicates the tendency of the soil to move toward the remolded state. When the bonds are completely broken or the pre-compression effect is completely overcome, the soil behavior is similar to that of the remolded soil or a normal consolidated or compressed soil. In other words, all the

compression curves for the same soil composition converge to a unique void ratio at very high-applied stresses.

The two zones are separated by the pre-compression stress ( $\sigma_p$ ) and the soil has different deformation behavior in either zone. However, the compression curve changes continuously within both zones and through the transition associated with the pre-compression stress. The continuity of the curve, the sharp curvature, the gentle decrease of the void ratio at the normally compression region, and the boundary restrictions are the major characteristics of a one-dimensional compression curve for a compacted soil.

### **7.3 REVIEW OF EQUATIONS FOR ONE-DIMENSIONAL COMPRESSION CURVE**

The classical method for modeling 1-D strain is to assume a linear relationship between the void ratio  $e$  and the logarithm of vertical effective stress ( $\sigma_v'$ ). Other mathematical functions have been used to approximate the observed behavior. Various forms of these functions, ranging in complexity from constant values for the compressibility to logarithmic, exponential, and power functions, have been proposed and used with greater or lesser success (Nishida 1956; Janbu 1963; Hanson 1969; Garlanger 1972; Mesri, Rokshar and Bohor 1975; Monte and Krizek 1976; Butterfield 1979; Koppula and Morgenstern 1982; Gibson et al. 1981; Sridharan and Jayadeva 1982; Carrier and Beckman 1984; Krizek and Somogyi 1984; Christie and Tonks 1985; Nagaraj and Murphy 1986; Jose, Sridharan and Abraham 1989; Nagaraj et al. 1990; Den Haan 1992; Liu and Carter 2000).

While these approaches give reasonable results for most engineering applications, the equations are not applicable over the whole stress range. As a result, some major deficiencies may exist, such as the void ratio is not well defined in low stress range, sharp angle appears at the pre-compression stress, and void ratio tends to be negative at a certain high stress.

Juarez-Badillo (1981) proposed a general compressibility equation for soils, which could be the first published model capable of describing the curve over the complete stress range. The equation used the concept of a specific volume as the variable which was defined as:

$$[7-1] \quad V = \frac{V_0}{1 + \left(\frac{\sigma}{\sigma^*}\right)^N}$$

where  $V$  represents volume,  $V_0$  is volume under zero stress,  $\sigma$  is the applied stress,  $\sigma^*$  is the characteristic stress for  $V = V_0/2$ , and  $N$  is a coefficient related to soil compressibility.

Hardin (1989) proposed a  $1/e$  versus  $\sigma_v'$  model for one-dimensional, normally consolidated cohesive soils in the form:

$$[7-2] \quad \frac{1}{e} = \frac{1}{e_0} + \frac{1}{S_{1-D}} \left(\frac{\sigma_v'}{P_a}\right)^N$$

where  $e$  represents the void ratio of soil at an applied stress  $\sigma_v'$ , and  $e_0$  is the initial void ratio.  $1/e_0$  is the intercept at  $\sigma_v' = 0$ , and the reciprocal slope  $S_{1-D}$  is the dimensionless stiffness coefficient for one-dimensional strain.  $P_a$  is a constant that represents the atmospheric pressure to eliminate the unit of stress.  $N$  is a fitting parameter that originally was represented by a symbol  $p$  in Hardin (1989). Clearly, the initial void ratio is well defined at zero effective stress with  $e = e_0$ .

Hardin's equation can be rewritten in a simpler form as Equation 7-3.

$$[7-3] \quad e = \frac{1}{\frac{1}{e_0} + \left(\frac{\sigma}{p}\right)^N}$$

where parameter  $p$  has units of stress, which combines both  $S_{1-D}$  and  $P_a^N$  in Eq. 7-2. Equation 7-3 will be referred to as the simplified Hardin equation later in this chapter.

In fact, Hardin's equation is the same type of equation as presented by Juarez-Badillo (1981) except it uses different variables. The major improvement would be the change of the location of parameter  $e_0$ , which separates from the stress variable. This change reflects the soil basic behavior that the initial void ratio has no influence on soil void ratio in the high stress range.

Liu and Znidarcic (1991) presented an extended power-function model for modeling compression of normally consolidated and overconsolidated soils with the form:

$$[7-4] \quad e = A(\sigma' + Z)^B$$

in which  $A$  and  $B$  are constants, having the usual notation as in other power-function models, and  $Z$  is an additional soil parameter having unit of stress. Because parameter  $B$  is actually negative, the equation is more suitably represented as:

$$[7-5] \quad e = \frac{A}{(\sigma' + Z)^B}$$

Although small differences could be recorded during curve fitting, all three equations are in a form of inversed polynomial equations. Their applications are thus comparable. Each model is reported to be capable of modeling both normally and overconsolidated soil behaviors, but has difficulty in properly modeling the sharp curvature observed in the experimental data of sensitive clay such as Mexico City clay (Liu and Znidarcic 1991). This conclusion is illustrated in Figure 7-2 and it shows that these equations do not

satisfied the sharp curvature of the overconsolidated soil used in Liu and Znidarcic's paper (Drammen clay, data from Butterfield 1979).

In fact, all three equations can be combined in a more general form with an additional parameter.

$$[7-6] \quad e = e_0 \cdot \left( \frac{1}{1 + \left( \frac{\sigma}{p} \right)^N} \right)^M$$

A combination of  $M$  and  $N$  give Equation 7-6 more flexibility to fit the curve in  $e$ -log  $\sigma$  space. When  $M$  is equal to 1, the equation is virtually the same as the equations presented by Juarez-Badillo (1981) and Hardin (1989). When  $N$  is equal to 1, the equation is the same as presented by Liu and Znidarcic (1991).

Equation 7-6 is virtually the same as the equation proposed by van Genuchten (1980) to describe the soil water retention curve (WRC), which has a similar shape to the one-dimensional compression curve and plays a similar role in unsaturated soil mechanics (Fredlund and Xing 1994; Leong and Rahardjo 1997). WRC is referred to as soil-water characteristic curve (SWCC) in geotechnical engineering. Van Genuchten's equation is the most popular equation for the WRC in soil science. However, the use of the power law function limits its application in describing compression curves for soils with compaction or pre-compression history. Mathematically, when modeling the sharp curvature over the yield point of the compression curve,  $N$  needs to be very large. But the cost of a large value of  $N$  is that the void ratio drops rapidly to zero over a narrow stress range. This does not agree with actual soil compression test results. These comparisons were presented in Fredlund and Xing (1994) when they discussed the equations used to describe the SWCC or WRC.

The decrease of void ratio with logarithm stress is one of the characteristics of a soil compression curve. Evident is the widely used logarithm linear relationship, e.g. Cam Clay (Schofield and Wroth 1968). Fredlund and Xing (1994) show a logarithmic relationship better represents the SWCC in most cases than other models based on power law function. The relationship between volumetric water content ( $\theta$ ) and suction ( $\psi$ ) according to these authors is best represented as:

$$[7-7] \quad \theta = \theta_s \left[ \frac{1}{\ln \left( 2.71828 + \left( \frac{\psi}{a} \right)^n \right)} \right]^m$$

where  $\theta_s$  is the volumetric water content at saturation and the three parameters  $a$ ,  $n$ , and  $m$  are used for fitting the *S*-shaped SWCC. By replacing the volumetric water content ( $\theta$ ) and suction ( $\psi$ ) with void ratio ( $e$ ) and compression stress ( $\sigma$ ), this equation can be also used to fit an *S*-shaped soil compression curve fairly well. However, the Fredlund and Xing equation assumes the initial saturated  $\theta_s$  (or  $e$  in compression curve) has an influence over the complete stress (suction) range. This in fact conflicts with the observation of the compression test results.

The concept of using a logarithm relationship in the normal compression region is adopted in this research to develop a suitable equation to describe the complete compression curve.

#### **7.4 PROPOSED EQUATION FOR ONE DIMENSIONAL COMPRESSION CURVE**

To properly define an equation of a complete compression curve, the parameters in the equation must be clearly defined to quantify the variation of the initial condition, structure, and compaction pressure applied to the soil.

It is evident that the initial void ratio dominates the curve before the yield stress  $\sigma_p$  and has little effect on the deformation behavior at higher stress. On the other hand, the applied stress has little effect before the yield stress  $\sigma_p$  but dominates in the normal compression range. Therefore, the whole curve can be divided into two zones separated by the yield stress  $\sigma_p$ . The lower stress zone (Zone 1) is dominated by the initial void ratio and the high stress zone (Zone 2) controlled by the virgin (normal) compression curve of soils after the yield point (Fig. 7-1). This concept suggests that the initial void ratio and compression stress are independent of each other and should be separately included in a two variable equation.

Based on the previous discussion, the void ratio after  $\sigma_p$  is assumed to follow the power law in semi-logarithm  $e$ -log  $\sigma$  space. The following two equations mathematically represent the influence of the initial void ratio and the power law curve in  $e$ -log  $\sigma$  space.

$$[7-8] \quad \begin{cases} e = e_0 \\ e = \frac{1}{M \cdot \ln \left( 1 + \left( \frac{\sigma}{p} \right)^N \right)} \end{cases}$$

where  $e_0$  is the initial void ratio. Parameters  $M$ ,  $N$ , and  $p$  are used to define the logarithm power law in  $e$ -log  $\sigma$  space with a maximum of flexibility. Both formulas in Equation 7-8 are valuable over the whole stress range. Den Haan (1992) found using three parameters substantially improved the fit of the virgin compression curves for soils, where a power law equation was used. The logarithm power law expression in Equation 7-8 allows the void ratio to decrease slowly with the stress, which is a better representation of the behavior than the power law expression.



To combine the two-separated conditions together, the following equation is obtained when all the boundary requirements are satisfied.

$$[7-9] \quad e = \frac{1}{\frac{1}{e_0} + M \cdot \ln \left( 1 + \left( \frac{\sigma}{p} \right)^N \right)}$$

Equation 7-9 is used to describe a complete soil compression curve in this paper. The curves from the two original functions of Equation 7-8 and the combined curve represented by Equation 7-9 are compared in Fig. 7-3.

In order to physically understand Equation 7-9, the equation is rewritten as:

$$[7-10] \quad \frac{1}{e} = \frac{1}{e_0} + M \cdot \ln \left( 1 + \left( \frac{\sigma}{p} \right)^N \right)$$

A plot in  $1/e$ - $\log \sigma$  space is shown in Figure 7-4 where two straight lines are smoothly connected around stress  $p$ . It is evident that the horizontal line ( $1/e_0$ ) is dominated by the initial ratio, while the logarithm power law relationship indicate a straight line with a slope of  $MN$  in  $1/e$ - $\log \sigma$  space. The value of  $N/M$  reflects the rate of transition of the two straight lines. The linear relationship between  $1/e$  and  $\log \sigma$  can be used to explain the proposed logarithm power law relationship physically.

The expression  $1/e$  represents the concept of the solid ratio (solid volume  $V_s = 1$  divided by the void volume  $e$ ), which is proposed as a useful new concept in geotechnical engineering. A related definition (solids content) is more commonly used in chemical engineering and mine tailing engineering. In this model, the solid ratio increases constantly with the increase of logarithmic applied stress in the virgin compression region. The capability and limitation of Equation 7-9 will be discussed in the following section.

For a compression curve without the obvious *S*-shape, a three-parameter equation would be sufficient to properly fit the complete compression curve. The parameter  $M$  may then be assumed as 1 so a single parameter ( $N$ ) is used to define the slope of the curve in transition zone.

## 7.5 INFLUENCES OF THE PARAMETERS

Each of the four parameters  $e_0$ ,  $p$ ,  $M$  and  $N$  has specific effect on the shape and position of the compression curve.

The parameter  $e_0$  is the initial void ratio when the compression stress is zero. In Figure 7-5, it can be seen that when other parameters are held constant, changing the initial void ratio  $e_0$  has a substantial influence in the low stress range but has less influence when the stress level increases, which agrees well with previous discussion about the equation and the typical compression curve.

Increasing the value of the parameter  $p$  moves the curve in  $e$ - $\log p$  space parallel to the right without appreciably changing its shape and either end boundary conditions (Fig. 7-6). It is obviously that  $p$  is a parameter that controls the location of transition of the curve and thus is strongly depend on the pre-compression stress. The value of  $p$  is not necessary equal to the stress at the maximum curvature of the compression curve, but it is close to the yield stress of the compression curve as shown in Figure 7-6 and later examples. Parameter  $p$  reflects the stress history influence on natural soils.

Figures 7-7 and 7-8 illustrate the influences of parameters  $M$  and  $N$  on the shape of the curve. Both parameters have mixed effects on the shape of the curve. Parameter  $M$  mainly has influence on the void ratio at the high stress level and parameter  $N$  controls the slope of the compression curve in the transition zone. The influence on the shape of curve by the parameters  $M$  and  $N$  is clearer when they are combined together to analyze a data set.

If the compression stress  $\sigma$  is assumed to be greater than  $p$ , then with a large value of  $N$ ,  $\left(\frac{\sigma}{p}\right)^N$  would be much greater than 1. Equation 7-9 can be then simplified by neglecting the less influential part as shown in Equation 7-11.

$$[7-11] \quad e \cong \frac{1}{\frac{1}{e_0} + M \cdot \ln \left[ \left( \frac{\sigma}{p} \right)^N \right]} = \frac{1}{\frac{1}{e_0} + MN \cdot \ln \left( \frac{\sigma}{p} \right)}$$

If the stress is much greater than  $p$ , Equation 7-11 can be further simplified by neglecting the more minor effects of  $1/e_0$  and  $\ln p$ .

$$[7-12] \quad e \cong \frac{1}{\frac{1}{e_0} + MN \cdot [\ln \sigma - \ln p]} \approx \frac{1}{MN \cdot \ln \sigma}$$

In Equation 7-12 only the product of  $M$  and  $N$  has influence on the final void ratio. If the value of  $MN$  is considered as a constant for a given soil, the model will give a unique void ratio at a given high-applied stress. This actually agrees with the fundamental behavior of the observed compression curves for a given soil, in which the void ratio at high stress level is seldom affected by either the initial void ratio ( $e_0$ ) and previous stress history ( $p$ ) associated with the soil.

If assuming  $MN$  is constant for a soil, a series of curves are plotted in Figure 7-9 by changing the ratio of  $N/M$  in the lower stress region. This shows that with the increase of  $N/M$ , the curve becomes steeper. The variation of the curves suggests the same features as observed for samples with different degree of disturbance (Rutledge 1944; Bozozuk 1971; Lacerda et al. 1977; Holtz and Kovacs 1981; Kabbaj et al. 1985; Wang and Wei 1996).

When  $N/M$  approaches infinite (i.e.  $N$  is much greater than  $M$  but  $MN$  is still a constant), Equation 7-9 actually separates into two parts. When the compression stress  $\sigma$  is smaller than the value of parameter  $p$ ,  $\left(\frac{\sigma}{p}\right)^N$  would be close to zero due to the large value of  $N$ . Therefore the void ratio at stresses less than  $p$  from Equation 7-9 equals  $e_0$ . When the stress  $\sigma$  is greater than  $p$ ,  $\left(\frac{\sigma}{p}\right)^N$  is much greater than 1, so  $\left(1 + \left(\frac{\sigma}{p}\right)^N\right)$  can be represented by  $\left(\frac{\sigma}{p}\right)^N$ . The void ratio after  $p$  is then well represented by Equation 7-11.

Therefore the compression curve when  $N/M$  approach infinite becomes

$$[7-13] \quad \begin{cases} e = e_0 & \text{when } \sigma \leq p \\ e = \frac{1}{\frac{1}{e_0} + MN \cdot \ln\left(\frac{\sigma}{p}\right)} & \text{when } \sigma > p \end{cases}$$

The two expressions of the ultimate compression curve from Equation 7-13 are asymptotic curves for a family of curves with  $MN$  as constant. They are continuous at point  $\sigma = p$  as shown in Figure 7-9, where  $e = e_0$ . The sharp angle at the stress equal to  $p$  indicates that  $p$  is the yield stress when  $N/M$  approach infinity. The sudden angle change also gives the equation tremendous ability to continuously model the compression curve of soils with a previous stress history, which are characterized by a sharp curvature when the applied stresses approaches the yield point (pre-compression stress). This overcomes the major shortcoming in previously equations proposed to describe the complete compression curve (Juarez-Badillo 1981; Hardin 1989; Liu and Znidarcic 1991).

Additionally, it would be convenient to change Equation 7-9 to incorporate elastic recompression for soils. An elastic recompression equation ( $e_k - C_k \ln \sigma$ ) is used to

replace the originally proposed constant initial void ratio ( $e_0$ ) (Atkinson and Bransby 1978). Then Equation 7-9 can be written as:

$$[7-14] \quad e = \frac{1}{\frac{1}{e_k - C_k \cdot \ln \sigma} + M \cdot \ln \left( 1 + \left( \frac{\sigma}{p} \right)^N \right)}$$

where  $C_k$  is the recompression index and  $e_k$  is the void ratio when the applied stress is unity. A curve represented by Equation 7-14 is shown in Fig. 7-10, in which the part of curve before yield point represents an inclined line in  $e$ -log  $\sigma$  space.

## 7.6 EXPERIMENTAL EVALUATION OF PROPOSED EQUATION

There are many one-dimensional compression test results for different soils available in published literature. Most are from consolidation tests. The results for compacted soils were usually carried out using unconfined or triaxial compression test. Test data from normal consolidated soils, overconsolidated soils, compacted soils, and structured and remolded clays have been selected to verify the usefulness of Equation 7-9. The regression parameters were obtained using statistic software SPSS.

Consolidation data of marine postglacial clay from Drammen, Norway (Berre and Iversen 1972) was chosen to evaluate the efficiency of different equations. The clay was described as soft sensitive normal consolidated clay. The data was calculated from vertical strain and the curve is plotted using void ratio versus stress in Fig. 7-11. Only one curve from Sample-H6 is presented since the other curves are of similar shape. The simplified Hardin's equation (Eq. 7-3), Liu and Znidarcic's extended power-function model (Eq. 7-4) and the proposed equation (Eq. 7-9) are compared with the published data. Because the curve show no "S" shape, Equation 7-9 was simplified by setting parameter  $M$  equal to 1 for the clay. Table 7-1 summarizes the regression results and Figure 7-11 shows the fitted curves. It is obvious the simplified Hardin's and the

proposed equation fit the data better than Liu and Znidarcic's model for this particular clay.

For typical *S*-shaped curves which are generally associated with overconsolidated clay such as San Francisco Bay Mud (Holtz and Kovacs 1981), the results from the simplified Hardin's, Liu and Znidarcic's and Equation 7-9 with  $M=1$  do not reproduce the data well (Fig. 7-12 and Table 7-2). This illustrates the limitation of the 3-parameter function in describing the sharp curvature of the *S*-shaped curve over the narrow range of yielding. The four-parameter version of Equation 7-9 produces a superior fit to the data for this clay (Fig. 7-12).

Chicago silty clay is a typical glacial lake clay, which has undergone preconsolidation in the past that is much higher than its current overburden stress. Equation 7-9 again fits the results from Taylor (1948) as is shown in Fig. 7-13 using the parameters summarized in Table 7-3.

Figure 7-14 shows the consolidation characteristics of Mexico City clay (Mesri et al. 1975). This sediment is not really a clay but is composed primarily of microfossils and diatoms. The porous structure of the fossils gives the soil a very high initial void ratio, natural water content, and compressibility (Holtz and Kovacs 1981). Mexico clay has been preconsolidated although it is known geologically as a normally consolidated soil. The higher stress was caused by variations of the water table, aging and structure or cementing (Diaz-Rodriguez, et al. 1992). Data from Mesri et al. (1975) for undisturbed, sedimented and remolded samples are compared to Equation 7-9 and this comparison is shown in Fig. 7-14. Remolding almost completely destroys the pre-consolidation effect. It was observed that the value of parameter  $p$  to produce the fit is very high as the remolded curve is not the typical *S*-shaped (Table 7-4).

Understanding and utilizing one-dimensional compression curve of compacted soils is the major focus of this research. To the authors' surprise, little data under one-dimensional compression on compacted soils is published in the literature. The test results for this

research project presented in Chapter 6 were therefore used. The one-dimensional compression curve for Pleistocene Lacustrine clay ( $P_1$ ) compacted at a water content of 15% are shown in Figure 7-15. It was observed that the initial void ratio is substantially decreased after kneading compaction and a sharp curvature is observed near the applied compaction foot pressure. This pressure for a compacted soil is similar to the pre-consolidation pressure of overconsolidated soils. The curves were fitted using Equation 7-9 and the fit shows good agreement with the laboratory data. Table 7-5 summarizes the parameters used and information on the fit.

Although the proposed equation fits the compression behavior of most soils well with or without previous stress history, it is unlikely the Equation 7-9 is a universal equation to fit any *S*-shaped curve. It may not fit well the structured clay such as cemented Canadian marine clay, where some of the bond strength is suddenly destroyed during the test. Curves of Leda clay from Quigley and Thompson (1966) were apparently fitted well as is illustrated in Figure 7-16. The regression data are presented in Table 7-6. However it was found that the increase of solid ratio ( $1/e$ ) after yield stress is not a straight line as predicted using Equation 7-9 and as is shown in Fig. 7-17. This non-linearity is more evident for the curves of two different Eastern Canadian sensitive clays shown in Figure 7-18 that were reported by Tavenas et al. (1981). There is generally no bi-linear relationship existing in  $1/e$ - $\log \sigma$  space for Matagami clay and Louiseville clay in Figure 7-19. The regression results for Louiseville clay using Equation 7-9 were included in Table 7-7.

In fact, the compression curve for structured clay does not change smoothly at the “yield stress” since the bond strength is sudden destroyed. The variation of void ratios before and after the yield stress is not continuous. Therefore, using a single equation such as Equation 7-9 to fit the complete compression curve for this kind of soils would not be satisfied.

## 7.7 PREDICTION OF A FAMILY OF COMPRESSION CURVES

Based on the fact that the same soil has a unique void ratio at high stress during one-dimensional compression test, Equation 7-9 allows a family of compression curves to be created by assuming  $MN$  is constant for a given soil. The virgin compression curve for a compacted soil prepared at a certain water content is unique and it is independent of the applied compaction effort. This suggests the value of  $N/M$ , which controls the slope of the virgin compression curve, is also constant. Therefore it would be reasonable to assume that both  $M$  and  $N$  are constants for a given soil compacted at the same water content. Using this concept, the compression curves for the soil can thus be predicted if the compaction pressure and resulting dry density (initial void ratio) are known.

Figure 7-20 shows the Pleistocene Lacustrine clay ( $P_1$ ) prepared at a water content of 17%. Three samples compacted using 98, 196, and 784 kPa foot pressures were used for one-dimensional compression tests. The initial void ratios for the three samples were obtained as  $e_k = 1.237, 1.004$  and  $0.594$  respectively from the plot. The elastic recompression index ( $C_k$ ) is  $0.0124 \text{ (kPa}^{-1}\text{)}$  in the 98-kPa compression curve. The compression curve for the sample prepared under 98 kPa was fitted using Equation 7-14, where  $M$  (0.0666) and  $N$  (9.3831) were established. Assuming parameter  $p$  equals the compaction pressures 196 and 784 kPa, the one-dimensional compression curves for each of the other applied footing pressures were calculated and the comparison is shown in Fig. 7-20. Table 7-8 summarized the data used to predict the results for the samples prepared at the 17% water content.

When a given soil with the same water content is used, the virgin compression curve is independent of the compactive effort, which indicates the ultimate asymptote curve is unique. An extra relationship among parameter  $e_0$ ,  $p$  and  $MN$  can be derived from Equation 7-13 as following Equation 7-15:



$$[7-15] \quad \frac{1}{e} - MN \cdot \ln \sigma = \frac{1}{e_0} - MN \cdot \ln p$$

Equation 7-15 would be useful in creating a family of compression curves for a given compacted soils. For the case when the compaction pressure is unknown, Equation 7-15 can be used to estimate the parameter  $p$ . The predicted compression curves for  $P_1$  at a water content of 17% using compactive pressures of 196 and 784 kPa are shown in Fig. 7-21 with good agreement. The calculated parameter  $p$  is 145.9 and 438.5 kPa and the results are summarized in Table 7-9.

In a field embankment, where dry density is usually measured but where the applied stress is unknown, one can predict the compression curve based on a single one-dimensional compression test carried out on the soil using this approach. It thus has the potential for use by practicing professionals.

## 7.8 CONCLUSIONS AND RECOMMENDATIONS

The one-dimensional compression test is commonly used for settlement calculations in geotechnical practice. Equation 7-9 or 7-14 is proposed to accurately represent the one-dimensional compression curve over the complete stress range. Examples with various types of soils illustrated its usefulness for geotechnical practice, with the exception of some highly structured sensitive clays. The parameters within the equation are physically defined as the initial void ratio ( $e_0$ ), the pre-compression stress or yield stress ( $p$ ), the slope of the transition ( $N/M$ ), and the boundary condition at high stress ( $MN$ ). They can be obtained using the regression method. Considering the initial elastic recompression equation, ( $e_k - C_k \ln \sigma$ ) can be used to replace the constant initial void ratio ( $e_0$ ). The values of  $M$  and  $N$  for a given soil at the same moisture condition can be considered constant. When only the initial condition (such as the in-situ dry density) is known, the parameter ( $p$ ) can be estimated using Equation 7-15. This helps using the equation to predict a family of compression curves within a layer of compacted soils and for settlement estimation.

Since Equations 7-9 and 7-14 can precisely describe a compression curve, the settlement at any stress level can be thus mathematically formulated. The model has the potential to be expanded to three-dimensions. It has been shown to be useful in representing the soil water characteristic curve (SWCC) of unsaturated soil mechanics. It is believed the parameters  $M$  and  $N$  are related to soil physical properties such as particle size distribution, plastic limit, or liquid limit. Hence, further research into this matter should allow prediction of the soil compression curve using only basic soil physical properties.

---

<sup>1</sup> SPSS for Windows is a proprietary product of SPSS Inc. Headquarters, 233 S. Wacker Drive, 11th floor, Chicago, Illinois 60606.

## 7.9 REFERENCES

- Atkinson, J.H. and Bransby, P.L 1978. **The Mechanics of Soils**. McGraw-Hill. 118-144.
- Berre T. and Iversen K. 1972. Oedometer test with different specimen heights on a clay exhibiting large secondary compression. *Geotechnique*, **22**(1): 53-70.
- Bishop, A.W. 1959. The principle effective stress, Lecture delivered in Oslo, Norway, in 1955, published in *Teknisk Ukeblad*, **106**(39): 859-863.
- Bozozuk, M. 1971. Effect of sampling, size, and storage on test results for marine clay. *Sampling of Soil and Rock*, ASTM STP **483**, American Society for Testing and Materials: 121-131.
- Burland, J.B. 1990. On the compressibility and shear strength of natural clays. *Geotechnique*, **40**(3): 329-378.
- Butterfield, R. 1979. A natural compression law for soils (an advance on  $e$ - $\log p'$ ). *Geotechnique*, **29**(4): 469-480.
- Carrier, W.D. and Beckman, J.F. 1984. Correlations between index tests and the properties of remoulded clays. *Geotechnique*, **34**(2): 211-228.

- Christie, I.F. and Tanks, D.M. 1985. Developments in the time lines theory of consolidation. *In* Proceedings of 11th International Conference on Soil Mechanics and Foundation Engineering. San Francisco, Vol. 2: 423-426.
- Den Haan, E.J. 1992. The formulation of virgin compression of soils. *Geotechnique*, **42**(3): 465-483.
- Diaz-Rodriguez, J.A., Leroueil, S., and Aleman, J.D. 1992. Yielding of Mexico City clay and the other natural clays. *ASCE Journal of Geotechnical Engineering*, **118**(7): 981-995.
- Fredlund, D.G. and Morgenstern, N.R. 1977. Stress state variables for unsaturated soils. *ASCE Journal of the Geotechnical Engineering Division*, **103**(GT5): 447-466.
- Fredlund, D.G. and Xing, A. 1994. Equations for the soil-water characteristic curve. *Canadian Geotechnical Journal*, **31**(4):521-532.
- Garlanger, J.E. 1972. The consolidation of soils exhibiting creep under constant effective stress. *Geotechnique*, **22**(1): 71-78.
- Gibson, R.E., Schiffman, R.L., and Cargill, K.W. 1981. The theory of one-dimensional consolidation of saturated clays, II. Finite nonlinear consolidation of thick homogeneous layers. *Canadian Geotechnical Journal*, **18**(2): 280-293.
- Hanson, B. 1969. A mathematical model for creep phenomena in clay. *In* Proceedings of 7<sup>th</sup> International Conference on Soil Mechanics and Foundation Engineering, Mexico City, Speciality session 12.
- Hardin, B. 1989. 1-D strain in normal consolidated cohesive soils. *ASCE Journal of Geotechnical Engineering*, **115**(5): 689-710.
- Holtz and Kovacs, 1981. **An introduction to geotechnical engineering**, Prentice-Hall, Inc, New Jersey, p291-293, p327.
- Janbu, N. 1963. Soil compressibility as determined by oedometer and triaxial tests. *In* Proceedings of the European Conference on Soil Mechanics and Foundation Engineering, Wiesbaden, West Germany, Vol. 1: 19-25.
- Jose, B.T., Sridharan, A., and Abraham. B.M. 1989. Log-log method for determination of preconsolidation pressure. *ASTM Geotechnical Testing Journal*, **12**(3): 230-237.

- Juarez-Badillo, E. 1981. General compressibility equation for soils. *In* Proceedings of 10th International Conference on Soil Mechanics and Foundation Engineering, Stockholm, Vol. 1: 171-178.
- Kabbaj, M., Oka, F., Leroueil, S., and Tavenas, F. 1985. Consolidation of natural clays and laboratory testing. Symposium on Consolidation Behavior of Soils, Fort Lauderdale, ASTM STP **892**: 378-403.
- Koppula, S.D. and Morgenstern, N.R. 1982. On the consolidation of sedimenting clays. *Canadian Geotechnical Journal*, **19**: 260-268.
- Krizek, R.J. and Somogyi, F. 1984. Perspectives on modeling consolidation of dredges materials. *In* Proceeding of the Symposium on Sedimentation-Consolidation Models: Predictions and Validation, ASCE, San Francisco, California: 296-332.
- Lacerda W.A., Costa Filho, L.M., Coutinho, R.Q., Duarte, A.E.R. 1977. Consolidation characteristics of Rio de Janeiro soft clay. *In* Proceeding of International Symposium on Soft Clay, Bangkok, Thailand: 231-235.
- Lambe, T.W. 1964. Methods of estimating settlement. *In* Proceedings of Design of Foundations for Control of Settlement, ASCE: 47-71.
- Leong, E.C. and Rahardjo, H. 1997. A review on soil-water characteristic curve equations. *ASCE Journal of Geotechnical and Geoenvironmental Engineering*, **123**(12): 1106-1117.
- Leroueil, S. and Kabbaj, M. 1987. Discussion on 'Composition and compressibility of typical samples of Mexico City clay' by Mesri et al. *ASCE Journal of Geotechnical Engineering*, **113**(9): 1067-1070.
- Li, H. and Sego, D.C. 1999. Deformation of dumped fined-grained soil. *In* Proceeding of 52nd Canadian Geotechnical Conference, Regina, Saskatchewan, Canada, October 25-27, 1999. 453-460.
- Li, H. and Sego, D. C. 2000a. Equation for complete compaction curve of fine-grained soils and its applications. *Constructing and Controlling Compaction of Earth Fills*, ASTM STP 1384, Shanklin, D.W., Rademacher, K.R., and Talbot, J.R. (Eds.), American Society for Testing and Materials, West Conshohocken, PA. pp. 113-125.
- Li, H. and Sego, D. C. 2000b. Equation of compaction curve for fine-grained soils: its origin, implementation and application. Submitted to *Canadian Geotechnical Journal*.

- Liu, J-C. and Znidarcic, D. 1991. Modeling one-dimensional compression characteristics of soils, *ASCE Journal of Geotechnical Engineering*, **117**(1): 162-169.
- Liu, M.D. and Carter, J.P. 1999. Virgin compression of structured soils. *Geotechnique*, **49**(1): 43-57.
- Liu, M.D. and Carter, J.P. 2000. Modeling the destructuring of soils during virgin compression. *Geotechnique*, **50**(4): 479-483.
- Lutenegger, A.J. and Saber, R.T. 1988. Determination of collapse potential of soils. *ASTM Geotechnical Testing Journal*, **11**(3): 173-178.
- Monte, J.L. and Krizek, R.J. 1976. One-dimensional mathematical model for large-strain consolidation. *Geotechnique*, **26**(4): 495-510.
- Mesri, G., Rokshar, A., and Bohor, B.F. 1975. Composition and compressibility of typical samples of Mexico City clay. *Geotechnique* **25**(3): 528-554.
- Nagaraj, T.S. and Murthy, B.R.S. 1986. A critical appraisal of compression index equations. *Geotechnique*, **36**(1): 27-32.
- Nagaraj, T.S., Murthy, B. R. S., Vatsala, A., and Joshi, R.C. 1990. Analysis of compressibility of sensitive soils. *ASCE Journal of Geotechnical Engineering*, **116**(1): 105-118.
- Nishida, Y. 1956. A brief note on compression index of soil. *ASCE Journal of Soil Mechanics and Foundation Engineering*, **82**(3): 1027-1to1027-14.
- Quigley, R.M. and Thompson, C.D. 1966. The fabric of anisotropically consolidated sensitive marine clay. *Canadian Geotechnical Journal*, **3**(2): 61-73.
- Rutledge, G.P. 1944. Relation of undisturbed sampling to laboratory testing. *Transactions of American Society of Civil Engineers*, **109**: 1155-1183.
- Scheffield, A.N. and Wroth, C.P. 1968. **Critical State Soil Mechanics**, McGraw-Hill, London, 310pp.
- Schmertmann, J.H. 1955. The undisturbed consolidation of clay. *Transaction of American Society of Civil Engineers*, **120**: 1201-1233.
- Skempton, A.W. and Bjerrum, L. 1957. A contribution to the settlement analysis of foundation on clay, *Geotechnique*, **7**: 168-178.
- Skempton, A.W. 1960. Terzaghi's discovery of effective stress. **From Theory to Practice in Soil Mechanics**, John Wiley and Sons, Inc., New York, N.Y., 42-53.

- Sridharan, A. and Jayadeva, M.S. 1982. Double layer theory and compressibility of clays. *Geotechnique*, **32**(2): 133-144.
- Taylor, D.W. 1948. Chapter 10: "One-dimensional consolidation", Problem 7, **Fundamentals of Soil Mechanics**, John Wiley & Sons, Inc., New York, p. 248.
- Tavenas, F., Jean, P., Leblond, P., and Leroueil S. 1983. The permeability of natural soft clays. Part II: Permeability characteristics. *Canadian Geotechnical Journal*, **20**(4): 645-660.
- Terzaghi, K. 1944. Discussion on "Relation of undisturbed sampling to laboratory testing". *Transaction of American Society of Civil Engineers*, **109**: 1196-1201.
- Van Genuchten, M.T. 1980. A closed form equation for predicting the hydraulic conductivity of unsaturated soils. *Soil Science Society of America Journal*, **44**: 892-898.
- Wang, N. and Wei, R. 1996. Evaluation of sample quality of soft clay. *In Proceeding of 2nd International Conference on Soft Soil Engineering*, Nanjing, 120-125.
- Yamamuro, J.A., Bopp, P.A., and Lade, P.V. 1996. One-dimensional compression of sands at high pressures. *ASCE Journal of Geotechnical Engineering*, **122**(2): 147-154.

**Table 7-1 Regression results for normal consolidated clay, Drammen, Norway**

Normal consolidated clay, Drammen, Norway						
Equation	Parameters				R-SS	R <sup>2</sup>
Simplified Hardin (Eq. 7-3)	$e_0=$ 1.542	$p=$ 335.3 kPa	nil	$N=$ 1.3424	0.000073	99.95%
Liu & Znidarcic (Eq. 7-4)	$A=$ 345.4	$Z=$ 269.3 kPa	$B=$ -0.9609	nil	0.001787	98.74%
Li & Sego (Eq. 7-9 with $M=1$ )	$e_0=$ 1.536	$p=$ 280.6 kPa	$M= 1$ (assumed)	$N=$ 1.4792	0.000152	99.89%

**Table 7-2 Regression results for overconsolidated clay, San Francisco Bay Mud**

Overconsolidated clay, San Francisco Bay Mud						
Equation	Parameters				R-SS	R <sup>2</sup>
Simplified Hardin (Eq. 7-3)	$e_0=$ 2.793	$p=$ 225.6 kPa	nil	$N=$ 0.7012	0.00423	97.54%
Liu & Znidarcic (Eq. 7-4)	$A=$ 13.41	$Z=$ 20.15 kPa	$B=$ -0.5333	nil	0.0555	97.01%
Eq. 7-9 with $M=1$	$e_0=$ 2.777	$p=$ 145.7 kPa	$M=$ 1	$N=$ 0.8086	0.00327	98.10%
Eq. 7-9	$e_0=$ 2.588	$p=$ 7.065 kPa	$M=$ 0.04017	$N=$ 4.371	0.00139	99.93%



**Table 7-3 Regression results for overconsolidated clay, Chicago silty clay**

Overconsolidated clay, Chicago silty clay						
Equation	$e_0=$	$p=$	$M=$	$N=$	R-SS	$R^2$
Equation 7-9	1.425	112.4 kPa	0.07887	3.001	0.000461	99.91%

**Table 7-4 Special normal consolidated clay, Mexico City clay**

Special normal consolidated clay, Mexico City clay (Mesri et al. 1975)						
Equation 7-9	$e_0=$	$p=$	$M=$	$N=$	R-SS	$R^2$
Undisturbed	10.677	159.2 kPa	0.08998	1.5211	0.0918	99.92%
Sedimented	10.499	755.9 kPa	0.3592	0.8418	0.0411	99.97%
Remolded	10.254	4084.8 kPa	0.8075	0.6834	0.0254	99.98%

**Table 7-5 Compacted lacustrine clay of Syncrude overburden ( $P_1$  at  $w= 15\%$ )**

Glacial lacustrine clay of Syncrude overburden ( $P_1$ at $w= 15\%$ )						
<b>Equation 7-9</b>	$e_0=$	$p=$	$M=$	$N=$	R-SS	$R^2$
pl-15%-98kPa-N25	1.081	89.9 kPa	0.2289	2.6011	0.00207	99.69%
pl-15%-245kPa-N4	0.900	102.8 kPa	0.0890	6.2475	0.00051	99.85%
pl-15%-fld0	11.112	20.60 kPa	1.1852	0.4035	0.00052	99.97%

**Table 7-6 Leda clay**

Canadian marine clay, Leda clay (Quigley and Thompson 1966)						
<b>Equation 7-9</b>	$e_0=$	$M=$	$N=$	$p=$	R-SS	$R^2$
Undisturbed	2.159	0.00359	78.3069	176.6 kPa	0.00969	99.65%
Leda clay						
Remolded Leda	1.938	0.19317	0.87686	54.94 kPa	0.000086	99.99%
clay						
Remolded Leda	2.058	0.497	0.56589	285.2 kPa	0.000607	99.94%
clay						
(MN = constant)						

**Table 7-7 Louiseville clay (Tavenas 1981)**

Louiseville clay (Tavenas et al. 1981)						
<b>Equation 7-9</b>	$e_0=$	$p=$	$M=$	$N=$	R-SS	$R^2$
Louiseville clay	1.961	135.6 kPa	0.01049	27.619	0.0175	96.94%

**Table 7-8 Prediction of compression curve (P<sub>1</sub>-17%) with known compactive pressure**

Glacial lacustrine clay of Syncrude overburden (P <sub>1</sub> at w= 17%)							
Equation 7-14	$e_k$	$C_k$	$M$	$N$	$p$	R-SS	R <sup>2</sup>
Compacted with 98 kPa	1.237	0.0124	0.0666	9.3831	108.1 kPa	0.000083	99.99%
Compacted with 196 kPa	1.004	same	same	same	196 kPa	nil	nil
Compacted with 784 kPa	0.594	same	same	same	784 kPa	nil	nil

**Table 7-9 Prediction of compression curve (P<sub>1</sub>-17%) with compactive pressure unknown (using Equation 7-15)**

Glacial lacustrine clay of Syncrude overburden (P <sub>1</sub> at w= 17%)							
Equation 7-14	$e_k$	$C_k$	$M$	$N$	$p$	R-SS	R <sup>2</sup>
Compacted with 98 kPa	1.237	0.0124	0.0666	9.3831	108.1 kPa	0.000083	99.99%
Compacted with 196 kPa	1.004	same	same	same	145.9 kPa (predicted)	nil	nil
Compacted with 784 kPa	0.594	same	same	same	438.5 kPa (predicted)	nil	nil

**Figure 7-1 Characteristics of a typical compression curve**

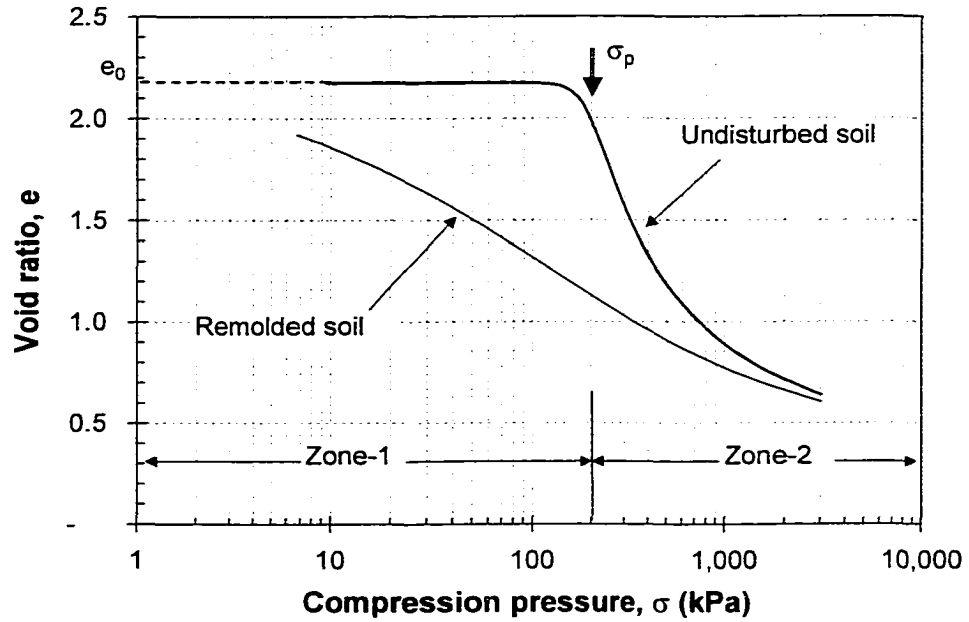


**Figure 7-2 The fitting curves by Hardin (1989) and Liu and Znidarcic (1991) on field samples of overconsolidated Drammen Clay (data from Butterfield 1979)**

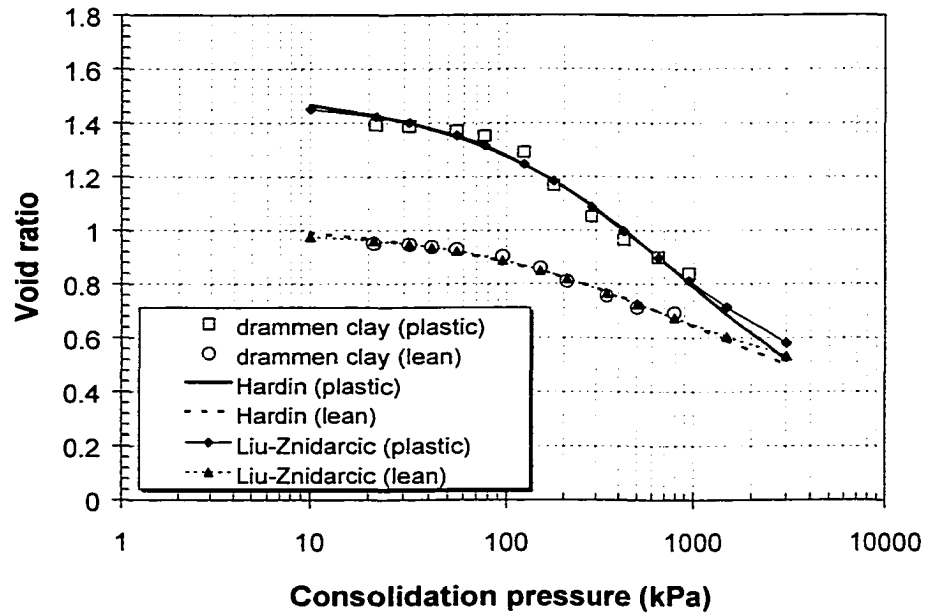


**Figure 7-3 The curves from two original functions and the combined proposed Equation 7-8**

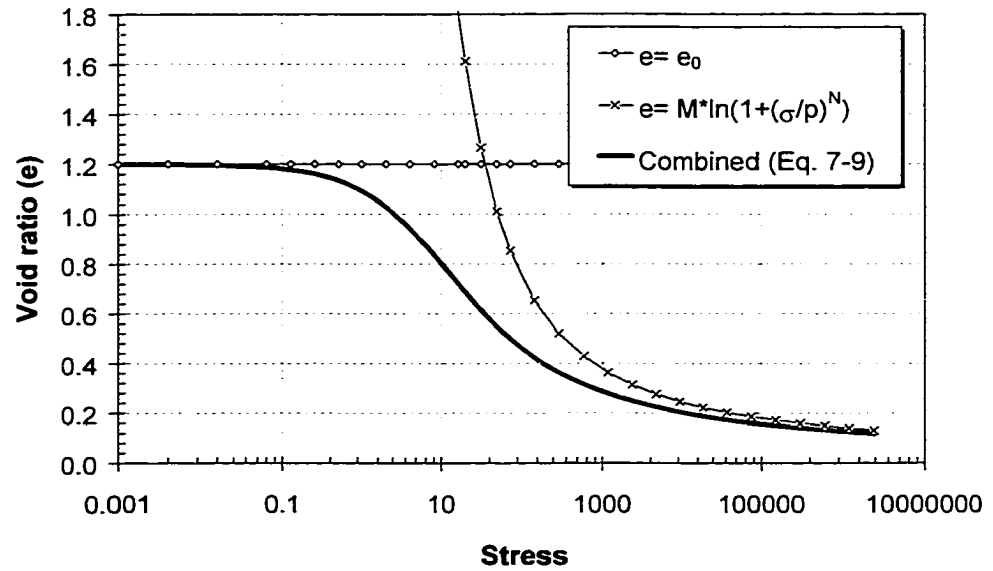


**Figure 7-4 The curve of solid ratio versus logarithm compression stress**

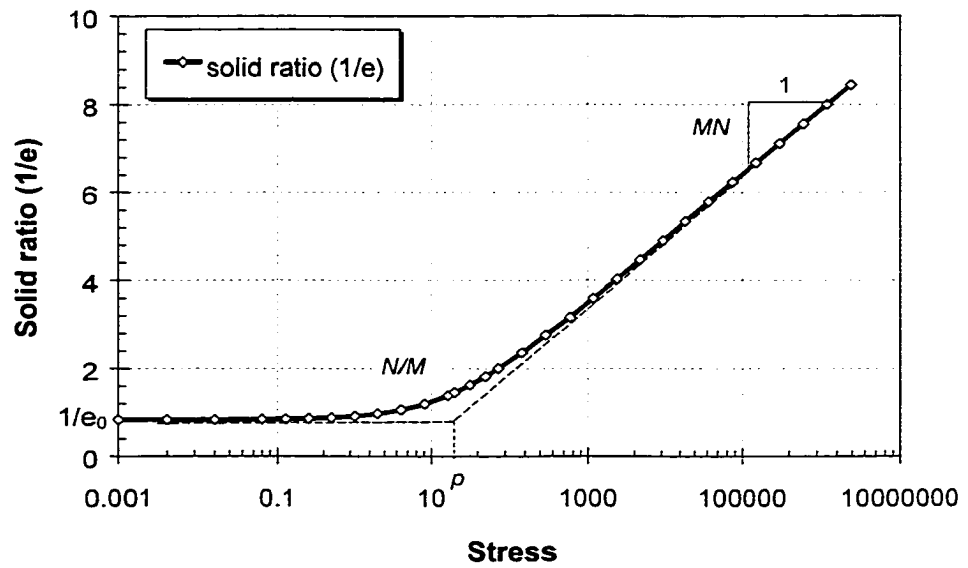


**Figure 7-5 The effects of parameter  $e$  (initial void ratio) on the compression curve (Eq. 7-9)**

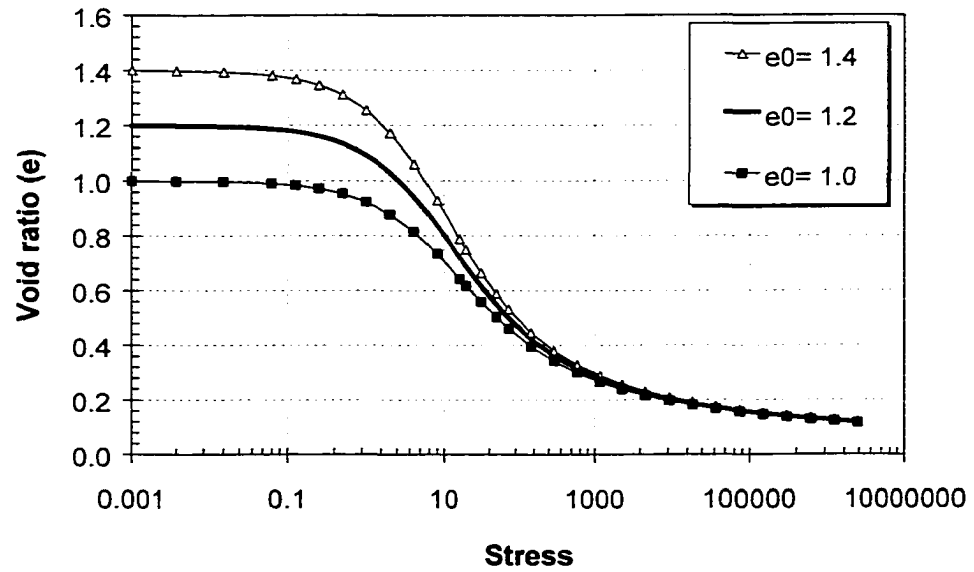


**Figure 7-6 The effects of parameter  $p$  (pre-compression stress) on the compression curve (Eq. 7-9)**

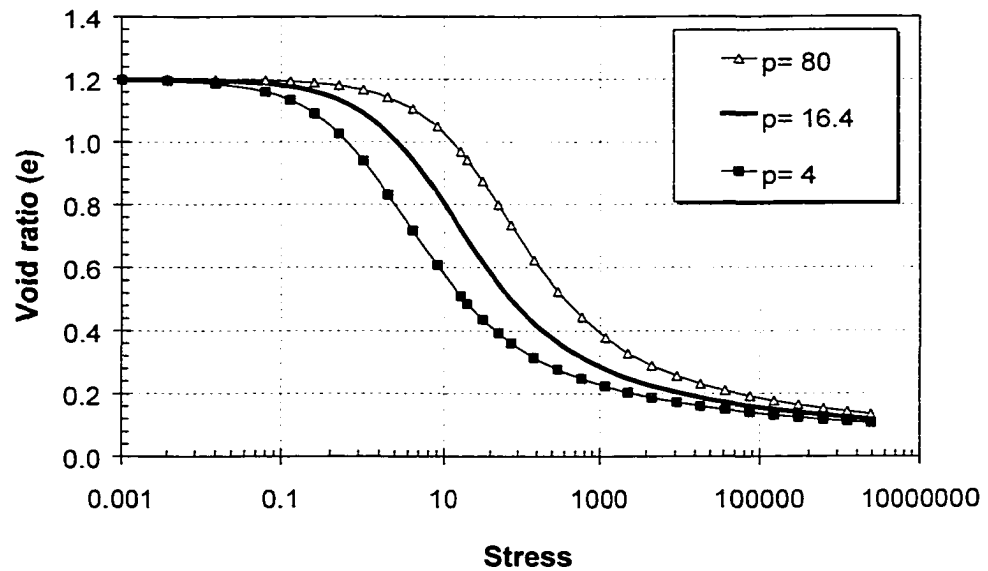


**Figure 7-7** The effects of parameter  $M$  on the compression curve ( $N = 0.8$ ) (Eq. 7-9)

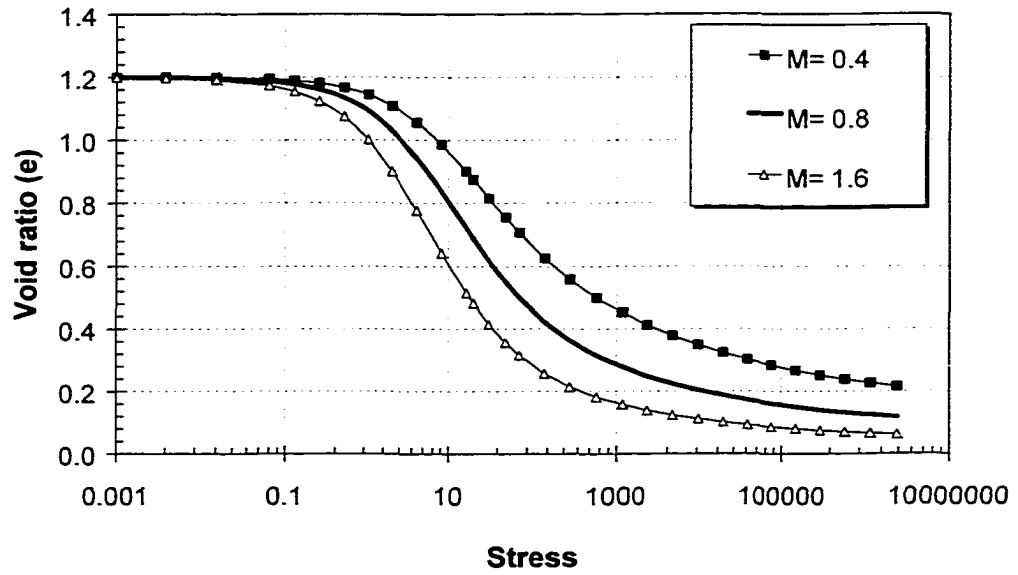


**Figure 7-8** The effects of parameter  $N$  on the compression curve ( $M = 0.8$ ) (Eq. 7-9)

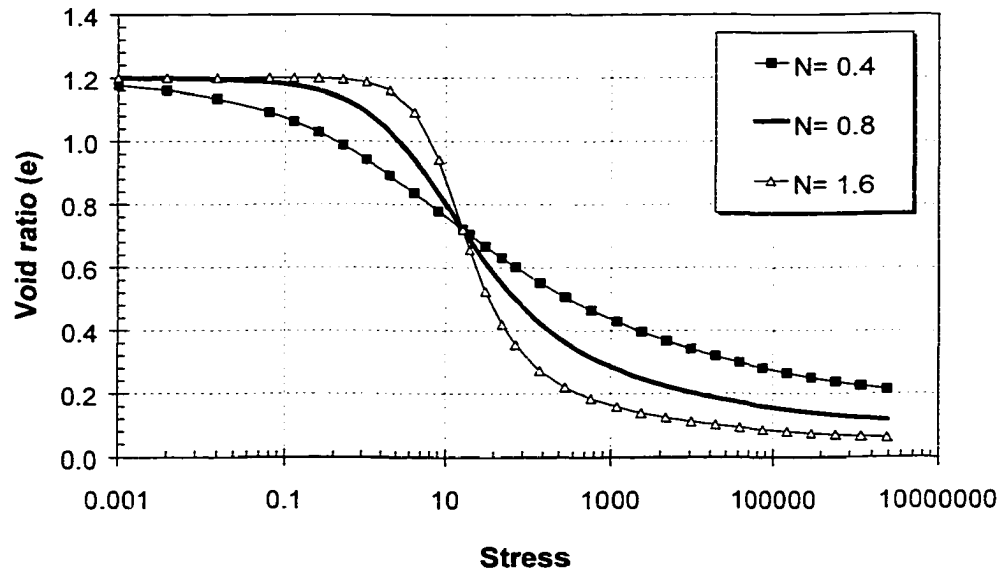




**Figure 7-9 The effects of  $N/M$  on the compression curve when  $MN$  is a constant (Eq. 7-9 and Eq. 7-13)**

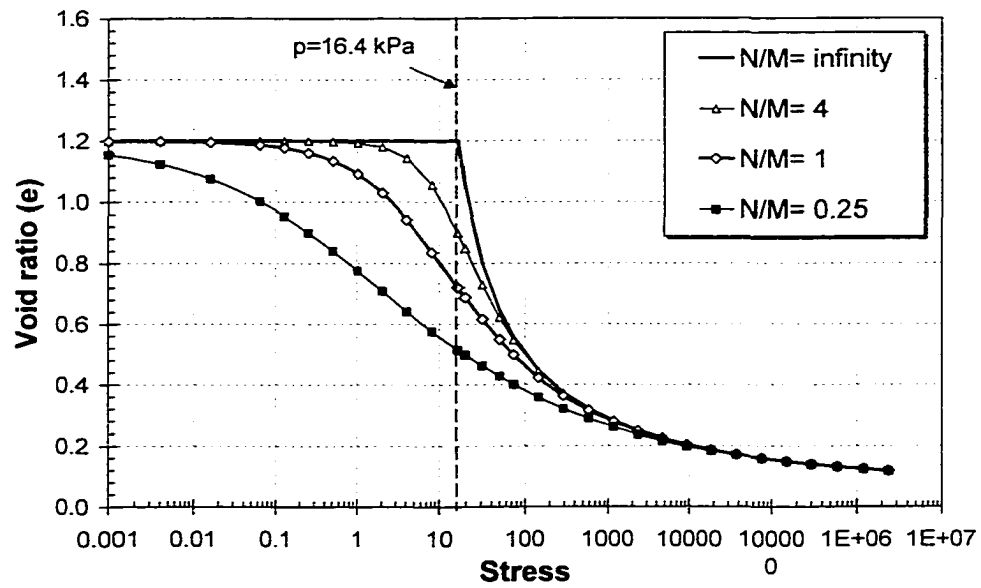


**Figure 7-10 The compression curve with consideration of elastic recompression effects (Eq. 7-14 and Eq. 7-9)**

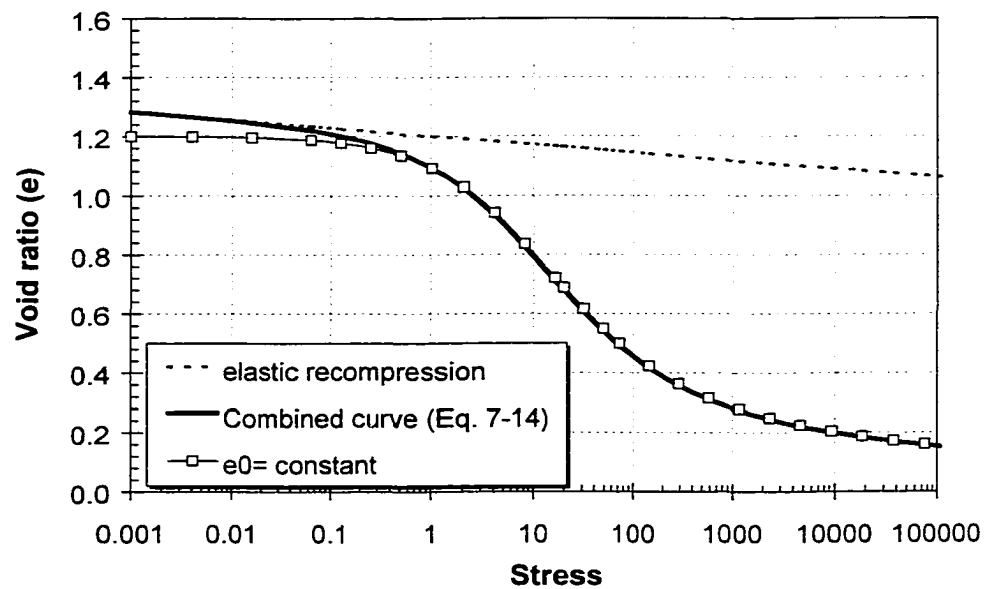


**Figure 7-11 Fitting normal consolidated Drammen clay by equations from simplified Hardin (1989), Liu & Znidarcic (1991), and proposed Equation 7-9 (Berre and Iversen 1972)**

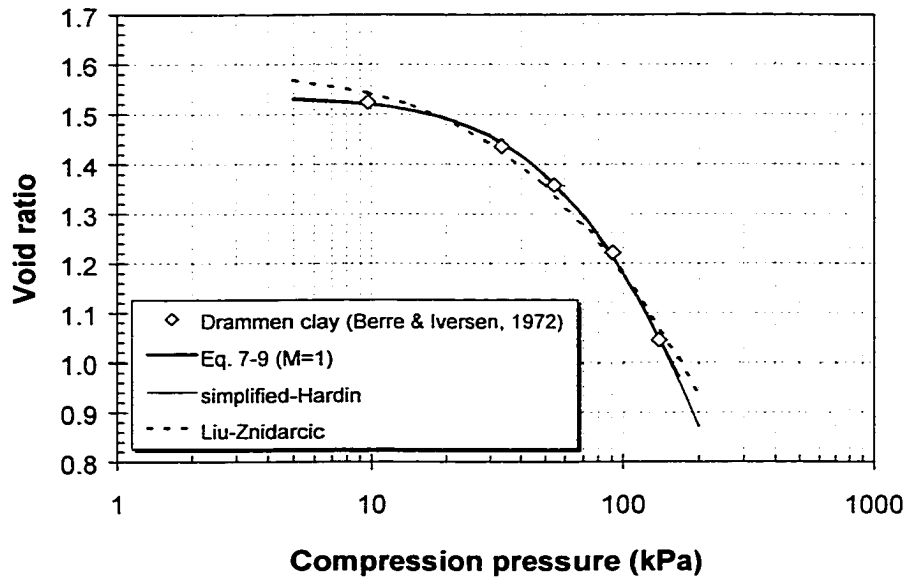


**Figure 7-12 Fitting over consolidated San Francisco Bay Mud by equations from proposed Equation 7-9 with or without  $M = 1$ , simplified Hardin (1989), and Liu-Znidarcic (Holtz and Kovacs 1981)**

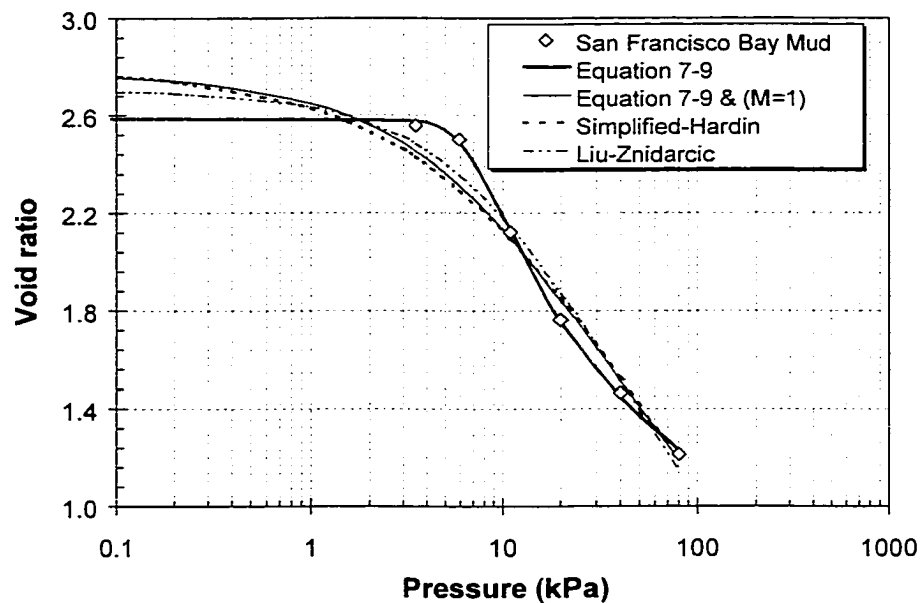


**Figure 7-13 Fitting over consolidated Chicago silty clay (Taylor 1948) by proposed Equation 7-9**

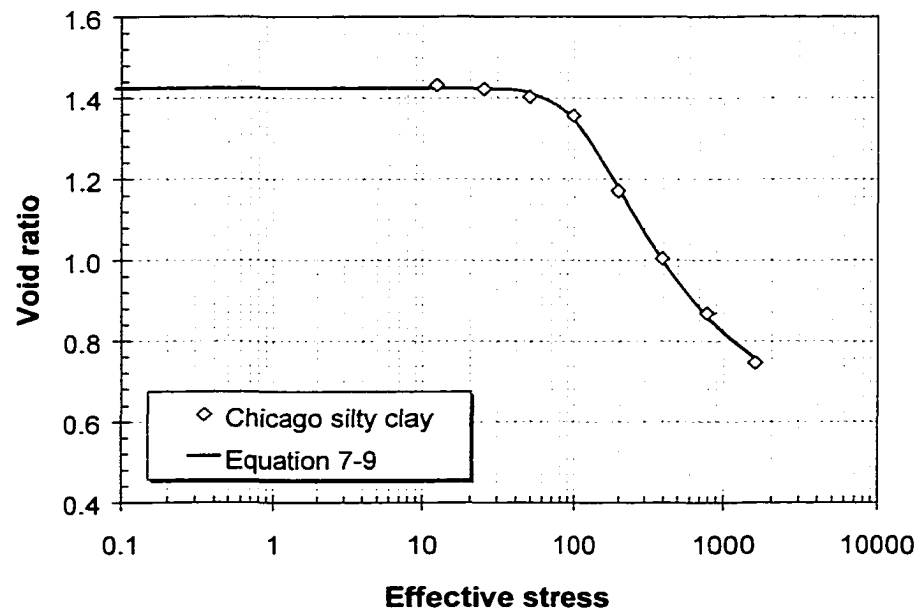


**Figure 7-14 Fitting structured Mexico City clay by proposed Equation 7-9 (Mesri et al. 1975)**

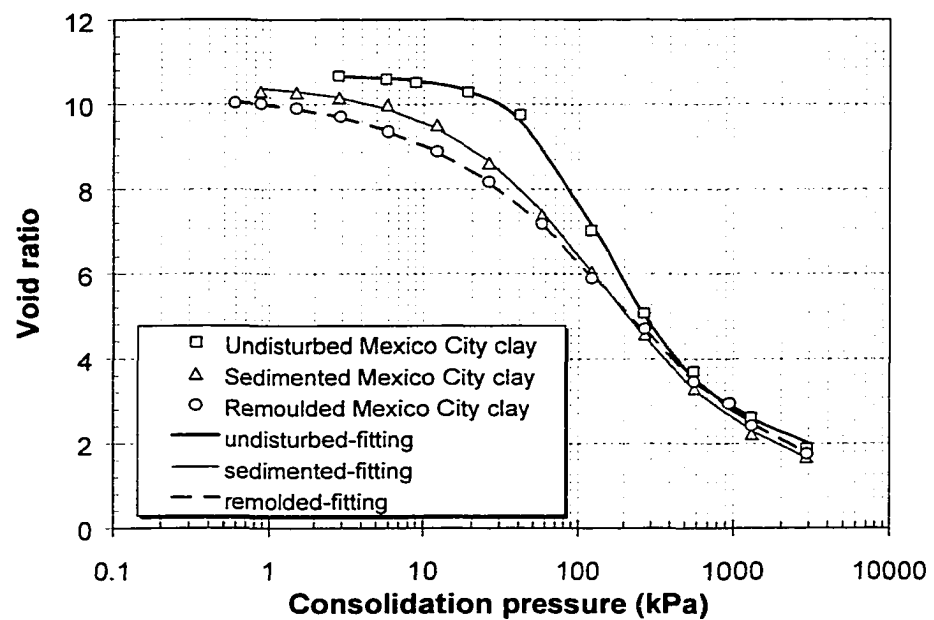


**Figure 7-15 Regression of one-dimensional compression curve for  $P_1$  at  $w = 15\%$  after compaction**

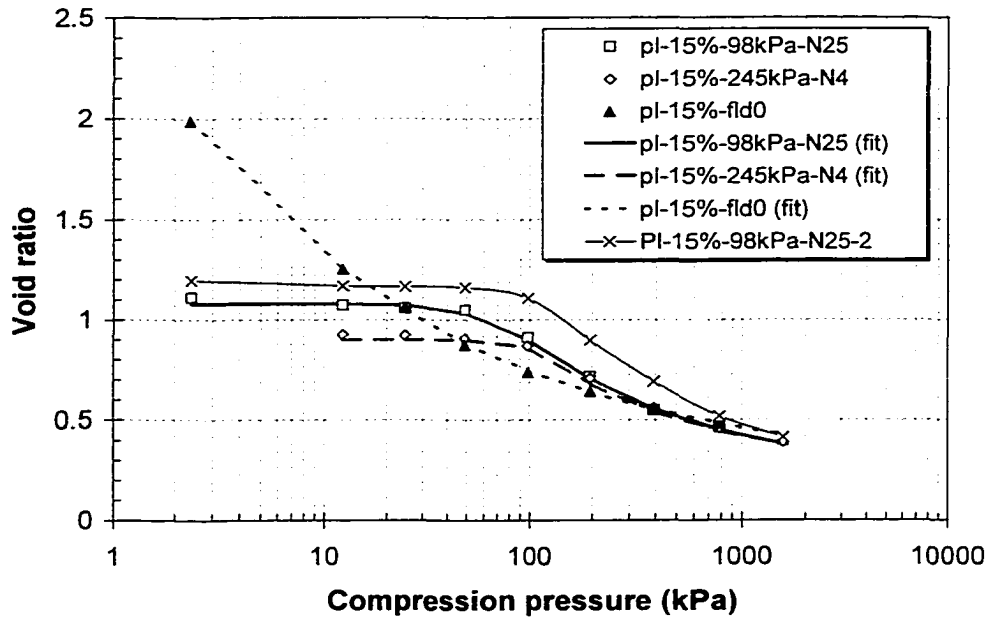


**Figure 7-16 The regression of consolidation curve of Canadian marine clay - Leda clay (Quigley and Thompson 1966)**

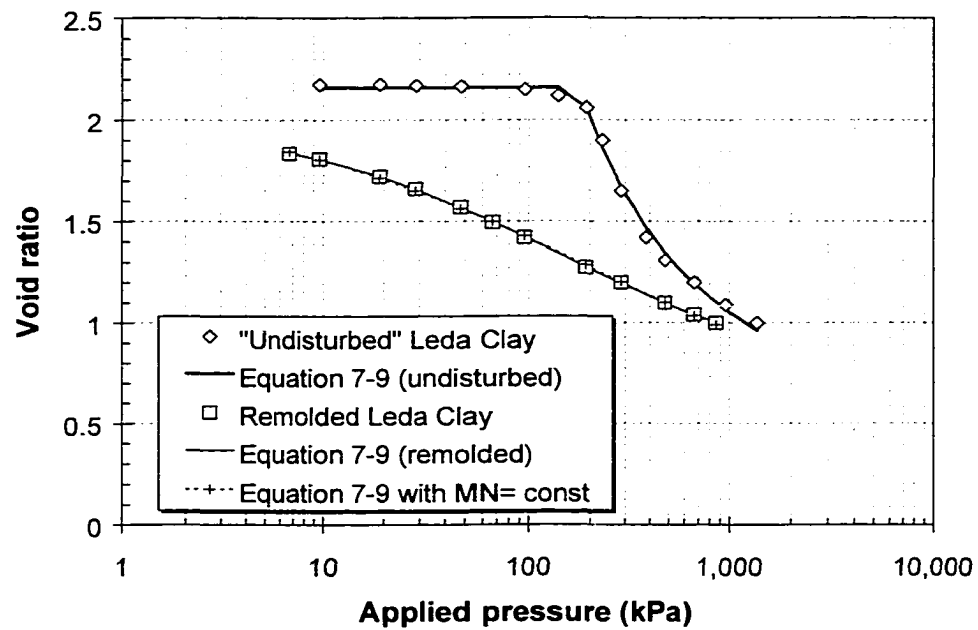


**Figure 7-17 The curve of solid ratio ( $1/e$ ) versus stress of Canadian marine clay - Leda clay (Quigley and Thompson 1966)**

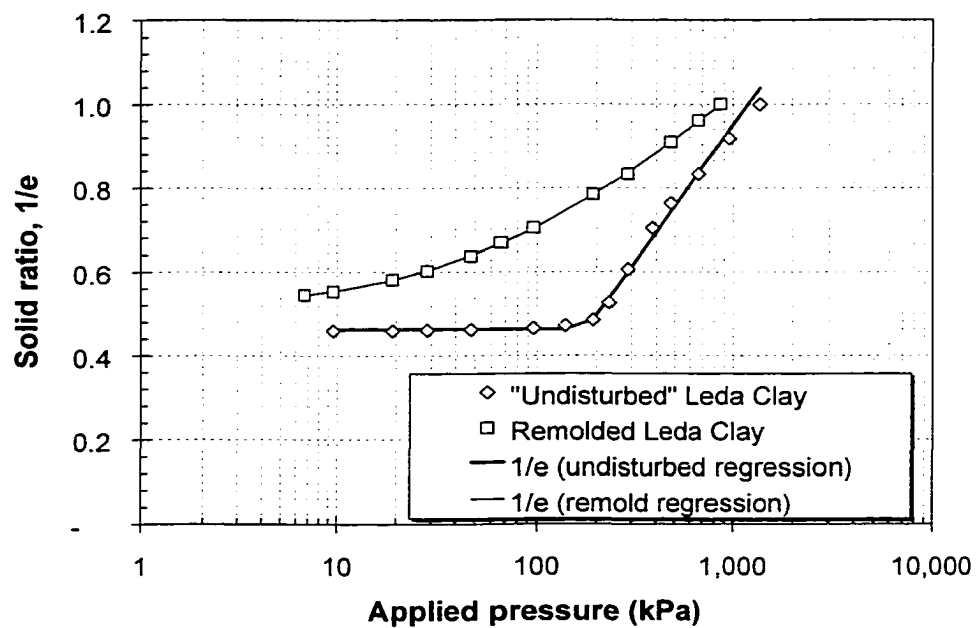


**Figure 7-18 The consolidation curve of two Eastern Canadian marine clays (Tavenas et al. 1981)**

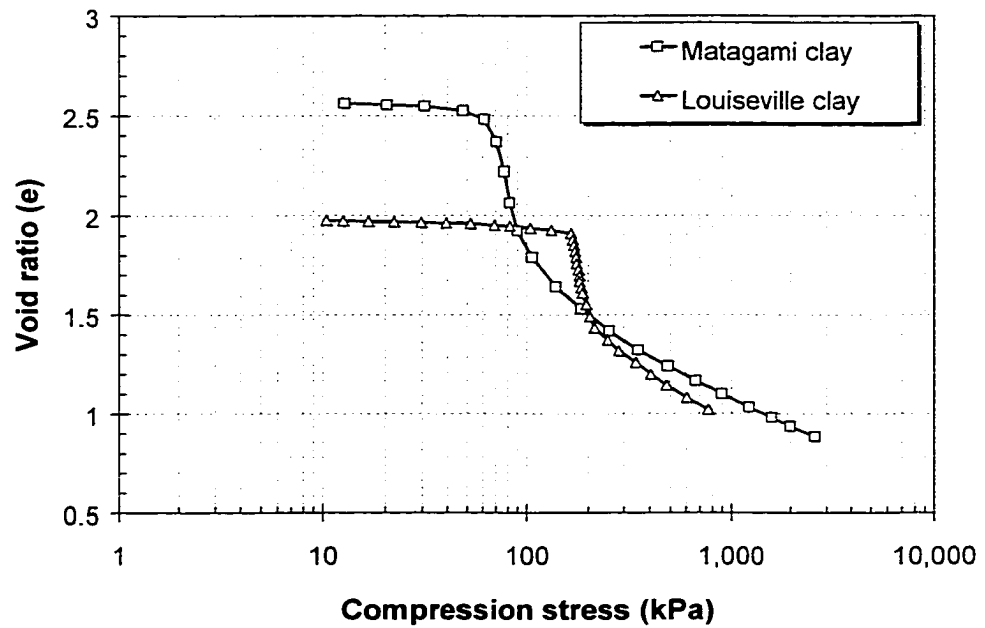


**Figure 7-19 The curve of solid ratio ( $1/e$ ) versus stress of two Eastern Canadian marine clay (Tavenas et al. 1981)**

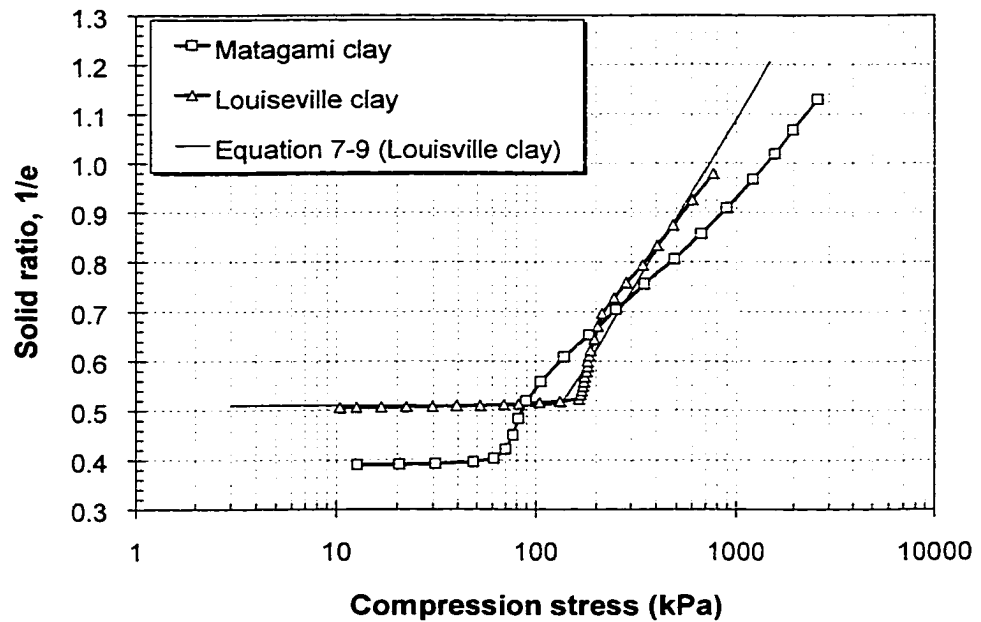


**Figure 7-20 The prediction of compression curves for  $P_1$ -17% with known previous compactive pressure**

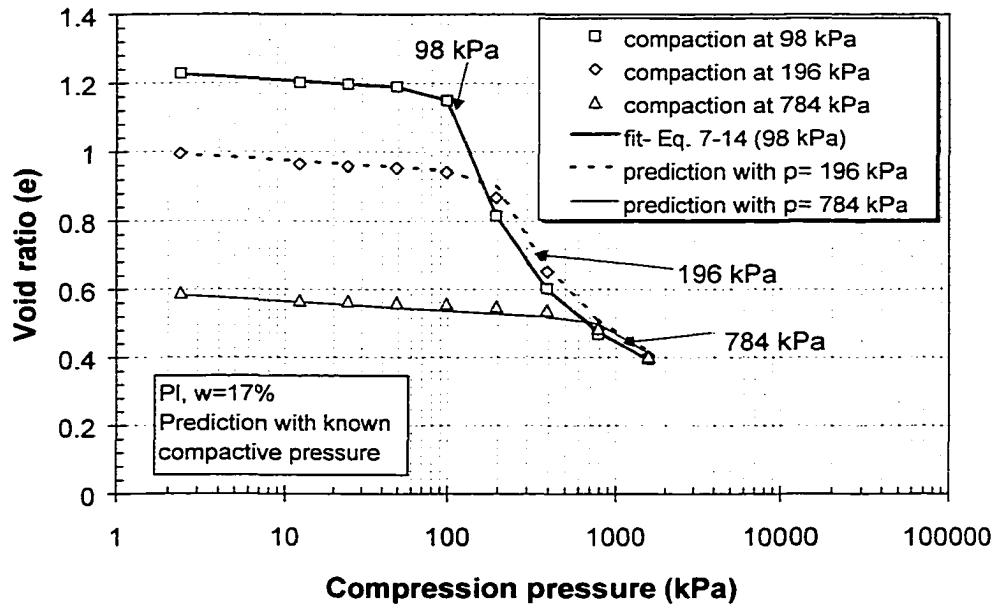
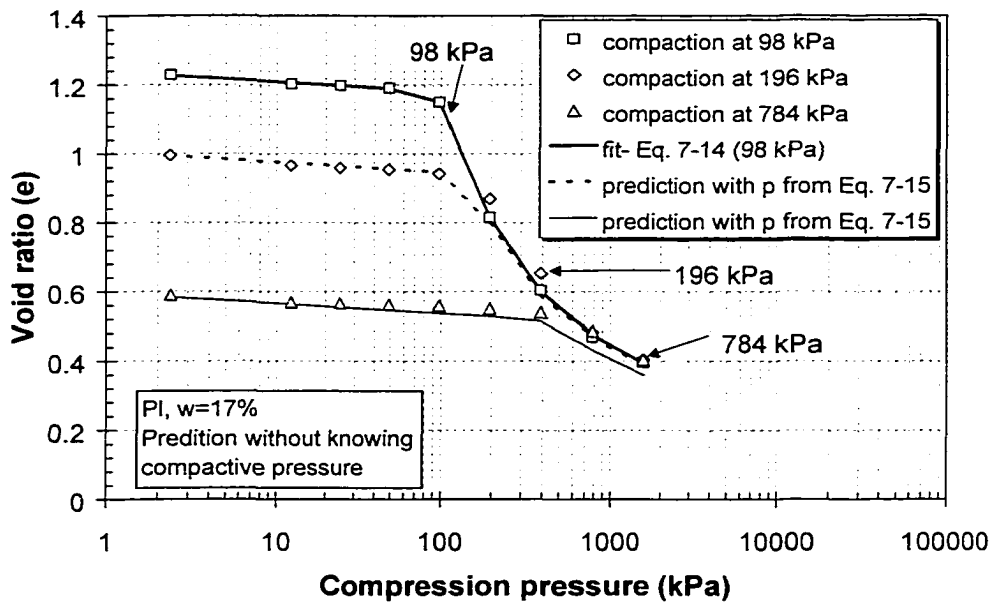


**Figure 7-21 The prediction of compression curves for  $P_1$ -17% without knowing the previous compactive pressure**



# CHAPTER 8 SETTLEMENT ESTIMATION FOR A THICK COMPACTED LAYER USING A FAMILY OF COMPRESSION CURVES

## 8.1 INTRODUCTION

The settlement calculation for consolidation or compression is a common calculation undertaken in geotechnical engineering. It is generally understood that the settlement of a foundation (or ground surface in general) is obtained by integration of the vertical strain over the depth of the compressible soil layer using the appropriated compressibility properties for the given layer.

The basis for consolidation settlement theory for a uniform layer is traditionally found using the approximately straight-line portion of the  $e$ -log  $p$  curve measured using a laboratory consolidation test carried out in an oedometer. For normally consolidated soils, a straight line with the slope  $C_c$  (the compression index of the soil) represents the nonlinear stress-strain relationship (US Army Corps of Engineers 1994). Using this slope, the void ratio change and then the settlement corresponding to an effective stress change from the initial value to a new value can be calculated as follows:

$$[8-1] \quad \Delta s = \frac{\Delta e}{1 + e_i} \cdot H_i = \frac{C_c \cdot \log \left( \frac{\sigma_f'}{\sigma_i} \right)}{1 + e_i} \cdot H_i$$

where  $\Delta s$  is the settlement of the uniform layer caused by an increase in load;  $e_i$  is the in-situ void ratio of the soil layer;  $\Delta e$  is the increase of void ratio ( $\Delta e = e_f - e_i$ ) caused by the increase in load, typically due to the construction of a building or of fills at ground surface;  $H_i$  is the in-situ thickness of the layer;  $C_c$  is the compression index from the



virgin consolidation curve;  $\sigma_i'$  is the original in-situ effective stress; and  $\sigma_f'$  is the final applied effective stress which is the sum of the original in-situ effective stress and the stress caused by the structure.

For overconsolidated soil, a bi-linear relationship rather than single straight line is suggested (US Army Corps of Engineers 1994). The reconstruction of the field virgin consolidation curve requires the determination of the maximum past pressure (pre-consolidation pressure)  $\sigma_p'$  and the recompression index  $C_r$ . If the final stress is less than the preconsolidation pressure, a similar equation to Equation 8-1 is used:

$$[8-2] \quad \Delta s = \frac{\Delta e}{1 + e_i} \cdot H_i = \frac{C_r \cdot \log\left(\frac{\sigma_f'}{\sigma_i'}\right)}{1 + e_i} \cdot H_i \quad \sigma_f' < \sigma_p'$$

where  $C_r$  is the recompression index, obtained from the recompression portion of the consolidation curve.

If the final stress is greater than the preconsolidation pressure, the settlement may be estimated as the sum of recompression and the virgin compression settlements.

$$[8-3] \quad \Delta s = \frac{C_r \cdot \log\frac{\sigma_p'}{\sigma_i'}}{1 + e_i} \cdot H_i + \frac{C_c \cdot \log\frac{\sigma_f'}{\sigma_p'}}{1 + e_i} \cdot H_i \quad \sigma_f' > \sigma_p'$$

The above equations should be used for a uniform thin layer, in which the indexes  $C_c$  and  $C_r$  are constants within the layer, and the average stresses is approximately equal to the stresses at the middle of the layer. If the layer is thick, and particularly if it is close to the foundation where the stress change from its top to its bottom is greater than 50 percent of the average, this procedure can lead to errors. This develops because neither the stress variation with depth nor the soil compression curve is a linear relationship. For a thick

uniform layer, McPhail et al. (2000) indicated that a possible 100% to 300% error could occur in most instances when compared with the exact solution. The error will increase if using constant indexes  $C_c$  and  $C_r$  for a thick non-uniform layer. It is therefore better practice to subdivide the layer into several sublayers as Figure 8-1, each of which is thin enough so that the stress change within the layer is less than about 50%. The settlement for each sublayer is computed as if it were a separate layer (Sowers 1962). References found in other geotechnical engineering textbooks published in the last several decades also recommended numerical integration using the sublayer method (Holtz and Kovacs 1981; Craig 1993; Bowles 1996; Terzaghi et al. 1996; Das 1998).

Overburden excavation such as oil sands mining in Northern Alberta results in a large volume of material for disposal. The use of increasing larger trucks to haul, dump, and compact these waste materials requires the use of thick placement layers in the waste dumps (Morgenstern et al. 1988). The embankments constructed using this technique were later used as the foundation for a highway for another project (Cameron et al. 1995). It is necessary to estimate the settlement for this kind of layer system constructed using thick-layered placement. The laboratory results in Chapter 6 indicated that the compression curve for a compacted soil is similar to the consolidation curve for an overconsolidated soil. The compactive effort plays the similar role as the preconsolidation pressure on a soil consolidation curve for the soil compacted at the dry side of optimum water content (OWC). In most dumps and less compacted soils, this is the condition to be dealt with.

Since the stress distribution during compaction using the heavy haulers varies with the depth, the resulting dry density over the thick layer is not uniform. It is therefore better practice to subdivide the thick layer into several sublayers. As the number of sublayers is increased, a more accurate solution can be obtained. However, the indexes  $C_c$  and  $C_r$  to represent the compression behavior for each sublayer must be individually determined as the compression curve is non-linear. To use Equation 8-2 or 8-3, the preconsolidation pressure  $\sigma_p$  needs to be determined for each sublayer, which requires a large number of soil compression tests over the depth. This makes the traditional calculation method

neither economical nor practical in geotechnical design when dealing with the same type of soil.

The concept of a family of compression curves within the thick compacted layer could provide a solution to this issue. It considers the multi-sublayer system as a family. The existence of the family of compression curves is based on the fact that, no matter what the initial void ratio, structure or stress history, the void ratio under high pressure for a given soil is unique. A relationship has been proposed in Chapter 7 to precisely describe a complete non-linear compression curve for a given soil. The proposed equation can predict a family of compression curves based on a single laboratory compression test carried out on a sample of compacted soil. It is the objective in this chapter to apply the proposed compression equation to settlement calculation for a thick compacted layer.

## 8.2 EQUATION FOR ONE-DIMENSIONAL COMPRESSION CURVE AND A FAMILY OF COMPRESSION CURVES

Equation 7-9 was shown to properly describe a compression curve for compacted soils over the complete applied stress range. It is a combination of the initial void ratio and the logarithm relationship for virgin compression.

$$[8-4] \quad e = \frac{1}{\frac{1}{e_0} + M \cdot \ln \left( 1 + \left( \frac{\sigma}{p} \right)^N \right)}$$

where  $e_0$  is the initial void ratio. Parameters  $M$ ,  $N$ , and  $p$  are used to define the logarithm power law in  $e$ -log  $\sigma$  space while maintaining maximum flexibility.

It was found in Chapter 7 that the product of  $MN$  controls the void ratio at high compression pressure. The uniqueness of the void ratio for a given soil at the high stress level suggests that it is appropriate to assume  $MN$  is a constant for a given soil. Thus

changing the ratio of  $N/M$  while keeping  $MN$  constant can create a family of compression curves as shown in Fig. 7-9. It was shown that with the increase of  $N/M$ , the curve becomes steeper. The variation of the curves suggests the same features as observed for samples with different degree of disturbance (Rutledge 1944; Bozozuk 1971; Lacerda et al. 1977; Holtz and Kovacs 1981; Kabbaj et al. 1985; Wang and Wei 1996).

When  $N/M$  approach infinity (i.e.  $N$  is much greater than  $M$  but  $MN$  is a still constant), an ultimate compression curve is obtained as Equation 8-5:

$$[8-5] \quad e = \frac{1}{\frac{1}{e_0} + MN \cdot \ln\left(\frac{\sigma}{p}\right)}$$

Equation 8-5 represents the asymptote of the family of compression curves, i.e. the undisturbed compression curve, or the virgin compression curve for a given soil. The parameter  $p$  in Equation 8-5 is the yield stress or the maximum pre-compression stress. For a given soil, the virgin compression curve should be unique and independent of the applied compactive effort. Therefore, the relationship among parameter  $e_0$ ,  $p$  and  $MN$  can be derived from Equation 8-5 as:

$$[8-6] \quad \frac{1}{e} - MN \cdot \ln \sigma = \frac{1}{e_0} - MN \cdot \ln p = A$$

where  $A$  is a constant for a given soil at a given water content.

Equation 8-6 is useful in creating the family of compression curves for a given compacted soil. In a field embankment, where the dry density ( $\gamma_d$ ) could be measured while the applied stress is unknown, one can use this equation to calculate the previous maximum pressure ( $p$ ) from  $e_0$  ( $e_0$  is obtained using the measured  $\gamma_d$ ).

The compression curves for a given soil prepared using different water contents are different as shown in Chapter 6 (e.g. Fig. 6-6). Only the samples prepared at the same moisture condition showed the same virgin compression curve (e.g. Fig. 6-13 to 6-17). This suggests the value of  $N/M$ , which controls the slope of the compression curve, may be considered as a constant for a given soil. Therefore it would be reasonable to assume that the both  $M$  and  $N$  are constants for a given compacted soil prepared at the same water content. This assumption plus Equation 8-6 leave only one unknown variable in Equation 8-4. For the thick layer of soil, if the dry densities over the depth are measured, i.e. parameter  $e_0$  is known, another parameter  $p$  can be obtained using Equation 8-6. Therefore all the compression curves can be predicted. Two compression curves for Pleistocene Lacustrine clay ( $P_1$ ) prepared at 17% water content but compacted under different compactive stress have been predicted in Chapter 7 and have shown general agreement with the laboratory data.

To incorporate elastic recompression for soils, an elastic recompression equation ( $e_r - C_r \ln \sigma$ ) can be used to replace the originally proposed constant initial void ratio ( $e_0$ ). Then Equation 8-4 can be written as:

$$[8-7] \quad e = \frac{1}{\frac{1}{e_k - C_k \cdot \ln \sigma} + M \cdot \ln \left( 1 + \left( \frac{\sigma}{p} \right)^N \right)}$$

where  $C_k$  is the recompression index and  $e_k$  is the void ratio when the applied stress is unity.

### 8.3 ESTIMATING SETTLEMENT OF THIN SUBLAYER USING PROPOSED COMPRESSION EQUATION

Since Equation 8-4 or 8-7 can describe a compression curve for an undisturbed sample over the complete stress range, the void ratio at a given stress can be directly obtained

from the equation with no need to check its relationship with the precompression pressure  $\sigma_p$  or the yield point. By substituting the original in-situ stress  $\sigma_i$  and the final stress  $\sigma_f$  after construction into the equation such as Equation 8-4, the void ratios  $e_i$  and  $e_f$  can be calculated respectively. For a layer of soil with an initial thickness  $H_i$ , the settlement  $\Delta s$  in terms of the void ratio is given as:

$$[8-8] \quad \Delta s = \frac{\Delta e}{1 + e_i} \cdot H_i = \frac{e_i - e_f}{1 + e_i} \cdot H_i$$

Since Equation 8-8 is the same as the traditional settlement calculation, this calculation method is called the **traditional method** in this chapter.

Since soil elastic rebound during sampling is relatively small, the initial void ratio in one-dimensional compression test ( $e_0$ ) is close to the initial in-situ void ratio of the soil layer ( $e_i$ ), i.e.  $e_i \approx e_0$ . By replacing  $e = e_f$ ,  $\sigma = \sigma_f$  and observing  $\Delta e = e_0 - e_f$  in Equation 8-4, the following expression for  $\Delta e$  may be written:

$$[8-9] \quad \Delta e = e_0 e_f \cdot M \ln \left( 1 + \left( \frac{\sigma_f}{p} \right)^N \right)$$

where  $e_f$  is the final void ratio after construction, and  $\sigma_f$  is the final stress, which is the sum of initial in-situ vertical stress and the increase in load due to the subsequent construction. The derivation of Equation 8-9 is presented in Appendix 8-A.

Substituting Equations 8-9 and 8-4 into Equation 8-8, the settlement under any given load ( $\sigma$ ) thus can be closely calculated using following equation:

$$[8-10] \quad \Delta s = \frac{H_0}{\left(1 + \frac{1}{e_0}\right) \cdot \left[1 + \frac{1}{e_0 \cdot M \ln \left(1 + \left(\frac{\sigma_f}{p}\right)^N\right)}\right]}$$

The advantage of Equation 8-10 is in its single analytical relationship and it is continuous over the complete stress range. The deformation of a uniform thin layer at any stress can be calculated immediately. Therefore this settlement calculation method is called the **one-step method**. Since Equation 8-10 does not include the small elastic rebound during sampling, it is a close solution to the **traditional method** using Equation 8-8.

As discussed previously, when considering the elastic recompression instead of using a constant initial void ratio ( $e_0$ ), one needs only to replace  $e_0$  with  $e_r - C_r \ln \sigma$  in Equation 8-10.

The Pleistocene Lacustrine clay test results reported in Chapter 6 are used throughout this example. The sample was prepared using a water content of 17% and compacted using 25 applications of foot pressure of 98 kPa. Its one-dimensional compression results and the fitted curve using Equation 8-7 are shown in Fig. 8-2. There is a sudden increase of deformation after the compression stress reached the applied compaction foot pressure of 98 kPa. The required parameters for use in Equation 8-4 as regressed and summarized in Chapter 7 are:  $e_0 = 1.237$ ,  $C_r = 0.0124$ ,  $M = 0.0666$ ,  $N = 9.383$ ,  $p = 108.1$  kPa. This allows the settlement at any stress to be easily calculated using Equation 8-10 if the layer thickness is assumed 10 centimeters. The results can also be presented using the vertical strain ( $\varepsilon = \Delta s/H_0$ ) without assuming the thickness. Both the settlement and the vertical strain at different loading pressure are illustrated in Figure 8-3. The vertical strain at the

compaction pressure (98 kPa) is only 1.4%, it increase rapidly to over 30% when the applied stress increase to 700 kPa.

#### **8.4 SETTLEMENT ESTIMATION FOR A THICK COMPACTED LAYER**

The estimation of the settlement of a thick compacted layer is more complicated than a thin compacted layer because the compression curve varies with the depth in the compacted layer. Considering the compacted thick layer as a single uniform layer would lead to potentially large errors, it is therefore better to subdivide a thick layer into several sublayers and calculate their settlement separately. The total settlement is an integration of the settlements of the individual layers. However dividing the thick layer into multi-sublayers would require many samples to be tested and parameters to be determined. The concept of a family of compression curves can then be used to predict a series of curves for a given soil type. Since the non-linear behavior of the compression curve is well defined using the relationships developed, the method should provide a reasonable solution for a thick layer in the settlement estimation.

Consider a thick-layer in Figure 8-1 with an original height  $H_0$ . The original dry density or void ratio profile is represented by  $\gamma_{d0}(z)$  or  $e_0(z)$ , where  $\gamma_{d0}(z)$  is the as-compacted dry density varying with the depth  $z$ ,  $e_0(z)$  is the initial void ratio varying with depth.

Dividing the whole thick layer into a multi-sublayer system. Each sublayer has a thickness of  $dz$ .

Using the Equation 8-10 in the paper to calculate the settlement of each sublayer under a compression stress  $\sigma(z)$ . The thickness has been replaced by  $dz$  in Equation 8-11.



$$[8-11] \quad \Delta s = \frac{dz}{\left(1 + \frac{1}{e_0(z)}\right) \cdot \left[1 + \frac{1}{e_0(z) \cdot M \ln \left(1 + \left(\frac{\sigma(z)}{p(z)}\right)^N\right)}\right]}$$

The parameters of  $M$  and  $N$  are assumed constant for a given soil at certain water content.  $\sigma(z)$  is the final stress applied to the sublayer. The void ratio function  $e_0(z)$  can be obtained from measurement or calculated using the dry density function  $\gamma_{d0}(z)$ .  $p(z)$  is then calculated from the ultimate asymptote curve by rearranging Equation 8-6:

$$[8-12] \quad p(z) = \exp\left(\frac{\frac{1}{e_0(z)} - A}{MN}\right)$$

The total settlement at the surface ( $S_c$ ) due to a surcharge loading after placement can then be integrated from depth 0 to  $H_0$  as follows:

$$[8-13] \quad S_c = \int_{z=0}^{z=H_0} \frac{1}{\left(1 + \frac{1}{e_0(z)}\right) \cdot \left[1 + \frac{1}{e_0(z) \cdot M \ln \left(1 + \left(\frac{\sigma(z)}{p(z)}\right)^N\right)}\right]} \cdot dz$$

where  $\sigma(z)$  is the compression stress at the depth  $z$ , which is the sum of the soil self-weight ( $\sum \gamma_i z_i$ ) and the stress increase due to construction surcharge. The stress increase in loading can be calculated using methods such as Boussinesq (1885, as shown in Timoshenko and Goodier 1951), the approximate 2:1 distribution, and for stratified soil using Westergaard (1938) (Sowers 1962; US Army Corps of Engineers 1994).

Equation 8-13 is the analytical expression to calculate the total settlement of a thick compacted layer. Given the rapid development in computer technology, the solution of the equation is no longer a challenge. A convenient approach is to use a spreadsheet. Alternately, a number of commercial mathematical computer programs can be used, which have emerged over the past couple of decades for the solution of math related problems. One of the common packages in Canada is Maple<sup>1</sup>.

## 8.5 METHODS AND EXAMPLES

To estimate the precompression pressure ( $\sigma_p$ ) over the whole layer, the density over the depth must be measured or assumed. If the initial dry density over the thick layer is known and assumed to decrease linearly with the depth (Fig. 8-4), the function of dry density can be written as

$$[8-14] \quad \gamma_d(z) = \gamma_{d1} - \frac{\gamma_{d1} - \gamma_{d2}}{H_0} \cdot z$$

where  $\gamma_{d1}$  indicate the dry density at the top of the layer ( $z = 0$ ),  $\gamma_{d2}$  is the dry density at the bottom of the layer ( $z = H_0$ ).

Therefore the initial void ratio at depth  $z$  is  $e_0(z)$  is

$$[8-15] \quad e_0(z) = \frac{\gamma_w G_s}{\gamma_d(z)} - 1 = \frac{\gamma_w G_s}{\left( \gamma_{d1} - \frac{\gamma_{d1} - \gamma_{d2}}{H_0} \cdot z \right)} - 1$$

$$= \frac{\gamma_w G_s}{\frac{\gamma_w G_s}{1 + e_{01}} - \frac{\gamma_w G_s}{1 + e_{02}} \cdot \frac{z}{H_0}} - 1 = \frac{1 + e_{01}}{1 - \frac{e_{02} - e_{01}}{1 + e_{02}} \cdot \frac{z}{H_0}} - 1$$

where  $e_{01}$  and  $e_{02}$  represents the initial void ratio at the top and the bottom of the thick layer.

Consider a 10 meter thick layer within a dump. The soil is assumed to be Pleistocene Lacustrine clay (P<sub>1</sub>) compacted at water content of 17%. From the previous discussion, only a single one-dimensional curve is required. In this case, the curve under compactive effort of 98 kPa with 25 applications in Figure 8-2 is used. The input parameters for the calculations are shown in Table 8-1.

The soil is assumed to be compacted in the field using a small compactive effort 98 kPa, which resulted in the dry density  $\gamma_{d1}$  at  $1.20 \text{ Mg/m}^3$  (or  $e_{01} = 1.24$ ) on the surface. The initial void ratio at the bottom is assumed based on the possible overburden pressure at the position. If the average unit weight over the thick layer is assumed to be about  $18 \text{ kN/m}^3$ , the void ratio  $e_{02}$  at the bottom is close to 0.82 for the soil prepared at 17% water content according to test results in Figure 6-16 ( $\gamma_{d2} = 1.48 \text{ Mg/m}^3$ ). Substituting them into Equation 8-15, the expression of  $e_0(z)$  becomes:

$$[8-16] \quad e_0(z) = \frac{2.24}{1 - 0.0232 \cdot z} - 1$$

The profile of initial void ratio  $e_0(z)$  and dry density  $\gamma_d(z)$  are shown in Fig. 8-4.

In case the dry density is not measured, the family of compaction curves presented in Chapter 2 can be used to roughly predict it by combining the stress distribution analysis and the dry density versus compactive effort relationship.

The function of  $p(z)$  can be calculated directly from Equation 8-12:

$$[8-17] \quad p(z) = \exp\left(\frac{\frac{1}{e_0(z)} + 2.120}{0.625}\right)$$

Substituting Equation 8-16 and 8-17 into Equation 8-13, the settlement under various surcharges can be calculated using a spreadsheet (e.g. MS Excel).

The following assumptions were made for the base case of the load: area of the load is 2-m by 2-m; the applied stress on the surface is assumed 700 kPa, which is equal to the inside inflation pressure of a heavy truck tire; and the embedment depth is zero. The stress distribution beneath the center of a rectangle loaded area is calculated using Boussinesq method and is shown in Figure 8-5. The in-situ stress and the final stress are also presented in the figure.

The number of the divided sublayers affects the final calculated settlement. Figure 8-6 shows the relationship between the calculated surface settlement and the number of the sublayers for a surcharge loading of 700 kPa. It shows there is little change of the result when the total number of sublayers is more than 5. McPhail et al. (2000) indicated that it is possible to obtain at least three digits correct using 64 sublayers for a uniform thick layer. Since it is very easy to use more sublayers in computer worksheet, the following results are based on the calculation where the thick layer is divided into 100 sublayers.

The relationship between surface settlement and the amount of surcharge loading is shown in Fig. 8-7. The settlements under surcharges that are below the initial pressure of 100 kPa are very small (< 0.015 m). This is because the previous compactive pressure applied at the surface (with the minimum dry density) is 98 kPa. The settlement rapidly increases above 100 kPa stress and reaches a large settlement (0.77 m) at 700 kPa applied stress. It confirms that a substantial settlement could occur under subsequent loading if a fill is not or less compacted. The results from the **traditional method** (Eq. 8-8) and the

**one-step method** (Eq. 8-10) are compared in Fig. 8-7. The difference between them is very small as expected.

The settlement curve for a thin layer in Figure 8-3 shows a different shape from the curve for a thick layer in Figure 8-7. It is evident that a thick non-uniform layer should not be considered as a one-layer system.

The vertical strain of each sublayer under a 700 kPa surcharge is shown in Figure 8-8 over the thickness. The greatest strain is at the top with 33.4% and the least is at the bottom at 0.18% for the soil with the highest placement density. The cumulative settlement at each depth is also shown in the figure.

## 8.6 DISCUSSION

The traditional procedures for calculation of settlement of a compressible stratum includes the following steps:

Evaluate the previous maximum stress  $\sigma_p$  from the results of one-dimensional compression tests on undisturbed specimens;

Estimate the average initial compression pressure  $\sigma_i$  in each sublayer;

Determine the soil initial void ratio  $e_i$  based on the 1-D compression test results;

Evaluate the compression index  $C_c$  and recompression index  $C_r$  from results of a 1-D compression test using the slope of the virgin compression line and recompression line;

Estimate the final applied effective pressure  $\sigma_f$ , where  $\sigma_f = \sigma_i + \sigma_{st}$ , soil pressure caused by the structure;

Determine the ultimate 1-D compression settlement of each sublayer using Equation 8-2 if  $\sigma_f < \sigma_p$  or 8-3 if  $\sigma_f > \sigma_p$ ;

Determine the total settlement from the sum of the settlement of each sublayer;

The **traditional method** discussed in this chapter follows the above procedures with little modifications. In the proposed **traditional method**, the continuous compression curve for each sublayer is represented using Equation 8-4 instead of a simplified straight line with slope of the compression index  $C_c$ . This change represents a better description of the actual soil compression behavior. And because of the continuity of the equation over the complete stress range, there is no need to check the final stress value in relation to the precompression pressure.

The family of compression curves exists for a given soil which has undergone various compactive effort. The concept of a family of compression curves give Equation 8-4 an extra advantage for a compacted thick layer of a given soil. Based on a one-dimensional compression curve, a series of compression curves over the thick layer can be predicted. This would substantially reduce the number of test samples.

Theoretically, with the stress distribution calculated, only a single compression curve is sufficient to construct the whole family of compression curves using Equation 8-12. The method proposed in this chapter uses the additional dry density profile or the initial void ratio profile, which would eliminate the possible errors resulting due to inaccuracy of the determination of initial void ratio when using the stress distribution analysis. Since the dry density profile can be measured or estimated by various techniques in the field, this method is applicable for use in practice.

The **One-step method** keeps the use of non-linear curve description in Equation 8-4 while neglecting the volume change of the soil rebound during sampling. It results in a single integrated equation in Equation 8-13 for the settlement estimation. Although the equation is complicated in form, it is easy to calculate using a spreadsheet. Equation 8-13 is more precise for the cases where the in-situ stress and the soil dry density (or modulus) are both low; most dump fills fall into this category.

The procedure to use the family of compression curves to calculate the settlement for a thick compacted layer is summarized using the following steps:

Investigate the dry density profile within thick compacted layer, i.e. of  $\gamma_d(z)$ ;  
Calculate  $e_0(z)$  from  $\gamma_d(z)$ . The profile can be measured or estimated by combining the stress distribution analysis and the dry density versus compactive effort relationship presented in Chapter 2.

Use the one dimensional compression curves from laboratory measurements or field tests to obtain parameters  $M$  and  $N$  in Equation 8-4 and the constant  $A$  in Equation 8-6.

Calculate  $p(z)$  using Equation 8-12.

With all four parameters obtained, calculate the settlement ( $\Delta s$ ) for each layer using Equation 8-8 or 8-10.

Calculate the total settlement by integrating the sublayers over the thick layer. For one-step method, Equation 8-13 can be used directly.

## 8.7 CONCLUSIONS

The settlement estimation for a thick compacted layer is more complicated and can result in large errors if one uses the compression index to estimate the settlement. It is therefore better practice to subdivide the thick layer into a number of sublayers. As the number of sublayers is increased, a more accurate solution can be obtained. However, the indexes  $C_c$  and  $C_r$  to represent the compression behavior for each sublayer must be individually determined as the compression curve is non-linear, which requires a large number of soil compression tests over the depth.

The concept of a family of compression curves within the thick compacted layer could provide a simpler solution to this problem. The complete compression curve for each sublayer can be described using Equation 8-4. An analytical method presented in this chapter is based on this equation and the concept of a family of compression curves. The method only requires a single one-dimensional compression curve and the dry density profile within the thick layer. The final settlement of the thick compacted layer is integrated from the settlement of multi-sublayers calculated using the traditional method

(Equation 8-8) or the one-step method (Equation 8-10). The integration of one-step method finally results in a single Equation 8-13. Although the equation is complicated in form, it is easy and fast to use with spreadsheet programs.

The approach presented in this chapter is just one of the many possible applications that the proposed compression equation and the concept of the family of compression curves can be used to improve the estimate of settlements. The usefulness of this approach needs to be established in practice, and other applications are anticipated in the future.

---

<sup>1</sup> Maple is a proprietary product of Waterloo Maple Inc., 57 Erb Street W. Waterloo, Ontario, Canada N2L 6C2.

## 8.8 REFERENCES

- Bowles, J.E., 1996. **Foundation Analysis and Design**, McGraw-Hill, Fifth Edition.
- Cameron, R., Ashton, Colin, Fong, V., and Strueby, B. 1995. Sun crude highway berm: Part 1 of 5 – project overview and design philosophy. *In* Proceedings of 48<sup>th</sup> Canadian Geotechnical Conference, Vol. 2: 789-797.
- Bozozuk, M. 1971. Effect of sampling, size, and storage on test results for marine clay. *Sampling of Soil and Rock*, ASTM STP 483, American Society for Testing and Materials: 121-131.
- Craig, R.F. 1993. **Soil Mechanics Chapman and Hall**, Fifth Edition.
- Das, B.M. 1998. **Principles of Geotechnical Engineering**, PWS Publishing Company.
- Holtz, R.D. and Kovacs, W.D. 1981. **An Introduction to Geotechnical Engineering**, Prentice-Hall.
- Kabbaj, M., Oka, F., Leroueil, S., and Tavenas, F. 1985. Consolidation of natural clays and laboratory testing. *Symposium on Consolidation Behavior of Soils*, Fort Lauderdale, ASTM STP 892: 378-403.



- Lacerda W.A., Costa Filho, L.M., Coutinho, R.Q., Duarte, A.E.R. 1977. Consolidation characteristics of Rio de Janeiro soft clay. *In* Proceeding of International Symposium on Soft Clay, Bangkok, Thailand: 231-235.
- McPhail, J., Hellen, P., Britton, S., Colvin, C., Silvey, T., and Jones, J. 2000. Evaluation of consolidation settlement using the sublayer method. *Electronic Journal of Geotechnical Engineering*, Vol. 5.
- Morgenstern, N.R., Fair, A.E., and McRoberts, E.C. 1988. Geotechnical engineering beyond soil mechanics – a case study. *Canadian Geotechnical Journal*, **25**: 637-661.
- Rutledge, G.P. 1944. Relation of undisturbed sampling to laboratory testing. *Transactions of American Society of Civil Engineers*, **109**: 1162-1163.
- Sowers, G.F. 1962. Shallow Foundations. Chapter 6, *Foundation Engineering*, Leonards, G.A. Ed. pp. 570-575.
- Terzaghi, K., R. Peck, and G. Mesri, 1996. **Soil Mechanics in Engineering Practice**, John Wiley and Sons.
- Timoshenko, S.P. and Goodier, J.N. 1951. **Theory of Elasticity**, McGraw-Hill Book Company, Inc., New York.
- U.S. Army Corps of Engineers. 1994. Engineering Manual, EM 1110-2-1904, Settlement Analysis, ASCE Press.
- Wang, N. and Wei, R. 1996. Evaluation of sample quality of soft clay. *In* Proceeding of 2nd International Conference on Soft Soil Engineering, Nanjing, 120-125.
- Westergaard, H.M. 1938. A problem of elasticity suggested by a problem in soil mechanics: a soft material reinforced by numerous strong horizontal sheets, in *Mechanics of Solids: S. Timoshenko Sixtieth Anniversary Volume*, The Macmillan Company, New York.

## 8.9 APPENDIX 8-A DERIVATION OF EQUATION 8-9

The equation of Equation 8-4 for a complete compression curve is rewritten as:

$$[8-A1] \quad \frac{1}{e_f} = \frac{1}{e_0} + M \cdot \ln \left[ 1 + \left( \frac{\sigma_f}{p} \right)^N \right]$$

where  $e_0$  is the initial void ratio and  $e_f$  is the final void ratio at an applied stress  $\sigma_f$ . The equation 8-A1 can be also rewritten as:

$$[8-A2] \quad \frac{e_0 - e_f}{e_0 e_f} = M \cdot \ln \left[ 1 + \left( \frac{\sigma_f}{p} \right)^N \right]$$

Since soil elastic rebound during sampling is relatively small, the initial void ratio in one-dimensional compression test ( $e_0$ ) is close to the initial void ratio of the in-situ soil ( $e_i$ ), i.e.  $e_i \approx e_0$ . Therefore, the void ratio change is

$$[8-A3] \quad \Delta e = e_i - e_f \approx e_0 - e_f$$

Substituting Equation 8-A3 into Equation 8-A2, the following expression is obtained:

$$[8-A4] \quad \Delta e = e_0 e_f \cdot M \ln \left( 1 + \left( \frac{\sigma_f}{p} \right)^N \right)$$

**Table 8-1 Parameters for  $P_1$  at  $w=17\%$  under compaction of 98 kPa foot pressure and 25 applications**

Regressed Parameters	Compression curve of compacted soil (98 kPa foot pressure, 25 applications)	Dry density profile
$e_k=$	1.237	$e_{01}= 1.24$ (top)
$C_k=$	0.0124	$\gamma_{d1}= 1.20 \text{ Mg/m}^3$ (top)
$M=$	0.0666	
$N=$	9.383	$e_{02}= 0.82$ (bottom)
$p=$	108.1 kPa	$\gamma_{d2}= 1.48 \text{ Mg/m}^3$ (bottom)
$MN=$	0.6252	
$1/e_k - MN * \ln(p) = A =$	-2.120	

**Figure 8-1 The cross-section of a thick-layer and multi-sublayer system**

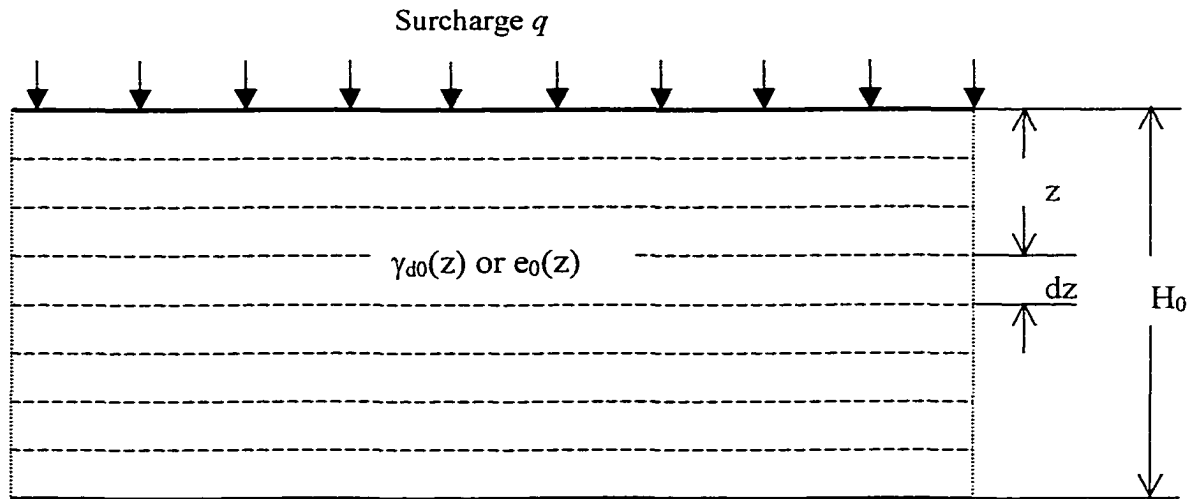


**Figure 8-2 The one-dimension compression curve and fitting for compacted Pleistocene Lacustrine clay prepared at 17% water content using a foot pressure of 98 kPa**

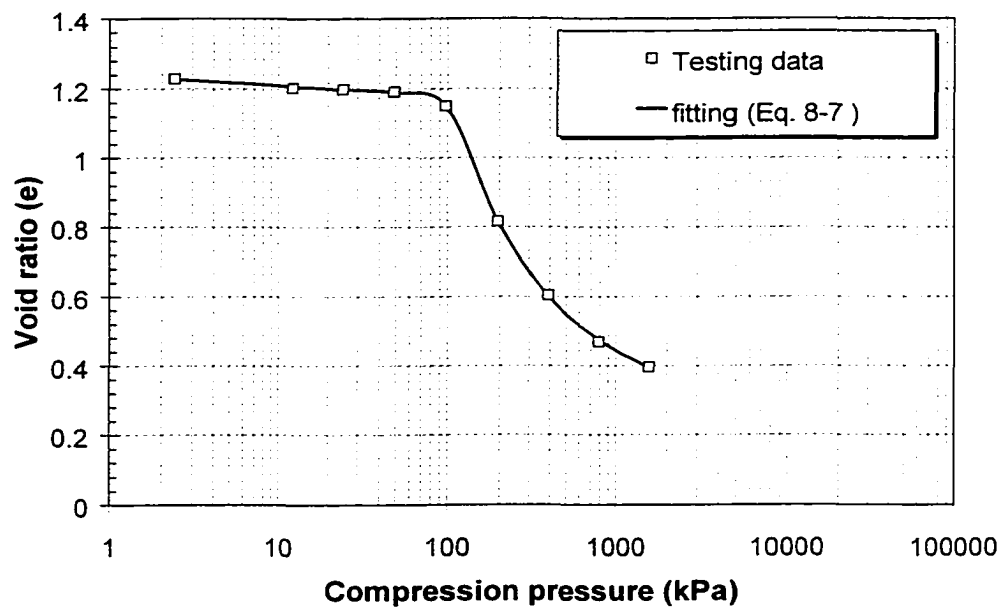


**Figure 8-3 The calculated settlement and vertical strain ( $\epsilon = \Delta s/H_0$ ) for thin compacted layer of Pleistocene Lacustrine Clay using Equation 8-10**

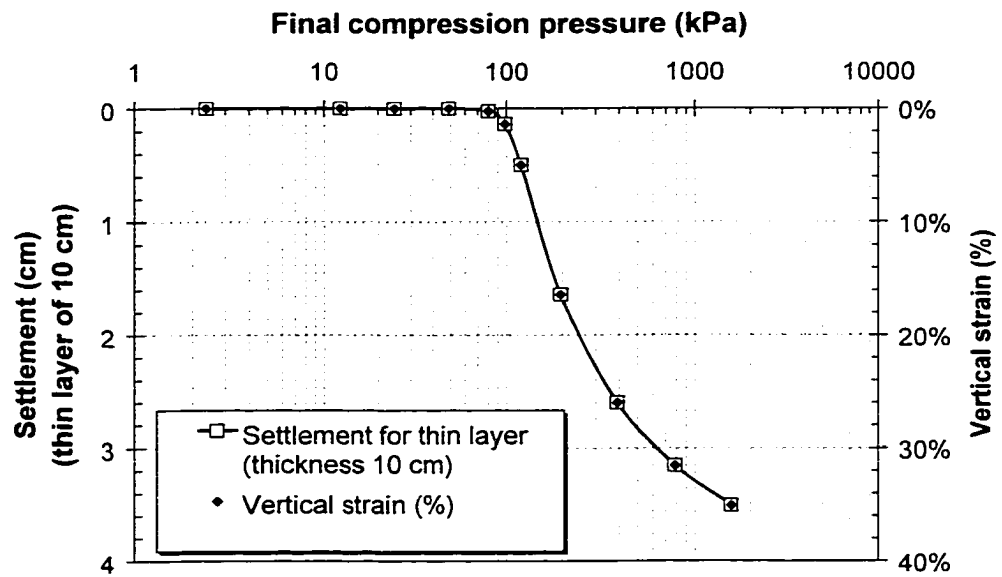


**Figure 8-4 Void ratio profile  $e_0(z)$  and dry density profile  $\gamma_d(z)$  over the thick layer**

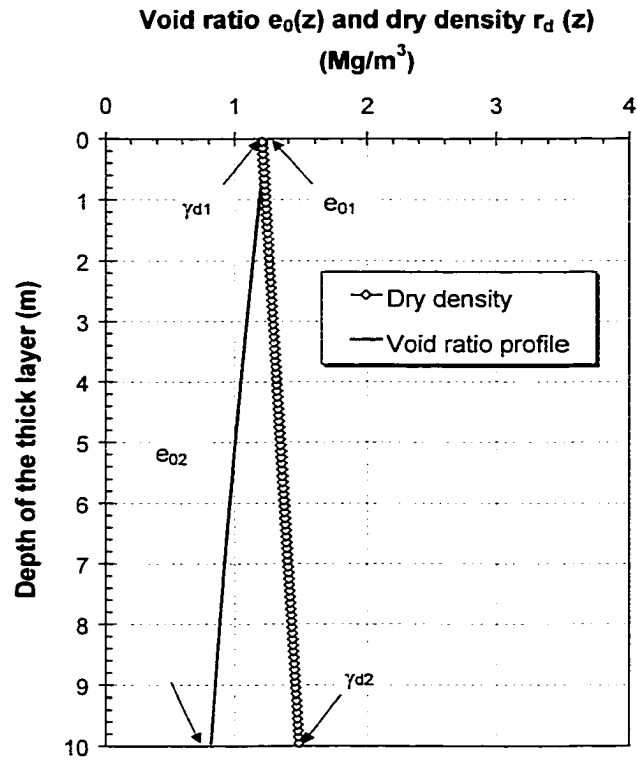


**Figure 8-5 Stress distribution over the thick layer**

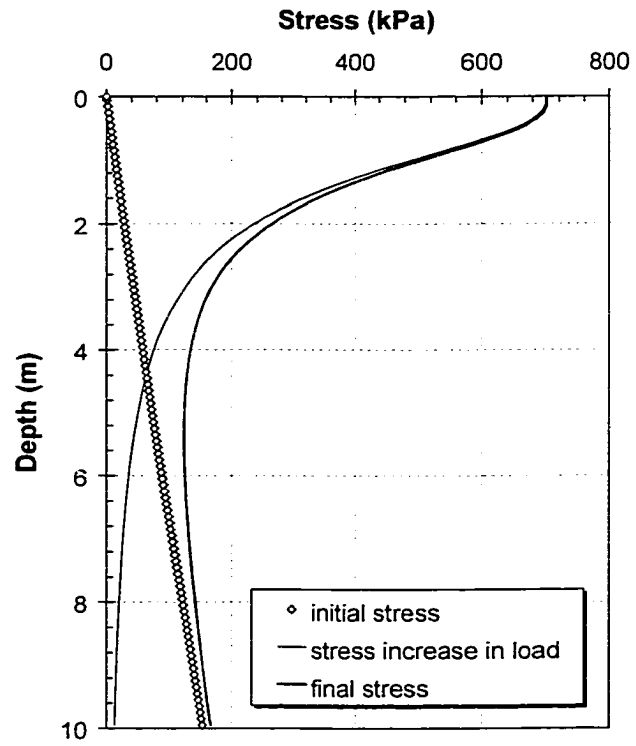


**Figure 8-6 Influence of the total number of divided sublayers on the results of calculated settlement**

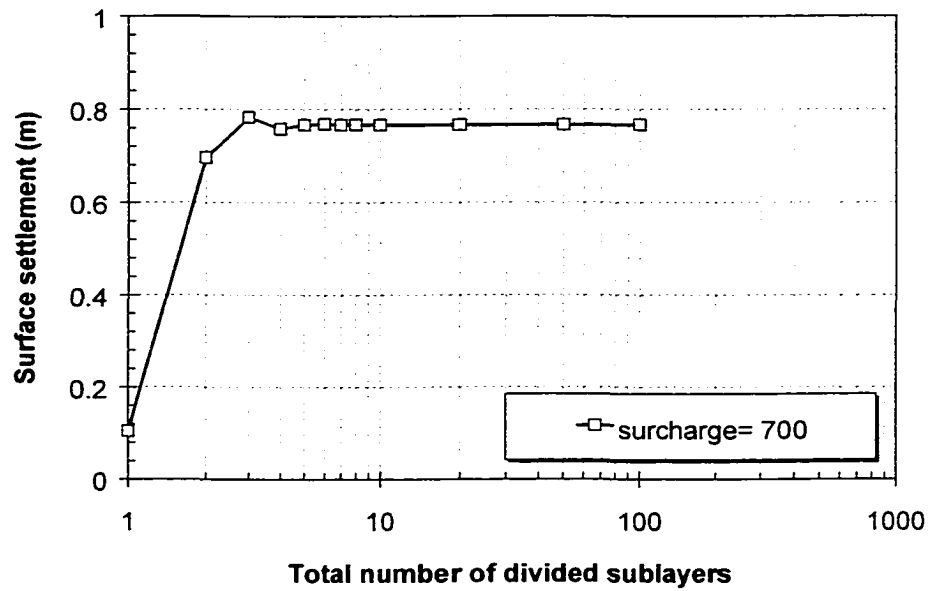


**Figure 8-7 The settlement estimation for thick compacted layer (10 m) under different surcharge loading using Equation 8-12**

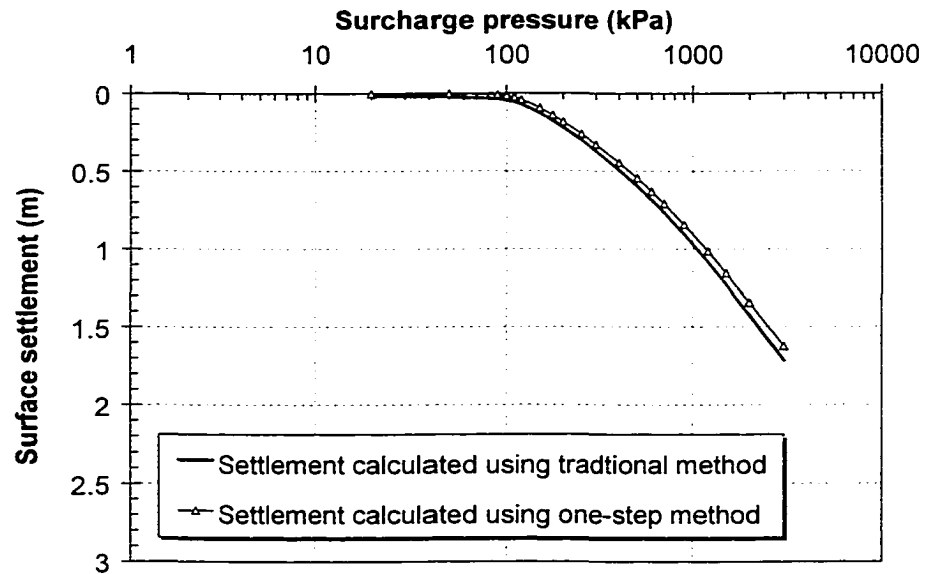
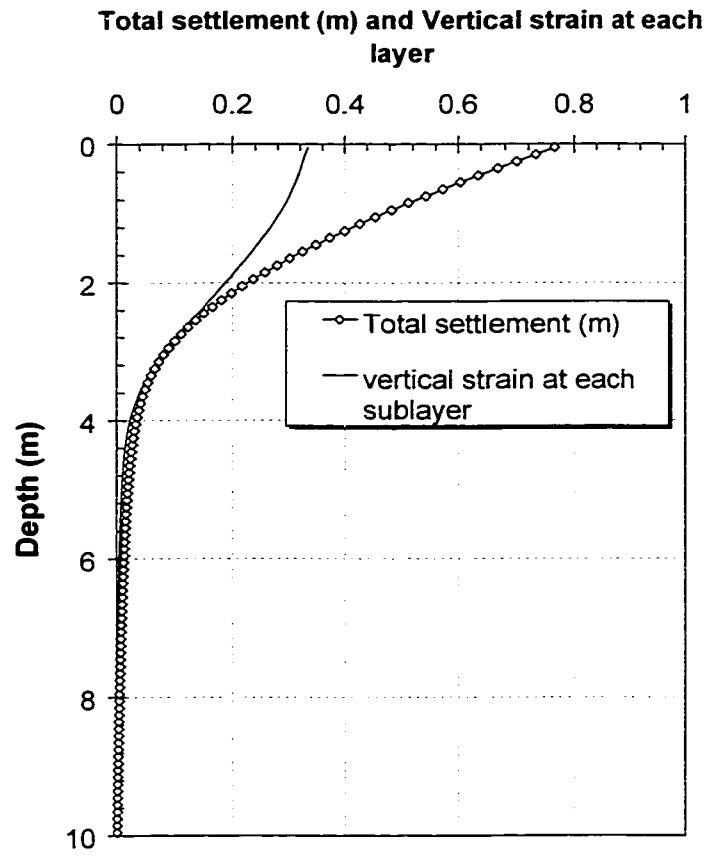




**Figure 8-8 The vertical strain at each sublayer and its accumulated settlement under surcharge of 700 kPa**



# **CHAPTER 9 SUMMARY AND CONCLUSIONS, AND RECOMMENDATION FOR FUTURE WORK**

## **9.1 SUMMARY**

The objectives of this study were to investigate soil compaction theory and the deformation behavior of compacted fine-grained soils. The thesis can be divided into two major categories:

- The compaction theory for fine-grained soils, which includes a description and explanation of the characteristics of a complete compaction curve, its formulation, and the existence and prediction of a family of compaction curves. The compaction parameters and the strength variation along the complete compaction curve are also discussed.
- The one-dimensional compression behavior of compacted fine-grained soils, its formulation, the concept and creation of a family of compression curves, and the settlement estimation for a thick, under compacted layer.

The complete compaction curve for fine-grained soil and its characteristics are discussed in Chapter 2. A promising relationship describing the compaction curve for fine-grained soils, based on the relationship between the degree of saturation and water content, is proposed. It is the first non-pure-curve-fitting equation since Proctor introduced the compaction theory in 1933. The equation has four parameters which are physically defined as the boundary conditions, shape and size of the compaction curve. The parameters can be obtained either directly from the curve or using regression analysis. The equation can easily be used to predict a family of compaction curves for the same soil for varying compactive efforts. The examples show the equation adequately represents the traditional as well as the complete compaction curves for fine-grained

soils. The curves predicted by the proposed equation show excellent agreement with laboratory test results.

The four parameters in the proposed compaction equation and their relationship to the physical properties of a particular soil are discussed in Chapter 3. Standard compaction test results from four different soils from Northern Alberta are used to estimate the parameter's value for the different soils. It is found that the shape factor, which is very useful because it is constant when a soil is compacted using different energy, is related to the soil uniformity coefficient. The dry density of soil in the dry region increases with average particle size for a given compaction test. The index of compactable range is related to the soil plastic limit and average particle size. The maximum degree of saturation varies in a small range for different soils.

The unconfined compression strength of a compacted sample is always important and of interest, especially the maximum strength and its relationship to the optimum water content (OWC). Complete profiles of unconfined compression strength along the complete compaction curves are presented in Chapter 4. The strength shows an increase at the point of the compaction sensitivity threshold (CST) where the dry density of the compacted soil also increases substantially. The strength reached a maximum midway between CST and OWC, and then the strength and deformation modulus decreased. The location of CST turned out to be another critical point on the compaction curves. Matric suction measurement found that the suction value at CST is equal to compactive stress applied during the test, which is important for understanding the compaction mechanism and determining the effective compaction region and the water content with the maximum compressive strength.

The particle size distribution of soil is a key factor to its engineering behaviors. The evolving particle size for residual soils due to weathering was analyzed using uniform fragmentation theory in Chapter 5. A general analytical method is developed to calculate the evolution of the particle size distribution. The calculated curves of particle size distribution curves after weathering are parallel to each other, which indicates similar

shape of compaction curves according to the study in Chapter 3. This conclusion can explain the origin of the Type A family of compaction curves that is widely used in practice. It provides a theoretical foundation for the one-point method.

The deformation behavior of less compacted fine-grained soils is another focus in this research. A new testing procedure is proposed in Chapter 6. It combines compaction, compression and wetting collapse testing in one apparatus. The samples were prepared over wide moisture range with water content from the air-dried condition to  $1.25 w_L$  (liquid limit). The compression curves of the samples joined together at high compression pressure, which becomes the base of the family of compression curves. The wettest sample (46%) reached the lowest void ratio for each different applied stress due to the lubrication effect of the water.

When the sample is prepared dry of the optimum water content (OWC), the compactive pressure has a similar effect on the compression curve to the preconsolidation pressure for the consolidation curve of saturated soils. When the sample is prepared wet of the OWC, compaction is not effective. This is due to the compaction causing pore pressure increases and that the pressures cannot dissipate during the short period. When the subsequently applied compression stress is beyond the previous compaction pressure, the compaction effect becomes insignificant to the measured deformation.

The samples compacted wet of OWC have yield pressure from their compression curves that are less than the applied compaction pressure. If the future compression pressure is greater than the effective compaction pressure, the compacted soil should behave as a less compacted soil and thus large compression deformation should be expected. Therefore, choosing an appropriate compaction pressure and placement water content and anticipating future loading pressure are both important for controlling the future compression and wetting collapse of dumped waste soils.

The wetting-induced collapse is independent of loading-wetting sequence and decreased when either the initial water content increases or the compression pressure increases. The

lower void ratio of a wetted soil can be estimated from the compression curve of a sample with its initial water content between  $w_L$  and  $1.5w_L$  or from the samples prepared at a given water content and flooded prior to conducting the compression test.

The one-dimensional compression test is commonly used for settlement calculations in geotechnical practice. Equations are proposed in Chapter 7 to properly represent the one-dimensional compression curve over the complete stress range. Examples with various types of soils illustrated its usefulness for geotechnical practice, with the exception of some highly structured sensitive clays. The parameters within the equation are physically defined. The boundary condition at high stress ( $MN$ ) and the ultimate asymptote curve are considered unique for a given soil at the same moisture condition. This helps to predict a family of compression curves within a layer of compacted soils and for settlement estimation.

Since the proposed compression equation can properly describe a single compression curve, the settlement for a thin layer at any stress level can be thus mathematically formulated. The settlement estimation for a thick compacted layer is more complicated and can result in large errors if one uses the simplified straight line with slope (compression index) to estimate the settlement. The analysis method described in Chapter 8 is based on the equation and its prediction of a family of compression curves. The method only requires a single one-dimensional compression curve and the dry density profile within the thick layer. The final settlement of a thick compacted layer is integrated from the settlement of multi-sublayers calculated using the traditional method or the one-step method. The integration of one-step method results in a single equation. Although the equation is complicated in form, it is easy and fast to use with readily available spreadsheet programs.

## 9.2 CONCLUSIONS

The family of compaction curves for fine-grained soils and their engineering behaviors were systematically studied. In conclusion, several findings and improvements in the

practice of geotechnical engineering have been achieved during this research. Major contributions that are viewed by the author as original work are summarized as follows:

- Proposed equation to describe the complete compaction curves for fine-grained soils. The equation can also be used to predict a family of compaction curves for different applied compactive efforts.
- Physically defined the compaction parameters used with this equation. The parameters can be obtained directly from the complete compaction curve. An effort has been made to relate the parameters to basic soil physical properties.
- Discovered the similarity of soil compaction curve and the unconfined compression strength profile around the compaction sensitivity threshold (CST). The strength reached a maximum midway between CST and optimum water content (OWC), and then the strength decreased.
- The location of CST was discovered to be an equilibrium point where the compactive pressure equals the soil matric suction.
- Created the original mathematical method to model the evolution of particle size distribution. The concept of uniform fragmentation was used to simulate the phenomenon of weathering. This result suggests the existence of family of compaction curves for residual and other geological similar soils.
- Developed a testing procedure that can combine the compaction test and one-dimensional compression test together. A series of soil deformation behaviors was summarized with variety in water content, compactive efforts, and wetting-flooding sequences.
- Proposed the continuous model to describe the one-dimensional compression curve over the complete stress range.
- Introduced the new concept of a family of compression curves and proposed the prediction method of the curves.
- Proposed a new method to estimate the settlement for a thick, under compacted layer using the family of compression curves.

### **9.3 RECOMMENDATIONS FOR FUTURE WORK**

This research focuses on the soil compaction theory and the deformation behavior for compacted fine-grained soils. The concept of the family of compaction curves and the family of compression curves are emphasized. Fundamental equations and methods have been developed to apply the concepts for prediction of the compaction and compression curves. The author is aware of the fact that this study deals with a field that is familiar to most researchers and engineers. The focus of this study is a new procedure and there is considerable additional work to be undertaken before its final acceptance in geotechnical practice. Toward that, the future work recommended falls into three categories:

The first category is topics associated with the soil compaction theory. The progress on soil compaction in this research makes the prediction of a family of compaction curves possible and it also physically defines four compaction parameters. The study based on limit data from Northern Alberta indicates that the compaction parameters have a close relationship to basic soil properties, such as particle size distribution and plastic limit. These results suggest that a soil compaction curve could be predicted using the soil basic properties. The predicted curve would be important for the selection of construction materials for use in embankments, highways, dams, landfills, pipelines, and even as nuclear waste disposal buffer material. To achieve this, a database using typical soils around the world should be created to allow for comparison between actual and predicted compaction curves.

The research results will be of interest to engineers to aid in selection of construction materials and to guide field compaction control related to highway or other infrastructure projects. It is more useful in a country like Canada with its variable soil conditions to have this database. It is anticipated that its completion and use will assist in reducing the costs associated with future infrastructure construction.

The second category deals with topics associated with the general analysis method on evolution of particle size distribution. The method provides a new solution in

mathematical modeling the change of soil particles due to various natural and human processes. In addition to using the uniform fragmentation for weathering in a long geological period, particle crushing due to loading or blasting in a very short time can be described using the concept of fractal. Combining these two concepts together, it would be possible and useful to discuss the evolution of particle size distribution of any soil types mathematically in the future.

The third category relates to applications of the equation for the one-dimensional compression curve. The compression model is continuous over complete stress range and can represent a family of compression curves. It has the potential to be expanded to three-dimension which would be more useful as a practical soil constitutive model. The model has been shown to be useful in representing soil water characteristic curve (SWCC) of unsaturated soil mechanics. It is believed that the parameters  $M$  and  $N$  are related to soil physical properties such as particle size distribution, plastic limit, or liquid limit. Further research should allow prediction of the soil compression curve using only basic soil physical properties.

The results of this study can have some significant implications for some conventional areas in geotechnical engineering. The methodology used here depends directly on the use of soil test results. It focuses on the precise description of the final outcomes of tests and avoids using constitutive assumptions. This could be the solution to simplify the processes while respecting the non-linear behaviors of soils. Fortunately, the development in computer technology allows the approach to become as simple as using spreadsheet. The usefulness of this approach needs to be established in practice, and other applications are anticipated in the future.



**APPENDIX INSTRUMENT PHOTOS AND MATRIC  
SUCTION MEASUREMENT RESULTS**

**Figure 0-1 Kneading compaction machine (photo)**

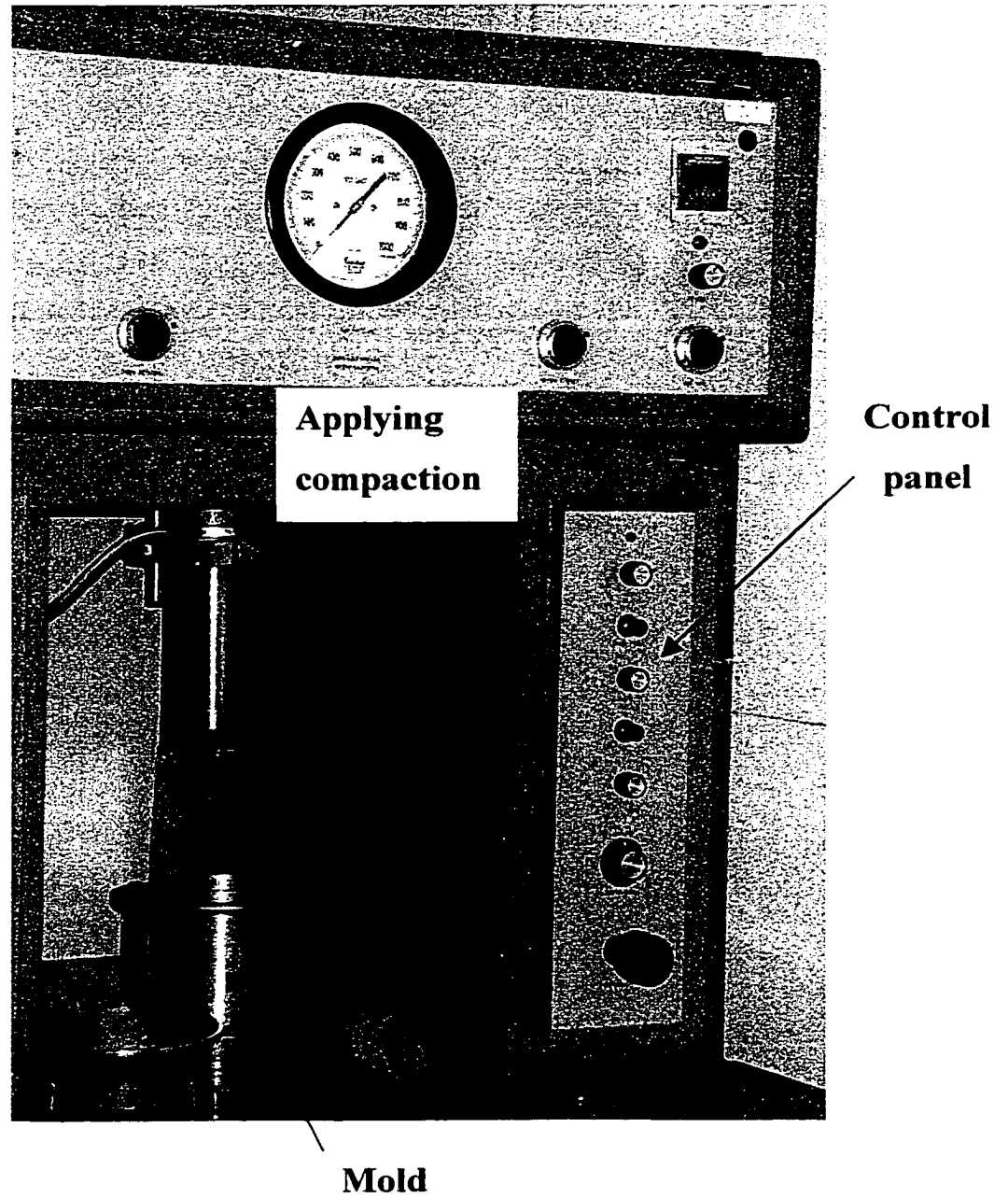


**Figure 0-2 Thermo-conductivity sensor and mold for suction measurement (photo)**

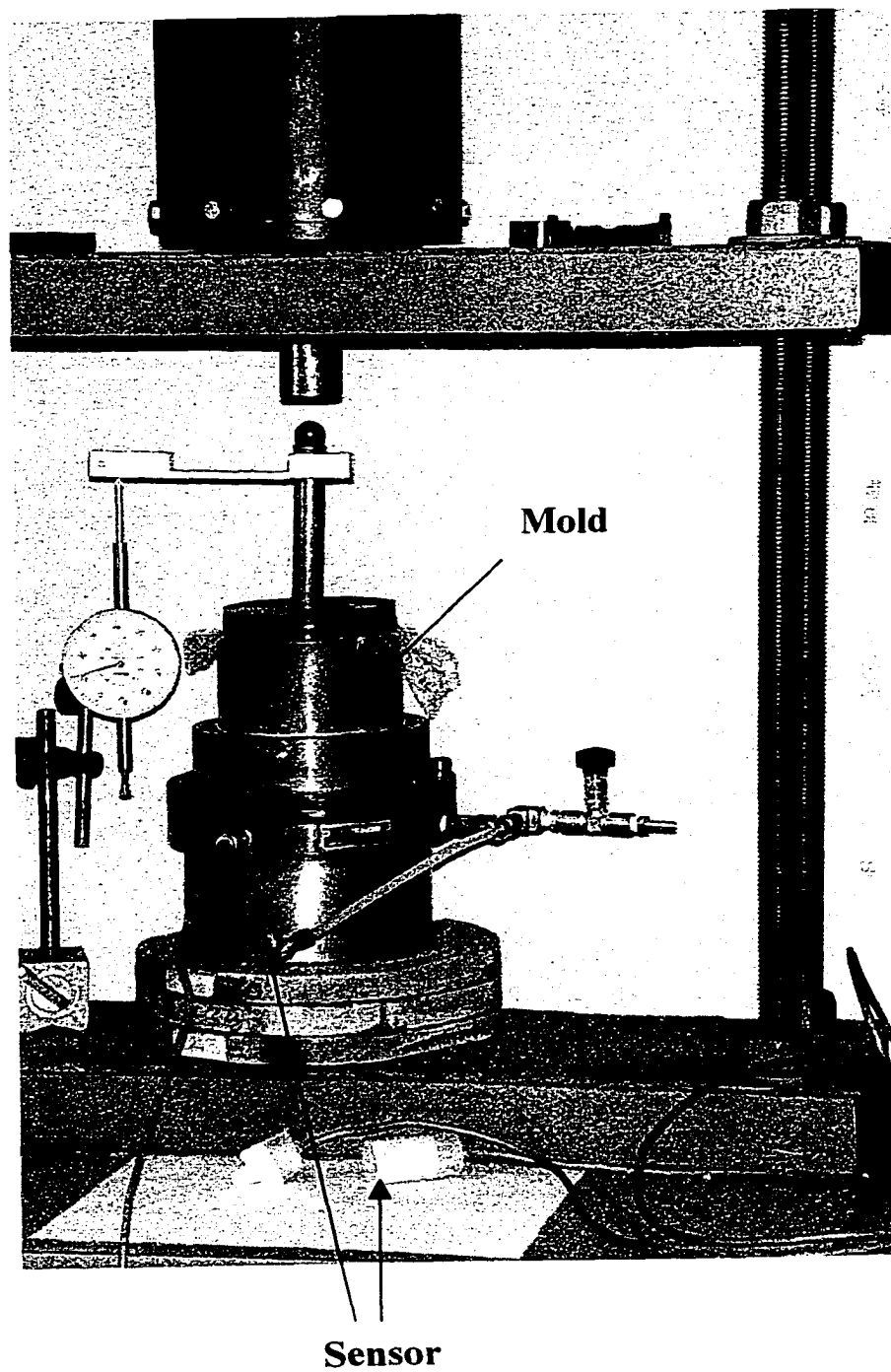


**Figure 0-3 Apparatus that combines pneumatic compaction test and one-dimensional compression test (photo)**

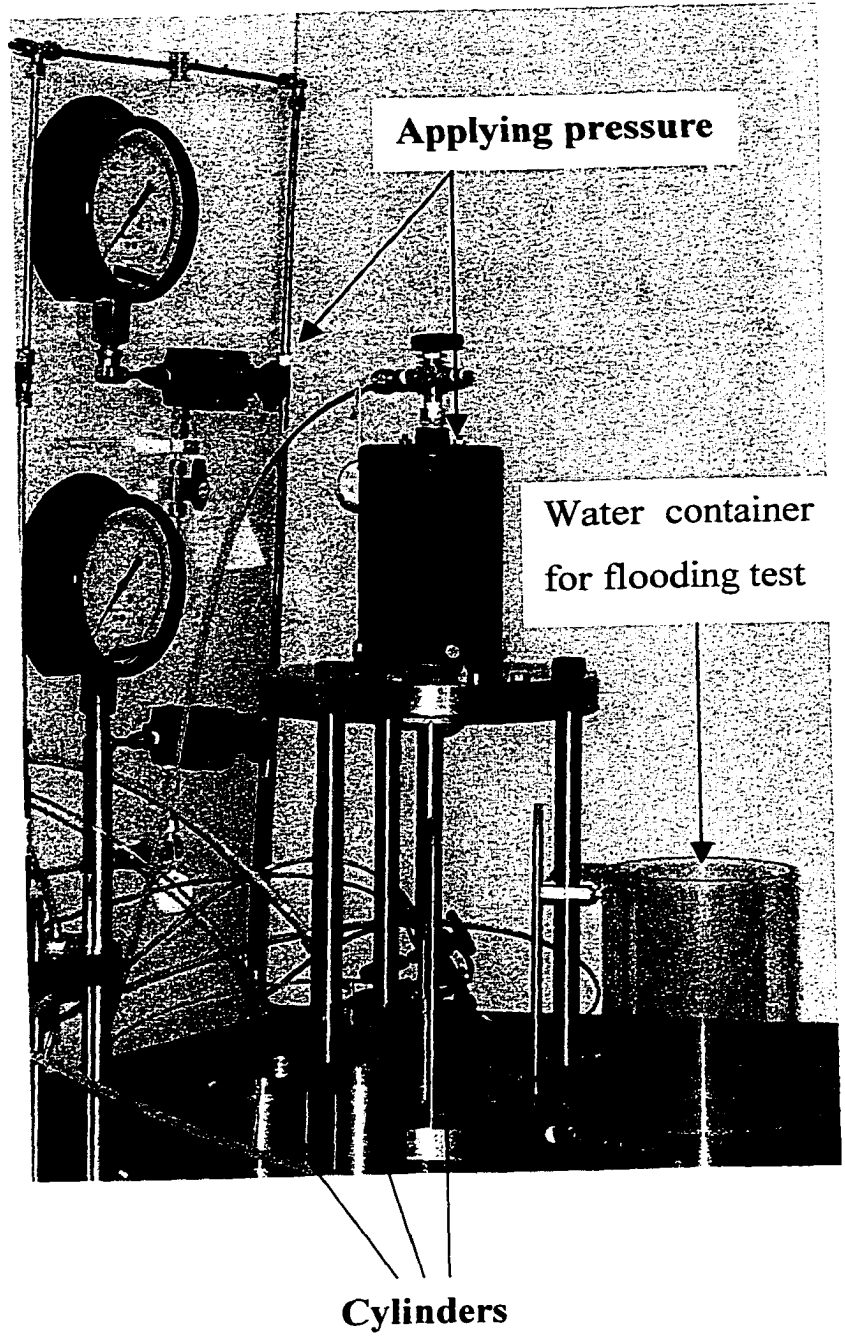


**Figure 0-4 The suction measurement of glacial till ( $P_g$ ): sample suc-P2g-3%-c1**

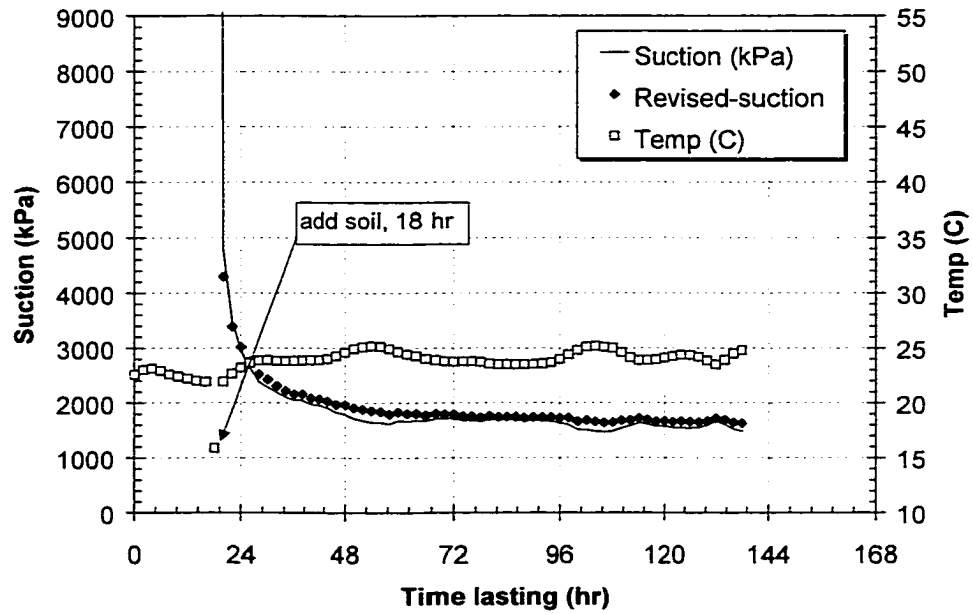


**Figure 0-5 The suction measurement of glacial till ( $P_g$ ): sample suc-P2g-7%-c2**

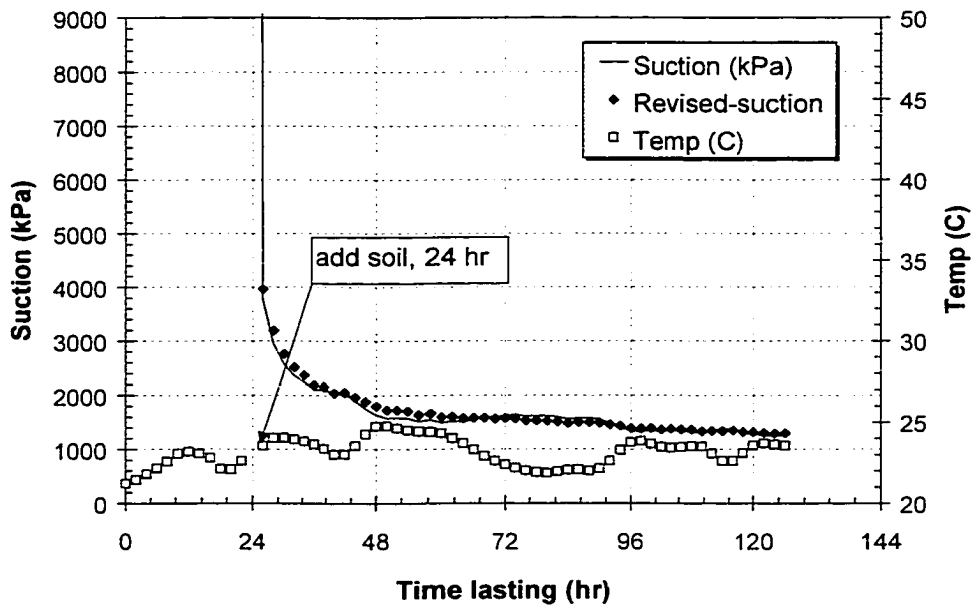


**Figure 0-6 The suction measurement of glacial till ( $P_g$ ): sample suc-P2g-9%-c3**

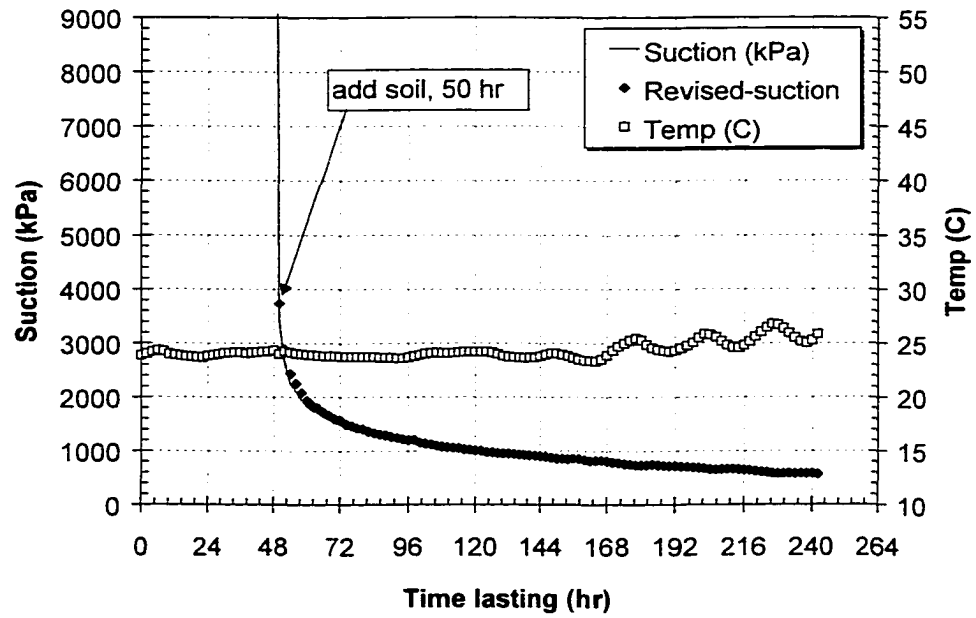


**Figure 0-7 The suction measurement of glacial till ( $P_g$ ): sample suc-P2g-12%-c4**

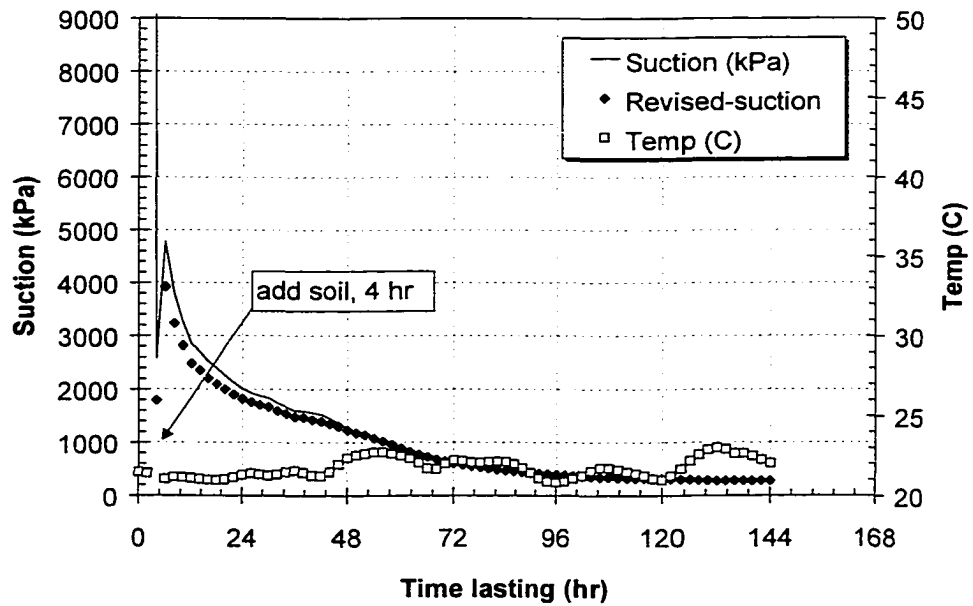


**Figure 0-8 The suction measurement of lacustrine clay (P<sub>1</sub>): sample suc-P2I-11%-a1**

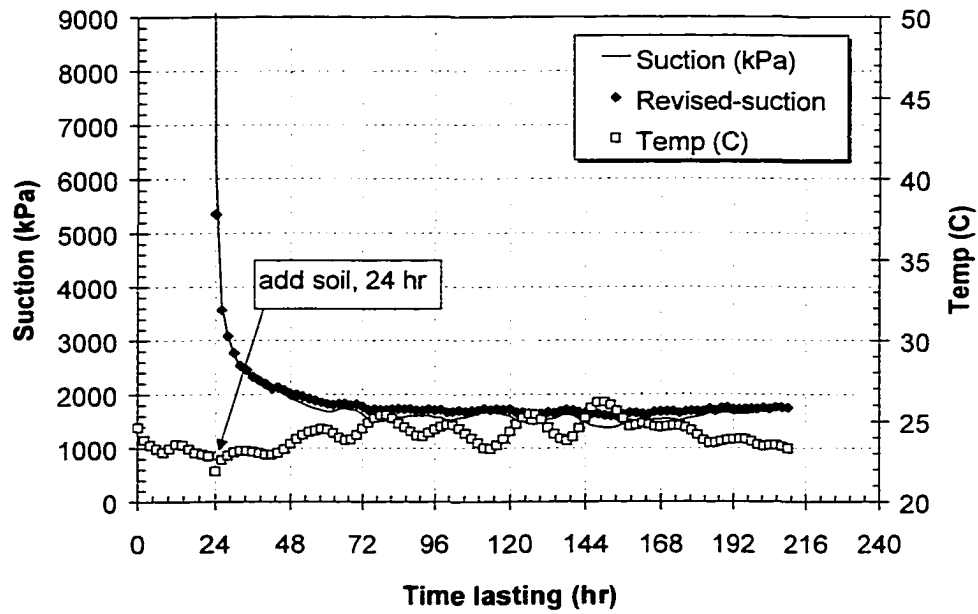


**Figure 0-9 The suction measurement of lacustrine clay (P<sub>1</sub>): sample suc-P2I-14%-a2**

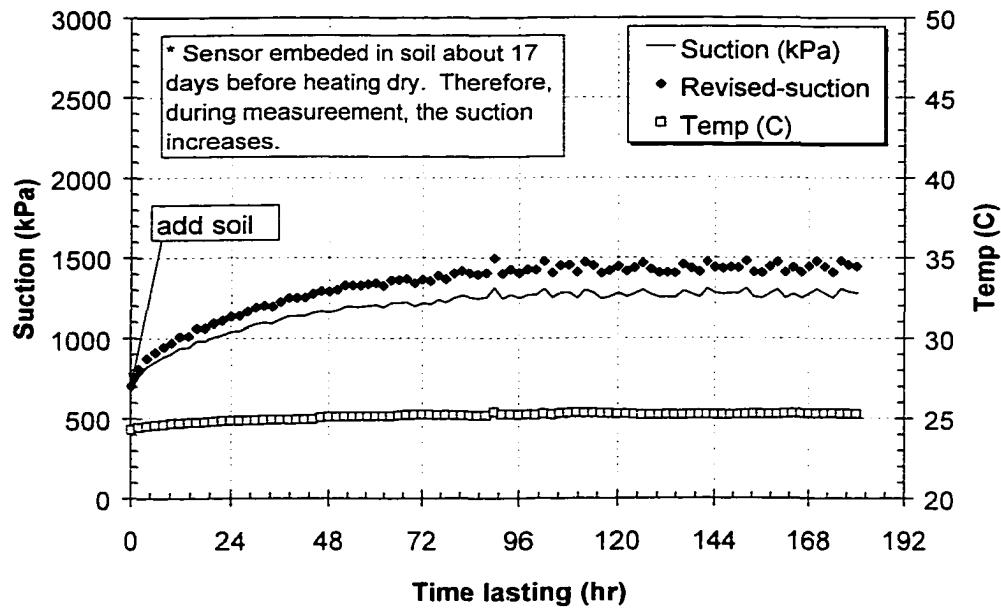


**Figure 0-10 The suction measurement of lacustrine clay (P<sub>1</sub>): sample suc-P21-18%-a3**

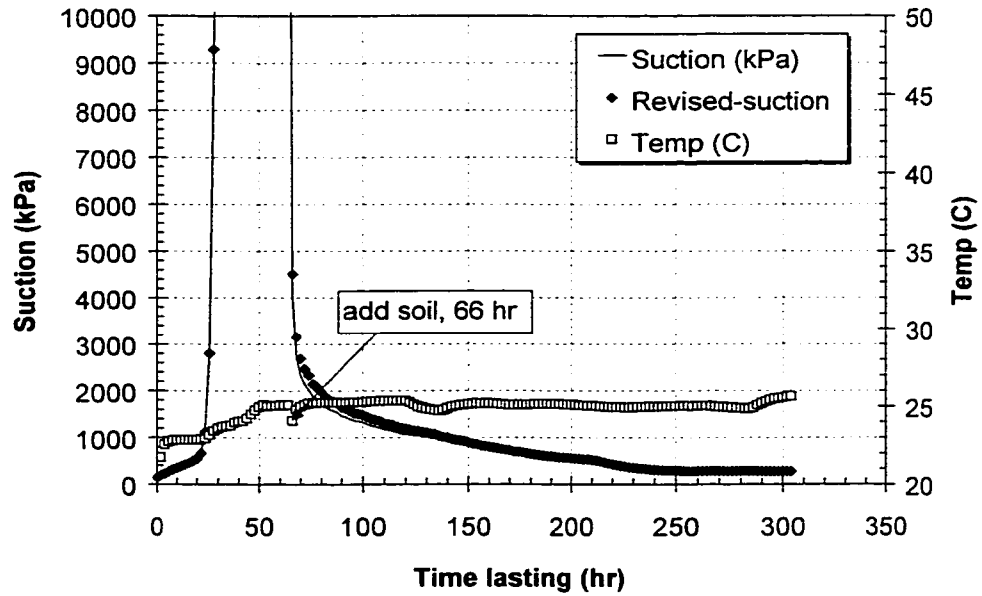


**Figure 0-11 The suction measurement of lacustrine clay (P<sub>1</sub>): sample suc-P21-24%-a4**

